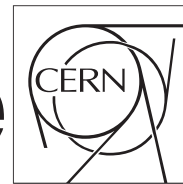




The Compact Muon Solenoid Experiment

CMS Draft Note

Mailing address: CMS CERN, CH-1211 GENEVA 23, Switzerland



2018/06/04

Head Id: 460082

Archive Id: 463220

Archive Date: 2018/05/13

Archive Tag: trunk

A search for beyond the Standard Model light bosons decaying into muon pairs at CMS at $\sqrt{s} = 13$ TeV

Alfredo Castaneda², Sven Dildick¹, Teruki Kamon¹, Bouhali Othmane², Paul Padley³, Luca Pernie¹, Jamal Rorie³, Alexei Safonov¹, and Wei Shi³

¹ Texas A&M University

² Texas A&M University at Qatar

³ Rice University

Abstract

A dataset corresponding to 35.9 fb^{-1} of proton-proton collisions at $\sqrt{s} = 13$ TeV was recorded during 2016 by the CMS experiment at the CERN LHC. These data are used to search for pair production of new light bosons with a mass between 0.25 - 8.5 GeV/c^2 which decay into muon pairs. No excess is observed in the data, and a model-independent upper limit on the product of the cross section, branching fraction, and acceptance is derived. The results are interpreted in the context of two benchmark models, namely, the next-to-minimal supersymmetric standard model, and dark SUSY models including those predicting a non-negligible light boson lifetime.

This box is only visible in draft mode. Please make sure the values below make sense.

PDFAuthor:	Alfredo Castaneda, Sven Dildick, Benjamin Michlin, Luca Pernie, Jamal Rorie
PDFTitle:	A search for beyond the Standard Model light bosons decaying into muon pairs at CMS
PDFSubject:	CMS
PDFKeywords:	CMS, physics, software, computing

Please also verify that the abstract does not use any user defined symbols

1 Contents

2	1	Introduction	2
3	2	Analysis Strategy	10
4	3	Samples	12
5	3.1	Data Samples	12
6	3.2	Simulated Samples for Signal	12
7	4	Analysis Selections and Efficiencies	18
8	4.1	Trigger	18
9	4.2	Muon Selection	22
10	4.3	Further Event Selection	23
11	4.4	Summary of the Selection Efficiencies	29
12	5	Modeling of the Signal Shape	36
13	6	SM Backgrounds and Their Shapes	37
14	6.1	EWK $pp \rightarrow 4\mu$ Background	37
15	6.2	QCD $pp \rightarrow b\bar{b} \rightarrow 4\mu$ Background	39
16	6.3	QCD Prompt $pp \rightarrow 2J/\psi \rightarrow 4\mu$ Background	46
17	6.4	Conclusions	54
18	7	Systematic Uncertainties	55
19	7.1	Instrumental Uncertainties	55
20	7.2	Theoretical Uncertainties	56
21	7.3	Summary of the Systematic Uncertainties	56
22	8	Results	58
23	8.1	Model Independent Limit	58
24	8.2	Constraints on Benchmark Models	60
25	9	Conclusions	66
26	A	List of the Data and MC Signal Samples	73
27	B	Efficiencies of the Event Selection Requirements for Benchmark MC Samples	97
28	C	BB Background Fit Results	129
29	D	Separation of prompt and non-prompt J/ψ using the lifetime method	131
30	E	Vertex Recovery for Parallel Muon Pairs	133
31	F	Dimuon Tracker Isolation	134
32	G	Extraction SF for muon ID and Isolation	139
33	G.1	Cross-check of the low- pT contribution with J/ψ	139
34	H	Model of the Event Acceptance as a Function of m_{γ_D} and $c\tau_{\gamma_D}$	142
35	I	Example of an Candidate Signal Event	143
36	J	Comparison 8 vs 13 TeV	145

37 1 Introduction

38 The CERN Large Hadron Collider (LHC), being one of the most energetic and luminous par-
 39 ticle accelerator ever created, presents a unique opportunity to search for new physics in a
 40 previously inaccessible energy regime with an increasing data sample. Our analysis looks for
 41 signals where pairs of new particles are produced and each of these new particles decays to
 42 muon pairs. This search criteria does not depend on how such new particles are produced, re-
 43 sulting in an analysis that is independent of any particular model or class of models. However,
 44 tuning selection criteria does require models against which we can benchmark performance
 45 and verify model independence. For this reason, we examine two classes of models featuring
 46 non-SM decays of the $125\text{ GeV}/c^2$ Higgs boson discovered at the LHC [1–3].

47 We present an analysis that explores one of the non-Standard Model (SM) decay modes of a
 48 Higgs boson (h), which includes production of two new light bosons (a), each of which subse-
 49 quently decays to a boosted pair of oppositely charged muons which are isolated from the rest
 50 of the event activity:

$$h \rightarrow 2a_1 + X \rightarrow 4\mu + X,$$

51 where X denotes possible additional particles from cascade decays of a Higgs boson. This
 52 signature is schematically shown in Fig. 1, where h can either be an SM-like Higgs boson or a
 53 new boson:

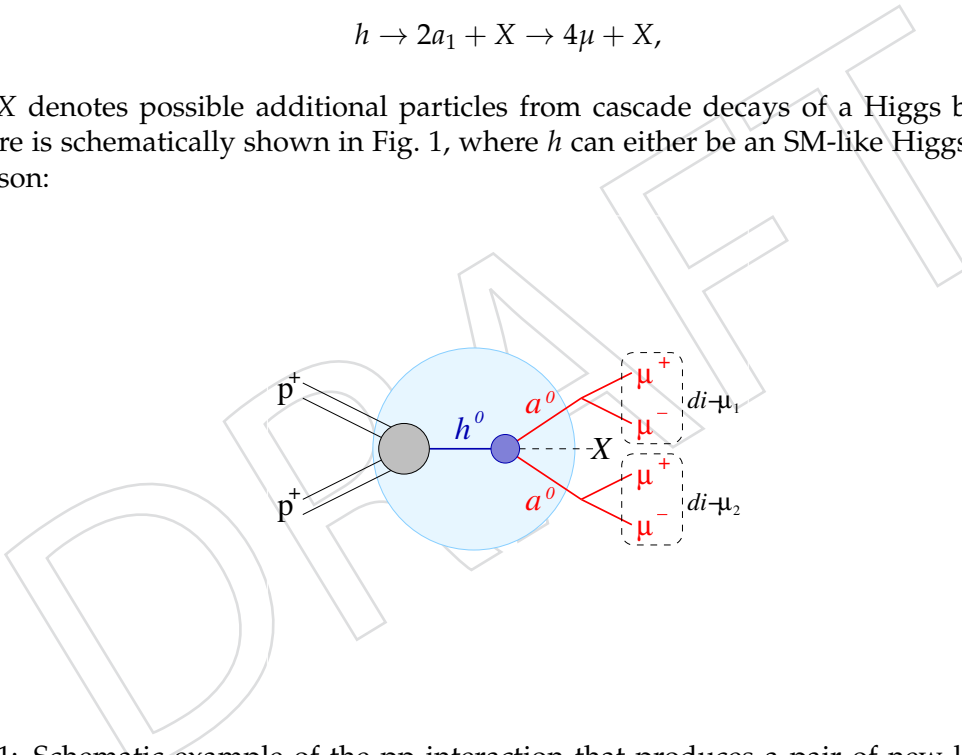


Figure 1: Schematic example of the pp interaction that produces a pair of new light bosons which decay into boosted, isolated, dimuons with consistent masses.

54 In this scenario the SM-like Higgs boson production cross section may or may not be enhanced
 55 compared to the SM prediction depending on the specific parameters of the model. The search
 56 described in this paper is designed to be independent of the details of specific models, and
 57 the results can therefore be interpreted in the context of other models predicting the same
 58 final state. We also study two specific scenarios: next-to-minimal supersymmetric standard
 59 model (NMSSM), and supersymmetric models with additional “hidden” or “dark” sectors
 60 (dark SUSY) including cases with long-lived new particles.

The NMSSM [4–12] extends the minimal supersymmetric standard model (MSSM) [13–15] by an additional gauge singlet field S under a new $U(1)_{PQ}$ (Peccei-Quinn) symmetry in the Higgs

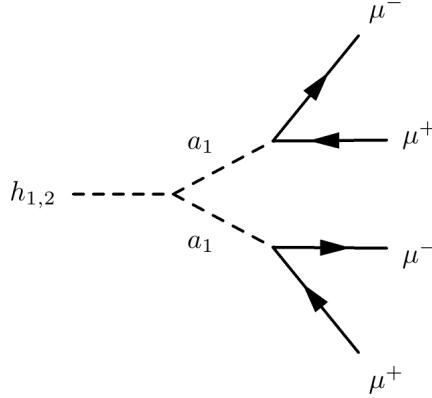


Figure 2: Feynman diagram of the NMSSM benchmark process $h_{1,2} \rightarrow 2a_1 \rightarrow 4\mu$.

sector of the superpotential:

$$\mu \hat{H}_u \cdot \hat{H}_d \rightarrow \lambda \hat{S} \hat{H}_u \cdot \hat{H}_d + \frac{\kappa}{3} \hat{S}^3. \quad (1)$$

In this expression, \hat{H}_u and \hat{H}_d are the Higgs fields for the up-type and down-type quarks, and κ is the self-interaction. In the NMSSM the parameter $\tan \beta$ is defined as

$$\tan \beta = \{\hat{H}_u / \hat{H}_d\}. \quad (2)$$

- 61 Compared to the MSSM, the NMSSM naturally generates the mass parameter (μ) in the Higgs
 62 superpotential at the electroweak scale [16] and significantly reduces the amount of fine tun-
 63 ing required [17–19]. This leads to an extension of the Higgs sector compared to the MSSM,
 64 and the Higgs sector of the NMSSM consists of 3 CP -even Higgs bosons ($h_{1,2,3}$) and 2 CP -odd
 65 Higgs bosons ($a_{1,2}$) [20–24]. Note that new light Higgs boson a_1 can couple to the SM-like
 66 Higgs $h_{1,2}$ and substantially broaden the phenomenology of the Higgs sector if the mass of
 67 the lighter CP -odd light Higgs boson, m_{a_1} , satisfies the condition $m_{a_1} < \frac{1}{2}m_{h_{1,2}}$. The CP -even
 68 Higgs bosons $h_{1,2}$ can thus decay via $h_{1,2} \rightarrow 2a_1$, where one of the CP -even Higgs bosons is
 69 a SM-like Higgs boson that could correspond to the newly observed particle at the LHC with
 70 a mass near $125 \text{ GeV}/c^2$. The Higgs boson production cross section may differ substantially
 71 from that of the SM depending on the parameters of a specific model. The new light boson a_1
 72 couples weakly to SM particles with the coupling to fermions proportional to the fermion mass
 73 and can have a substantial branching fraction $\mathcal{B}(a_1 \rightarrow \mu^+ \mu^-)$ if its mass is within the range
 74 $2m_\mu < m_{a_1} < 2m_\tau$ [25, 26]. The Feynman diagram of the NMSSM process $h_{1,2} \rightarrow 2a_1 \rightarrow 4\mu$ is
 75 shown in Fig. 2.
- 76 For values of the NMSSM parameters that give the lightest CP -even Higgs (h_1) a large singlet
 77 field component, $h_1 \rightarrow a_1 a_1$ can be as large as 100%. If this is the case, then the strongest
 78 constraints on the NMSSM scenarios with light a_1 come from the most general LEP Higgs
 79 boson search that yields $m_h > 82 \text{ GeV}/c^2$ [27], independent of the Higgs boson decay. If $2m_\tau <$
 80 $m_{a_1} < 2m_b$, then the $\mathcal{B}(a \rightarrow 2\mu)$ is suppressed by a factor $(m_\mu^2/m_\tau^2) / [\sqrt{1 - (2m_\tau/m_{a_1})^2}]$, the
 81 a_1 decays primarily to $\tau^+ \tau^-$, and the limit from LEP becomes $m_h > 86 \text{ GeV}/c^2$ [28]. Searches at
 82 BaBar and CLEO for direct production of a_1 [29, 30] have little impact on the allowed parameter
 83 space because in the vast majority of the parameter space the coupling of the a_1 to SM particles
 84 is too weak to produce an excess of signal events. The DØ search [31] that employed the same
 85 signature as this analysis has only a moderate impact on the allowed parameter space due to
 86 low Higgs boson production cross section at the Tevatron as compared to the LHC. A previous

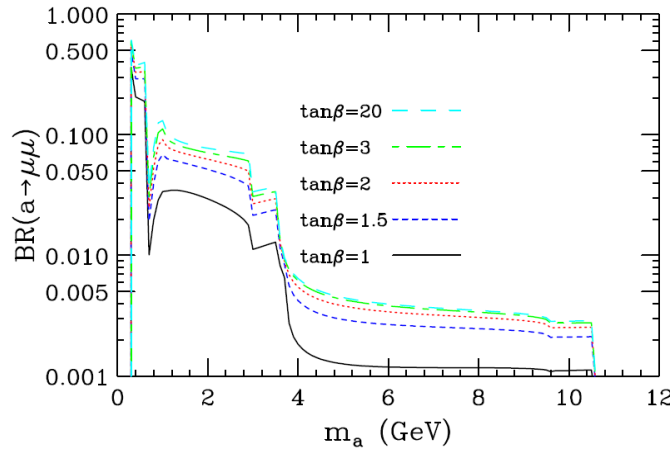


Figure 3: Branching fraction of light CP-odd Higgs boson $a_1 \rightarrow \mu\mu$ in the NMSSM scenario as a function of m_{a_1} for a variety of $\tan\beta$ values. Excerpt from [26].

87 CMS search that used 5.3 fb^{-1} of data at $\sqrt{s} = 7 \text{ TeV}$ [32] also set limits on this region of
 88 parameter space, but the analysis presented here has more sensitivity due to the larger center-
 89 of-mass energy and available integrated luminosity.

90 In this paper we follow the phenomenological studies published in [25, 26] and explore the
 91 scenario where h_1 and h_2 can decay via $h_{1,2} \rightarrow a_1 a_1$. There are no strong indications as to what
 92 the mass of a_1 should be, so very low masses are allowed. Because a_1 typically carries a large
 93 fraction of the NMSSM singlet field, the direct production $pp \rightarrow a_1$ is extremely suppressed.
 94 Helicity suppression causes the a_1 boson to decay to the heaviest pair of particles kinematically
 95 allowed [26, 33]. Below the $3m_\pi$ threshold, $\mathcal{B}(a_1 \rightarrow 2\mu)$ is expected to be close to 100% as
 96 hadronic decays are prohibited by spin and hadronization effects and $\mathcal{B}(a_1 \rightarrow \gamma\gamma)$ is small. If
 97 $2m_\mu < m_{a_1} < 2m_\tau$ then it has a substantial branching fraction (about 7.7% for $m_{a_1} \sim 2 \text{ GeV}/c^2$,
 98 see Fig. 3) for decays into muon pairs, and the $h_{1,2} \rightarrow a_1 a_1 \rightarrow 4\mu$ decay channel makes detection
 99 of a_1 in the muon channel viable at the LHC with the total integrated luminosity as of the end
 100 of Run II 2016.

101 Both the production rate for the CP-even Higgs bosons $h_{1,2}$ (via gluon fusion predominantly)
 102 as well as the branching fraction for $h_{1,2} \rightarrow a_1 a_1$ can vary significantly depending on the chosen
 103 NMSSM parameters (notably the singlet fraction of $h_{1,2}$). It is possible for either h_1 or h_2 to be
 104 almost completely decoupled from the gauge singlet, in which case that particle could acquire
 105 a non-negligible singlet component and decay to two a_1 bosons [25]. For the majority of the
 106 relevant parameter space one of the Higgs bosons $h_{1,2}$ is very similar to the predicted SM Higgs
 107 boson, with a production cross section negligibly different from the SM prediction and has a
 108 small branching fraction $\mathcal{B}(h_i \rightarrow 2a_1)$, while the other one has a suppressed cross section (due
 109 to the weak coupling to SM fermions and bosons) but a large branching fraction $\mathcal{B}(h_i \rightarrow 2a_1)$.
 110 There are three potential scenarios that are relevant to this analysis:

- 111 1. the lightest h_1 is a non-SM-like Higgs boson with $m_{h_1} < 125 \text{ GeV}/c^2$, reduced cross section
 112 and large $\mathcal{B}(h_1 \rightarrow 2a_1)$, and h_2 is the SM-like Higgs with negligible $\mathcal{B}(h_2 \rightarrow 2a_1)$, with
 113 respect to the sensitivity of this analysis
- 114 2. h_1 is the SM-like Higgs with SM cross section and negligible $\mathcal{B}(h_1 \rightarrow 2a_1)$, and h_2 is a
 115 heavier non-SM higgs boson with reduced cross section and large $\mathcal{B}(h_2 \rightarrow 2a_1)$, to which
 116 this analysis can be sensitive

117 3. the non-SM-like Higgs boson is either lighter or heavier than $125\text{ GeV}/c^2$, it has a large
 118 branching ratio but too small production cross section resulting in this analysis not being
 119 sensitive to it, in which case the sensitivity is driven by the decays of the SM-like Higgs
 120 into $2a$ (even if the branching ratio is small).

121 Typical production cross sections $\sigma(pp \rightarrow h_{1,2})$ can range from ~ 0.05 to $\sim 10\text{ pb}$ while
 122 $\mathcal{B}(h_{1,2} \rightarrow a_1 a_1)$ can be as high as 100% depending on the free parameters of the model. This is
 123 especially true for λ , the trilinear coupling between the singlet field S and the Higgs fields in
 124 the NMSSM superpotential.

125 In dark SUSY [34–36], $U(1)_D$ is broken, giving rise to light dark photons (γ_D) that weakly couple
 126 to the SM particles via a small kinetic mixing [37–39] with photons. The lightest neutralino
 127 n_1 in the *visible* (as opposed to *hidden*) part of the SUSY spectrum is no longer stable and can
 128 decay via processes such as $n_1 \rightarrow n_D + \gamma_D$, where n_D is a light dark fermion (dark neutralino)
 129 that escapes detection. In these models, the decays of the γ_D are often mediated by very weak
 130 interactions with the SM, and in much of the available parameter space they have long life-
 131 times. If dark SUSY is realised in nature the dark photon decays could occur promptly, some
 132 distance into the detector, or potentially even far outside of it.

133 In the simple benchmark model that we consider in this analysis, the SM-like Higgs boson
 134 can decay via $h \rightarrow 2n_1$, if $m_h > 2m_{n_1}$. The branching fraction $\mathcal{B}(h \rightarrow 2n_1)$ can vary from
 135 very small to large, bounded by the LHC measurements in the context of Higgs searches, since
 136 the bounds obtained at LEP can be circumvented [36]. The lack of an anti-proton excess in
 137 the measurements of the cosmic ray spectrum constrains the mass of γ_D to be $\leq 2m_p$ [40].
 138 Assuming that γ_D can only decay to SM particles the branching fraction $\mathcal{B}(\gamma_D \rightarrow \mu^+ \mu^-)$ can
 139 be as large as 45%, depending on m_{γ_D} [36]. If the coupling to SM particles is highly suppressed
 140 then the m_{γ_D} can also have a non-negligible lifetime and travel some distance prior to decaying.
 141 It is therefore important to accommodate the possibility of long-lived dark photons in searches.

142 The new hidden forces in Dark SUSY scenarios can couple to the SM hypercharge through a
 143 kinetic mixing term in Lagrangian:

$$L_{KM} \sim \frac{\epsilon}{2} F_{\mu\nu}^Y F^{D\mu\nu}, \quad (3)$$

144 where $F_{\mu\nu}^D = \partial_\mu A_\nu^D - \partial_\nu A_\mu^D$ and A^D is the dark gauge field [37–39]. If the A^D is massive then
 145 the SM particles acquire an additional charge ϵe under the dark interaction. Note that in typical
 146 Dark SUSY scenarios with kinetic mixing the parameter ϵ is within the range $10^{-8}\text{--}10^{-2}$.

147 It is shown in [41] that due to the kinetic mixing the dark photon will decay to SM leptons with
 148 a partial width given by:

$$\Gamma_{\gamma_D \rightarrow ll} = \frac{1}{3} \alpha \epsilon^2 m_{\gamma_D} \sqrt{1 - \frac{4m_l^2}{m_{\gamma_D}^2}} \left(1 + \frac{2m_l^2}{m_{\gamma_D}^2} \right), \quad (4)$$

149 where m_l is mass of the lepton and different decay modes start from $m_{\gamma_D} > 2m_l$. Also, the dark
 150 photon will decay to SM hadrons for masses $m_{\gamma_D} > 2m_\pi$, with partial width:

$$\Gamma_{\gamma_D \rightarrow \text{hadrons}} = \frac{1}{3} \alpha \epsilon^2 m_{\gamma_D} \sqrt{1 - \frac{4m_\mu^2}{m_{\gamma_D}^2}} \left(1 + \frac{2m_\mu^2}{m_{\gamma_D}^2} \right) R(s = m_{\gamma_D}^2), \quad (5)$$

where $R = \sigma_{e^+e^- \rightarrow \text{hadrons}} / \sigma_{e^+e^- \rightarrow \mu^+\mu^-}$. The hadronic cross section data is available in recent compilation of various experimental measurements [42] but it is measured only starting at $\sqrt{s} = 0.36 \text{ GeV}/c^2$ which is above $2m_\pi = 0.28 \text{ GeV}/c^2$ threshold. Therefore, in the region where $2m_\pi < \sqrt{s} < 0.36 \text{ GeV}/c^2$, we use the cross section for the $e^+e^- \rightarrow \pi^+\pi^-$ process evaluated using the technique presented in Ref. [43] and constants defined in Ref. [44]. Finally, for the region where $\sqrt{s} < 2m_\pi$, we sum only the lepton partial widths.

Table 1: Total width and $f(m_{\gamma_D})$.

	$m_{\gamma_D}, \text{ GeV}/c^2$								
	0.250	0.275	0.300	0.400	0.700	1.000	1.500	2.000	8.500
$\Gamma_{\gamma_D \text{Total}}/\epsilon^2 [\text{MeV}]$	1.0	1.2	1.9	2.1	11.4	8.0	15.5	20.3	114.6
$f(m_{\gamma_D}) [\text{GeV}^{-1}]$	952.9	817.2	538.9	480.2	87.4	125.1	64.6	49.2	8.7

According to expressions (4) and (5), the partial width's dependences on ϵ and m_{γ_D} are factorized, i.e. $(\Gamma_{\gamma_D}/\epsilon^2)^{-1} = f(m_{\gamma_D})$, where $f(m_{\gamma_D})$ is a function of the dark photon mass only. The partial widths for the different decay modes of the dark photon and its total width (all divided by ϵ^2 to demonstrate only the dependence of the widths on m_{γ_D}) are shown in Tab. 1 and Fig. 4 (top left). The branching ratio for the decay of the dark photon to a pair of muons $B_{\gamma_D \rightarrow \mu\mu} = \Gamma_{\gamma_D \rightarrow \mu\mu} / \Gamma_{\gamma_D \text{Total}}$ does not depend on ϵ due to the factorized dependence on the ϵ , as was noted above, and it is shown in Fig. 4 (right) as a function of m_{γ_D} . This branching ratio $B_{\gamma_D \rightarrow \mu\mu}$ has a minimum at $m_{\gamma_D} \sim 0.8 \text{ GeV}/c^2$, where dark photon decays to hadrons dominates.

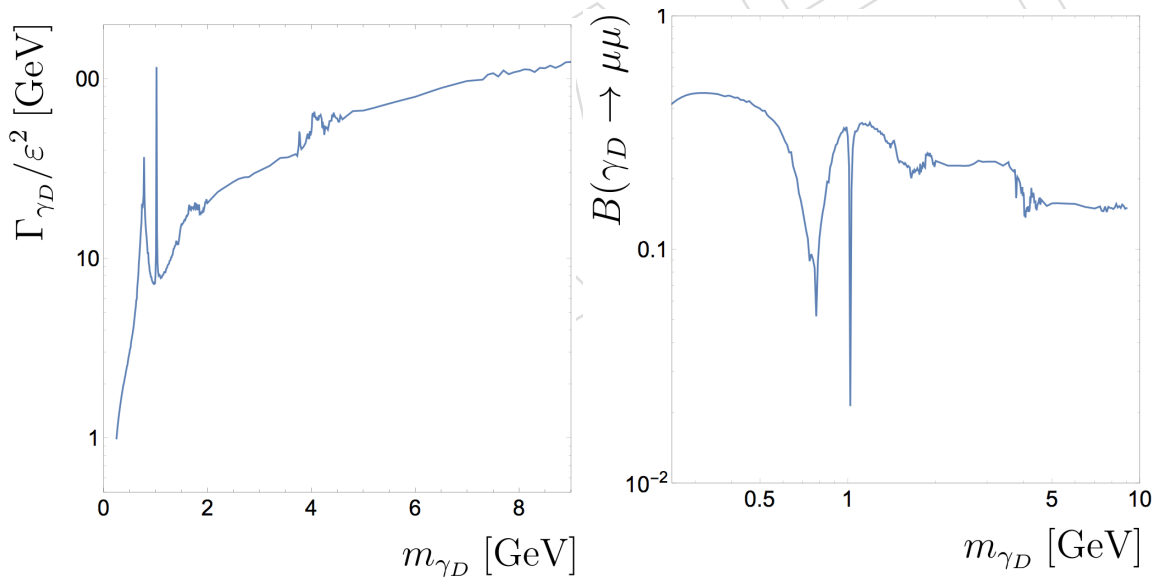


Figure 4: Left: Total width considering the different decay modes of the dark photon, normalized by ϵ^2 . Right: Branching ratio for $\gamma_D \rightarrow \mu\mu$ decay mode.

The expressions for the partial widths allow for the calculation of the lifetime of dark photon via:

$$\tau_{\gamma_D} = \frac{\hbar}{\Gamma_{\gamma_D \text{Total}}} = \frac{1}{\Gamma_{\gamma_D \rightarrow e^+e^-} + \Gamma_{\gamma_D \rightarrow \mu^+\mu^-} + \Gamma_{\gamma_D \rightarrow \text{hadrons}}} \quad (6)$$

The lifetime is directly related to the parameter ϵ and the mass of dark photon via:

$$\tau_{\gamma_D}(\epsilon, m_{\gamma_D}) = \frac{1}{\epsilon^2} \times f(m_{\gamma_D}), \quad (7)$$

168 It is convenient to represent the lifetime τ_{γ_D} as a distance $c\tau_{\gamma_D}$, where c is speed of light. It is
 169 also convenient to measure $c\tau_{\gamma_D}$ in millimeters because the sensitivity of the analysis to this
 170 variable is $\mathcal{O}(\text{mm})$. Including all unit-conversion coefficients, expression (7) becomes:

$$c\tau_{\gamma_D}(\epsilon, m_{\gamma_D})[\text{mm}] = \frac{c[\text{mm/s}] \times \hbar[\text{GeV} \cdot \text{s}]}{\epsilon^2} \times f(m_{\gamma_D})[\text{GeV}^{-1}], \quad (8)$$

171 or numerically:

$$c\tau_{\gamma_D}(\epsilon, m_{\gamma_D})[\text{mm}] = \frac{1.97 \cdot 10^{-13}[\text{GeV} \cdot \text{mm}]}{\epsilon^2} \times f(m_{\gamma_D})[\text{GeV}^{-1}], \quad (9)$$

172 where $c = 3 \cdot 10^8 \text{ m/s} = 3 \cdot 10^{11} \text{ mm/s}$ and $\hbar = 1.055 \cdot 10^{-34} \text{ J}\cdot\text{s} = 6.58 \cdot 10^{-25} \text{ GeV}\cdot\text{s}$.

173 The constraints on ϵ and the mass of dark photon could be obtained from the constraints on
 174 the lifetime of the dark photon because they are directly related to each other, as shown above.

175 The Feynman diagram of the dark SUSY process $h \rightarrow 2n_1 \rightarrow 2n_D + 2\gamma_D \rightarrow 2n_D + 4\mu$ is
 176 shown in Fig. 5. This benchmark model is only one possible scenario, and is chosen as a sin-
 177 gular representation of a very wide range of available parameter space. This simple model of
 178 the dark sector can be extended in a number of ways; more complex versions involve other
 179 dark Higgs, W, and Z bosons [45]. There are also many other allowed processes, such as
 180 $pp \rightarrow h \rightarrow Z_D Z/Z_D Z_D/Za \rightarrow 4\mu$, for example. In this analysis we present the results in a
 181 way that allows for further reinterpretations in the framework of other models.

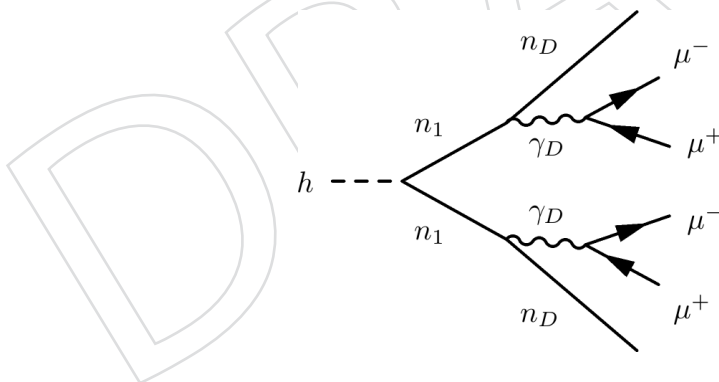


Figure 5: Feynman diagram of the dark SUSY benchmark process $h \rightarrow 2n_1 \rightarrow 2n_D + 2\gamma_D \rightarrow 2n_D + 4\mu$.

182 In the MSSM the Higgs boson can naturally have a substantial branching fraction to a pair of
 183 LSPs if the LSPs are predominantly binos (e.g. 90% bino and 10% higgsino), often much larger
 184 than to the SM channels. These scenarios are strongly constrained in the MSSM due to the
 185 limits from LEP on invisible Higgs boson decays. However, if the LSPs are no longer stable and
 186 decay into the hidden sector, becoming the lightest visible supersymmetric particles (LVSPs),
 187 these constraints are substantially weakened. There are large fractions of parameter space with
 188 a light LVSP (typically $m_{n_1} < 40 \text{ GeV}/c^2$) and large branching fraction of $h \rightarrow n_1 n_1$. Similarly,
 189 the branching fraction can be moderate or even small, which could lead to an experimental
 190 observation of the Higgs boson with only slightly reduced branching fractions in the channels

191 dominating the LHC sensitivity to the SM Higgs boson. Distinguishing between the SM Higgs
 192 boson and the Higgs boson in this scenario can only be done by exploring final states sensitive
 193 to these exotic Higgs boson decays.

194 Note that the same class of models predicts other Higgs boson decay channels that this anal-
 195 ysis is sensitive to. For example, if at least one of the sneutrinos is light, decays $h \rightarrow \tilde{\nu}\tilde{\nu}$ are
 196 possible with generally unconstrained branching fraction. The sneutrinos then can decay via
 197 $\tilde{\nu} \rightarrow \nu n_1 \rightarrow \nu n_D \gamma_D$ leading to the same signature. This scenario is viable if the sneutrino mass
 198 is above $\frac{m(Z)}{2}$ as otherwise it could have been detected in LEP Z width measurements.

199 As mentioned earlier, there is a connection between this analysis and a number of other searches
 200 for evidence of a dark sector, under the assumption that the dark photons couple via the
 201 Higgs sector. Low energy e^+e^- colliders and fixed target experiments, including APEX [46],
 202 BaBar [47, 48], HADES [49] and KLOE [50, 51] (among others) have performed complementary
 203 searches. These experiments search for slightly different topologies, such as the associated pro-
 204 duction of a dark photon and a photon, with the dark photon then decaying into SM fermions.
 205 This type of dark photon production could be detected as a narrow resonance in radiative
 206 $e^+e^- \rightarrow \gamma \ell^+ \ell^- (\ell = e, \mu)$ events, and low energy e^+e^- colliders provide a clean environment
 207 in which to perform these searches. However, these searches involve two suppressed vertices
 208 and therefore scale with ϵ^4 (rather than ϵ^2 as in the analysis described in this note), preventing
 209 the low energy experiments probing very small values of ϵ . The status of the current exper-
 210 imental constraints is reviewed in [52], and current experimental exclusion limits in the 2D
 211 plane of ϵ^2 and m_{γ_D} , excerpted from [53], is shown in Fig. 6.

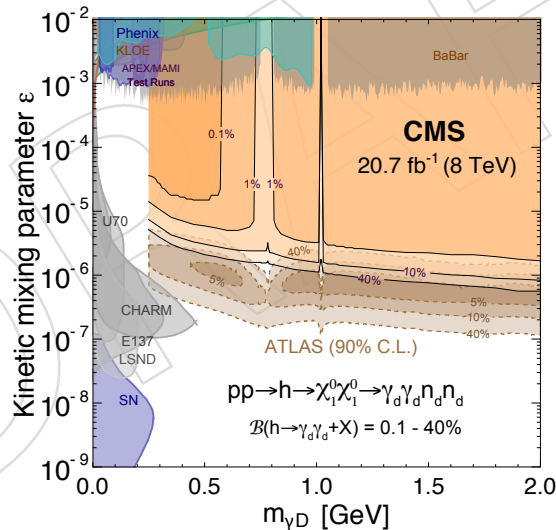


Figure 6: Experimental constraints in the plane of two parameters for the Dark SUSY scenarios:
 ϵ and m_{γ_D} (figure from [54]).

212 Previous searches for the pair production of new light bosons decaying into dimuons have
 213 been performed at the Tevatron with 4.2 fb^{-1} data sample [31] at $\sqrt{s} = 1.96 \text{ TeV}$ and more
 214 recently at the LHC with 35 pb^{-1} [55, 56] (7 TeV), 1.9 fb^{-1} [57] (7 TeV), 5.3 fb^{-1} [32, 58] (7 TeV),
 215 20.3 fb^{-1} [53] (8 TeV), and 20.7 fb^{-1} [54] (8 TeV). The two latest results, from ATLAS and CMS
 216 respectively, consider models in which the γ_D can be long-lived.

217 Associated production of the light CP -odd scalar bosons has been sought at e^+e^- colliders as
 218 in the case of BaBar [29, 30] and BESIII [59, 60] experiments, also at the Tevatron [61]. Direct

²¹⁹ production of the a_1 has been studied at the LHC [62], but in the framework of NMSSM the
²²⁰ sensitivity of these searches is limited by the very weak coupling of the a_1 to SM particles. The
²²¹ most stringent limits on the Higgs sector of the NMSSM are provided by the WMAP data [63]
²²² and LEP searches [27, 28, 64] ($m_{h_1} > 86 \text{ GeV}/c^2$). In the framework of dark SUSY experimental
²²³ searches for γ_D have focused on the production of dark photons at the end of SUSY cascades
²²⁴ at the Tevatron [65–67] and at the LHC [56].

²²⁵ This analysis is based on a data sample corresponding to an integrated luminosity of 35.9 fb^{-1}
²²⁶ of proton-proton collisions at $\sqrt{s} = 13 \text{ TeV}$ collected by the CMS detector during the 2016 data
²²⁷ taking campaign during Run II.

DRAFT

2 Analysis Strategy

The general search strategy is to select events with two distinct muon pairs. Each muon pair must be consistent with having originated from the decay of a light resonance. Muons of opposite charge are paired if:

- each muon has $p_T > 8 \text{ GeV}/c$
- the pair has sufficiently low invariant mass ($m_{\mu\mu} < 9 \text{ GeV}/c^2$)
- the trajectories of the two muon are consistent with originating from the same vertex.

The integrated luminosity of the data used in this analysis is 35.9 fb^{-1} ; the data are collected using a trimuon trigger requiring at least one muon candidate with $p_T > 15 \text{ GeV}/c$ and at least two others with $p_T > 5 \text{ GeV}/c$. Each event is then required to contain exactly two muon pairs with no restriction on additional unpaired muon candidates; such muons are referred to as “orphans”. The impact of orphan muons is discussed further in section 4.3. The main SM background contributions to the selected topology are $b\bar{b}$, the electroweak production of 4μ , and prompt double J/ψ production. In $b\bar{b}$, production muon pairs are produced via either semileptonic decays or from decays of light resonances. The contribution of other SM processes has been found to be negligible, e.g. low mass Drell-Yan production is heavily suppressed by the requirement of additional muons, and $\text{pp} \rightarrow Z/\gamma^* \rightarrow 4\mu$ production is suppressed by the requirement of small and mutually consistent masses of the dimuons. In double J/ψ production, muons are produced via the decay $J/\psi \rightarrow \mu^+ \mu^-$, and this background is relevant in the region where $m_{\mu\mu_1} \sim m_{\mu\mu_2} \sim m(J/\psi)$. A requirement that the muon pair candidates are isolated suppresses the $b\bar{b}$ contribution, resulting in an almost zero background final state. The isolation requirement relies only on the charged tracks and is sufficiently loose to ensure that the efficiency of this selection for signal-like topologies is nearly completely insensitive to systematic effects owing to overlapping interactions per bunch crossing, as well as effects of initial and final state radiation. To ensure that the analysis has high and well-understood trigger and reconstruction efficiencies, each dimuon is required to have been produced in the region bounded by the third pixel layer in the barrel and the second pixel layer in the endcap.

The reconstructed invariant masses of the boosted dimuons which originate from the new light boson decay is a narrow peak around m_a . Fig. 7 (left) shows an example dimuon mass distribution for NMSSM production of a_1 with $m_{a_1} = 2 \text{ GeV}/c^2$. At the final stage of the analysis the two dimuons are required to have invariant masses consistent within the detector resolution. This is because, in signal events both pairs of dimuons are produced from decays of particles with the same mass. The signal, if observed, will be somewhere on the diagonal of a 2D invariant mass plot of the dimuons as illustrated in Fig. 7 (right) for the same NMSSM example with $m_{a_1} = 2 \text{ GeV}/c^2$. Background events from $b\bar{b}$ do not have such an intrinsic correlation as decays of each b-quark are uncorrelated, as is shown in Fig. 7 (right) as the intensity of the shading. The backgrounds will be distributed across the entire 2D space. Known resonances may form enhancements near the diagonal, but those will also appear as vertical or horizontal lines of enhancements in events that have only one of the dimuons coming from a resonance. This effect constrains the size of the corresponding enhancement on the diagonal. We therefore analyze the 2D distribution of dimuon masses and search for an enhancement near the diagonal, while the background rate is extrapolated from the off-diagonal regions of the distribution. The signal region in the 2D space of dimuon invariant masses m_1 and m_2 is defined as a “corridor” near the diagonal: $|m_1 - m_2| < 0.13 + 0.065(m_1 + m_2)/2$, with the width corresponding to at least 5σ in detector resolution (see Sec. 5).

A fit is performed in the signal region, while the normalization for background is determined

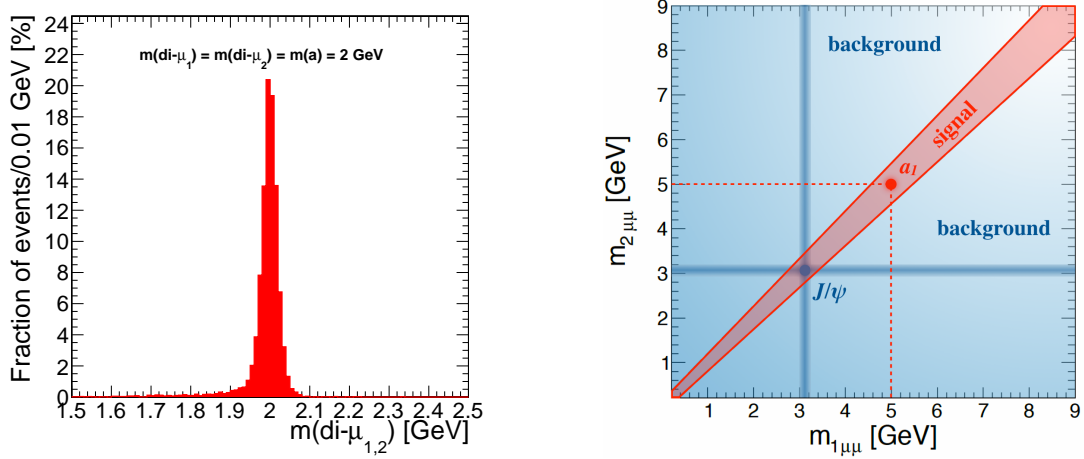


Figure 7: Left: the distribution of the invariant mass of the dimuons is a sharp peak centered at the mass of the new light boson ($m_a = 2 \text{ GeV}/c^2$ in this example). Right: schematic of a two-dimensional search for a signal in the events with pairs of dimuons. The signal, if observed, will appear as a peak somewhere on the diagonal corridor ($m_a = 5 \text{ GeV}/c^2$ in this example) while the background events will have a distribution spread across the entire 2D space. Known resonances (J/ψ is shown as an example) may form an enhancement near the diagonal, but those will also appear as vertical or horizontal enhancements in events that only have one of the dimuons coming from such resonances.

274 from a fit in the side-band (off-diagonal) region. The posterior for the signal normalization
 275 is used to either discover or set limits on the production rate of a non-SM Higgs boson. The
 276 analysis of this 2D spectra is performed using a binned likelihood fit where the signal shape
 277 is modeled using a Crystal Ball function and background shape is determined from properly
 278 defined background-enriched samples.

279 3 Samples

280 In this section we describe the details of the data and Monte Carlo (MC) samples used in the
 281 analysis.

282 **3.1 Data Samples**

283 The analysis is based on the full 25 ns data sample recorded in 2016 by the CMS detector in
 284 pp collisions at center-of-mass energy $\sqrt{s} = 13$ TeV at $B = 3.8T$. The analysis data sample
 285 includes only runs¹ where the LHC was providing stable beams, where the CMS silicon tracker,
 286 muon system and trigger were performing well, and where the luminosity was measured. This
 287 data corresponds to a total integrated luminosity of 35.9 ± 0.9 fb⁻¹. The signal search was
 288 performed in events stored in DoubleMuon primary data set (PD) based on
 289 HLT_TrkMu15_DoubleTrkMu5NoFiltersNoVtx trigger (See Sec. 4). Details on the dataset used
 290 can be found in appendix A.

291 **3.2 Simulated Samples for Signal**

292 Simulated signal MC events are fully reconstructed with the CMS software and used to opti-
 293 mize the selection criteria, to check the agreement with data, to calculate acceptances, to obtain
 294 corrections to the efficiencies, and to evaluate some of the systematic uncertainties. Two signal
 295 benchmark scenarios (NMSSM and dark SUSY) are simulated for the analysis (see motivation
 296 in Sec. 1). As the widths of all decaying particles in the benchmark scenarios are expected to be
 297 very narrow (so called *narrow width approximation*) the detector resolution is dominant and no
 298 precise calculation of the widths is required. Further, calculation of the cross sections for gen-
 299 erated events is not required, as we set a 95% confidence level (CL) upper limit on the number
 300 of signal events.

301 All benchmark samples are generated using the leading-order NNPDF2.3LO [68] set of parton
 302 distribution functions (PDF). The dark SUSY samples are interfaced with PYTHIA 8.205 while
 303 the NMSSM samples use PYTHIA 8.212 using the Monash tune [69] for “underlying event” (UE)
 304 activity at the LHC and to simulate jet fragmentation, when applicable. The generated events
 305 are hadronized with PYTHIA and then they are passed through the GEANT4-based detector
 306 simulation and processed with the CMSSW_8_0_X release of the CMS software. Also all MC
 307 samples contain a valid simulation of the pileup effects on the number of primary vertexes cor-
 308 responding to the real pileup present in the data sample used in the analysis. The MC samples
 309 are then fully reconstructed using CMSSW_8_0_X.

310 **Higgs production.** NMSSM and dark SUSY MC samples in this analysis are generated using
 311 only the dominant channel for SM-like Higgs boson production at LHC: gluon-gluon fusion
 312 pp → H. The Feynman diagram for the channel is shown in Fig. 8 (left). The contribution
 313 from other channels for SM-like Higgs boson production (vector-boson fusion pp → qq+H;
 314 association with vector boson pp → W/Z+H; association with top quark pair pp → t̄t +
 315 H) are neglected. For illustration, the cross sections for all channels for SM-like Higgs boson
 316 production are shown in Fig. 8 (right). More details on the calculation of the Higgs boson
 317 production cross sections can be found in Ref. [70].

318 **NMSSM scenario.** The MC samples for the NMSSM benchmark scenario are simulated using
 319 PYTHIA 8.212 event generator [71]. In the analysis the production of NMSSM Higgs boson $h_{1,2}$
 320 was simulated which was forced to decay into the pair of NMSSM CP-odd Higgs bosons a_1
 321 with all other decay modes switched off. And finally, both a_1 ’s are forced to decay into the pair

¹The run list: Cert_271036284044_13TeV_23Sep2016ReReco_Collisions16_JSON.txt

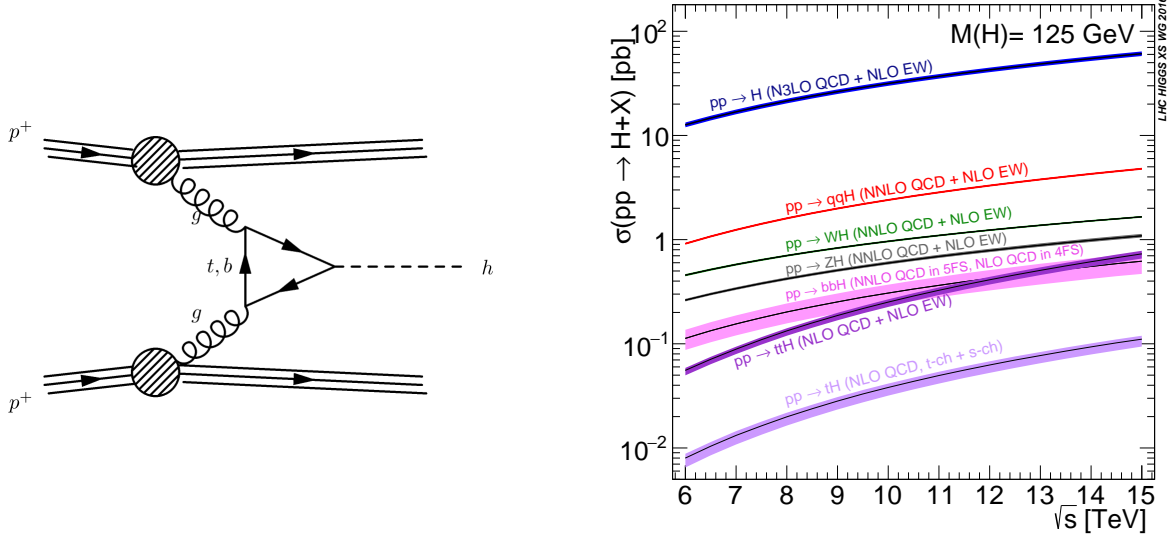


Figure 8: Left: Feynman diagram of the dominant SM Higgs boson production process (gluon-gluon fusion) in pp collisions at $\sqrt{s} = 13$ TeV. Right: Cross sections of all leading-order SM Higgs boson production processes in pp collisions at $\sqrt{s} = 13$ TeV versus Higgs boson mass. Figure reproduced from Ref. [70]

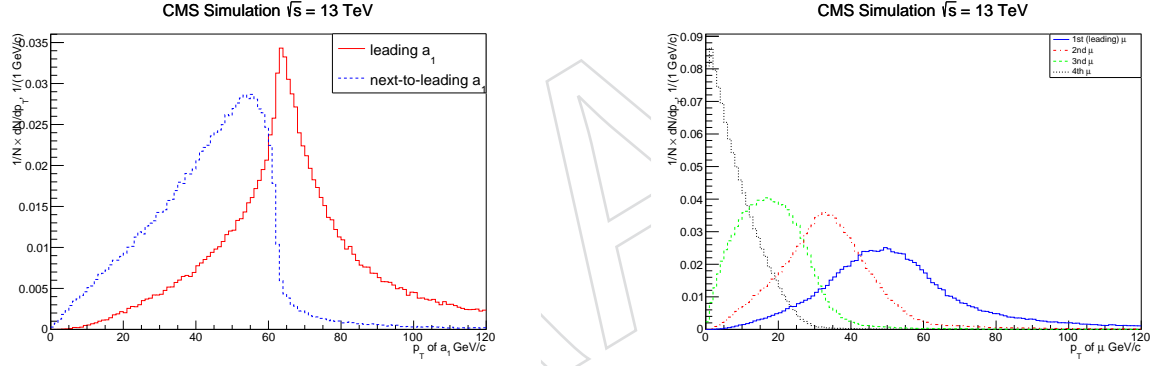


Figure 9: Left: Distributions of the transverse momentum of CP-odd Higgs bosons a_1 (leading and next-to-leading) in NMSSM scenario with $m_{h_{1,2}} = 125$ GeV/ c^2 and $m_{a_1} = 2$ GeV/ c^2 . Right: Distributions of the transverse momentum of muons (ordered in p_T) that originate from decays of a_1 in the same NMSSM scenario with $m_{h_{1,2}} = 125$ GeV/ c^2 and $m_{a_1} = 2$ GeV/ c^2 .

322 of muons with 100% branching fraction. Several NMSSM samples with different masses of
323 the $h_{1,2}$ and a_1 were produced to scan the NMSSM parameter space as summarized in Tab. 13.
324 Figure 9 shows the transverse momentum distributions of the light bosons and the muons a
325 representative NMSSM sample.

326 **Dark-SUSY scenario.** To quantify the sensitivity of this analysis we use several dark SUSY
327 benchmark models. The specific scenario we use considers Higgs boson decay via $h \rightarrow n_1 n_1$
328 (where h is the SM-like Higgs discovered at the LHC) followed by decays of the LVSPs into the
329 hidden sector via $n_1 \rightarrow n_D \gamma_D$ [35, 36]. The γ_D can also be long lived, traversing some region
330 of the detector prior to decaying. This corresponds to approximately the simplest realization
331 of such models as there could be a wider variety of decays if the hidden dark sector is more
332 complex (it can include a whole hierarchy of light dark Higgs bosons, h_D , leading to a large

Table 2: The NMSSM MC samples used in the analysis.

$m_{h_{1,2}}, \text{GeV}/c^2$	$m_{a_1}, \text{GeV}/c^2$	Number of events
90	0.50	200,000
90	0.75	196,949
90	1.00	194,299
90	2.00	199,598
90	3.00	199,351
90	3.55	199,360
100	0.75	200,000
100	1.00	200,000
100	2.00	200,000
100	3.00	198,826
100	3.55	200,000
110	0.50	199,400
110	0.75	200,000
110	1.00	197,892
110	2.00	200,000
110	3.00	200,000
110	3.55	200,000
125	0.50	192,848
125	0.75	200,000
125	1.00	196,985
125	2.00	190,593
125	3.00	199,015
125	3.55	200,000
150	0.50	200,000
150	0.75	200,000
150	1.00	197,874
150	2.00	195,495
150	3.00	199,004
150	3.55	190,704

variety of possible cascade decays). Note that stable dark fermions n_D escape detection giving rise to measurable missing transverse energy in these events. We do not place requirements on the missing transverse energy in this analysis since the final signature already has a small SM background. Further, by avoiding a cut on the missing transverse energy the analysis remains model independent. This is important given that the benchmark models used in this analysis provide only a representation of the large available parameter space and the results need to be interpretable in a range of different models.

The specific benchmark model used to illustrate the power of this search uses an LVSP mass of $m_{n_1} = 10 \text{ GeV}/c^2$, a dark fermion mass of $m_{n_D} = 1 \text{ GeV}/c^2$, and a dark photon mass in the range $m_{\gamma_D} = 0.25 - 8.5 \text{ GeV}/c^2$, with a proper lifetime ($c\tau$) between 0 and 100 mm. The $\mathcal{B}(\gamma_D \rightarrow \mu\mu)$ for dark photons as a function of $m(\gamma_D)$ is shown in Fig. 10. To simulate $pp \rightarrow h \rightarrow n_1 n_1 \rightarrow n_D \gamma_D n_D \gamma_D$ events, we use MADGRAPH 4.5.2 [72] where the Higgs boson is produced via gluon fusion, dark photons are then forced to decay via $\gamma_D \rightarrow \mu\mu$ 100% of the time. The LHE format events are then processed using PYTHIA 8.205 for hadronization and then standard CMS simulation, including trigger emulation, and reconstruction procedures are applied. The reconstructed events are used to evaluate the acceptance for these kinds of signatures. The results of the analysis are quantified in terms of its sensitivity to measuring or excluding $\sigma(pp \rightarrow h) \times \mathcal{B}(h \rightarrow n_1 n_1)$ so the exact value of the cross section used for $pp \rightarrow h$ is unimportant. For illustrative purposes, we will use the SM Higgs boson cross section when needed in order to keep things simple. This is a safe assumption in this scenario as h is taken to be the SM-like Higgs and current LHC results are consistent with the predicted SM cross

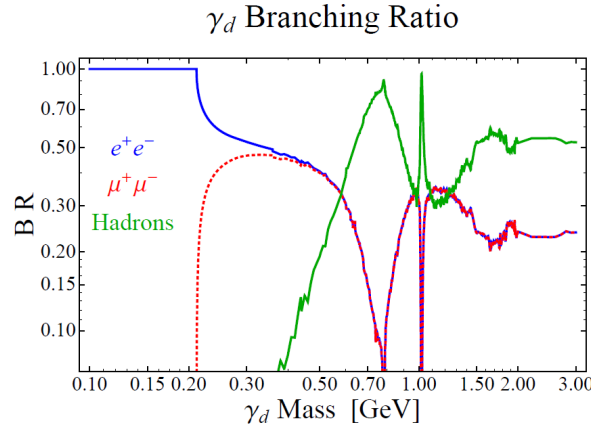


Figure 10: Branching fraction of light dark photon to pairs of electrons, muons, and hadrons through the electromagnetic current in dark SUSY scenario as a function of m_{γ_D} . Excerpt from [36].

354 section.

355 The MC samples for the dark SUSY benchmark scenario are simulated using the MADGRAPH
 356 event generator. Initially gluon-gluon fusion of SM Higgs boson h_{SM} was simulated (using
 357 HEFT model within Madgraph with QCD= 99, QED= 0 and HIG= 1 input process parameters). Then custom extension for SM was created, namely 4 new particles were introduced:

- 359 • n_1 – neutralino, lightest SUSY particle from visible sector (LSP)
- 360 • n_D – dark neutralino
- 361 • γ_D – dark photon
- 362 • μ_1 – custom muon with mass set to $m = 105.66 \text{ MeV}/c^2$

363 Note, the custom muon (μ_1) was required because in MADGRAPH the default mass of SM muon
 364 is set $0 \text{ MeV}/c^2$. Three additional vertexes were introduced into the custom model:

- 365 • $h_{SM} \rightarrow n_1 n_1$
- 366 • $n_1 \rightarrow n_D \gamma_D$

367 The couplings for all three vertexes were reset from default value (which is 1) to a small
 368 value (which is 10^{-3}) that corresponds to *narrow width approximation* for all decaying custom
 369 particles. Then the BRIDGE software package [73] was used to calculate all widths and branch-
 370 ing ratios and to decay SM Higgs bosons in initially generated events.

371 We simulated several dark SUSY samples with fixed masses of Higgs boson, lightest SUSY
 372 neutralino, and dark neutralino, corresponding to $m_h = 125 \text{ GeV}/c^2$, $m_{n_1} = 10 \text{ GeV}/c^2$, $m_{n_D} =$
 373 $1 \text{ GeV}/c^2$ respectively and various masses of dark photon in the range $0.25 \text{ GeV}/c^2 \leq m_{\gamma_D} \leq$
 374 $8.5 \text{ GeV}/c^2$ to scan the parameter space, as summarized in Tab. 16 and Appendix A. Figure 11
 375 shows the transverse momentum distributions of the light bosons and the muons in a repre-
 376 sentative dark SUSY sample. Figure 11 shows the transverse momentum distributions of the
 377 SUSY neutralino and dark neutralino in a representative dark SUSY sample.

378 Tables with names of all MC samples (as published in the CMS DAS) used in the analysis can
 379 be found in Appendix A.

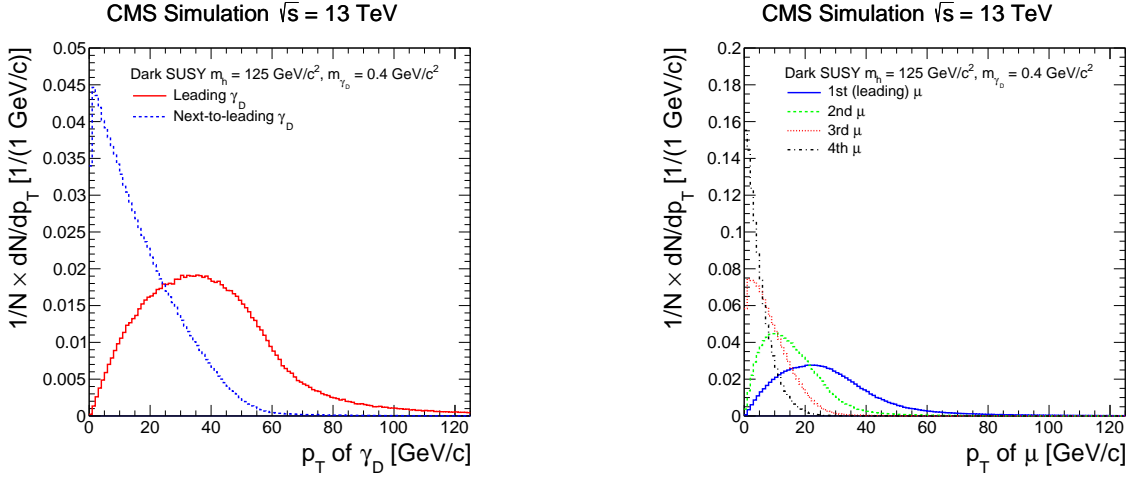


Figure 11: Left: Distributions of the transverse momentum of dark photon γ_D (leading and next-to-leading) in dark SUSY scenario with $m_h = 125 \text{ GeV}/c^2$, $m_{n_1} = 10 \text{ GeV}/c^2$, $m_{n_D} = 1 \text{ GeV}/c^2$ and $m_{\gamma_D} = 0.4 \text{ GeV}/c^2$. Right: Distributions of the transverse momentum of muons (ordered in p_T) that originate from decays of γ_D in the same dark SUSY scenario with $m_h = 125 \text{ GeV}/c^2$, $m_{n_1} = 10 \text{ GeV}/c^2$, $m_{n_D} = 1 \text{ GeV}/c^2$ and $m_{\gamma_D} = 0.4 \text{ GeV}/c^2$.

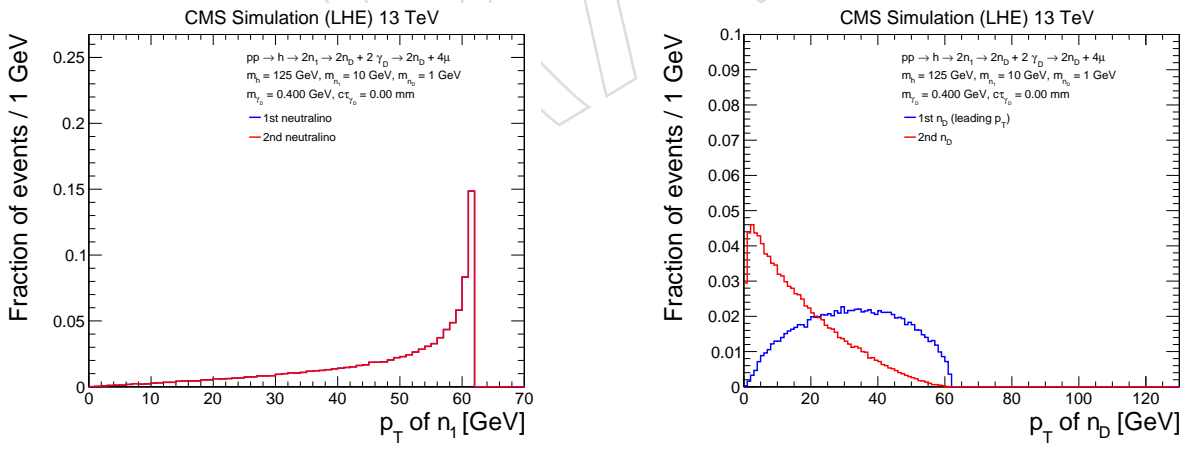


Figure 12: Left: Distributions of the transverse momentum of the SUSY neutralino n_1 in dark SUSY scenario with $m_h = 125 \text{ GeV}/c^2, m_{n_1} = 10 \text{ GeV}/c^2, m_{n_D} = 1 \text{ GeV}/c^2$ and $m_{\gamma_D} = 0.4 \text{ GeV}/c^2$. Right: Distributions of the transverse momentum of the dark neutralino (ordered in p_T) that originate from decays of n_1 in the same dark SUSY scenario with $m_h = 125 \text{ GeV}/c^2, m_{n_1} = 10 \text{ GeV}/c^2, m_{n_D} = 1 \text{ GeV}/c^2$ and $m_{\gamma_D} = 0.4 \text{ GeV}/c^2$.

Table 3: The dark SUSY MC samples used in the analysis

$m_h, \text{GeV}/c^2$	$m_{h_1}, \text{GeV}/c^2$	$m_{n_D}, \text{GeV}/c^2$	$m_{\gamma_D}, \text{GeV}/c^2$	$c\tau(\gamma_D), \text{mm}$
125	10	1	0.25	0
125	10	1	0.25	0.05
125	10	1	0.25	0.1
125	10	1	0.25	0.5
125	10	1	0.25	1
125	10	1	0.25	2
125	10	1	0.25	5
125	10	1	0.25	20
125	10	1	0.25	100
125	10	1	0.4	0
125	10	1	0.4	0.5
125	10	1	0.4	1
125	10	1	0.4	2
125	10	1	0.4	5
125	10	1	0.4	20
125	10	1	0.4	100
125	10	1	0.7	0
125	10	1	0.7	0.5
125	10	1	0.7	1
125	10	1	0.7	20
125	10	1	0.7	100
125	10	1	1	0
125	10	1	1	5
125	10	1	1	20
125	10	1	1	100
125	10	1	5	0
125	10	1	5	20
125	10	1	5	100
125	10	1	8.5	0
125	10	1	8.5	2
125	10	1	8.5	20
125	10	1	8.5	100

380 4 Analysis Selections and Efficiencies

381 In this section we describe the details of the muon selection, event selection and trigger choice.
 382 We also review algorithms used to evaluate selection efficiencies in data and simulated sam-
 383 ples. The scale factor correcting for experimental effects not accounted for by the simulation is
 384 also derived.

385 4.1 Trigger

386 4.1.1 Design considerations

387 Several aspects of the signal topology were taken into account in the selecting a good trigger
 388 for this analysis: (1) multiple close-by muons degrade the L1-trigger efficiency, (2) muon tracks
 389 from dark photon decays do not perfectly point back to the beamspot and may not have the
 390 same vertex z position with increasing mass or increasing life-time, (3) the muon p_T thresholds
 391 should be kept low as the acceptance falls fast for leading muon p_T above 15 – 20 GeV, and
 392 (4) isolation cannot be applied reliably per muon; the other muon has to be reconstructed and
 393 excluded from the track list. In addition, the trigger should be unprescaled: it accepts all events
 394 to maintain maximum sensitivity.

395 In previous iterations of this analysis the data were collected with the unprescaled, inclusive,
 396 non-isolated double muon trigger `HLT_Double_Mu17_Mu8`, that requires the presence of two
 397 muons with $p_T \geq 17$ GeV and $p_T \geq 8$ GeV in the event. While this trigger was suitable during
 398 Run-1. Prior to the start of Run-2 `HLT_Double_Mu17_Mu8` was replaced with a set of triggers,
 399 each of which would affect the model independence of t after all selection cuts are shown in
 400 the analysis.

401 It was found that the Run-2 trigger menu did not include a suitable double muon trigger that
 402 satisfied the criteria listed above. The available triggers (1) required ≥ 3 L1T muons, (2) placed
 403 cuts on the impact parameter d_{xy} or the longitudinal distance of the muon vertex to the IP d_z ,
 404 (3) significantly increased the offline p_T cuts affecting the acceptance, (4) applied track-based
 405 isolation on the muons or (5) were pre-scaled for Run-2 data taking so they would not take too
 406 much data.

407 In addition, new muon reconstruction algorithms optimized for displacement were imple-
 408 mented during LS1. These algorithms (labeled as “NoVtx”) allowed the implementation of
 409 triggers for displaced muons. However, a trigger with two displaced muons with $p_T \geq 17$ GeV
 410 and $p_T \geq 8$ GeV would have to be pre-scaled. Therefore, an additional muon would be needed
 411 to keep the trigger rate low. However, since the addition of an extra muon at the L1T step
 412 would violate criterium (1), the third muon would have to be inserted at a later stage in the
 413 trigger. It was decided to first reconstruct two displaced global muons and then use them as
 414 seeds for the displaced tracker muon reconstruction. With the requirement of three displaced
 415 tracker muons the trigger would satisfy criteria (1-4), would have sufficiently low trigger rate
 416 and high trigger efficiency.

417 4.1.2 Implementation

418 Two inclusive non-isolated triple muon triggers were implemented in the menu, a signal trig-
 419 ger `HLT_TrkMu15_DoubleTrkMu5NoFiltersNoVtx` and a backup trigger `HLT_TrkMu17_`
 420 `DoubleTrkMu8NoFiltersNoVtx`. Both require 2 L1 muons with $p_T > 12$ and $p_T > 5$ GeV
 421 (`L1_DoubleMu_12_5`) or $p_T > 10$ and $p_T > 3.5$ GeV (`L1_DoubleMu_11_3p5`). Next, Global
 422 muons are reconstructed from the L1 seeds using dedicated algorithm for non-pointing muons.
 423 Two muons are required with $p_T > 15$ and $p_T > 5$ GeV (or $p_T > 17$ and $p_T > 8$ GeV for the

424 backup trigger). Finally, three Tracker muons are reconstructed, again using a dedicated algo-
425 rithm for non-pointing muons. Two muons are required with $p_T > 5$ GeV and 1 muon with
426 $p_T > 15$ GeV. The backup trigger requires two muons with $p_T > 8$ GeV and 1 muon with
427 $p_T > 17$ GeV.

428 During the 2016 data taking period, the transverse momentum cuts on the muons in the L1T
429 paths were modified two times to handle the increasing LHC instantaneous luminosity. The
430 seed L1_DoubleMu_10_3p5 was replaced by L1_DoubleMu_11_4 soon after the start of data
431 taking. L1_DoubleMu_12_6 was added later as backup trigger in the later stages of data taking.
432 Tab. 4 lists the L1T and HLT versions used to take LHC data in their respective run ranges.

Table 4: List of triggers used to collect LHC data. All triggers were unprescaled during the entire 2016 data taking period.

L1T version	HLT version	Run range
L1_DoubleMu_10_3p5 OR L1_DoubleMu_12_5	HLT_TrkMu15_DoubleTrkMu5NoFiltersNoVtx_v2	272760 - 274443
L1_DoubleMu_11_4 OR L1_DoubleMu_12_5	HLT_TrkMu15_DoubleTrkMu5NoFiltersNoVtx_v3 HLT_TrkMu15_DoubleTrkMu5NoFiltersNoVtx_v4	274954 - 276244 276282 - 280385
L1_DoubleMu_11_4 OR L1_DoubleMu_12_5 OR L1_DoubleMu_13_6	HLT_TrkMu15_DoubleTrkMu5NoFiltersNoVtx_v6	281613 - 284044

433 4.1.3 Trigger efficiency and scale factor

434 There is a previously well understood feature (see details in Ref. [55]) of muon triggering in the
435 forward region, which leads to a diminished efficiency of reconstructing at least two muons
436 when there are two or more muons nearby. In this analysis, the situation is not as severe as
437 there are always at least four muons per event, but there is still a substantial loss in efficiency for
438 events with no offline muon of $p_T > 17$ GeV present in the barrel. This observation is illustrated
439 in Fig. 13. It shows the efficiency that a dark SUSY event, having at least four reconstructed
440 offline muons with $p_T > 8$ GeV of which one has to have $p_T > 17$ GeV, was triggered versus η of
441 the leading muon. The diminished trigger efficiency in the endcap region is model dependent,
442 e.g. it depends on the mass of a_1 . To minimize the model dependency of the results, we require
443 that there is at least one offline muon with $p_T > 17$ GeV and $|\eta| < 0.9$ in the offline selections.
444 The trigger fiducial requirement leads to a signal acceptance loss of about 20%. Once this
445 requirement is applied, the efficiency per event becomes high and independent of η .

446 The true trigger efficiency of HLT_TrkMu15_DoubleTrkMu5NoFiltersNoVtx on Monte Carlo
447 and real data was estimated using the orthogonal method. In the orthogonal method we rely
448 on a set of events that are contained in a data set other than the DoubleMuon data set. In this
449 study we selected events in data and Monte Carlo with large MET. Tab. 5 shows the used MET
450 data samples. Events were required to pass at least one of the trigger paths in Tab. 6.

451 For the Monte Carlo, we used the datasets in Tab. 7. We considered contributions from multi-
452 boson channels (such as WZ and ZZ), possibly in association with a top quark pair, decaying
453 to multiple leptons (electrons and/or muons). Drell-Yan might produce multiple leptons, but
454 has a negligible missing transverse energy, and thus was not taken into account.

455 Monte Carlo events were also required to pass at least one of the triggers in Tab. 6. To estimate
456 the trigger efficiency, the Monte Carlo and real data sample are cleaned by applying selections
457 on the muons in order to obtain a set of well-reconstructed WZ events. These selections are
458 derived from Ref. [74]. Exactly three reconstructed muons are required, with $|\eta| < 2.4$. Two
459 have the same charge and one has opposite charge (+ + – or – – +). The muons from heavy

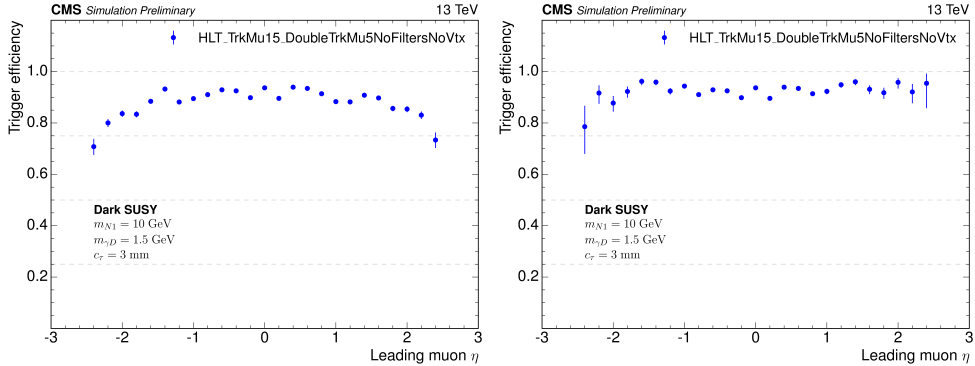


Figure 13: The per event trigger efficiency of the signal path HLT_TrkMu15_DoubleTrkMu5NoFiltersNoVtx measured in dark SUSY Monte Carlo versus η of the muon with leading p_T for different selections. Left: at least four muons with $p_T > 8 \text{ GeV}$ within $|\eta| < 2.4$. Right: at least four muons with $p_T > 8 \text{ GeV}$ within $|\eta| < 2.4$ of which one has $p_T > 17 \text{ GeV}$ within $|\eta| < 0.9$.

Table 5: Used data samples from the MET Primary dataset in AOD format

Dataset name	Run range	Disk size	Number of events
/MET/Run2016B-07Aug17_ver1-v1/AOD	272760-273017	106.1 GB	583,427
/MET/Run2016B-07Aug17_ver2-v1/AOD	273150-275376	6.9 TB	35,987,712
/MET/Run2016C-07Aug17-v1/AOD	275656-276283	3.9 TB	17,381,222
/MET/Run2016D-07Aug17-v1/AOD	276315-276811	4.8 TB	20,947,429
/MET/Run2016E-07Aug17-v1/AOD	276831-277420	5.8 TB	22,348,402
/MET/Run2016F-07Aug17-v1/AOD	277932-278808	3.5 TB	13,319,829
/MET/Run2016G-07Aug17-v1/AOD	278820-280385	7.3 TB	26,974,131
/MET/Run2016H-07Aug17-v1/AOD	284036-284068	302.0 GB	1,129,511
Total	272760-284068		

460 boson decay are required to be prompt, i.e. $d_{xy} < 0.01 \text{ cm}$ and $d_z < 0.1 \text{ cm}$. In addition, the
461 muons must pass the tight identification and tight PF isolation requirement. These cuts on the
462 muon tracks reject decays in flight. Muons with opposite charge and dimuon invariant mass
463 compatible with the Z mass ($|m(\mu_1\mu_2) - m_Z| < 15 \text{ GeV}$) are paired as muons from Z boson
464 decay. Cuts are applied on the muon transverse momentum of the three muons in each event
465 of 40:40:10 GeV. Events with at least one b jet with $p_T > 20 \text{ GeV}$ are vetoed.

466 Several distributions comparing data with Monte Carlo after all selection cuts are shown in
467 figure 14. The trigger efficiency versus leading muon p_T , η and ϕ in the Monte Carlo and real
468 MET data sample are shown in Fig. 15 and Fig. 16 respectively. The weighted average trigger
469 efficiency on Monte Carlo was calculated to be 95.5%, while efficiency on real data was 89.2%.
470 The trigger scale factor was calculated to be 93.4% with a statistical uncertainty of 6%. The
471 statistical uncertainty was taken as the inverse square root of the number of surviving events
472 in data after all selections. A systematic uncertainty of 15% was obtained by calculating the
473 difference in the normalization between the Monte Carlo and the data and then dividing by
474 the normalization in data.

475 When we lower the cuts from 40:40:10 GeV to 30:30:10 GeV, the trigger efficiency on data drops
476 by about 0.5%. The trigger scale factor also drops by about 0.5%. However, relaxing the cuts too
477 much would introduce a non-prompt contribution in data for which we do not have simulated
478 sample. This would bias the SF estimation. In [74], a data-driven background determination
479 was done to estimate the ‘non-prompt’ contribution using dijet events enriched in non-prompt
480 leptons. In our case we increased the pT cuts in order to have reasonable agreement between

Table 6: MET triggers used in MET Primary dataset

Trigger Path
HLT_MET100
HLT_MET150
HLT_MET200
HLT_MET250
HLT_MET300
HLT_MET600
HLT_MET700
HLT_PFMET110_PFMHT110_IDTight
HLT_PFMET120_PFMHT120_IDTight
HLT_PFMET170_BeamHaloCleaned
HLT_PFMET170_HBHECleaned
HLT_PFMET170_HBHE_BeamHaloCleaned
HLT_PFMET170_JetIdCleaned
HLT_PFMET170_NoiseCleaned
HLT_PFMET170_NotCleaned
HLT_PFMET300
HLT_PFMET400
HLT_PFMET500
HLT_PFMET600
HLT_PFMETTypeOne190_HBHE_BeamHaloCleaned

Table 7: Used Monte Carlo samples for the trigger scale factor studies.

Process	Dataset	Number of events
$WZ \rightarrow 3l\nu$	/WZTo3LNu_TuneCUETP8M1_13TeV-powheg-pythia8/_RunII Summer 16 DR80 Premix-PUMoriond17_80X_mcRun2_asymptotic_2016_TrancheIV_v6_ext1-v3/AODSIM	18,000,000
$ZZ \rightarrow 4\mu$	/EWK_13TeV_CALCHEP_50K_batch1_GEN_SIM_v1_TAMU/jrorie-EWK_13TeV_CALCHEP_50K_batch1_RAW2DIGI_L1Reco.RECO_v1_TAMU-2ddd25030f7878ebc0ae5f7f9cd4b430/USER	50,000
$ZZ \rightarrow 4\mu$	/EWK_13TeV_CALCHEP_50K_batch1_GEN_SIM_v3_TAMU/jrorie-EWK_13TeV_CALCHEP_50K_batch2_RAW2DIGI_L1Reco.RECO_v1_TAMU-2ddd25030f7878ebc0ae5f7f9cd4b430/USER	50,000
$t\bar{t}W \rightarrow 3l\nu$	/TTWJetsToLNu_TuneCUETP8M1_13TeV-amcatnloFXFX-madspin-pythia8/RunII Summer 16 DR80 Premix-PUMoriond17_80X_mcRun2_asymptotic_2016_TrancheIV_v6_ext1-v3/AODSIM	2,160,168
$t\bar{t}Z \rightarrow ll\nu\nu$	/TTZToLLNuNu_M-10_TuneCUETP8M1_13TeV-amcatnloFXFX-madspin-pythia8/RunII Summer 16 DR80 Premix-PUMoriond17_80X_mcRun2_asymptotic_2016_TrancheIV_v6_ext1-v3/AODSIM	5,934,228

481 data and MC before extracting the SF.

482 We also tried the orthogonal method with the SingleElectron dataset. We required at least
 483 three PF loose muons with transverse momenta 20:10:10 GeV, and at least one electron with 30
 484 GeV. No ID or isolation was applied on the electron. Each muon was required to pass $d_{xy} < 0.05$
 485 cm and $d_z < 0.05$ cm, and must have a PF relative isolation less than 0.15. In addition, the event
 486 must pass at least one single electron trigger. Events in Monte Carlo simulated datasets (WZ ,
 487 ZZ , $t\bar{t}Z$, WWZ , WZZ and ZZZ) were required to pass exactly the same selections. Less than 50
 488 events survive in the SingleElectron data, which is too few to obtain reliable results. We
 489 did not further pursue the orthogonal method with the SingleElectron dataset.

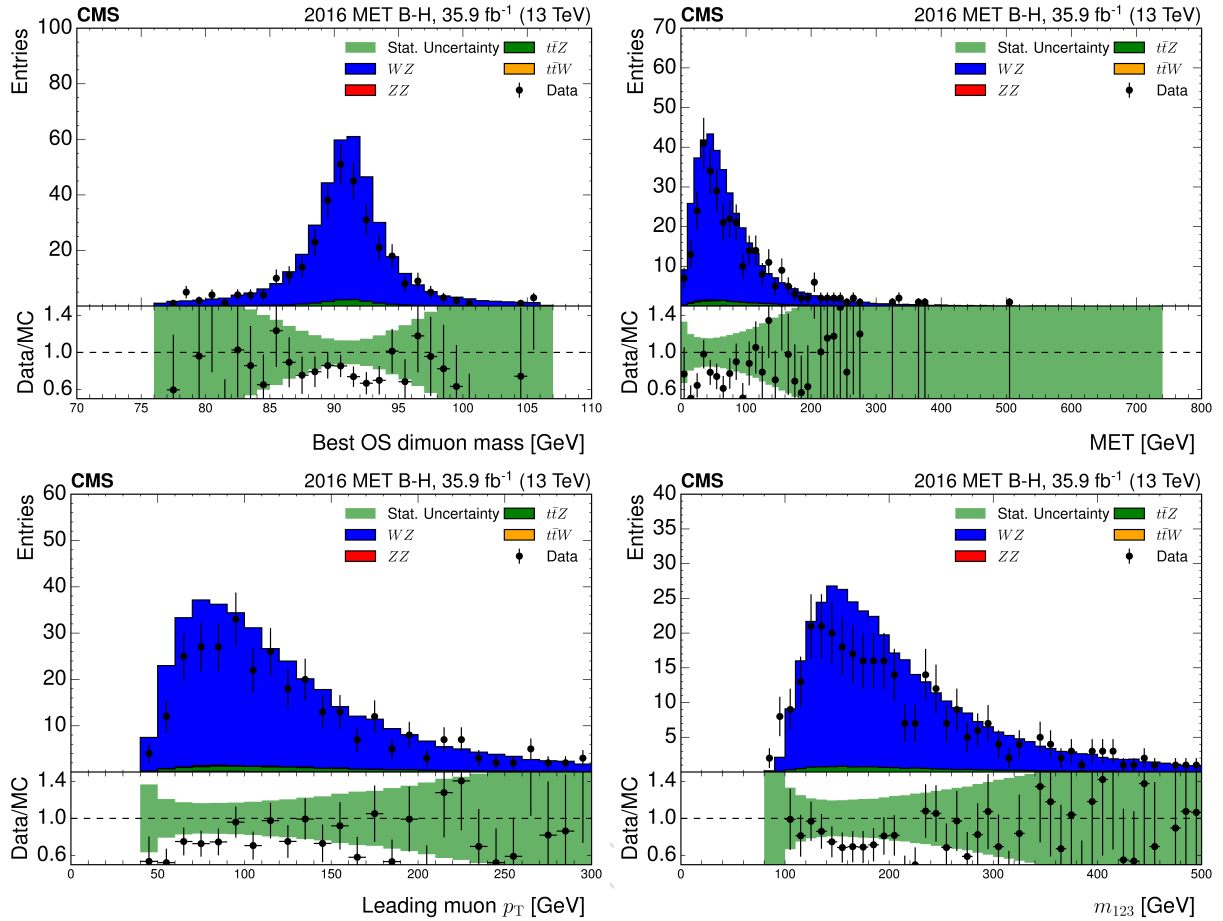


Figure 14: Dimuon invariant mass (top left), MET (top right), leading muon transverse momentum (bottom left) and invariant mass of the 3-muon system (bottom right) in Monte Carlo and Data.

4.2 Muon Selection

Offline muon reconstruction. In this analysis, offline muon candidates are defined as particle-flow (PF) muons [75]. The PF reconstruction algorithm combines information from all CMS subdetectors to identify and reconstruct individual particles like electrons, hadrons or muons. For muons, the PF approach applying the particular selection criteria to the muon candidates reconstructed with the *Global* and *Tracker* muon algorithms are chosen. Depending on the environment of the muon (for example, whether it is isolated or not) the selection criteria are adjusted making use of information from other subdetectors (for example, the energy deposition in the calorimeters). In general, the selection is optimized in order to identify muons within jets with high efficiency while maintaining a low rate for the misidentification of charged hadrons as muons.

Baseline muon identification. Particles identified as a muon by the PF event reconstruction algorithm are also required to satisfy baseline *Loose* selection requirements ², namely muon candidate must be reconstructed with *Tracker* or *Global* PF algorithms.

Kinematic muon selection. In this analysis, the following kinematic and geometric requirements are applied to Loose PF muons:

²See twiki: https://twiki.cern.ch/twiki/bin/view/CMSPublic/SWGuideMuonId#Loose_Muon

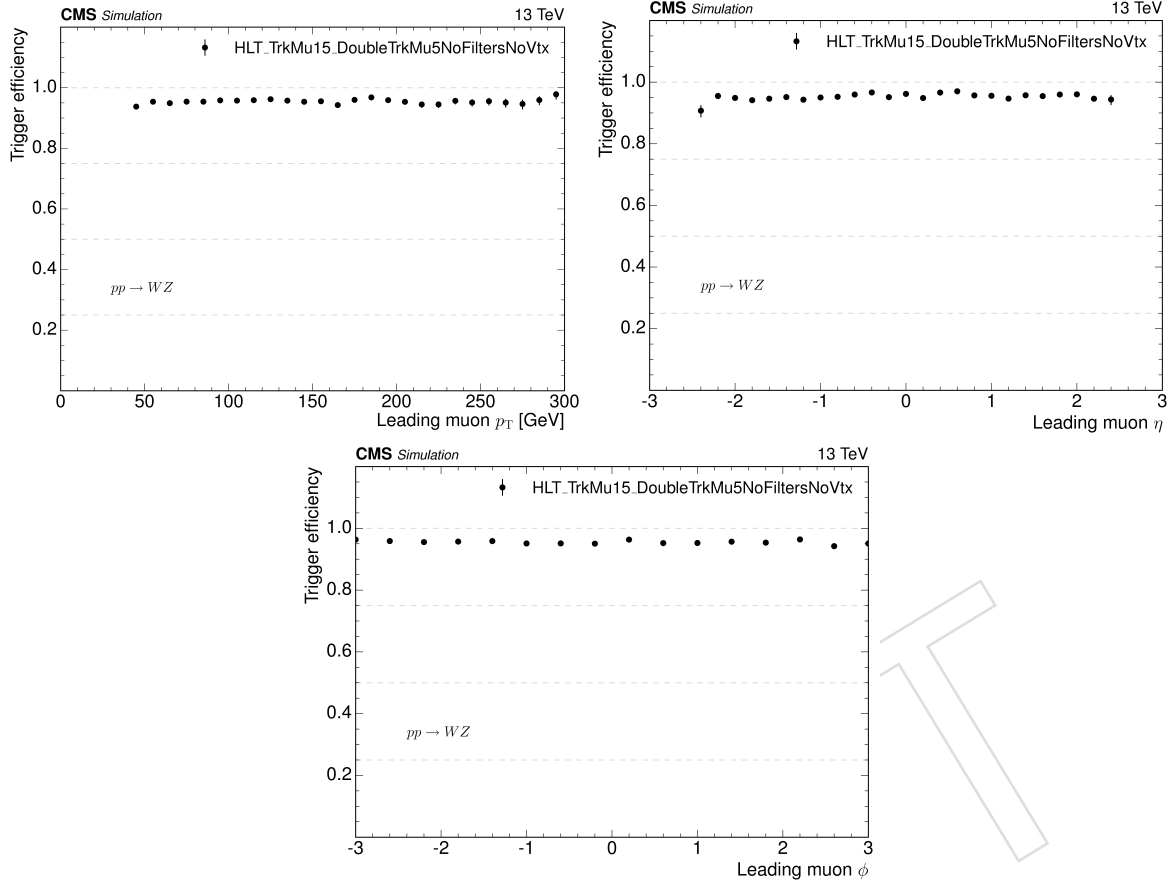


Figure 15: Trigger efficiency versus leading muon p_T (top left), η (top right), and ϕ (bottom) in the $WZ \rightarrow 3\mu\nu$ Monte Carlo sample.

- transverse momentum $p_T > 8$ GeV,
- pseudorapidity within $|\eta| < 2.4$.

Basic event selection. Events are required to have at least four PF muons selected as described above in Subsection 4.2. In addition, at least one of these muons is required to be in the barrel region $|\eta| < 0.9$ and have a transverse momentum $p_T > 17$ GeV to ensure that the trigger efficiency for selected events is high (96-97%) and independent of η of either of the dimuons (see Sec. 4.1).

The acceptance (α_{reco}) of the basic event selection requirements applied to *reconstructed* muons are shown in the Tables in Appendix B. We use the simulated signal events for representative choices for masses of h_1 and a_1 or h and γ_D , respectively for the NMSSM and Dark SUSY benchmark scenarios. For the Dark SUSY samples a range of representative values of $c\tau$ is also considered. These tables also show acceptance at of the basic event selection requirements applied to muons at the generator level (α_{gen}). Other aspects of the signal selection are chosen in such a way that they allow for the full selection efficiency to be easily calculated from α_{gen} with only a single scale factor.

4.3 Further Event Selection

Construction of Dimuon Candidates. In events that satisfy the basic event selection, all selected muons are iteratively grouped into dimuon candidates using the following algorithm:

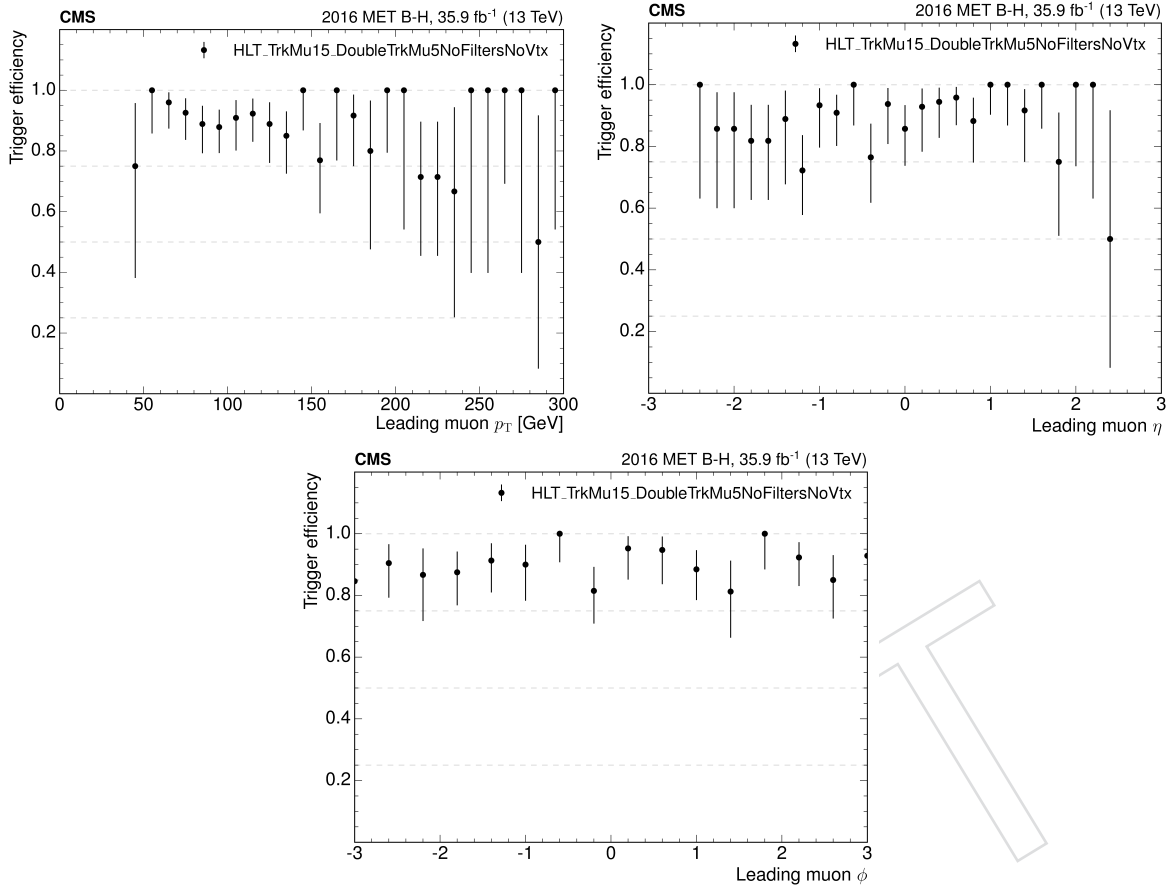


Figure 16: Trigger efficiency versus leading muon p_T (top left), η (top right), and ϕ (bottom) in the 2016 MET sample.

- 524 1. **Association of muons into “muon pairs”.** Pairs of oppositely charged muons are grouped
 525 together if they have a pairwise invariant mass $m(\mu^+\mu^-) < 9$ GeV and one of the two
 526 following spatial conditions: either the fit of the tracker tracks associated with the two
 527 muons for a common KalmanFitter vertex has the vertex probability $P_v(\mu^+\mu^-) > 1\%$ or
 528 the two muons are within $\Delta R(\mu^+\mu^-) < 0.01$ of each other. The latter requirement en-
 529 sures that pairs of muons with closely spaced nearly parallel tracks at the common vertex
 530 (in which case the efficiency of the vertex fit requirement is significantly reduced) are ac-
 531 cepted with high efficiency. This requirement does not introduce any significant increase
 532 in the background contamination as the probability of two unrelated muon candidates
 533 being in such close proximity to each other is negligible; further details concerning this
 534 issue can be found in Appendix E. At this stage, a particular muon may be associated with
 535 more than one “muon pair”. The procedure continues until all “muon pairs” satisfying
 536 these criteria are constructed.
- 537 2. **Association of “muon pairs” into “dimuon candidates”.** We only select events where
 538 two muon pairs that do not share any muon are present. No limit on ungrouped muons
 539 (“orphans”) is applied. The two muon pairs will be referred as “dimuon candidates”.

540 **Requirement on dimuons.** We select events with exactly two dimuon candidates, each with
 541 exactly two reconstructed muons that appear in nowhere else in the event. This follows the
 542 analysis strategy that targets only events with non-standard-model Higgs boson decays to pairs
 543 of new light bosons, each of which decays into the $\mu^+\mu^-$ final state. Such dimuon candidates

544 are referred to as *dimuons*. The Tables in Appendix B show that this selection is highly efficient
 545 for the signal benchmark scenarios, where the small inefficiency arises from the common vertex
 546 fit requirement.

547 Note again, that no restriction on the number of “orphan” muons in the event is applied. While
 548 we could reject events with “orphans,” it would introduce unnecessary model dependency
 549 into the results. One example could be Higgs boson production in association with one or
 550 more energetic jet, where the probability that a non-muon track from a jet to be incorrectly
 551 associated with some of the 16 muon stubs available in the event resulting in a reconstructed
 552 “orphan” can be not negligible.

553 **Requirement on each dimuon containing at least one muon with a hit in one of the three
 554 layers of the pixel detector.**

The average transverse decay length, L_{xy} , of the dark photon depends on its lifetime and mass as follows:

$$L_{xy} = \gamma c \tau_{\gamma_D} \frac{p_T}{p} = \frac{E}{m_{\gamma_D}} c \tau_{\gamma_D} \frac{p_T}{p}, \quad (10)$$

555 where γ , E , p and p_T are the Lorentz factor, average energy, momentum, and transverse mo-
 556 mentum of the dark photons respectively.

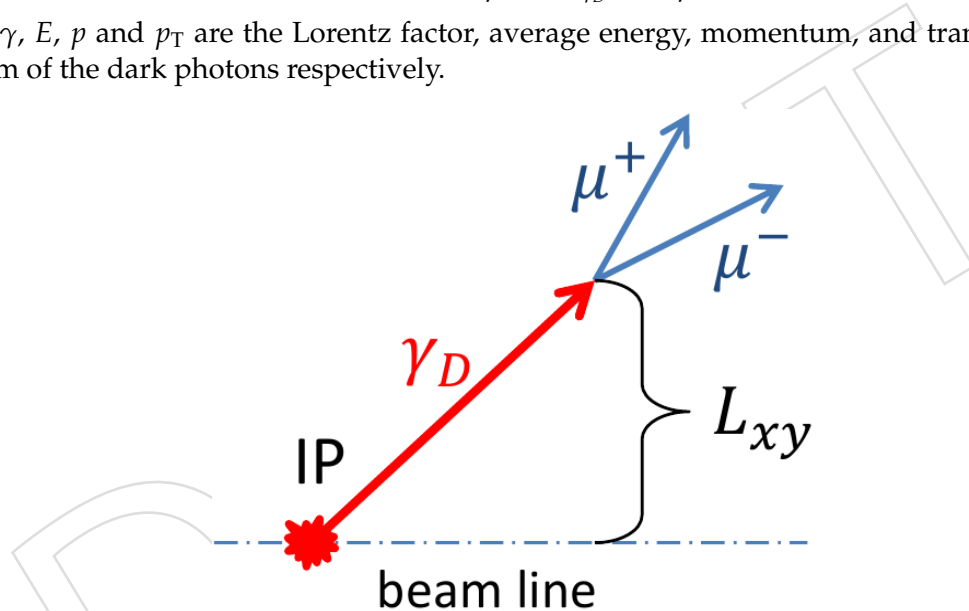


Figure 17: Sketch to illustrate definition of the transverse decay length L_{xy} between the beam line and the displaced decay vertex of the dark photon.

557 Dark photons with a long enough lifetime can decay at a non-negligible distance from the inter-
 558 action point, and these relatively largely displaced dimuon vertices result in a decrease in the
 559 trigger and reconstruction performance for these dimuons. The dimuon reconstruction perfor-
 560 mance with respect to the transverse decay length, L_{xy} , has been extensivelyyy studied. L_{xy} , the
 561 distance between the beam line and the dimuon vertex in the transverse plane is illustrated in
 562 Fig. 17. L_{xy} is the natural variable to use when studying the dimuon and muon reconstruction
 563 efficiency because of the cylindrical symmetry of the CMS detector. The distribution of the L_{xy}
 564 for dark photons in different MC samples is shown in Fig. 18 (for each sample the distributions
 565 for leading and next-to-leading dark photons are plotted). The longitudinal decay length, L_z ,
 566 is also considered.

567 Quantifying the reconstruction efficiency as a function of the transverse and longitudinal decay
 568 length of the new light boson is done in two ways. The first is to study the efficiency per
 569 dimuon, and the second is to study the efficiency per muon.

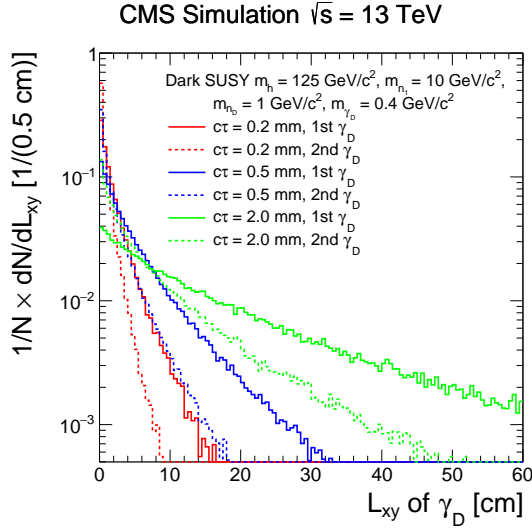


Figure 18: Distribution of L_{xy} for the leading and next-to-leading dark photons in the Dark SUSY MC simulated samples with different $c\tau_{\gamma_D}$.

570 The efficiency per dimuon is defined as

$$\frac{N_{GEN\mu\mu-2\times RECO\mu \text{ Match}}}{N_{GEN\mu\mu}}. \quad (11)$$

571 Here, $N_{GEN\mu\mu}$ is the number of new light bosons (dark photons) with both generator level
572 muons (the decay products of the dark photon) satisfying the p_T and η analysis requirements
573 in events which fired the HLT. Due to the different p_T thresholds that must be satisfied by each
574 of the dimuons in an event the efficiencies for both types of dimuons were separately studied:

575 1. one muon with $p_T > 17 \text{ GeV}$ and $|\eta| < 0.9$, and the other muon with $p_T > 8 \text{ GeV}$ and
576 $|\eta| < 2.4$

577 2. both muons with $p_T > 8 \text{ GeV}$ and $|\eta| < 2.4$

578 The light boson (dark photon) satisfying (1) is labelled a_0 and the other is labelled a_1 . In the
579 case that both dimuons in an event satisfy (1), containing a 17 GeV muon in $|\eta| < 0.9$, the labels
580 of a_0 and a_1 are assigned randomly.

581 The numerator in equation 11, $N_{GEN\mu\mu-2\times RECO\mu \text{ Match}}$, is the number of new light bosons (dark
582 photons) in which the generator level (GEN) dimuon has two reconstruction level (RECO)
583 muon matches meeting a $\Delta R < 0.1$ criteria in events which fired the HLT. The reconstructed
584 muons considered are required to have a $p_T > 8 \text{ GeV}$ and $|\eta| < 2.4$. The resulting dimuon
585 reconstruction efficiency as a function of the vertex L_{xy} and L_z for a_0 is shown in Fig. 19. Note,
586 that the efficiency is high and stable for $L_{xy} \lesssim 9.8 \text{ cm}$ (corresponding to the inner radius of
587 the third layer in the pixel barrel detector), and then it begins to gradually decrease up to
588 $L_{xy} \approx 22 \text{ cm}$ (corresponding to the radius of the first layer of the silicon tracker), after which
589 the efficiency proceeds to decreases much more steeply as the new light bosons decay further
590 and further inside the silicon tracker up to $L_{xy} \approx 60 \text{ cm}$ (corresponding to the radius of the last
591 layer of the silicon tracker inner barrel), before falling to zero for higher L_{xy} . Furthermore, a

592 reduction of the dimuon reconstruction efficiency is seen from the muon system overlap region
 593 ($|\eta| = 0.9$) until the start of CSC ring ME1/1 ($|\eta| = 1.5$). This loss of efficiency is then recovered
 594 in the CSC endcap ($1.5 < |\eta| < 2.4$).

595 It is also interesting to study the dimuon efficiency from equation 11 when constrained by only
 596 considering new light bosons decaying within the third pixel barrel layer ($L_{xy} < 9.8\text{cm}$) and the
 597 second pixel endcap ($L_z < 48.5\text{cm}$). This 1-dimensional efficiency as a function of L_{xy} and L_z ,
 598 which is a projection of the 2-dimensional efficiency shown in Fig. 19, is shown in Figure 20. It
 599 is clear that within this region dimuons are accurately reconstructed with a very high efficiency.

600 The trigger inefficiency and consequent reduced dimuon reconstruction efficiency with increasing
 601 dimuon vertex L_{xy} and L_z provides the strongest motivation for including an effective
 602 “fiducial” constraint on the dimuons in this analysis.

603 The trigger inefficiency is the driving factor behind the decision to bound the fiducial region
 604 for this analysis by the third layer of the pixel barrel and the second layer of the pixel endcap.
 605 Figure 21 shows the dimuon efficiency separated by regions in η . It is clear that the efficiency is
 606 high and flat for all dimuons within the chosen fiducial region. Alongside the effects due to the
 607 trigger and reconstruction the inefficiency also has a complex dependence on a range of event
 608 kinematics, including the direction, momentum, vertex position and decay kinematics of the
 609 γ_D . It would be extremely challenging to attempt to measure these efficiencies experimentally
 610 and it would also detract from the model independence of this analysis.

611 By constraining our search to the region bounded by the third layer of the pixel barrel and
 612 second layer of the pixel endcap the trigger and reconstruction inefficiencies are minimal. This
 613 additional kinematic selection mimics a requirement that the new boson decays within the
 614 volume defined by the third layer of the pixel barrel and second layer of the pixel endcap,
 615 and ensures that the trigger and reconstruction efficiencies remain high and independent of
 616 the specific model details considered here. In order to implement this at generator level we
 617 apply cuts on the new boson of $L_{xy} < 9.8\text{ cm}$ and $L_z < 46.5\text{ cm}$, corresponding to the distance
 618 from the center of the detector to the third layer in the pixel barrel (BPIX) and the second pixel
 619 endcap (FPIX) respectively. For reconstructed muons we require that at least one muon in each
 620 dimuon has at least one hit in one of the three layer of the pixel barrel, or one hit in at least one
 621 of the two pixel endcaps.

622 **Requirement on valid primary vertex.** Only events with at least one primary vertex are se-
 623 lected. The following quality requirements applied to select a primary vertex:

- 624 • status = not “fake”,
- 625 • number of tracks ≥ 4 ,
- 626 • global z coordinate within 24 cm from the CMS origin.

627 **Reconstruction of dimuon vertex.** We reconstruct the position of the light boson “production
 628 vertex” at the beamline $z_{\mu\mu}$, which we later also use to apply tracking isolation requirements
 629 and to verify that the two light boson candidates are originating from the same pp interaction in
 630 the same bunch crossing. When defining $z_{\mu\mu}$, we assume that each new light boson is produced
 631 sufficiently close to the beamline but allow for non-negligible lifetime before decaying to a
 632 muon pair. We first calculate the 3D direction of the momentum of the light boson candidate
 633 $\vec{p}_{\mu^+} + \vec{p}_{\mu^-}$ at the position of the reconstructed “common vertex” of the two muons (or, for
 634 muons with very close directions where the vertex is not reconstructed, at the points on the
 635 respective trajectories where the two tracks are the closest to each other in xy -plane). Next,
 636 we project a straight line along the dimuon direction vector from the common vertex (or the

637 point in the middle of the segment connecting the points on the trajectories where momenta
 638 of the two muons are calculated) towards the beamline. The z -coordinate of the projected line
 639 at the point of closest approach to the beamline in the xy -plane becomes the reconstructed $z_{\mu\mu}$
 640 of the “production vertex”. As Higgs boson lifetime is negligible, in signal events $z_{\mu\mu}$ for each
 641 dimuon tags the primary vertex position and therefore the two positions should be consistent
 642 within the detector resolution.

643 **Requirement on vertices of dimuons.** We use the reconstructed vertices of dimuons to require
 644 that the two light boson candidates are produced in the same pp collision:

$$645 \quad |\Delta z| = |z_{\mu\mu_1} - z_{\mu\mu_2}| < 0.1 \text{ cm} \quad (12)$$

646 This requirement is loose enough to ensure that signal events are never rejected by this selec-
 647 tion, which is illustrated in Fig. 22. The red histogram shows the distribution of the Δz for the
 648 simulated signal events (Dark SUSY benchmark sample with $m_{h_1} = 125$ GeV) proving that the
 649 requirement is much looser than the typical Δz resolution making sure this is a safe choice.

650 For comparison, in the same Fig. 22, the blue histogram shows the distribution of $\Delta z = z_{\mu\mu} - z_\mu$
 651 obtained from $b\bar{b}$ -background-dominated data sample with events selected by requiring ex-
 652 actly one dimuon (with $z_{\mu\mu}$ vertex coordinate) and one *orphan* muon (with z_μ vertex coordi-
 653 nate). This topology is very much unlike our signal events as neither the *orphan* muon nor the
 654 dimuon are capturing the direction of the original b -quarks correctly, owing to the b -decay ver-
 655 tex being frequently displaced from the beamline and the unaccounted b -jet constituents. Yet,
 656 while the distribution is expectedly broader than the distribution from the signal-like topolo-
 657 gies, the selection remains highly efficient even in this case, providing additional confidence
 658 that the choice is safe and robust. Tightening the cut will not lead to any sizable improvement
 659 in sensitivity of the analysis at present luminosity as it is already a near zero background anal-
 660 ysis. A too tight Δz cut will decrease sensitivity due to reduced signal acceptance and due to
 661 potential systematic increase.

662 **Requirement on isolation of dimuons.** We use the absolute isolation of dimuons to suppress
 663 background events with muons from heavy-flavor $b\bar{b}$ decays. We choose to use the abso-
 664 lute isolation definition, because the relative isolation is always p_T dependent, which would
 665 severely complicate a model-independent interpretation of the results. Both of the two selected
 666 dimuons (candidates for light bosons) are required to be isolated using the following definition:

$$667 \quad Iso_{\mu\mu} = \sum_{\text{tracks}} p_T(\text{track}) < 2 \text{ GeV}, \quad (13)$$

668 where the summation runs over all reconstructed tracks with

- 669 • $p_T(\text{track}) > 0.5 \text{ GeV}$,
- 670 • $\Delta R(\text{track}, \mu\mu) < 0.4$,
- 671 • $|z_{\text{track}} - z_{\mu\mu}| < 0.1 \text{ cm}$,
- 672 • tracks associated with the muons forming the dimuon are excluded.

673 Note, in calculating the isolation variable, we only use tracks that have z_{track} position near
 674 the beamline consistent with the dimuon vertex $z_{\mu\mu}$. This “consistency” requirement is driven
 675 by the tracking resolution. With this definition, the isolation efficiency is almost completely
 676 insensitive to pileup as even with 30 pileup interactions, the typical distance between the z
 677 positions of two nearby interactions is substantially larger than 0.1 cm^3 , therefore tracks from
 678 nearby pileup collisions never contribute to the inefficiency of the isolation selections.

³If the size of the highly luminous region is taken to be $\sim 15 \text{ cm}$, for an event with ~ 30 pile-up collisions the

The requirement on dimuon isolation $Iso_{\mu\mu} < 2$ GeV has a signal efficiency about 90% per dimuon, independent of the sample mass of $c\tau$, while reducing the $b\bar{b}$ background contamination by a factor of about 50. Fig. 23 shows the distribution for $Iso_{\mu\mu}$ using the dark SUSY simulated sample (with a dark photon $m(\gamma_D) = 2.0$ GeV). This distribution is compared to the isolation distribution for dimuons in the background-enriched sample (one dimuon plus exactly one orphan muon). The full dimuon isolation distribution is shown (left) and a close-up log-scaled plot (right) is shown in the region near the 2.0 GeV cut. The isolation distributions for every dark SUSY MC sample that was generated and used in this analysis is shown in Appendix F. Further details related to the isolation can be found in the documentation describing the 5.3 fb^{-1} version of this analysis [32].

Consistent masses of dimuons. The very final requirement is that the masses of the two dimuons reconstructed in the event should be consistent with each other within the detector resolution:

$$|m_{\mu\mu_1} - m_{\mu\mu_2}| < 0.13 + 0.065 \times \frac{m_{\mu\mu_1} + m_{\mu\mu_2}}{2}. \quad (14)$$

This selection requirement appears as a *corridor* in the 2D plane (as shown in Fig. 7) of $m_{\mu\mu_1}$ vs. $m_{\mu\mu_2}$ distribution. The parameters are selected so that the size of the corridor is at least five times the size of the core resolution of the dimuon invariant mass measurement, accounting for the difference in resolution in the central (barrel) and forward (endcap) regions. The typical inefficiency of this selection is less than 5% owing to the radiative tails and is not related to the detector resolution. The off-diagonal sidebands of the $m_{\mu\mu_1}$ vs. $m_{\mu\mu_2}$ distribution are used to estimate the normalization of the background contribution in the signal region (the background shape is measured using data only as described further in this note). As with the isolation requirement, further details concerning this cut, including the study that determined the width of the signal corridor, can be found in the documentation describing the 5.3 fb^{-1} version of this analysis [32].

4.4 Summary of the Selection Efficiencies

Tables in Appendix B list efficiency of the event selections in terms of relative efficiencies at each step for several representative model points using fully-reconstructed simulated events. For reference, we also list cumulative efficiencies for baseline selection requirements for muons encompassing kinematic and geometrical acceptance and muon reconstruction efficiencies labeled as “Basic Acceptance”, and the rest of the selections labeled as “Auxiliary Selections”. To facilitate future re-interpretation of the results of this analysis, we calculate the efficiency of “Basic Acceptance” α_{Gen} using generator level information only (the case of a “perfect Monte Carlo”) defined as:

$$\alpha_{\text{Gen}} = \frac{N_{\text{GENSel.}}}{N_{\text{Events}}}, \quad (15)$$

where N_{Events} is the total number of generated Monte Carlo events, and $N_{\text{GENSel.}}$ is the number of events passing the GEN level muon selection requirements on η , p_T , and vertex position (fiducial cut). We also define the ratio of the efficiency of all analysis selections which we call the “acceptance”, ϵ_{Full} as:

$$\epsilon_{\text{Full}} = \frac{N_{\text{RECOSel.}}}{N_{\text{Events}}}, \quad (16)$$

“average distance” between the interactions would be of the order of 0.5 cm.

717 where N_{Events} is the total number of generated Monte Carlo events, and $N_{RECOsel.}$ is the total
 718 number of events satisfying the full RECO analysis selection described in the previous section.
 719 This full analysis selection at RECO level includes the muon selection requirements on η and
 720 p_T , exactly two dimuons in the event, one hit in one of the pixel barrel or endcap layers per
 721 dimuon, the isolation requirement, the requirement on the vertices of the dimuons, the mass
 722 compatibility requirement, and the requirement that the event fire the HLT.

723 These quantities, α_{Gen} and ϵ_{Full} , are useful for quantifying the sensitivity of this analysis in a
 724 model-independent fashion. For the dark SUSY sample, we check that the ratio $\epsilon_{Full}/\alpha_{Gen}$ is
 725 independent of the lifetime and mass of the dark photon. For the NMSSM sample, we check
 726 that $\epsilon_{Full}/\alpha_{Gen}$ is independent of the masses of the a_1 and $h_{1,2}$. Both the dark SUSY and NMSSM
 727 $\epsilon_{Full}/\alpha_{Gen}$ ratio plots are presented in Fig. 24. By verifying that $\epsilon_{Full}/\alpha_{Gen}$ is insensitive to
 728 variations of model parameters, we ensure that the analysis remains model independent. To
 729 calculate an overall $\epsilon_{Full}/\alpha_{Gen}$, an average of the $\epsilon_{Full}/\alpha_{Gen}$ is found. This averaging is weighted
 730 by each sample's uncertainty and included all samples except for the Dark SUSY samples with
 731 $c\tau_{\gamma_D} = 100$ mm.

732 The exclusion limit with respect to the mass of the dark photon is derived by design of the
 733 analysis. To derive the exclusion limit with respect to the dark photon lifetime, we simulated a
 734 grid of dark SUSY samples with a range of dark photon lifetimes. We generated a dark SUSY
 735 samples with values of $c\tau_{\gamma_D}$ in the range 0.05 mm – 100 mm, which allows for us to probe a
 736 wide range of the kinematic mixing parameter, ϵ . Since the average transverse decay length
 737 of the dark photons directly depends on its lifetime, such dependence allows evaluation of
 738 the acceptance $\alpha(m_{\gamma_D}, c\tau_{\gamma_D})$ of the analysis selection requirements in $(m_{\gamma_D}, c\tau_{\gamma_D})$ space. We
 739 generate dark photon masses in the range $0.25 < m_{\gamma_D} < 8.5$ GeV/ c^2 while the masses of the
 740 Higgs boson, neutralino and dark fermion are fixed to $m_h = 125$ GeV/ c^2 , $m_{n_1} = 10$ GeV/ c^2 and
 741 $m_{n_D} = 1$ GeV/ c^2 . Samples for the second benchmark model, NMSSM, are also generated with
 742 a range of model parameters. In this case, the mass of the $h_{1,2}$ is varied between $80 < m_{h_{1,2}} <$
 743 150 GeV/ c^2 while the mass of the a_1 ranges between $0.50 < m_a < 3.55$ GeV/ c^2 .

744 We used the simulated MC samples for several sets of m_{γ_D} and $c\tau_{\gamma_D}$ (see exact choices in Tab. 16)
 745 and extrapolate the acceptance from Eqn 16 to other points in the $(m_{\gamma_D}, c\tau_{\gamma_D})$ space within area
 746 of the analysis sensitivity: 0.25 GeV/ c^2 $< m_{\gamma_D} < 8.5$ GeV/ c^2 and 0 mm $< c\tau_{\gamma_D} < 100$ mm.
 747 The obtained acceptance of the analysis selection requirements with respect to m_{γ_D} and $c\tau_{\gamma_D}$ is
 748 shown in Fig. 25 (right and left, respectively), where the solid bullets represent points for the
 749 simulated MC samples were used to evaluate the acceptance.

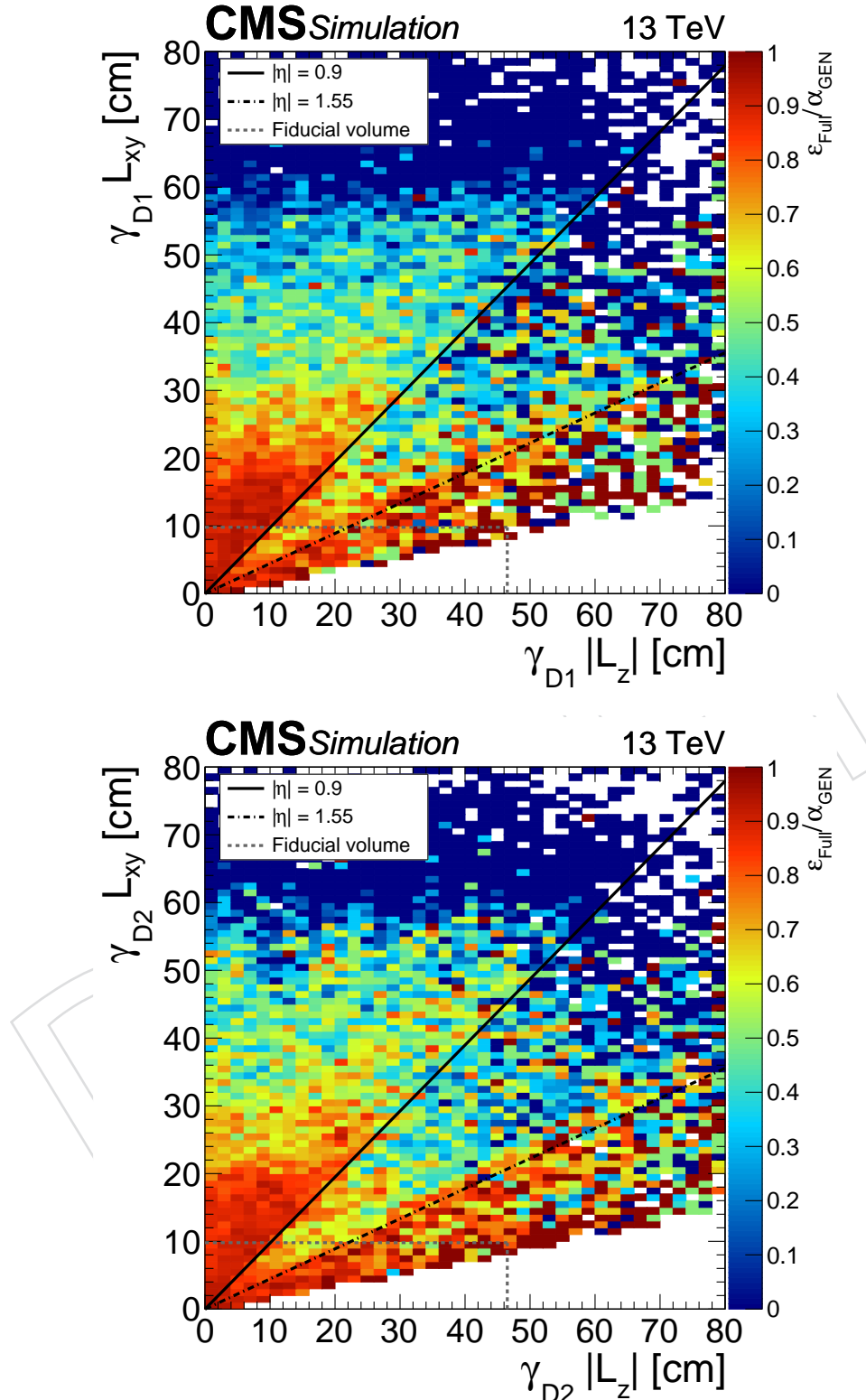


Figure 19: Plots show Dark SUSY MC samples corresponding to a dark photon mass of 0.25 GeV with all lifetimes ($c\tau_{\gamma_D}$) combined. Dimuon reconstruction efficiency as a function of L_{xy} and L_z for the dimuon pair requiring at least one muon with $p_T > 17 \text{ GeV}$ and $|\eta| < 0.9$ (left) and the other muon with $p_T > 8 \text{ GeV}$ and $|\eta| < 2.4$ (right).

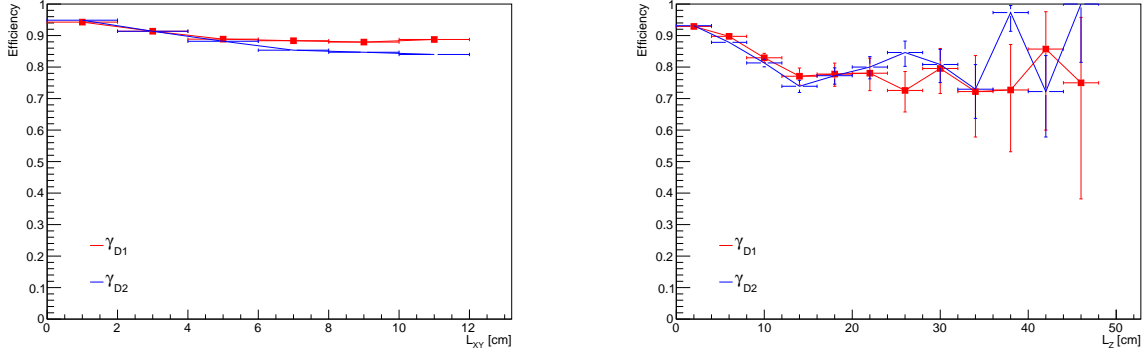


Figure 20: Reconstruction efficiency per dimuon as a function of L_{xy} (left) and L_z (right) for the Dark SUSY MC samples with $m(\gamma_D) = 0.25$ GeV/ c^2 and all lifetimes combined.

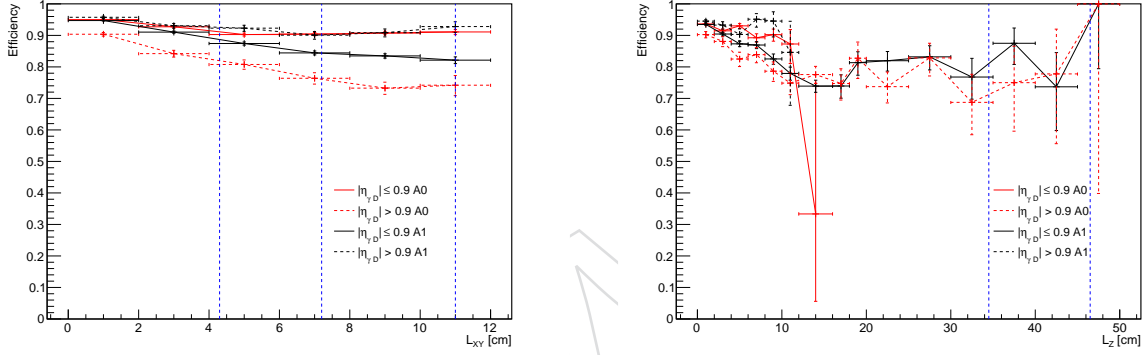


Figure 21: Reconstruction efficiency per dimuon as a function of L_{xy} (left) and L_z (right) for the Dark SUSY MC samples $m(\gamma_D) = 0.25$ GeV/ c^2 for all combined lifetimes separated by η regions corresponding to the CMS detector geometry. The blue dashed lines correspond to the layers of the pixel detector (barrel in L_{xy} , endcap in L_z). The dimuon that contains the leading p_T barrel muon is denoted as A0, the other is denoted as A1.

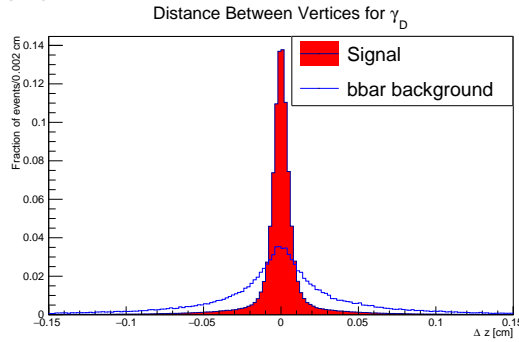


Figure 22: Distance between vertices measured for two dimuons ($\Delta z = z_{\mu\mu_1} - z_{\mu\mu_2}$) in the Dark SUSY simulated sample with $m_{h_1} = 125$ GeV for combined dark photon masses and lifetimes and for dimuon and “orphan” muon ($\Delta z = z_{\mu\mu} - z_\mu$) in events from $b\bar{b}$ -background-enriched part of data sample.

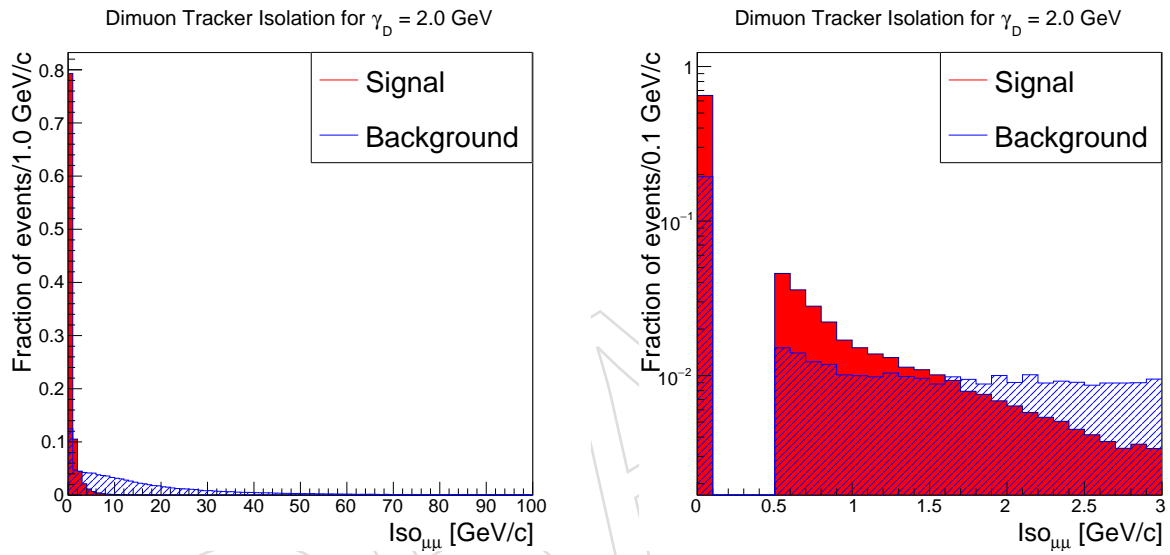


Figure 23: Isolation of the dimuons in events from the dark SUSY MC sample with a dark photon mass of 2.0 GeV and in events from the background-enriched part of data. The full normalized distribution (left) and a log-scale close-up near the 2.0 GeV isolation cut (right) are shown.

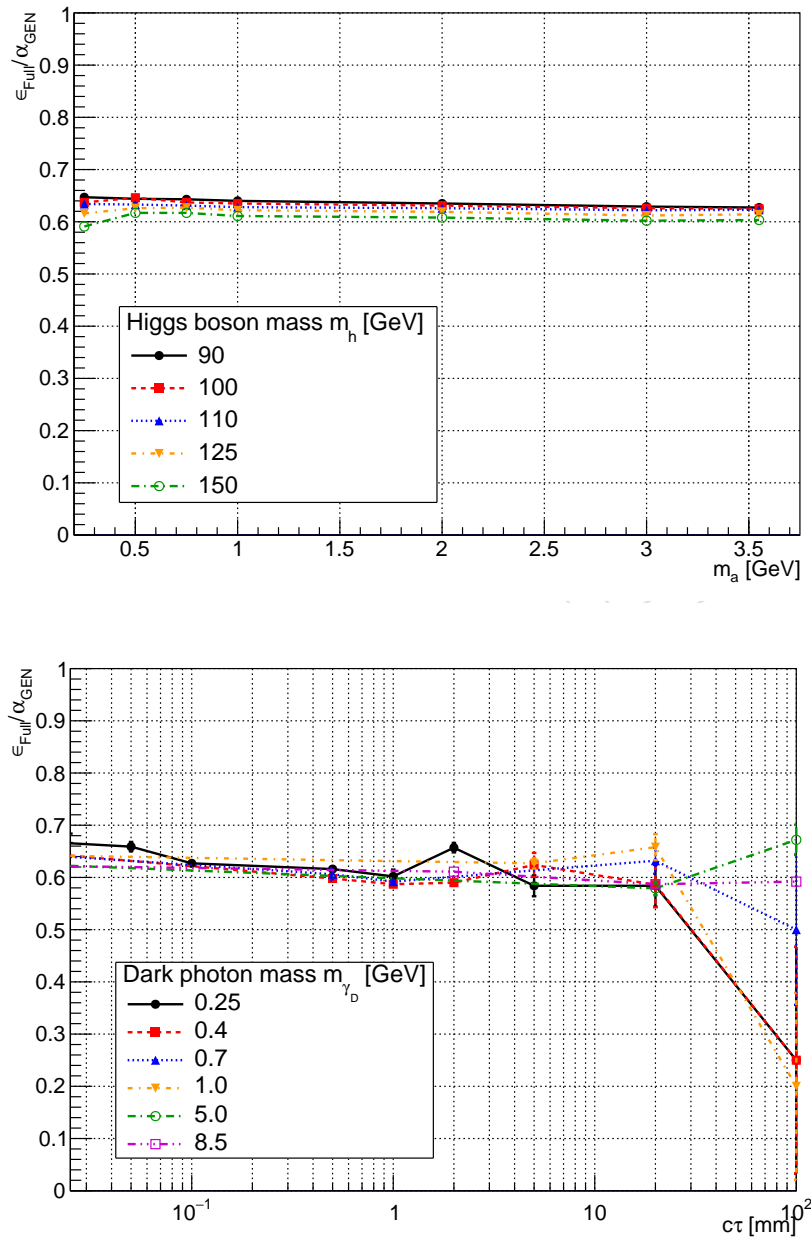


Figure 24: The ratio of the full analysis acceptance at reconstruction level to the generator level acceptance ($\epsilon_{\text{Full}}/\alpha_{\text{Gen}}$) for the NMSSM samples (top) as function of m_a , and for the dark SUSY benchmark samples (bottom), as function of the dark photon lifetime in log-scale.

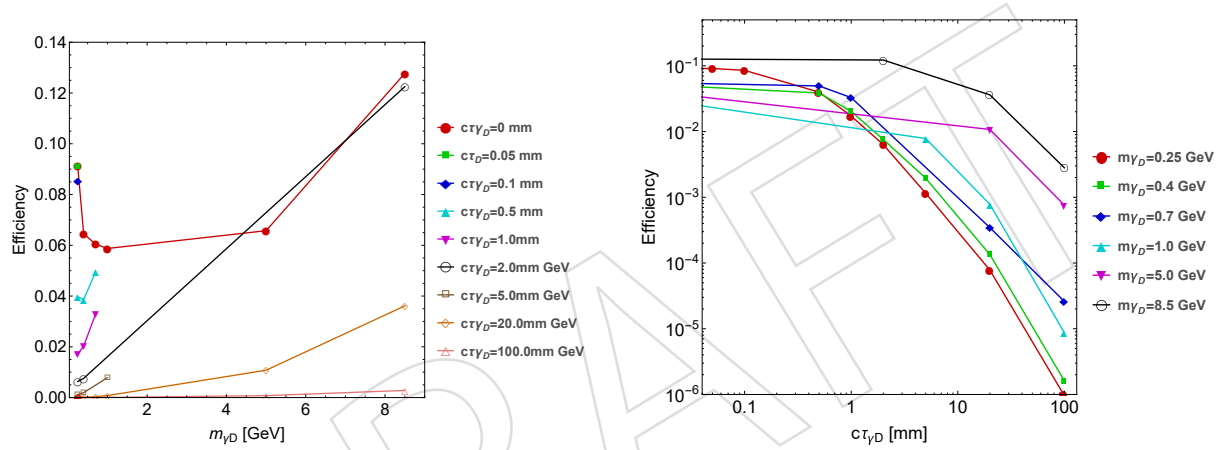


Figure 25: Acceptance of the analysis selection requirements evaluated using the simulated MC samples for several sets of $m_{\gamma D}$ and $c\tau_{\gamma D}$ (solid bullets). For these plots the bullet points at which the efficiency is evaluated are connected by a simple line to guide the eye.

750 5 Modeling of the Signal Shape

751 As final interpretation of results is performed by fitting the data surviving selections for a com-
752 bination of signal and background, modeling of the signal shape is important. It is particularly
753 important if an excess is found in the final signal region. If no events are observed in data the
754 the accuracy in the description of the signal shape is completely unimportant for this fitting
755 procedure.

756 As the new resonances decay to SM particles only and the coupling to SM is weak, they have
757 a narrow width and the shape of the dimuon invariant mass distribution is fully determined
758 by the detector resolution and final-state radiation of a photon from one of the muons. Though
759 extreme precision in modeling these shapes is not required in the presence of nearly zero back-
760 grounds, it has to be reasonably well-understood if we need to quantify properties of the new
761 resonances, assuming they are discovered.

762 The detector resolution has been extensively studied in the past (see Ref. [55]). The SM provides
763 four narrow, high cross section dimuon resonances in the mass ranges relevant for this analysis,
764 ω , ϕ , J/ψ , and ψ' , and these were used to calibrate the signal shapes. The resolution of each of
765 these resonances in data, modeled using a convenient Crystal Ball function. This approximation
766 has been found to be in a good agreement with the expectation based on simulation predictions.

767 The main effect relevant for the acceptance of the analysis is the efficiency of the requirement
768 that the two masses are compatible. The accuracy in the efficiency of the mass compatibility
769 requirement is driven by the accuracy with which simulation describes the radiative tail. The
770 size of the signal region (diagonal “corridor”) is much larger than the detector resolution. This
771 means that the inefficiency and also the potential systematic uncertainty is small. To estimate
772 the effect, the parameters of the Crystal Ball fit to J/ψ events in data (we use the background
773 enriched sample of dimuon and orphan) were deviated within the fit statistical uncertainties on
774 the parameters. Assuming that the distribution of signal events is similar to obtained template
775 the corresponding deviation 1.5% in the acceptance within signal region was calculated and
776 assigned as systematic uncertainty of this effect.



6 SM Backgrounds and Their Shapes

In this section we evaluate contribution from the SM to a signature with two light dimuons after final selections of the analysis. We study three main SM backgrounds: electroweak production of four muons, $b\bar{b}$ and prompt production of J/ψ pair. The contribution of other SM processes has been found to be negligible, e.g. the low mass Drell-Yan production is heavily suppressed by the requirement of two additional muons.

6.1 EWK $p p \rightarrow 4\mu$ Background

The electroweak $p p \rightarrow 4\mu$ contribution to the background events in the signal region is studied using a sample of 100,000 MC events. These events are generated with CalcHEP 3.6.25 [76]; the resulting LHE is then processed in CMSSW_8_0_20. The Feynman diagrams in Fig. 26 illustrate the processes that are included in this estimation: $q\bar{q} \rightarrow ZZ \rightarrow 4\mu$ and $q\bar{q} \rightarrow Z \rightarrow 2\mu$, the latter where a second Z is radiated and decays to a $\mu^+\mu^-$ pair. Other EWK processes are not included in this study due to their negligible (less than 1 per-mil) contribution to the signal region of this analysis. An example of such a process is the associated production of a Higgs boson and a Z boson with both decaying to a $\mu^+\mu^-$ pair; this is shown in Fig. 27. The η and p_T distributions for muons from the simulated SM EWK background are shown in Fig. 28. Based on the simulation, the expected EWK contribution to the total background in the signal region for an integrated luminosity of 35.9 fb^{-1} is found to be 0.36 ± 0.09 events. This contribution is of the same order of magnitude as the prompt double J/ψ background modeled in Sec. 6.3. Unlike the prompt double J/ψ background, this background is non-peaking, so its contribution to the background any one mass bin in the signal region is negligible compared to that of the $b\bar{b}$ background modeled in Sec. 6.2.

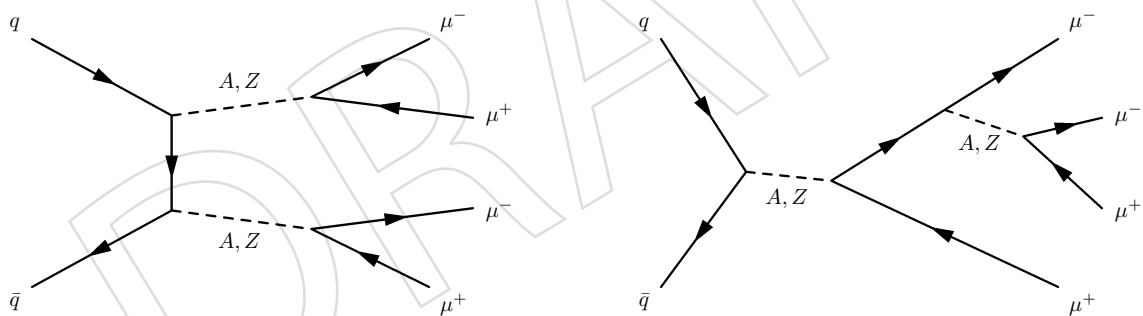


Figure 26: Feynman diagrams for the $p p \rightarrow 4\mu$ processes included in the MC samples used to estimate this background.

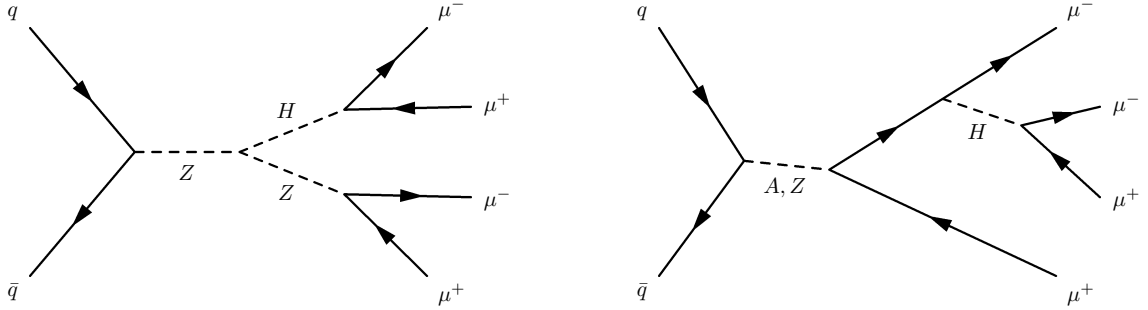


Figure 27: Feynman diagrams for the $pp \rightarrow 4\mu$ processes not included in the MC samples used to estimate this background.

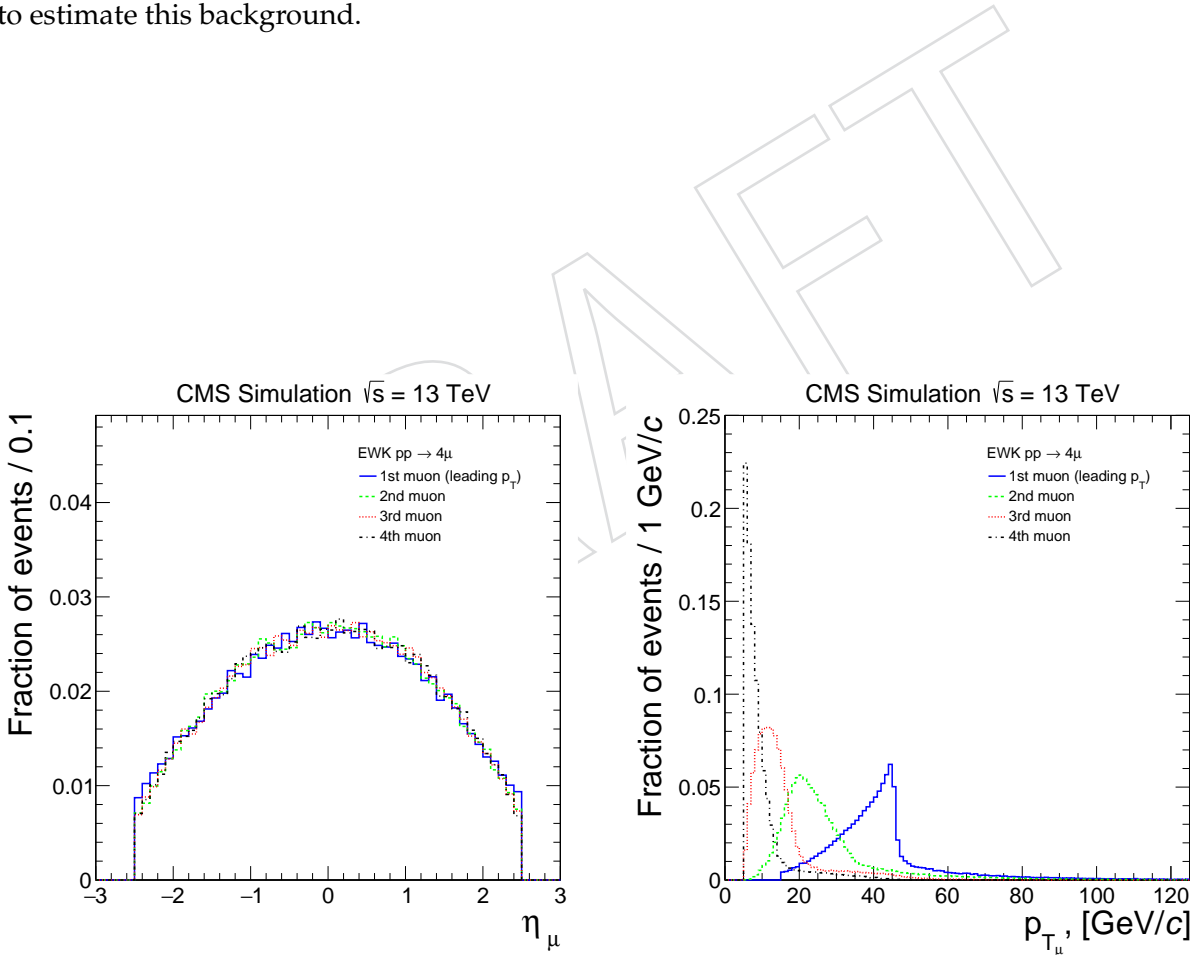


Figure 28: Distributions of pseudorapidity (left) and transverse momentum (right) for all 4 muons from the simulated EWK $pp \rightarrow 4\mu$ processes.

799 6.2 QCD $p\bar{p} \rightarrow b\bar{b} \rightarrow 4\mu$ Background

800 The leading part of the $b\bar{b}$ background contribution is dominated by events in which both b -
 801 quarks decay to pairs of muons ($\mu^+ \mu^- + X$) via double semileptonic decays or resonances,
 802 e.g. ω , ρ , ϕ , J/ψ , ψ . Fig. 29 shows an example event in which two b quarks decay double
 803 semi-leptonically into a total of four muons. A smaller contribution comes from events with
 804 a true muon from semileptonic b -quark decays and a charged track misidentified as another
 805 muon due to an occasional incorrect assignment of some of the true muon's tracklets recon-
 806 structed in the muon system to a nearby track, resulting in two muon candidates. The fraction
 807 of these cases decreases as the momentum of the two muons increases. The isolation require-
 808 ment imposed on dimuon candidates and a sufficiently broad upper mass bound used to form
 809 muon-jets ensures that the two dimuons always come from two well separated b -jets.

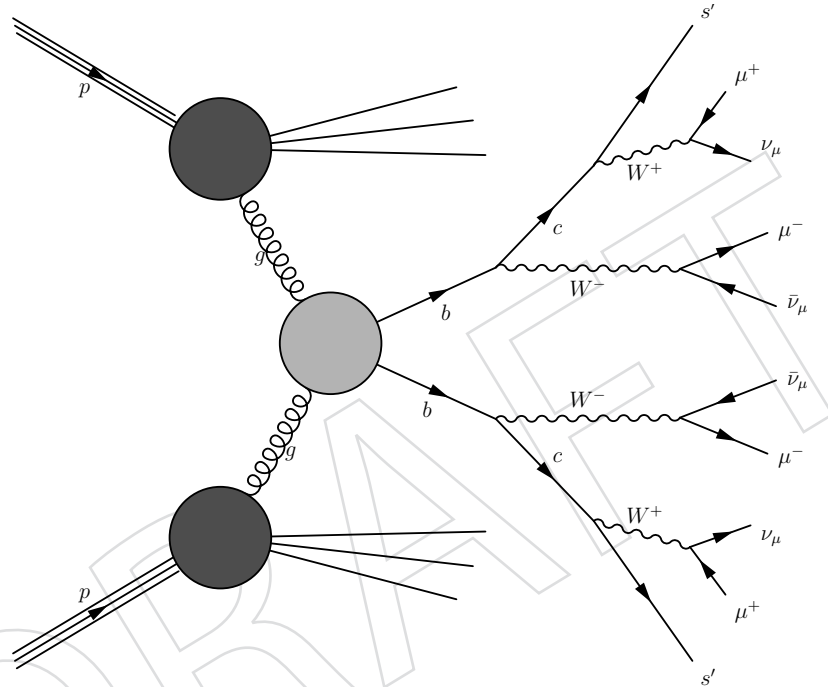


Figure 29: Example Feynman diagram of a four-muon event through $b\bar{b}$ pair production in which both b quarks decay double semi-leptonically.

810 **Modeling of the $b\bar{b}$ Background Shape.** In this analysis the data in the diagonal signal corri-
 811 dor in the plane of the two dimuon masses ($m_{di-\mu_1}, m_{di-\mu_2}$) is fitted with a sum of signal and
 812 background 2D templates. The signal normalization is allowed to float with the size of a pot-
 813 tential signal, while the background template has its normalization constrained using data in
 814 the “off-diagonal” portion (background-enriched region) of the ($m_{di-\mu_1}, m_{di-\mu_2}$) distribution.
 815 The modeling of the 2D signal shape is straightforward and is discussed in the Subsection 5.
 816 The modeling of the 2D shape for the background distribution in the ($m_{di-\mu_1}, m_{di-\mu_2}$) plane
 817 covering both the signal “corridor” and the “off-diagonal” part of the square ($0.2 < m_{di-\mu_1} <$
 818 $9 \text{ GeV}/c^2$, $0.2 < m_{di-\mu_2} < 9 \text{ GeV}/c^2$) is described in this Section.

819 Naïvely, because each b -quark decays independently of the other, the 2D background template
 820 can be modeled by a Cartesian product of two identical 1D mass templates describing the
 821 dimuon distribution in b -jets that happen to have two muons in them. However, the shape
 822 of dimuon invariant mass depends on the momentum thresholds used to select muons and
 823 whether the muons come from the barrel or from the endcap owing to different resolutions in
 824 the two systems. In the analysis at least one of the dimuons was required to contain at least one

825 muon with $p_T > 17 \text{ GeV}/c$ within $|\eta| < 0.9$, while the muons in the other dimuon only required
 826 to have $p_T > 8 \text{ GeV}/c$ and can be either in the barrel or the endcap $|\eta| < 2.4$. Therefore, there
 827 is a natural division of the dimuons into “high- p_T ” and “low- p_T ” types depending on whether
 828 they contain a quality muon with $p_T > 17 \text{ GeV}/c$ in the barrel $|\eta| < 0.9$ or they don’t. As
 829 these distributions may have somewhat different shapes, these 1D mass templates need to be
 830 obtained separately for each type and then properly convoluted building a 2D template.

831 In the analysis it is defined that background dimuons of the “high- p_T ” type have their invariant
 832 mass distribution following 1D shape $S_{17}(m_{di-\mu})$, while dimuons of the “low- p_T ” type have
 833 1D shape $S_8(m_{di-\mu})$. When filling the 2D distribution of dimuon masses $S(m_{di-\mu_1}, m_{di-\mu_2})$ (or
 834 $S(m_1, m_2)$ for short, where $m_1 = m_{di-\mu_1}$ is mass plotted against horizontal axis and $m_2 = m_{di-\mu_2}$
 835 is mass plotted against vertical axis), only two following situations can happen:

- 836 1. Only one dimuon is of the “high- p_T ” type (contains a quality muon with $p_T > 17 \text{ GeV}/c$
 837 within $|\eta| < 0.9$) and the other dimuon is of the ‘low- p_T ’ type. In this case the mass of
 838 the “high- p_T ” dimuon is taken as m_1 and the mass of the “low- p_T ” dimuon is taken as m_2
 839 resulting in the following 2D mass template: $S_{17}(m_1) \times S_8(m_2)$.
- 840 2. Both dimuons are of the “high- p_T ” type. In this case the dimuons are randomly assigned
 841 to be on m_1 or m_2 axis of the 2D distribution resulting in the following 2D mass template:
 842 $S_{17}(m_1) \times S_{17}(m_2)$.

If the rates of events entering the final distribution in the first and second category is $N_{8,17}$ and $N_{17,17}$, respectively, the normalized shape of the resultant 2D distribution is as follows:

$$S(m_1, m_2) = \frac{N_{17,8}}{N_{17,8} + N_{17,17}} \cdot [S_{17}(m_1) \times S_8(m_2)] + \frac{N_{17,17}}{N_{17,8} + N_{17,17}} \cdot [S_{17}(m_1) \times S_{17}(m_2)]. \quad (17)$$

The 2D distribution can be factorized:

$$S(m_1, m_2) = S_{17}(m_1) \times \left[\frac{N_{17,8}}{N_{17,8} + N_{17,17}} \cdot S_8(m_2) + \frac{N_{17,17}}{N_{17,8} + N_{17,17}} \cdot S_{17}(m_2) \right] \quad (18)$$

843 Note, the 2D distribution is a Cartesian product of the mass distribution S_{17} for “high- p_T ” type
 844 of dimuons and the proper mix S_{mix} of the mass distributions S_{17} and S_8 for “high- p_T ” and
 845 “low- p_T ” types of dimuons:

$$S(m_1, m_2) = S_{17}(m_1) \times S_{mix}(m_2), \quad (19)$$

846 which can be used as a recipe in building the background 2D template of the analysis.

847 To construct the background templates S_{17} and S_{mix} , background-enriched events in the topol-
 848 ogy containing exactly one dimuon and one orphan muon were used. These events are col-
 849 lected using the same trigger and exact same definitions as in the main analysis, except with
 850 three muons instead of four. This data is also heavily dominated by $b\bar{b}$ events and the topol-
 851 ogy and kinematics of these events are nearly identical to the events entering sample with
 852 two dimuons. Note that the mass range for the signal region is limited to 8.5 GeV. Thus, only
 853 dimuon resonances signalling b quark or light meson decay are expected.

854 To obtain the shape S_{17} , only events where the dimuon is of the “high- p_T ” type (contains a
 855 quality muon with $p_T > 17 \text{ GeV}/c$ within $|\eta| < 0.9$) were selected (the “orphan” muon is
 856 therefore only required to have $p_T > 8 \text{ GeV}/c$). The shape of the invariant mass distribution of

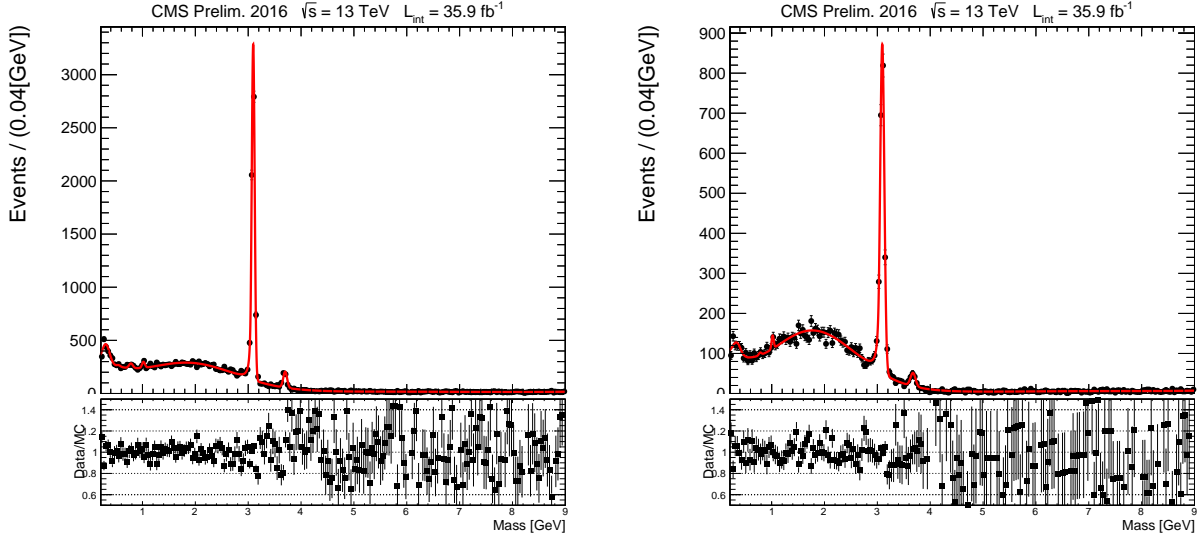


Figure 30: The S_{17} (top left) and S_{mix} (top right) templates (solid lines) for dimuons obtained with background-enriched data (solid circles) samples. The pull distribution of S_{17} and S_{mix} are shown bottom left and bottom right respectively.

the dimuons in the selected events is shown in Fig. 30 (left). In the second case, to obtain the shape S_{mix} , only events where the “orphan” muon was a quality muon with $p_T > 17 \text{ GeV}/c$ within $|\eta| < 0.9$ were selected (both muons in the dimuon are therefore only required to have $p_T > 8 \text{ GeV}/c$). The corresponding shape of the invariant mass distribution of the dimuons in the selected events is shown in Fig. 30 (right). The resulting dimuon mass distribution contains proper fraction of both “high- p_T ” and “low- p_T ” dimuons. One could split these events depending on whether the dimuon contains a muon with $p_T > 17 \text{ GeV}/c$ within $|\eta| < 0.9$ or not and measure S_8 , but it turns out to be not necessary. If one compares the topology of these events with that of the signal events with two dimuons, the fractions containing “high- p_T ” and “low- p_T ” dimuons in this sample should come out to be exactly the same, as both come from $b\bar{b}$ events in the same topology and kinematic conditions. Therefore, the obtained shape is exactly the same shape as S_{mix} in Eq. (19). The final 2D template is thus a Cartesian product of distributions S_{17} shown in Fig. 30 (left) and S_{mix} shown in Fig. 30 (right). While both shapes are fairly similar, one can notice that the distribution in Fig. 30 (right) has a slightly enhanced “bulk” component and slightly broader shape of the resonances (compare, for example, widths of J/ψ in the two cases). This is consistent with the expectation as the dimuons in this case are on average less energetic and a fraction of them fall into the endcap region of the CMS.

Parametrization of the Background Template. For convenience of future use of the templates in the final fit, the template shapes shown in Fig. 30 (left) and (right) are fitted with a parametric

analytical function using an extended unbinned likelihood fit:

$$\begin{aligned}
BG(m; p_\eta, p_\omega, p_\phi, p_{J/\psi}, \alpha_{J/\psi}, \sigma_{J/\psi}, p_\psi, p_B, p_{06}, \dots, p_{66}) \\
= p_\eta G(m; m_{0,\eta}, \sigma_\eta) + p_\omega G(m; m_{0,\omega}, \sigma_\omega) \\
+ p_\phi G(m; m_{0,\phi}, \sigma_\phi) + p_\psi G(m; m_{0,\psi}, \sigma_\psi) \\
+ p_{J/\psi} CB(m; m_{J/\psi}, \sigma_{J/\psi}, \alpha_{J/\psi}, n_{J/\psi}) \\
+ p_B B(m; p_{06}, \dots, p_{66}) \\
+ p_{AH} G(m; m_{0,AH}, \sigma_{AH}) \\
+ p_{E0} \left[\left(\frac{p_{E0}}{m} \right)^2 - 1 \right]^{p_{E1}} \times \exp \left[-p_{E2} \left[\left(\frac{p_{E0}}{m} \right)^2 - 1 \right] \right]
\end{aligned}$$

where η , ω , ϕ , and ψ resonances are parametrized using $G(m; m_0, \sigma)$, a Gaussian normalized to a unit integral in the region $0.25 < m < 9$ GeV/c². For each, m_0 is fixed to the corresponding PDG mass and σ (resolution) is fixed to the detector resolution. The mass (resolution) values are 0.548 (0.030) GeV for η , 0.782 (0.031) GeV for ρ , 1.019 (0.033) for Φ , 3.095 (0.04) for J/ψ , and finally 3.7 (0.05) GeV for ψ .

The J/ψ resonance shape is parametrized with a Crystal Ball function, normalized to unit area in $0.25 < m < 9$ GeV/c². $m_{J/\psi}$ is fixed to the PDG value, $\sigma_{J/\psi}$, $\alpha_{J/\psi}$, $n_{J/\psi}$ are obtained in Sec. 5, $\sigma_{J/\psi}$ is allowed to float in the fits. The bulk shape is described using $B(m; p_{06}, \dots, p_{66})$, a series expansion in the Bernstein polynomial basis⁴ of power 6. A Gaussian complemented with a decaying exponential were added in the low mass region (< 0.5 GeV) to model kinematic bumps in the low mass region. The p_η , p_ω , p_ϕ , $p_{J/\psi}$, p_B , and parameters are normalization factors for the resonances, bulk component, respectively, and are obtained from the fit. Results of the fit are shown in Figs. 30 (left) and (right) as solid red lines.

The parameters returned by the fit are 23. The Bernstein function is formed by 8 parameters (normalization included), the exponential and the gaussian distributions that describe the very low mass part of the mass spectrum are described by 6 parameters. The J/ψ resonance is described by 4 parameters, and for the other SM resonances only the normalization is allowed to vary, except the ψ resonance, where also the width is free to vary, for a total of 5 additional parameters. The ChiSquare test have been performed and has returned a value of about 1.3 per each fit (divided by the number of degrees of freedom).

The parametrized functional dependencies are then used to construct the 2D template shown in Fig. 31. The corresponding uncertainties in the fit parameters are saved including full correlation information to be used in the final fit.

Normalization of the Background Template. The 2D template is then normalized in the region 0.25 to 9 GeV, such that

$$\int_{0.25}^9 dm_{\mu\mu_1} \int_{0.25}^9 dm_{\mu\mu_2} S_{17}(m_{\mu\mu_1}) \times S_{\text{mix}}(m_{\mu\mu_2}) = 1.$$

To estimate the background contribution in the signal region, we calculate the ratio of the template integral in the diagonal region over the off-diagonal region:

$$R = \frac{\int_{0.25}^9 dm_{\mu\mu_1} \int_{0.25}^9 dm_{\mu\mu_2} S_{17}(m_{\mu\mu_1}) \times S_{\text{mix}}(m_{\mu\mu_2}) \times \theta(|m_{\mu\mu_1} - m_{\mu\mu_2}| < 5\sigma(m_{\mu\mu}))}{\int_{0.25}^9 dm_{\mu\mu_1} \int_{0.25}^9 dm_{\mu\mu_2} S_{17}(m_{\mu\mu_1}) \times S_{\text{mix}}(m_{\mu\mu_2}) \times \theta(|m_{\mu\mu_1} - m_{\mu\mu_2}| > 5\sigma(m_{\mu\mu}))}$$

⁴E.g., see <http://www.idav.ucdavis.edu/education/CAGDNotes/Bernstein-Polynomials.pdf>. Bernstein basis polynomials are positive-definite, thus, by providing n non-negative coefficients we can get a well behaving p.d.f. approximation. We use RooFit's implementation for Bernstein basis polynomials.

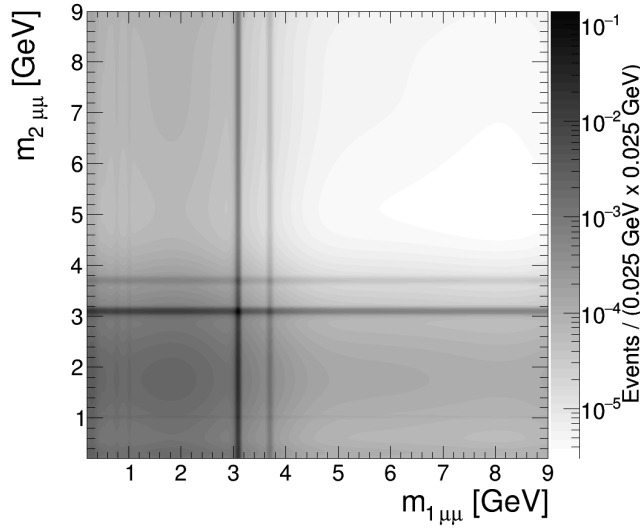


Figure 31: The 2D analytical template for distribution of the dimuon masses obtained using background-enriched data sample.

897 This ratio is calculated to be $R = 0.141291/0.8587$. A total of 56 events were observed in
 898 the off-diagonal region passing the signal selection. We can therefore estimate the number
 899 of background events passing the signal selection in the diagonal region as $N_{bb, \text{signal region}} =$
 900 $(56 \pm \sqrt{56}) \times 0.141291/0.8587 = 9.21 \pm 1.23$. Fig. 32 shows the background events in the off-
 901 diagonal sideband region overlayed on top of the 2D template.

902 **Validation of the Background Template.** To validate the technique, we return to the sample
 903 with two dimuons. The standard requirements were applied to select these events, except the
 904 isolation requirement for dimuons has been removed in this check to obtain a sample with
 905 large statistics. The diagonal region in the $(m_{di-\mu_1}, m_{di-\mu_2})$ plane has been excluded to avoid
 906 accidental unblinding of the analysis in case a large signal is present in data. Thus only the
 907 “non-diagonal” part of the 2D dimuon mass distribution was looked at in data.

908 In Fig. 33 (top, left) the 1D projection of this 2D distribution on horizontal axis m_1 is shown (as
 909 black dots) and compared to the corresponding template S_{17} (red line) obtained from background-
 910 enriched sample as described above. Also, in Fig. 33 (top, right) the 1D projection of the 2D
 911 distribution on vertical axis m_2 is shown (as black dots) and compared to the corresponding
 912 template S_{mix} (red line). Additionally, both 1D mass projections onto m_1 and m_2 axis were
 913 summed up (two entries per event) into one distribution for selected events as shown (black
 914 dots) in Fig. 33 (bottom) and compared to combined 1D template (red line) that comprises of
 915 both templates S_{17} and S_{mix} stacked together. Note, all 1D templates used for comparisons de-
 916 scribed above were normalized to number of selected events in the distributions obtained from
 917 data. All plots in Fig. 33 demonstrate good agreement between distributions obtained from
 918 events with two dimuons (no isolation requirement applied) and analytical templates obtained
 919 from background-enriched events with one dimuon and one “orphan” muon.

920 As additional test to confirm the stability of the $b\bar{b}$ estimation, we performed the same pro-
 921 cedure relaxing the isolation cut on the dimuon from 2 GeV to 5, 10, and 50 GeV in the Con-
 922 trol Region. For each different isolation cut, we recompute the template and the final number
 923 of $b\bar{b}$ events expected in the signal region. The initial number of 9.21 ± 1.23 varied for each
 924 different isolation threshold to 9.03 ± 1.162 , 8.74 ± 1.093 , and 7.88 ± 0.965 . Despite the dimuon

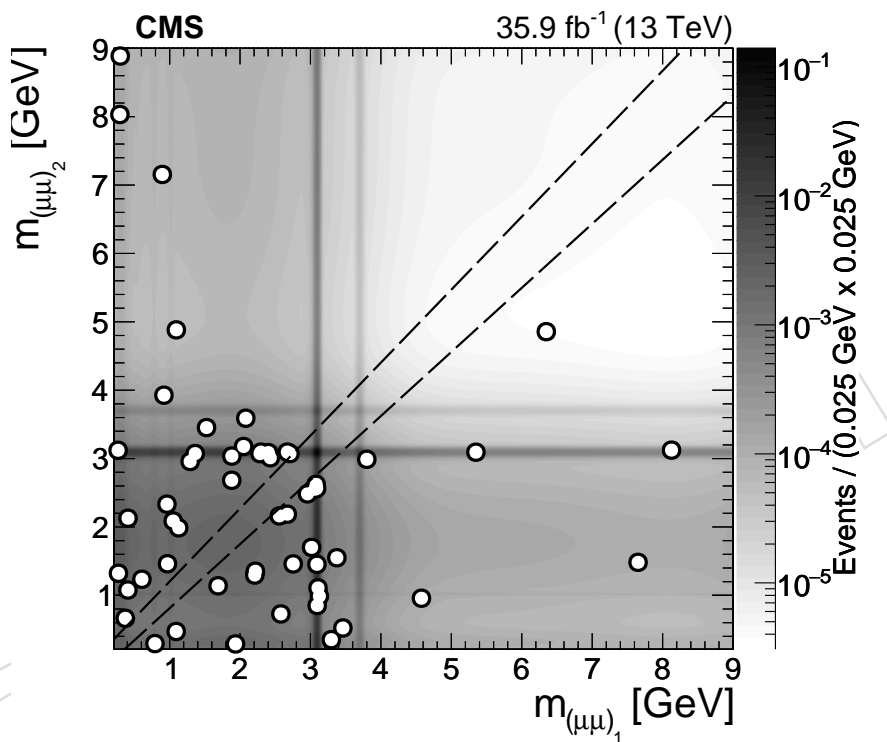


Figure 32: Distribution of the invariant masses $m_{\mu\mu_1}$ vs. $m_{\mu\mu_2}$ for the isolated dimuon systems for the 56 events in the data (shown as empty circles) surviving all selections but failing the $m_{\mu\mu_1} \simeq m_{\mu\mu_2}$ masses consistency requirement. The diagonal signal region $m_{\mu\mu_1} \simeq m_{\mu\mu_2}$ (outlined with dashed lines) remains blind.

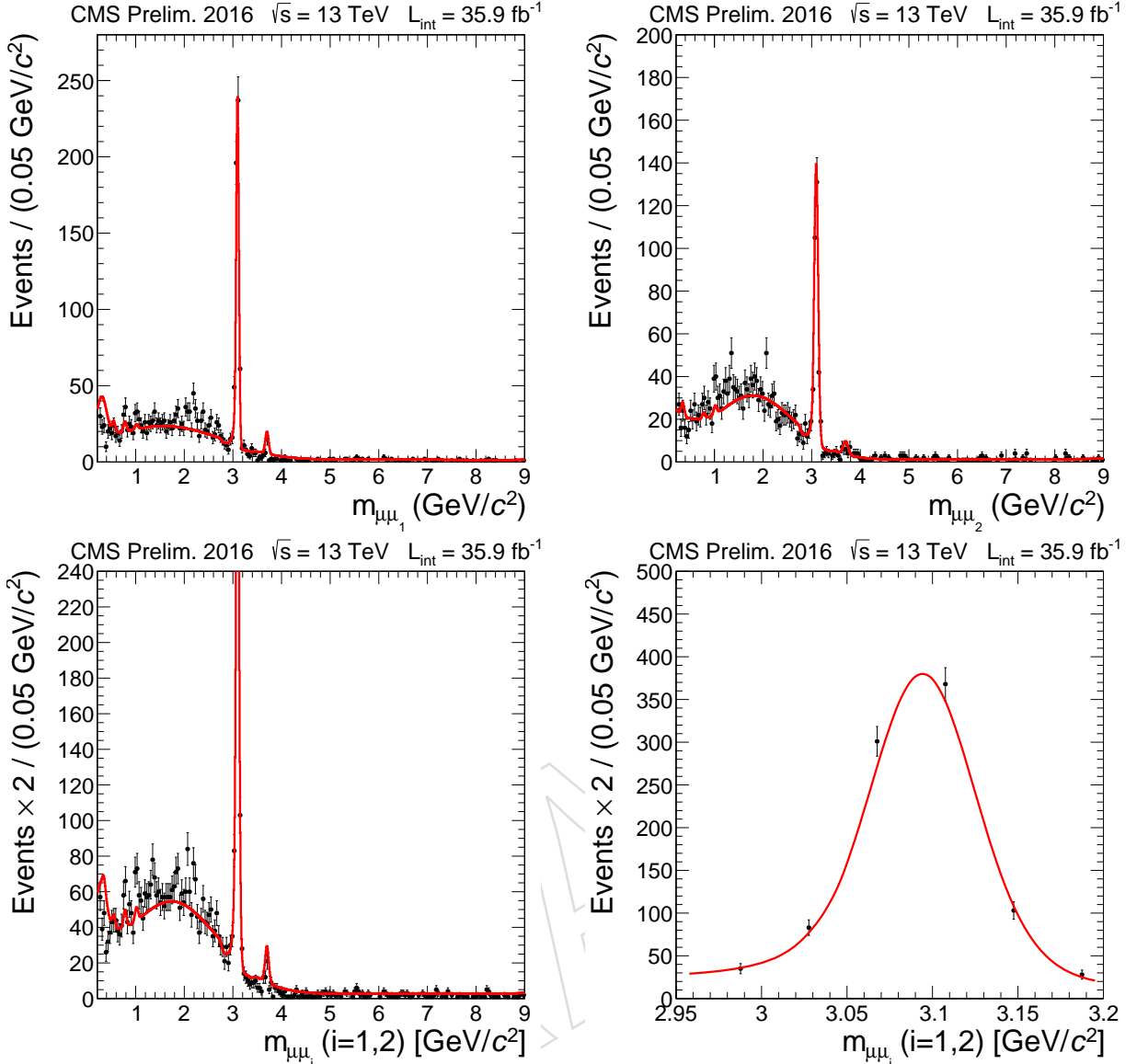


Figure 33: Comparison of the data (solid circles) failing the $m_{\mu\mu_1} \simeq m_{\mu\mu_2}$ requirement in the control sample where no isolation requirement is applied to reconstructed dimuons with the prediction of the background shape model (solid line) scaled to the number of entries in the data. Top, left: distribution for $m_{\mu\mu_1}$. Top, right: distribution for $m_{\mu\mu_2}$. Bottom, left: combined distribution for $m_{\mu\mu_1}$ and $m_{\mu\mu_2}$ (two entries per event). Bottom, right: combined distribution for $m_{\mu\mu_1}$ and $m_{\mu\mu_2}$ in vicinity of J/ψ resonance.

invariant mass is expected to be affected by the isolation cut, the final estimation is consistent within their uncertainty, and we assign a conservatively of 20% on the number of $b\bar{b}$ estimated in the signal region. Thus the $b\bar{b}$ contribution in the signal region is expected to be 9.21 ± 1.23 (stat.) ± 1.84 (syst.) or 9.21 ± 2.21 (stat + syst.).

929 6.3 QCD Prompt $pp \rightarrow 2J/\psi \rightarrow 4\mu$ Background

930 There are two mechanisms for the production of prompt double J/ψ events: "Single" and the
 931 "Double" Parton Scattering (SPS and DPS respectively). In the case of SPS two J/ψ mesons are
 932 produced from a single parton scattering, while for DPS each J/ψ originates from an indepen-
 933 dent parton interaction. If the two J/ψ both decay to a pair of opposite sign muons the final
 934 state topology mimics our analysis signal.

935 Figure 34 shows an example SPS process. Two partons scatter off colliding protons and fuse
 936 into two J/ψ mesons which decay into two muon pairs. Figure 35 shows an example DPS
 937 process. Each proton radiates two partons each which fuse into two J/ψ mesons.

938 The production of prompt" double J/ψ events has been measured in other experiments, for
 939 instance the LHCb collaboration reported the measurement of the cross section in a four muon
 940 final state using 35.4 pb^{-1} and a center of mass collision energy of 7 TeV, and a method to
 941 separate the contribution of SPS and DPS processes was proposed [77].

942 While a better understanding of the DPS mechanism constitutes a very active topic of study
 943 for the LHC collaborations, for this analysis the main goal is to have a reliable estimate of the
 944 contribution of double J/ψ events in the signal region. In order to have sufficient statistics for
 945 this background to be estimated a control sample was selected in which the content of double
 946 J/ψ events in data is enhanced.

947 Double J/ψ control sample

948 The object and event selections for this control sample was designed to be as similar as possible
 949 to the standard signal selection procedure. The specific requirements for this control sample
 950 are:

- 951 1. **Trigger:** Events are selected with HLT_Dimuon0_Jpsi_Muon, a dedicated trigger for B-
 952 Physics studies. This trigger requires the presence of at least three offline muon candi-
 953 dates, two of which have a common vertex and an invariant mass consistent with the J/ψ
 954 particle.
- 955 2. **Muon ID:** The Particle Flow muon reconstruction algorithm was used (as in the main
 956 analysis), but with a relaxed cut on the muon transverse momentum ($p_T > 3.5 \text{ GeV}$).
- 957 3. **Dimuon labeling:** For this control sample there is no distinction between di- μ_1 and di- μ_2 . The label is assigned randomly a high- p_T muon is not required to be in the event
 958 (from the trigger point of view) and also to avoid introducing a bias into any of the
 959 distributions, such as the dimuon isolation.
- 960 4. **Dimuon isolation:** The same definition as in the standard analysis selection (Section 4).
 At this preselection step there is no explicit cut on the dimuon isolation distribution since
 this is one of the variables that will be used to separate the contribution of "prompt" and
 "non-prompt" (from b -decay) J/ψ 's in data.

965 Monte Carlo distributions for DPS and SPS

966 It is hard to distinguish between J/ψ 's originating from DPS and SPS processes since both
 967 production mechanisms have similar isolation and invariant mass distributions, as shown in
 968 Figure 36. Distributions for dimuon displacement, leading muon transverse momentum and
 969 the rapidity difference between dimuons is shown in Figure 37. It is clear that the rapidity

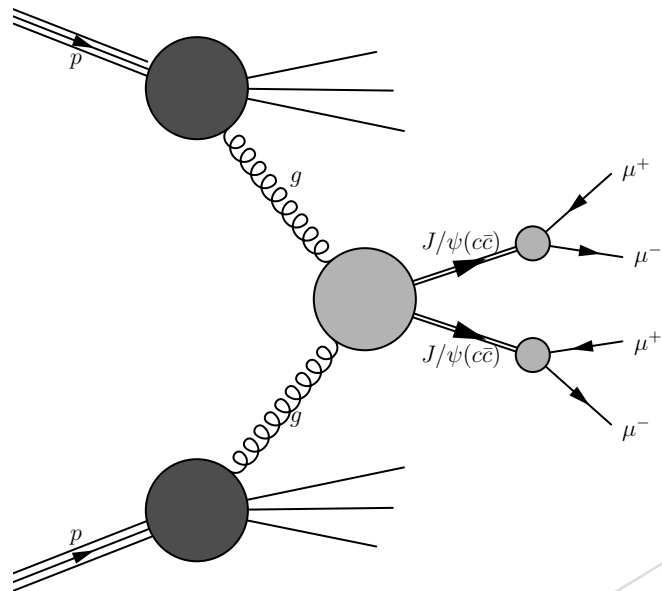


Figure 34: Diagram of prompt double J/ψ production to four muons through SPS.

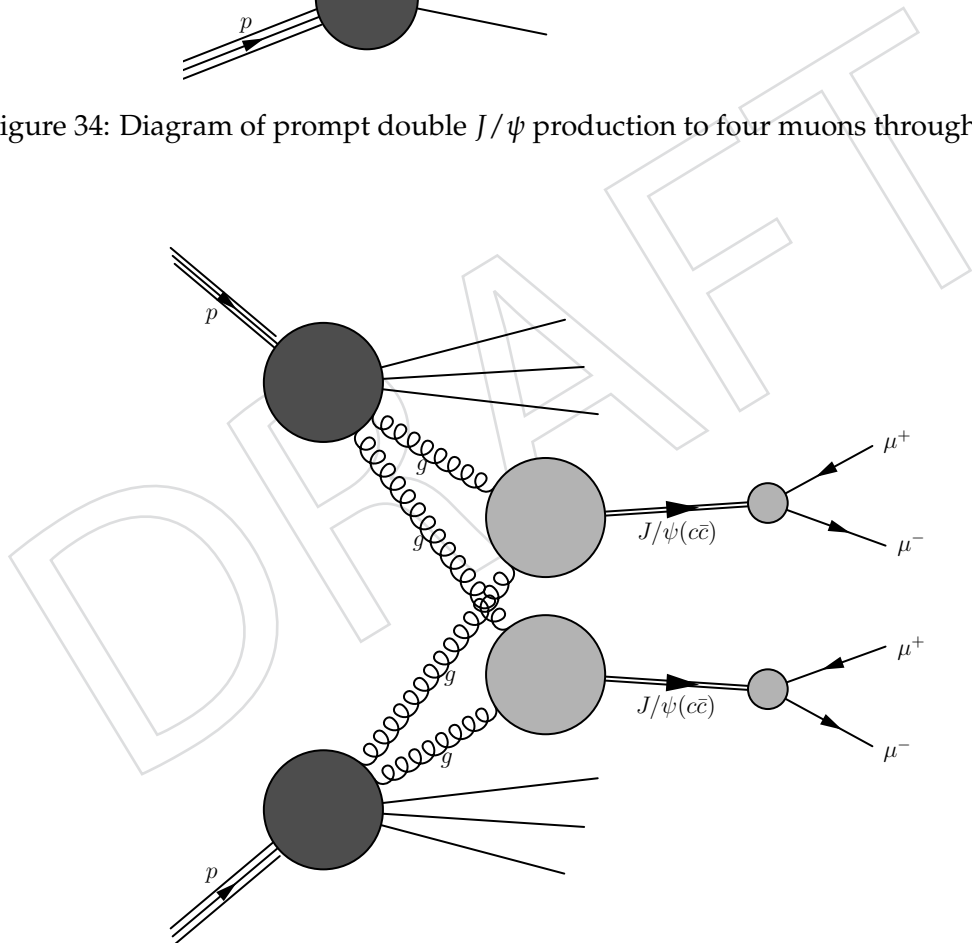


Figure 35: Diagram of prompt double J/ψ production to four muons through DPS.

970 difference is a much better discriminator between the DPS and SPS processes, than any other
971 variable.

972 **Additional cleaning cut in data**

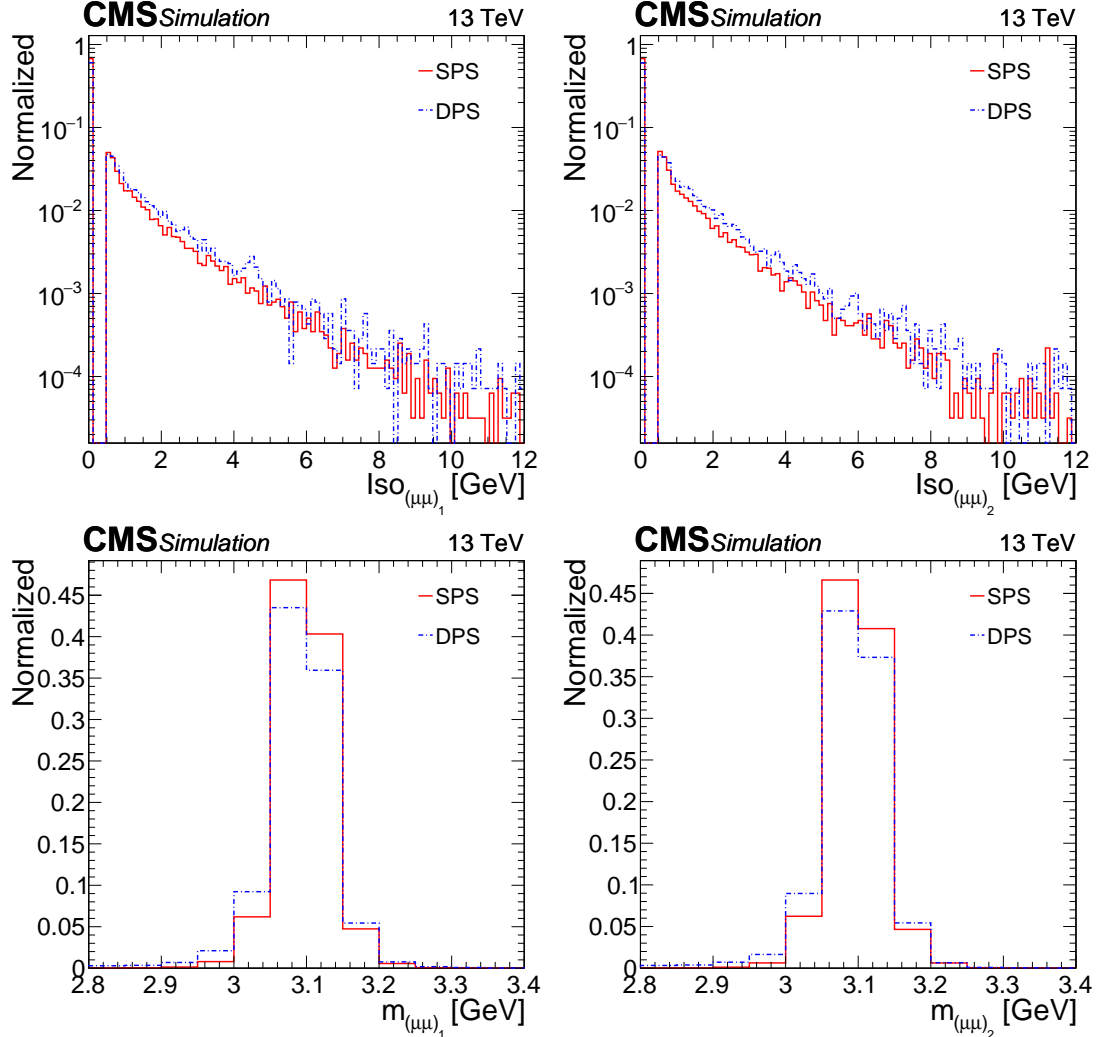


Figure 36: Comparison of several kinematic distributions for the SPS and DPS MC samples. Top left: $(\mu\mu)_1$ isolation. Top right: $(\mu\mu)_2$ isolation. Bottom left: $(\mu\mu)_1$ mass. Bottom right: $(\mu\mu)_2$ mass.

The data sample analyzed here is the MuOnia Primary Dataset, which is a sample that was selected via a set of triggers designed for B-Physics studies. After applying the control sample selection requirements to the data the composition of events is a mixture of "prompt" and "non-prompt" double J/ψ 's and non-resonant muon pairs coming from the semileptonic decay of b -quarks. To further clean the data and increase the content of double J/ψ events a cut on the invariant mass of both dimuons is imposed. Specifically, only events in which both dimuons have a mass between 2.8 and 3.3 GeV are selected. This is shown in the two dimensional plot in Figure 38. This requirement reduces the fraction of events not corresponding to genuine double J/ψ 's and avoids the possibility of having trigger "volunteers". After applying this requirement and looking at the isolation distribution of each dimuon (shown in Figure 38) it is clear that the data is now composed of events with "prompt" and "non-prompt" J/ψ 's. Even in the isolated region ($\text{Iso}_{\mu\mu_1, \mu\mu_2} < 2$ GeV) we expect a non-negligible contribution of "non-prompt" processes. For this specific background study we are only interested in the "prompt" component because the "non-prompt" background is estimated via the method described in Section 6.2. Thus, the "non-prompt" events have to be subtracted from the data. In order to do this, the so-called "ABCD" method is used which makes use of two uncorrelated variables with

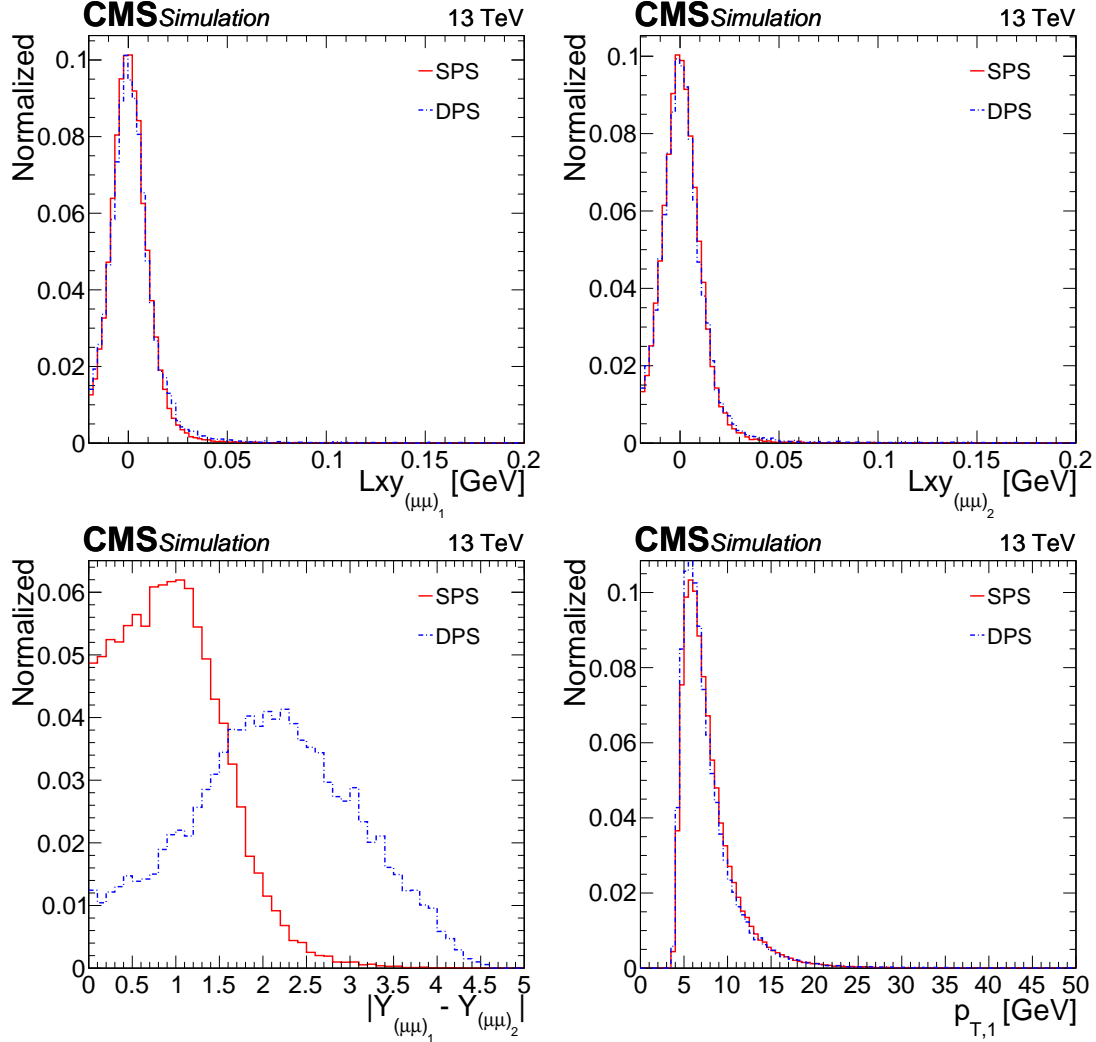


Figure 37: Comparison of several kinematic distributions for the SPS and DPS MC samples. Top left: Corrected $(\mu\mu)_1$ displacement L_{xy} . Top right: Corrected $(\mu\mu)_2$ displacement L_{xy} . Bottom left: $|Y_{(\mu\mu)_1} - Y_{(\mu\mu)_2}|$. Bottom right: Leading muon p_T .

discriminating power between the two processes. The ABCD method provides an accurate estimation of prompt and non-prompt contributions in data and is consistent with the results seen in the previous iteration of this analysis [54].

Separation of "prompt" and "non-prompt" J/ψ 's in data

ABCD method. This method relies on the discrimination power of two uncorrelated (or "weakly" correlated) variables, and for this specific case the dimuon isolation distributions were chosen because they provide a clear discrimination between "prompt" and "non-prompt" processes. This method works as follows:

- After the control sample cuts and dimuon invariant mass constraint is applied to data the isolation distributions of di- μ_1 and di- μ_2 are used to discriminate between the "prompt" and "non-prompt" contributions. For this method to be valid the variables should have at most a weak correlation. The correlation was estimated with the ROOT function GetCorrelationFactor. This function returns a number between 0 (no correlation between the variables) and 1 (full correlation). In the case of the dimuon isolation distributions the

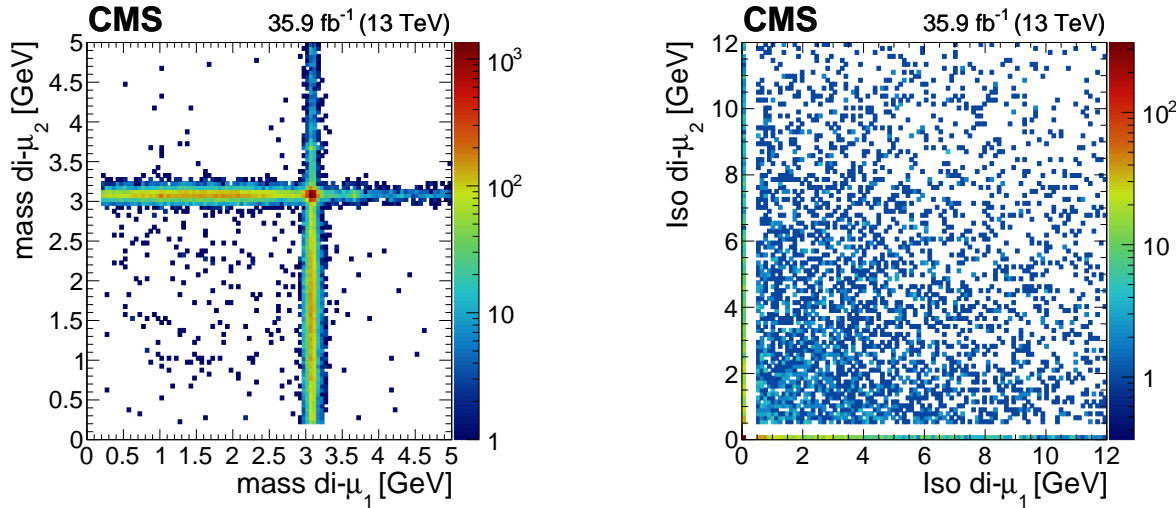


Figure 38: Left: Invariant mass distributions for di- μ_1 and di- μ_2 in data after applying the control sample cuts. The long tails correspond to J/ψ 's coming from b-decays or non-resonant dimuon pairs from semileptonic decays of b-quark. Only events in which the dimuon invariant mass is between 2.8 and 3.3 GeV are selected (events inside the box). Right: Isolation distribution for di- μ_1 and di- μ_2 after applying control sample cuts and the invariant mass constraint.

correlation was found to be 0.13, and according to this result the variables are "weakly" correlated and the next step of the ABCD method may be applied.

2. The events are then divided into four independent regions (labeled A, B, C, and D) based on the isolation distribution values, as shown in Figure 39. In region A both dimuons have an isolation value of $Iso_{\mu\mu_{1,2}} < 2$ GeV, and this corresponds to the cut used in the signal region. Regions B, C, and D act as non-isolated sidebands and are used to extrapolate the content of the "non-prompt" contribution into region A. A maximum isolation value of 12 GeV was imposed to both dimuons to avoid any effects from highly non-isolated dimuons.
3. The assumption is that for isolation values > 2 GeV the data is composed mostly of J/ψ 's from b-decays. This is a reasonable assumption as shown in Figure 39 where for the case of the SPS "prompt" double J/ψ Monte Carlo sample most of the events are located inside of the isolated region (region A). The relatively small "prompt" contamination in regions B, C, and D was studied and it was concluded that its impact on the final result is negligible.
4. If all the previous points are satisfied the following expressions must hold.

$$\frac{N_{A_{non-prompt}}}{N_B} \sim \frac{N_D}{N_C}, \quad (20)$$

$$N_{A_{non-prompt}} = N_B \times \frac{N_D}{N_C}, \quad (21)$$

$$N_{A_{prompt}} = N_A - N_{A_{non-prompt}} = N_A - N_B \frac{N_D}{N_C}, \quad (22)$$

where:

N_A : Number of data events in region A.

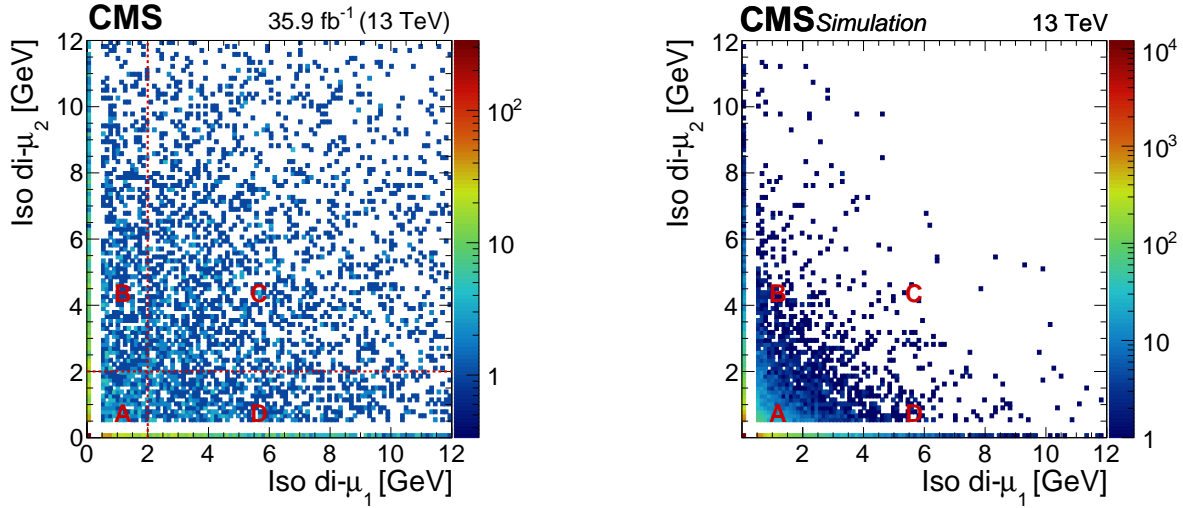


Figure 39: Left: Isolation distributions for di- μ_1 and di- μ_2 in data. The events are divided into four independent regions. Right: Isolation distributions for di- μ_1 and di- μ_2 for the SPS Monte Carlo sample where most of the events are located in the isolated region (< 2 GeV).

- 1021 N_B : Number of data events in region B.
- 1022 N_C : Number of data events in region C.
- 1023 N_D : Number of data events in region D.
- 1024 $N_{A_{non-prompt}}$: Estimated number of events with "non-prompt" J/ψ 's in region A.
- 1025 $N_{A_{prompt}}$: Estimated number of events with "prompt" J/ψ 's in region A.

- 1026
- 1027 5. Following the equations in step 4, the content of data events in each one of the four
- 1028 regions is presented in table 8 and the estimated contribution of "prompt" and "non-
- 1029 prompt" processes in region A is presented in table 9.

N_A	N_B	N_C	N_D
1219	1232	1999	1313

Table 8: Content of events in data for regions A,B,C, and D where the regions are defined as in Figure 39

$N_{A_{prompt}}$	$N_{A_{non-prompt}}$
$409.79 \pm 50.76(\text{stat}) \pm 61.79(\text{syst})$	809.21 ± 36.85

Table 9: Estimation of "prompt" and "non-prompt" contribution into region A, results obtained following the expressions in 22, the first uncertainty is the statistical uncertainty after correct error propagation, the second uncertainty is the systematical one which was obtained by varying the non-isolated sideband region and observing an effect of around 15% in the final result

- 1030 An alternative method to separate the "prompt" and "non-prompt" J/ψ contributions was
- 1031 also studied, and this method uses information about the dimuon lifetime (via the " L_{xy} " vari-
- 1032 able) as the discriminant. The assumption in this case is that J/ψ 's coming from b -decays will
- 1033 have a relatively larger lifetime than those "promptly" produced. As mentioned previously,

1034 in region A ($\text{Iso}_{\mu\mu_{1,2}} < 2 \text{ GeV}$) the data is composed of "prompt" and "non-prompt" double
 1035 J/ψ events. In order to find the contribution of each process the "prompt" lifetime template
 1036 was obtained, using the double J/ψ Monte Carlo samples (SPS and DPS give similar results),
 1037 while for the "non-prompt" contribution the template can be taken from the data using the
 1038 non-isolated sideband region (Region "C" in "ABCD" method). The results from this method
 1039 are presented in appendix D and are compatible within uncertainties to the ones obtained with
 1040 ABCD method.

1041 Separation of DPS and SPS contribution

1042 The next step after the separation of the "prompt" and "non-prompt" contributions in data
 1043 is to find what percentage of the "prompt" events correspond to the DPS and SPS production
 1044 mechanisms. This percentage can be obtained by fitting the SPS and DPS Monte Carlo template
 1045 to the data in region A. To do this we use the variable previously identified as that which offers
 1046 the best discriminating power (the rapidity difference) between the processes. Before applying
 1047 the fit of the rapidity difference the "non-prompt" component should be subtracted from the
 1048 distributions. The rapidity distributions for DPS, SPS and data is show in Figure 40 (left) and
 1049 the combined fit result in Figure 40 (right). The contribution of the DPS process corresponds to
 1050 $f_{DPS} = 0.38 \pm 0.02$, and the SPS contribution to $f_{DPS} 0.60 \pm 0.03$.

1051 Extrapolation of Double J/ψ events from control sample to "Signal" Region

1052 The information obtained from the control sample can then be used to get an estimation of the
 1053 number of double J/ψ events in the signal region using the following relations:

$$N_{DATA_{DPS}}(SR) = N_{MC_{DPS}}(SR) \times \frac{f_{DPS} * N_{DATA}(CR)}{N_{MC_{DPS}}(CR)}, \quad (23)$$

$$N_{DATA_{SPS}}(SR) = N_{MC_{SPS}}(SR) \times \frac{(1 - f_{DPS}) * N_{DATA}(CR)}{N_{MC_{SPS}}(CR)}, \quad (24)$$

1054 where:

- 1055 • $N_{MC_{DPS,SPS}}(SR)$: The number of Monte Carlo events surviving after applying "sig-
 1056 nal" region cuts to the SPS and DPS samples.
- 1057 • $N_{DATA}(CR)$: The estimated number of "prompt" double J/ψ events in data for the
 1058 control sample.
- 1059 • $N_{MC_{DPS,SPS}}(CR)$: The number of Monte Carlo events after applying control sample
 1060 cuts to SPS and DPS samples.
- 1061 • f_{DPS} : The fraction of "prompt" double J/ψ 's corresponding to the DPS process.

1062 The results are reported in table 10, from which we may conclude that the total contribution
 1063 from "prompt" double J/ψ events into the signal region is 0.33 ± 0.08 events.

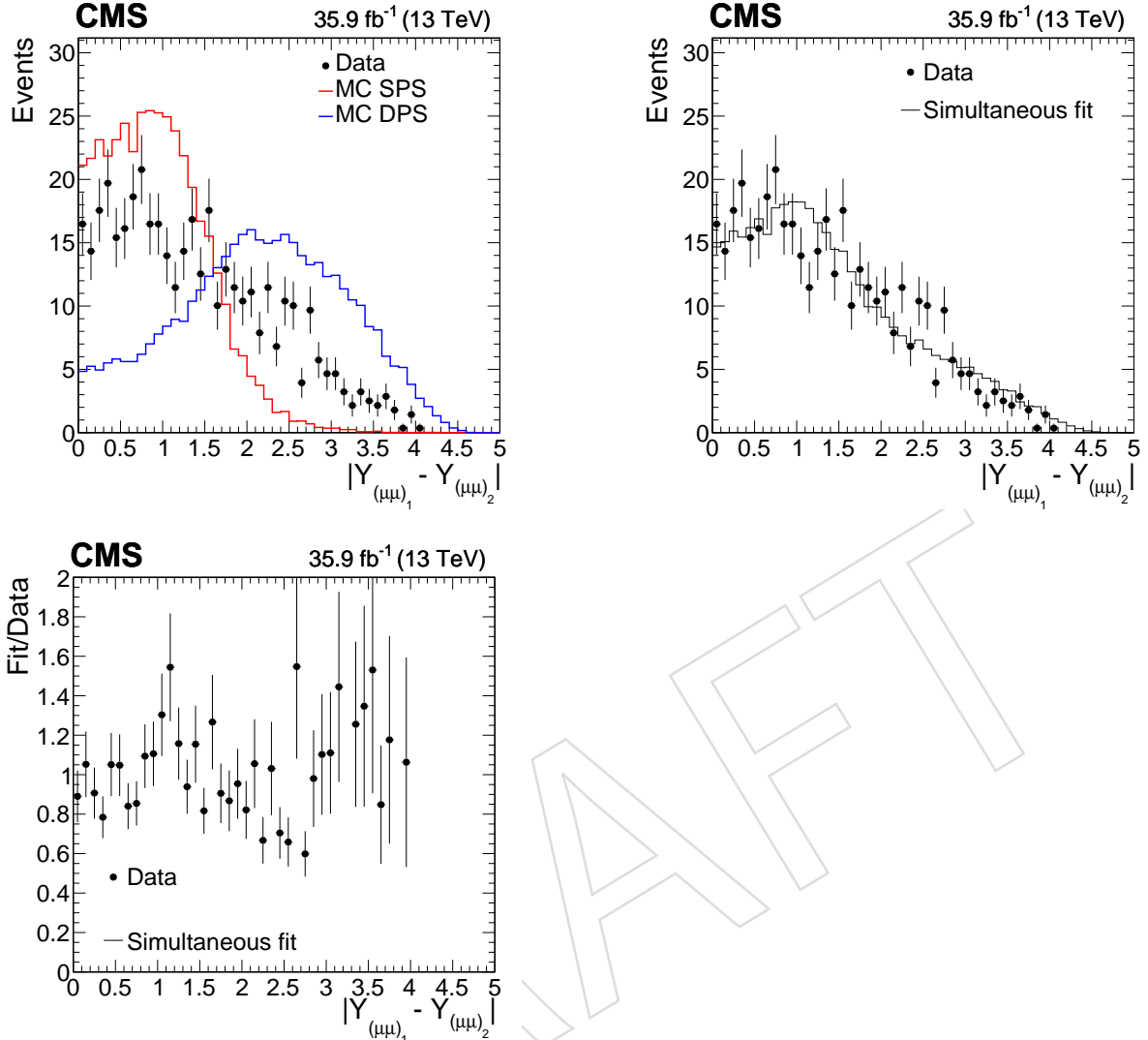


Figure 40: Left: Rapidity distribution for DPS, SPS and data normalized to number of entries in data. Right: Combined fit to data in order to extract the percentage contribution from DPS and SPS processes.

Process	$N_{MC}(SR)$	$\frac{N_{DATA}}{N_{MC}} (\text{CR})$	f	$N_{DATA} (\text{SR})$
DPS	5 ± 2.2	0.010 ± 0.002	0.40 ± 0.03	0.02 ± 0.01
SPS	27 ± 5.2	0.019 ± 0.003	0.60 ± 0.03	0.31 ± 0.08

Table 10: Summary table showing the estimate of DPS and SPS double J/ψ events into the "signal" region combining information from control sample and "signal" region and using the expressions in Equation 24.

1064 6.4 Conclusions

1065 The total number of background events was estimated to be 9.90 ± 1.24 (stat.) ± 1.84 (syst.) in
1066 the signal region. The dominant contribution is b -quark pair production, while the other two
1067 backgrounds contribute equally. Note that, unlike b -quark pair production and prompt double
1068 J/ψ production, the electroweak background contribution is not resonant, i.e. it is spread out
1069 across the entire signal region.

DRAFT

7 Systematic Uncertainties

7.1 Instrumental Uncertainties

Luminosity. The uncertainty on the luminosity measurement is estimated as 2.5% as recommended by CMS Lumi POG. [78]

Muon trigger The trigger scale factor was estimated to be $93\% \pm 6\%$ (stat.) using the orthogonal method as described in Sec. 4.1.3.

Muon ID. The scale factor and its uncertainty for muon identification in data and MC have been provided by the Muon POG. Using the *Tag and Probe* tool as described in Appendix G, we assign a systematic uncertainty of 0.6% per muons by varying the function used to fit the dimuon invariant mass distribution.

Dimuon isolation. The isolation is driven by the underlying event activity. The isolation efficiency scale factor in our analysis has been computed using the *Tag and Probe* described in Appendix G. We find an uncertainty of 0.1% per dimuon.

Pileup. The systematic uncertainty due to mischaracterization of the pileup distribution in MC was evaluated using a luminosity-based pileup estimation method. First, per-bunch luminosities were obtained from pixel detector information. Next, the delivered and recorded luminosity were calculated in each lumisection (which is about 23 seconds of data taking with CMS). The number of expected pileup interactions was then obtained from the per-bunch luminosities, the information in each lumisection and the $p\bar{p}$ total inelastic cross section. The pileup distribution was derived for the nominal case with $\sigma(pp)_{\text{nom}} = 69.2$ mb. Similar pileup distributions were derived for data with a 5% shifted up cross section $\sigma(pp)_{\text{up}} = 65.8$ mb and 5% shifted down cross section $\sigma(pp)_{\text{down}} = 72.3$ mb. The three pileup distributions in data were normalized to unity and divided by the pileup distribution in MC. The effect on $\varepsilon_{\text{Full}}/\alpha_{\text{GEN}}$ for a representative MC sample was calculated for each of the three cases (-5%, 0%, and 5%). The greatest absolute difference in magnitude in $\varepsilon_{\text{Full}}/\alpha_{\text{GEN}}$ was taken as the uncertainty. With this method, the systematic uncertainty was measured to be 0.17%.

Reconstruction of close muons in the muon system. To account for correlated effects of muon reconstruction when two muons are close to each other in the muon system, we use the results of the studies in [55], where the systematic uncertainty associated with this effect was conservatively evaluated by comparing the difference per leg efficiency for cases with and without a nearby muon present (so called crossing and non-crossing topologies), which yielded a systematic uncertainty of 1.3% per muon in the endcap region only. No such effect was observed in the barrel region. As in our events there is at most one dimuon in the endcap region, we assign the uncertainty of 2.6% per event to account for the uncertainties in reconstructing muons with overlapping trajectories in the muon system. There is only one relevant difference between muon identifications requirements in this analysis and in [55], which is the requirement on the number of muon stubs per muon (at least two in this analysis, at least three in [55]). As the muon reconstruction is unchanged, it is only a matter of what muons each analysis picks out of the pool of reconstructed muons. As this analysis has looser requirement, the importance of the effect of nearby muons only becomes smaller (we find all muons that would have been found by [55] and more, which makes the loss of efficiency due to overlaps smaller). Therefore, the uncertainty of 2.6% per event is a conservative estimate of the effects related to overlaps in the muon system.

Reconstruction of close muons in the tracker. In [55], a potential effect related to tracking was identified as low mass muon pairs at sufficiently high momentum can stay very close in the

tracking volume leading to reduced efficiency of reconstructing both tracks in the dimuon, due to merging of tracker hits into clusters. The assumption was that if the track hits size is larger in data than in the simulation by 20%, merging will be happening more frequently in data leading to lower efficiency to reconstruct both muons. As varying hit resolutions in simulation is a complicated endeavor, an easier but equivalent solution is to vary the momentum of the dimuons by the same 20%, which makes trajectories 20% closer and comparing efficiencies. We compared these efficiencies for reconstructed dimuons with transverse momenta from 16 to 60 GeV/c (typical in the current analysis) using Fig. 7 in [55]. As a result, the corresponding systematic uncertainty was estimated as 1.2% per dimuon.

Dimuons mass consistency: $m_{\mu\mu_1} \simeq m_{\mu\mu_2}$. To estimate the effect, the parameters of the Crystal Ball fit to J/ψ events in data (we use the background enriched sample of dimuon and orphan) were deviated within the fit statistical uncertainties on the parameters. Assuming that the distribution of signal events is similar to obtained template the corresponding deviation 1.5% in the acceptance within signal region was calculated and assigned as systematic uncertainty of this effect.

NNLO Higgs p_T re-weighting: The signal samples used in this analysis were produced at NLO and therefore it was important to estimate the effect of re-summation and to account for the effect that possible changes to the shape of the Higgs p_T could have for the kinematics and therefore acceptance. In order to do this, we used NNLO re-weighting functions with respect to the Higgs p_T to evaluate changes in the signal acceptance after all selection requirements have been applied. The estimations for several NMSSM and Dark SUSY samples were mostly found to be negligible, with small deviations observed for the $m_h = 125 \text{ GeV}$ sample. A conservative systematic of 2% is included to account for these deviations.

7.2 Theoretical Uncertainties

Theoretical systematic errors on the signal acceptance come from uncertainties in PDF+ α_s and from uncertainties evaluated by varying QCD renormalization and factorization scales (μ_R and μ_F). The uncertainties related to the parton distribution functions (PDFs) and the knowledge of the strong coupling constant α_s were calculated in Ref. [79] by following the PDF4LHC recommendations [80]. To this end, the QCD scale uncertainty was found by using MCFM [81] and varying μ_R and μ_F by a factor of two up and down. Further, the uncertainty due to the PDF choice was found by varying parametrization within the PDF as well as investigating alternative PDFs and comparing the central values. These uncertainties when treated as uncorrelated and added in quadrature were found to be 8%.

To exclude certain NMSSM points (in parameter space) it is important to include uncertainty on Higgs cross section and branching fraction $Br(h^0 \rightarrow a^0 a^0 \rightarrow 4\mu)$. Systematic errors on the signal total cross section for each production mechanism and for all Higgs boson masses are fully defined elsewhere [82]. They come from PDF+ α_s systematic errors and varying QCD renormalization and factorization scales. The uncertainties were treated as uncorrelated and total systematic uncertainty of 3.2% (Higgs boson mass independent) was assigned. The uncertainty on the branching fraction is taken to be 2% and assumed to be Higgs boson mass independent.

7.3 Summary of the Systematic Uncertainties

Table 36 lists systematic uncertainties which were used for setting upper limits on the signal search in the analysis. These systematics are referred to the signal events only, additional we also consider systematic uncertainties applied to the background. These include statistical

¹¹⁶⁰ uncertainties plus a conservative 20% uncertainty for $b\bar{b}$, coming from the closure test we pre-
¹¹⁶¹ formed releasing the isolation cut, and a 15% uncertainty for prompt double J/ψ , obtained by
¹¹⁶² varying the non-isolated sideband region in the double J/ψ estimation.

Table 11: Summary of the magnitude of systematic uncertainties.

Source of uncertainties	Error, %
Integrated luminosity	2.5%
Muon HLT	6%
Muon ID	$4 \times 0.6\%$
dimuon isolation	$2 \times 0.1\%$
Overlapping in Tracker	$2 \times 1.2\%$
Overlapping in Muon System	$2 \times 1.3\%$
Pile-up	0.17%
Dimuons mass consistency	1.5%
NNLO Higgs p_T re-weighting	2.0%
PDF+ α_s +QCD scales	8.0%
Higgs cross sec. and Br.	3.8%
Total	12.1%

8 Results

After the full analysis selection is applied to the data sample, 13 events were observed in the diagonal signal region, which is consistent with the standard model prediction of 9.90 ± 1.24 (stat.) ± 1.84 (syst.) events. These events are shown in Fig 41. Also shown are the 56 events that did not pass the dimuon mass compatibility requirement.

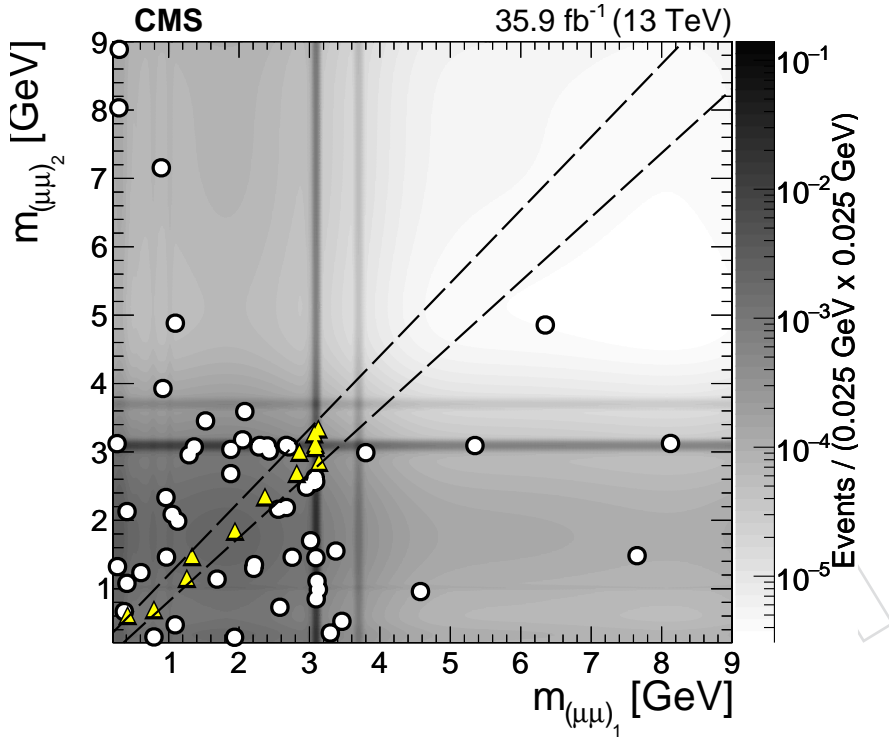


Figure 41: The distribution of the invariant masses $m_{\mu\mu_1}$ vs. $m_{\mu\mu_2}$ for the isolated dimuon systems for the 56 events in the data (solid bullets) surviving all selections but failing the $m_{\mu\mu_1} \simeq m_{\mu\mu_2}$ requirement. The diagonal signal region $m_{\mu\mu_1} \simeq m_{\mu\mu_2}$ (outlined with dashed lines) contains 13 events observed in data (triangle). The color scale indicates the expected SM background.

8.1 Model Independent Limit

For any new physics model predicting the signature investigated in this analysis, the results can be presented as the 95% confidence level (CL) upper limit on product of cross section times branching fraction squared times kinematic and geometric acceptance of the analysis at generator level:

$$\sigma(pp \rightarrow 2a + X) \times \mathcal{B}^2(a \rightarrow 2\mu) \times \alpha_{\text{Gen}} \leq \frac{N(m_{\mu\mu})}{\mathcal{L} \times r}.$$

The calculation uses the integrated luminosity $\mathcal{L} = 35.9 \text{ fb}^{-1}$, as measured in data, and takes the ratio $r = 0.56 \pm 0.06$, which is given by

$$r = \epsilon_{\text{Full}} / \alpha_{\text{Gen}} = \epsilon_{\text{Full}} / \epsilon_{\text{Full}}^{\text{MC}} \times \epsilon_{\text{Full}}^{\text{MC}} / \alpha_{\text{Gen}},$$

where $\epsilon_{\text{Full}} / \epsilon_{\text{Full}}^{\text{MC}} = 0.93 \pm 0.06$ is a scale factor correcting for experimental effects not accounted for by simulation and $\epsilon_{\text{Full}}^{\text{MC}} / \alpha_{\text{Gen}} = 0.61 \pm 0.06$ is the ratio of Full selection efficiency over kinematic and geometric acceptance of the analysis at generator level averaged over all of the

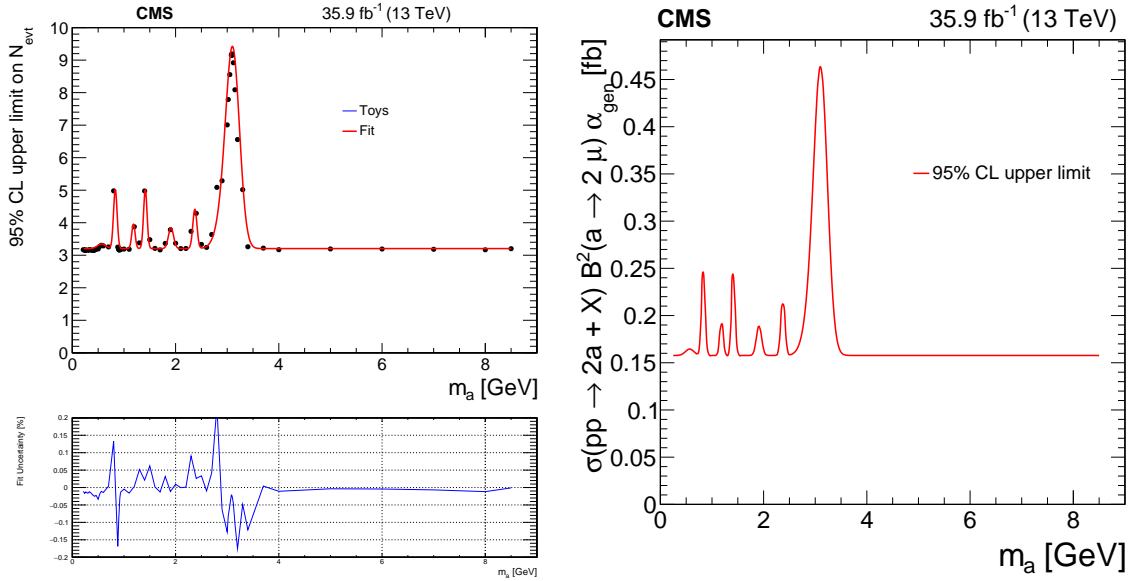


Figure 42: Left: The 95% CL upper limit on the number of signal events $N(\mu\mu)$: solid bullets show results of actual calculations for several values of m_a conveniently approximated with fit shown as solid line. Relative uncertainty between actual calculations and approximate function are also shown. Right: Model independent 95% CL upper limit on the product of the cross section times branching fraction squared times acceptance on generator level: $\sigma(pp \rightarrow 2a + X) \times B^2(a \rightarrow 2\mu) \times \alpha_{\text{Gen}}$.

benchmark points except for the Dark SUSY samples with $c\tau_{\gamma_D} = 100$ mm. $\epsilon_{\text{Full}}/\epsilon_{\text{Full}}^{\text{MC}}$ is the multiplicative product of scale factors from the trigger, isolation, and muon ID, where values are taken from Sec. 7. Further, $\epsilon_{\text{Full}}^{\text{MC}}/\alpha_{\text{Gen}}$ is derived from Fig. 24 by finding the weighted arithmetic mean over all of the benchmark points from the dark SUSY MC samples.

The overall statistical methodology used in this analysis was developed by the ATLAS and CMS Collaborations in the context of the LHC Higgs Combination Group and is described in Refs. [83–85]. The chosen test statistic is based on the profile likelihood ratio and is used to determine how signal-like or background-like the data are. Systematic uncertainties are incorporated in the analysis via nuisance parameters that are treated according to the frequentist paradigm. The actual outputs of the statistical tool for 95% CL limits on $N(\mu\mu)$ for several dimuon masses are shown as solid black dots in Fig. 42 (left top). The limit spectrum as a function of m_a has been fitted using series of Gaussians on top of a flat line that represents the limit obtained in absence of observed data. Using the proposed approximation the model independent limit of the analysis takes the form

$$\sigma(pp \rightarrow 2a + X) \times B^2(a \rightarrow 2\mu) \times \alpha_{\text{Gen}} \leq \text{Lim}(m_a) \quad (25)$$

Where the limits are of the form:

$$\begin{aligned} \text{Lim}(m_a) = & 3.18 + 0.23 * G(0.56, 0.1) + 2.31 * G(0.91, 0.03) + 2.10 * G(1.16, 0.02) + \\ & 2.25 * G(1.41, 0.04) + 3.00 * G(1.9, 0.08) + 1.82 * G(2.39, 0.05) + \\ & 0.68 * G(2.74, 0.04) + 4.7 * G(3.10, 0.09) \end{aligned} \quad (26)$$

The limit on $\sigma(pp \rightarrow 2a + X) \times B^2(a \rightarrow 2\mu) \times \alpha_{\text{Gen}}$ fluctuates between 0.16 and 0.4 over a range of new light boson masses from 0.25 GeV to 8.5 GeV as shown in Fig. 42 (right).

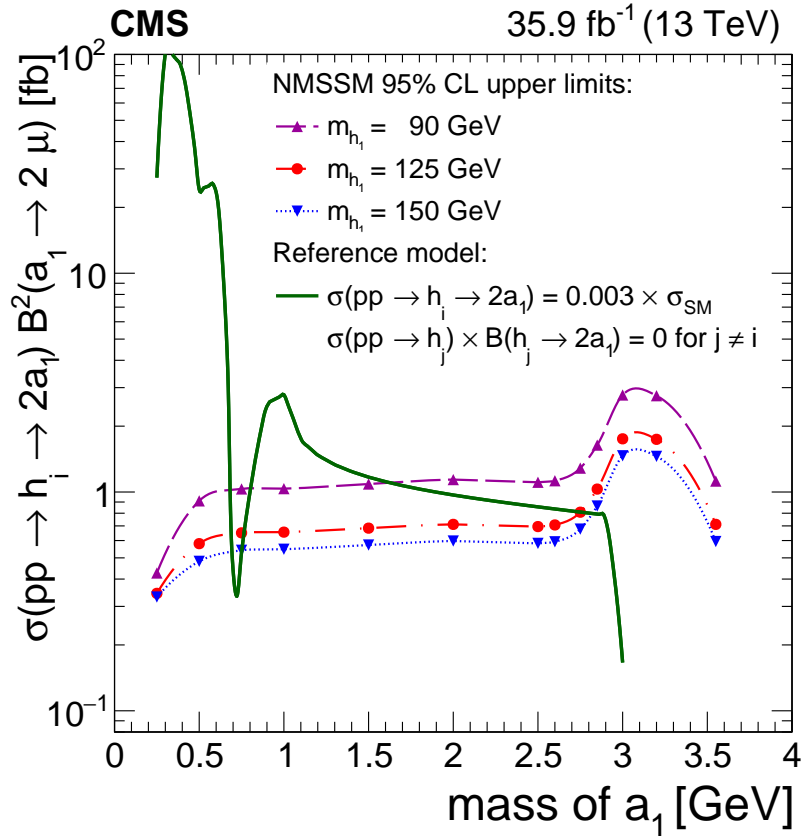


Figure 43: The 95% CL upper limits as functions of m_{a_1} , for the NMSSM case, on $\sigma(pp \rightarrow h_{1,2} \rightarrow 2a_1) \times \mathcal{B}^2(a_1 \rightarrow 2\mu)$ with $m_{h_1} = 90\text{ GeV}/c^2$ (dashed curve), $m_{h_1} = 125\text{ GeV}/c^2$ (dash-dotted curve), and $m_{h_1} = 150\text{ GeV}/c^2$ (dotted curve)). The limits are compared to the predicted rate (solid curve) obtained using a simplified scenario with $\mathcal{B}(h_1 \rightarrow 2a_1) = 0.3\%$, $\sigma(pp \rightarrow h_1) = \sigma_{SM}(m_{h_1} = 125\text{ GeV}/c^2)$ [82], $\sigma(pp \rightarrow h_2) \times \mathcal{B}(h_2 \rightarrow 2a_1) = 0$, and $\mathcal{B}(a_1 \rightarrow 2\mu)$ as a function of m_{a_1} which is taken from [26] for NMSSM parameter $\tan \beta = 20$.

1178 In regions with no signal it allows simple reinterpretation of the results in other models with
 1179 two pairs of muons coming from light bosons of the same type with a mass in range $0.25 <$
 1180 $m_a < 8.5$ GeV where the new light bosons are typically isolated and spatially separated (so as
 1181 to satisfy the isolation requirements).

1182 Generally the reinterpretation of results in a specific beyond the SM scenario requires there to
 1183 be an evaluation of the signal acceptance. As mentioned above, this analysis has been designed
 1184 in such a way that this is a simple procedure. Below we describe one approach to evaluate new
 1185 models that only requires the analyst to use generator level information and does not require
 1186 simulating the response from the CMS detector and reconstruction software.

1187 8.2 Constraints on Benchmark Models

1188 **Constraints on NMSSM Scenario.** For the NMSSM, the 95% CL upper limit is derived for
 1189 $\sigma(pp \rightarrow h_{1,2} \rightarrow 2a_1) \times \mathcal{B}^2(a_1 \rightarrow 2\mu)$ as a function of m_{a_1} . Such limit curves are shown in Fig. 43
 1190 for three choices of m_{h_1} .

1191 As the production cross sections and branching fractions for h_1 and h_2 can vary substantially
 1192 depending on the chosen NMSSM parameters, and the unknown mass of one of the two bosons

(the other one has mass of $\approx 125 \text{ GeV}/c^2$), the results obtained in this analysis cannot be easily presented with a single plot that would be usable for sufficiently large fraction of possible model parameters. An exact interpretation would instead require following the prescription for calculating the experimental acceptance using the generator level acceptance for each of the two $h_{1,2}$ bosons, and then using the measured upper limit on the sum of two contributions to derive limits for any choice of NMSSM model parameters.

Despite the above, one can present results in an easy to interpret fashion at the cost of somewhat overestimated (more conservative) upper limits in parts of the parameter space, in comparison to the exact approach described above. It turns out that in the NMSSM, for the vast majority of the parameter space relevant to this analysis, the two Higgs bosons “factorize” into separate categories. One of the Higgs bosons, $h_{1,2}$, is almost always very SM-like, with a production cross section negligibly different from the SM prediction and a small branching fraction $\mathcal{B}(h_i \rightarrow 2a_1)$, while the other one (“non-SM-like”) has a suppressed cross section (because of the weak coupling to SM fermions and bosons) but a large branching fraction $\mathcal{B}(h_i \rightarrow 2a_1)$. In the limiting case, there are three potential scenarios, as enumerated earlier in Section 1:

1. the lightest h_1 is a non-SM-like Higgs boson with $m_{h_1} < 125 \text{ GeV}/c^2$, with reduced cross section and large $\mathcal{B}(h_1 \rightarrow 2a_1)$, and h_2 is the SM-like Higgs with negligible $\mathcal{B}(h_2 \rightarrow 2a_1)$,
2. h_1 is the SM-like Higgs boson with SM cross section and negligible $\mathcal{B}(h_1 \rightarrow 2a_1)$ and h_2 is a heavier non-SM Higgs boson with reduced cross section and large $\mathcal{B}(h_2 \rightarrow 2a_1)$, to which this analysis can be sensitive,
3. the non-SM-like Higgs boson is either lighter or heavier than $125 \text{ GeV}/c^2$, it has a large branching ratio but such a small production cross section that this analysis is not sensitive to it. In this case the sensitivity is driven by the decays of the SM-like Higgs into $2a_1$ (even though small).

For scenario 1 with $m_{h_1} < 125 \text{ GeV}/c^2$ and h_2 being the SM-like Higgs we rely on the following inequality:

$$\begin{aligned} \sigma(pp \rightarrow h_1) \times \mathcal{B}(h_1 \rightarrow 2a_1) \times \mathcal{B}^2(a_1 \rightarrow 2\mu) \times \alpha(m_{h_1}) \leq \\ \sigma(pp \rightarrow h_1) \times \mathcal{B}(h_1 \rightarrow 2a_1) \times \mathcal{B}^2(a_1 \rightarrow 2\mu) \times \alpha(m_{h_1}) + \\ \sigma(pp \rightarrow h_2) \times \mathcal{B}(h_2 \rightarrow 2a_1) \times \mathcal{B}^2(a_1 \rightarrow 2\mu) \times \alpha(m_{h_2}) \leq X, \end{aligned}$$

where X is the limit from this analysis. Here, we effectively neglect the contribution from the second term as negligible. If, in a given model, its contribution is not completely negligible, we end up with a more conservative limit on $\sigma(pp \rightarrow h_1) \times \mathcal{B}(h_1 \rightarrow 2a_1) \times \mathcal{B}^2(a_1 \rightarrow 2\mu)$ than in the exact calculation.

For scenario 2 with $m_{h_2} > 125 \text{ GeV}/c^2$ we set the limit using:

$$\begin{aligned} \sigma(pp \rightarrow h_2) \times \mathcal{B}(h_2 \rightarrow 2a_1) \times \mathcal{B}^2(a_1 \rightarrow 2\mu) \times \alpha(m_{h_2}) \leq \\ \sigma(pp \rightarrow h_1) \times \mathcal{B}(h_1 \rightarrow 2a_1) \times \mathcal{B}^2(a_1 \rightarrow 2\mu) \times \alpha(m_{h_1}) + \\ \sigma(pp \rightarrow h_2) \times \mathcal{B}(h_2 \rightarrow 2a_1) \times \mathcal{B}^2(a_1 \rightarrow 2\mu) \times \alpha(m_{h_2}) \leq X, \end{aligned}$$

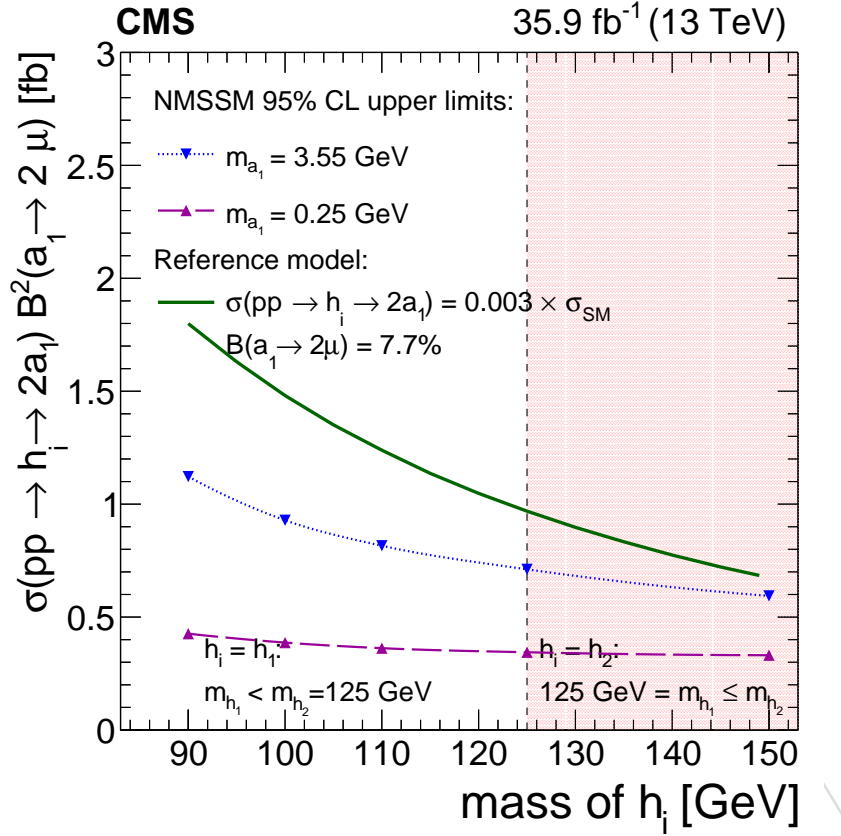


Figure 44: The 95% CL upper limits as functions of m_{h_1} in range $86 \text{ GeV}/c^2 < m_{h_1} < 126 \text{ GeV}/c^2$ and as functions of m_{h_2} in range $m_{h_2} > 126 \text{ GeV}/c^2$, for the NMSSM case, on $\sigma(pp \rightarrow h_{1/2} \rightarrow 2a_1) \times \mathcal{B}^2(a_1 \rightarrow 2\mu)$ with $m_{a_1} = 0.25 \text{ GeV}/c^2$ (dashed curve), $m_{a_1} = 2 \text{ GeV}/c^2$ (dash-dotted curve) and $m_{a_1} = 3.55 \text{ GeV}/c^2$ (dotted curve). As an illustration, the limits are compared to the predicted rate (solid curve) obtained using a simplified scenario with $\mathcal{B}(a_1 \rightarrow 2\mu) = 7.7\%$ and $\sigma(pp \rightarrow h_1) \times \mathcal{B}(h_1 \rightarrow 2a_1) = 0.003 \times \sigma_{\text{SM}}(m_{h_1})$, $\mathcal{B}(h_2 \rightarrow 2a_1) = 0$ in range $86 \text{ GeV}/c^2 < m_{h_1} < 126 \text{ GeV}/c^2$ or $\mathcal{B}(h_1 \rightarrow 2a_1) = 0$, $\sigma(pp \rightarrow h_2) \times \mathcal{B}(h_2 \rightarrow 2a_1) = 0.003 \times \sigma_{\text{SM}}(m_{h_2})$ in range $m_{h_2} > 126 \text{ GeV}/c^2$. The chosen $\mathcal{B}(a_1 \rightarrow 2\mu)$ is taken from [26] for $m_{a_1} = 2 \text{ GeV}/c^2$ and $\tan \beta = 20$.

in which case we neglect the potential contribution from the SM-like Higgs h_1 . if the contribution is indeed negligible, the limit for h_2 is exact. If the contribution for h_1 is not completely negligible, we end up with a more conservative limit.

For scenario 3:

$$\begin{aligned} \sigma(pp \rightarrow h_{\text{SM-like}}) \times \mathcal{B}(h_{\text{SM-like}} \rightarrow 2a_1) \times \mathcal{B}^2(a_1 \rightarrow 2\mu) \times \alpha(m_{h_{\text{SM-like}}}) &\leq \\ \sigma(pp \rightarrow h_{\text{SM-like}}) \times \mathcal{B}(h_{\text{SM-like}} \rightarrow 2a_1) \times \mathcal{B}^2(a_1 \rightarrow 2\mu) \times \alpha(m_{h_{\text{SM-like}}}) + \\ \sigma(pp \rightarrow h_{\text{non-SM-like}}) \times \mathcal{B}(h_{\text{non-SM-like}} \rightarrow 2a_1) \times \mathcal{B}^2(a_1 \rightarrow 2\mu) \times \alpha(m_{h_{\text{non-SM-like}}}) &\leq X. \end{aligned}$$

If the non-SM-like boson is way below the sensitivity of this analysis (either because it is light, but has severely suppressed cross section or because it is either too heavy to be produced or has cross section too suppressed), the limit becomes effectively a limit on potential rare decays

of SM-like Higgs via $h \rightarrow 2a_1 \rightarrow 4\mu$. Again, if the contribution from the non-SM Higgs boson is not negligible, the limit on SM-like Higgs boson branching ratio becomes more conservative than the exact limit. These limits can be easily put on a single plot versus $m(h)$ where, depending on the value of m , it should be interpreted as h_1 or h_2 or h_{SM} (either h_1 or h_2 when the other one is inaccessible) as shown in Fig. 44 (for three choices of m_{a_1}). The plot is limited at $m_h = 150 \text{ GeV}/c^2$, for the limit value for $m(h_2)$ above $150 \text{ GeV}/c^2$ one can either extrapolate the curve or just take the value at $150 \text{ GeV}/c^2$ as a conservative estimate of the limit above $150 \text{ GeV}/c^2$.

For the NMSSM simplified prediction scenario we use the representative value of $\mathcal{B}(a_1 \rightarrow 2\mu) = 7.7\%$ for $m_{a_1} \approx 2 \text{ GeV}/c^2$ and $\tan\beta = 20$ taken from [26]. We assume $\mathcal{B}(h_2 \rightarrow 2a_1) = 0$ in range $86 \text{ GeV}/c^2 < m_{h_1} < 125 \text{ GeV}/c^2$ or $\mathcal{B}(h_1 \rightarrow 2a_1) = 0$ in range $m_{h_2} > 125 \text{ GeV}/c^2$. We normalize the production cross section to that of the SM Higgs boson [82] assuming $\sigma(pp \rightarrow h_1) \times \mathcal{B}(h_1 \rightarrow 2a_1) = 0.003 \times \sigma_{SM}(m_{h_1})$ in range $86 \text{ GeV}/c^2 < m_{h_1} < 125 \text{ GeV}/c^2$ or $\sigma(pp \rightarrow h_2) \times \mathcal{B}(h_2 \rightarrow 2a_1) = 0.003 \times \sigma_{SM}(m_{h_2})$ in range $m_{h_2} > 125 \text{ GeV}/c^2$, where in both ranges we choose 0.003 coefficient, which yields predictions for the rates of dimuon pair events comparable to the obtained experimental limits.

For the NMSSM simplified prediction scenario we use $\mathcal{B}(a_1 \rightarrow 2\mu)$ as a function of m_{a_1} , calculated in [26] for $\tan\beta = 20$ with no hadronization effects included in the $m_{a_1} < 2m_\tau$ region. The branching fraction $\mathcal{B}(a_1 \rightarrow 2\mu)$ is influenced by the $a_1 \rightarrow s\bar{s}$ and $a_1 \rightarrow gg$ channels. The significant structures in the predicted curves visible in Fig. 43 arise from the fact that $\mathcal{B}(a_1 \rightarrow gg)$ varies rapidly in that region of m_{a_1} . The rapid variation in $\mathcal{B}(a_1 \rightarrow gg)$ occurs when m_{a_1} crosses the internal quark loop thresholds. The representative value of $\mathcal{B}(a_1 \rightarrow 2\mu)$ is equal to 7.7% for $m_{a_1} \approx 2 \text{ GeV}/c^2$. Finally, we choose $\mathcal{B}(h_1 \rightarrow 2a_1) = 0.3\%$, which yields predictions for the rates of dimuon pair events comparable to the obtained experimental limits.

Constraints on dark SUSY scenarios with non-zero lifetime of dark photon.

The results of this analysis will allow us to set exclusion limits on currently unconstrained region of ϵ and m_{γ_D} plane, as described in Sec. 1 and shown in Figure 6.

Evaluated 95% CL limits on the product of Higgs production cross section times branching ratios of all decays and known branching ratio of the dark photon decay to two muons (Fig. 4 (right)) will allow us to set 95% CL limit on the product of Higgs production cross section and branching ratio of the Higgs decay to pair of dark photons (in a cascade decay accompanied with something else) as follows:

$$\sigma(pp \rightarrow h) \times Br(h \rightarrow 2\gamma_D + X) < \frac{N(m_{\mu\mu})}{L \times r \times \alpha_{gen}(m_{\gamma_D}, c\tau_{\gamma_D}) \times Br_{\gamma_D \rightarrow \mu\mu}^2(m_{\gamma_D})}.$$

For this limit we normalize the product $\sigma(pp \rightarrow h) \times Br(h \rightarrow 2a + X)$ to the cross section of SM Higgs production $\sigma_{SM}(pp \rightarrow h_{125\text{GeV}})$ as follows:

$$\sigma(pp \rightarrow h) \times \mathcal{B}(h \rightarrow 2a + X) = \sigma_{SM}(pp \rightarrow h_{125\text{GeV}}) \times K$$

where K could be interpreted as an "effective" branching ratio $\mathcal{B}(h \rightarrow 2a + X)$.

We will then use the parameter K to set limits on several choices of the branching ratio $\mathcal{B}(h \rightarrow 2\gamma_D + X)$ as follows:

$$\sigma_{SM}(pp \rightarrow h_{125\text{GeV}}) \times K < \frac{N(m_{\mu\mu})}{L \times r \times \alpha(m_{\gamma_D}, c\tau_{\gamma_D}) \times Br_{\gamma_D \rightarrow \mu\mu}^2(m_{\gamma_D})}.$$

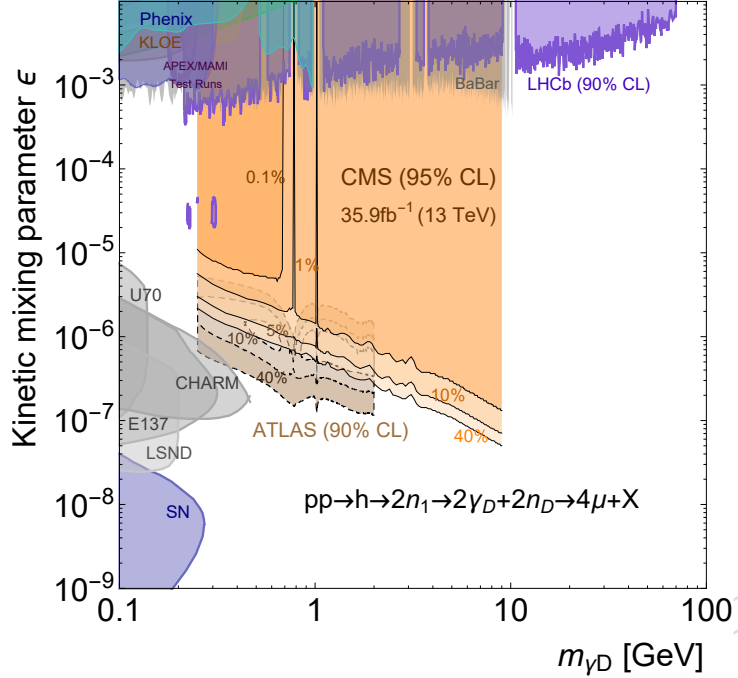


Figure 45: The 95% CL limits from this analysis and other experimental constraints, in the plane of two parameters for the dark SUSY scenarios: ϵ and m_{γ_D} . Different colors represent different values of $Br(h \rightarrow 2\gamma_D)$. The limit goes from 0.25 to 8.5 GeV.

1266 The choices of parameter K (0.001, 0.01, 0.1, 0.4) are color coded and represented in the "z"
 1267 axis. Using equation (9) we converted $(m_{\gamma_D}, c\tau_{\gamma_D})$ space to (m_{γ_D}, ϵ) space and represent the
 1268 95% CL limits in this plane. This is shown in Fig. 46. We can conclude that a large previously
 1269 unconstrained area of the parameters space is limited.

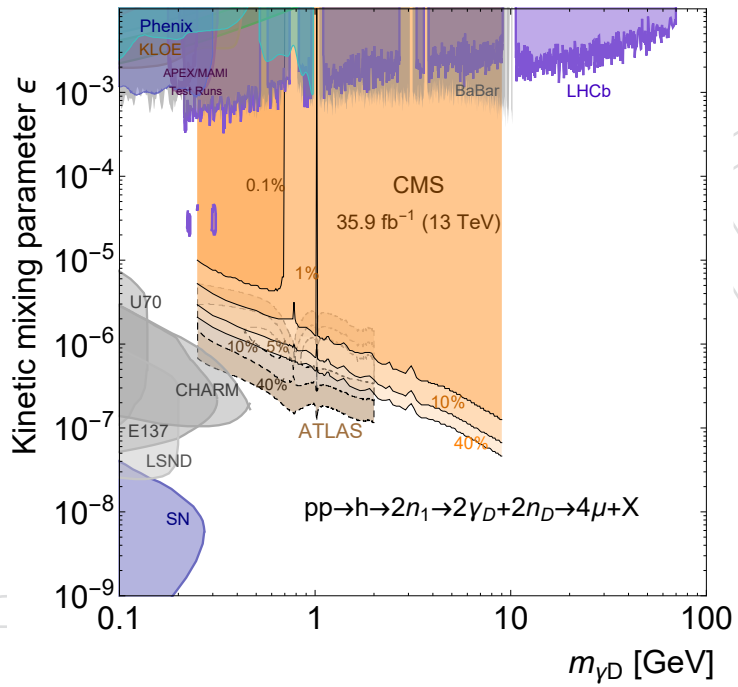


Figure 46: The 90% CL limits from this analysis and other experimental constraints, in the plane of two parameters for the dark SUSY scenarios: ϵ and m_{γ_D} . Different colors represent different values of $\text{Br}(h \rightarrow 2\gamma_D)$. The limit goes from 0.25 to 8.5 GeV.

1270 **9 Conclusions**

1271 A search for pairs of new light bosons, which could be produced in the decay of a Higgs boson
1272 that subsequently decays to pairs of oppositely charged muons ($h \rightarrow 2a + X \rightarrow 4\mu + X$), has
1273 been presented. The search is based on a data sample corresponding to an integrated lumi-
1274 nosity of 35.9 fb^{-1} collected by the CMS experiment in proton-proton collisions at $\sqrt{s} = 13 \text{ TeV}$
1275 in 2016. The results of the analysis are presented in a way which allows straightforward re-
1276 interpretation within a broad range of physics models predicting the same type of signature.
1277 Additionally, the results have been interpreted in the context of the NMSSM and the dark SUSY
1278 benchmark models.

DRAFT

1279 References

- 1280 [1] F. Englert and R. Brout, "Broken symmetry and the mass of gauge vector mesons", *Phys.*
1281 *Rev. Lett.* **13** (1964) 321, doi:10.1103/PhysRevLett.13.321.
- 1282 [2] P. W. Higgs, "Broken symmetries and the masses of gauge bosons", *Phys. Rev. Lett.* **13**
1283 (1964) 508, doi:10.1103/PhysRevLett.13.508.
- 1284 [3] G. S. Guralnik, C. R. Hagen, and T. W. B. Kibble, "Global conservation laws and massless
1285 particles", *Phys. Rev. Lett.* **13** (1964) 585, doi:10.1103/PhysRevLett.13.585.
- 1286 [4] P. Fayet, "Supergauge invariant extension of the higgs mechanism and a model for the
1287 electron and its neutrino", *Nucl. Phys. B* **90** (1975) 104,
1288 doi:10.1016/0550-3213(75)90636-7.
- 1289 [5] R. K. Kaul and P. Majumdar, "Cancellation of quadratically divergent mass corrections in
1290 globally supersymmetric spontaneously broken gauge theories", *Nucl. Phys. B* **199**
1291 (1982) 36, doi:10.1016/0550-3213(82)90565-X.
- 1292 [6] R. Barbieri, S. Ferrara, and C. A. Savoy, "Gauge models with spontaneously broken local
1293 supersymmetry", *Phys. Lett. B* **119** (1982) 343,
1294 doi:10.1016/0370-2693(82)90685-2.
- 1295 [7] H. P. Nilles, M. Srednicki, and D. Wyler, "Weak interaction breakdown induced by
1296 supergravity", *Phys. Lett.* **120** (1983) 346, doi:10.1016/0370-2693(83)90460-4.
- 1297 [8] J.-M. Frere, D. R. T. Jones, and S. Raby, "Fermion masses and induction of the weak scale
1298 by supergravity", *Nucl. Phys. B* **222** (1983) 11,
1299 doi:10.1016/0550-3213(83)90606-5.
- 1300 [9] J.-P. Derendinger and C. A. Savoy, "Quantum effects and $SU(2) \times U(1)$ breaking in
1301 supergravity gauge theories", *Nucl. Phys. B* **237** (1984) 307,
1302 doi:10.1016/0550-3213(84)90162-7.
- 1303 [10] M. Drees, "Supersymmetric models with extended Higgs sector", *Int. J. Mod. Phys. A* **4**
1304 (1989) 3635, doi:10.1142/S0217751X89001448.
- 1305 [11] M. Maniatis, "The next-to-minimal supersymmetric extension of the standard model
1306 reviewed", *Int. J. Mod. Phys. A* **25** (2010) 3505, doi:10.1142/S0217751X10049827,
1307 arXiv:0906.0777.
- 1308 [12] U. Ellwanger, C. Hugonie, and A. M. Teixeira, "The next-to-minimal supersymmetric
1309 standard model", *Phys. Rept.* **496** (2010) 1, doi:10.1016/j.physrep.2010.07.001,
1310 arXiv:0910.1785.
- 1311 [13] H. P. Nilles, "Supersymmetry, supergravity and particle physics", *Phys. Rept.* **110** (1984)
1312 1, doi:10.1016/0370-1573(84)90008-5.
- 1313 [14] S. P. Martin, "A Supersymmetry primer", *Adv.Ser.Direct.High Energy Phys.* **21** (2010)
1314 1–153, doi:10.1142/9789814307505_0001, arXiv:hep-ph/9709356.
- 1315 [15] D. J. H. Chung et al., "The soft supersymmetry breaking Lagrangian: theory and
1316 applications", *Phys. Rept.* **407** (2005) 1, doi:10.1016/j.physrep.2004.08.032,
1317 arXiv:hep-ph/0312378.

- [16] J. E. Kim and H. P. Nilles, "The μ -problem and the strong CP-problem", *Phys. Lett. B* **138** (1984) 150, doi:10.1016/0370-2693(84)91890-2.
- [17] J. A. Casas, J. R. Espinosa, and I. Hidalgo, "The MSSM fine tuning problem: a way out", *JHEP* **01** (2004) 008, doi:10.1088/1126-6708/2004/01/008, arXiv:hep-ph/0310137.
- [18] R. Dermisek and J. F. Gunion, "Escaping the large fine tuning and little hierarchy problems in the next to minimal supersymmetric model and $h \rightarrow aa$ decays", *Phys. Rev. Lett.* **95** (2005) 041801, doi:10.1103/PhysRevLett.95.041801, arXiv:hep-ph/0502105.
- [19] S. Chang, R. Dermisek, J. F. Gunion, and N. Weiner, "Nonstandard Higgs boson decays", *Ann. Rev. Nucl. Part. Sci.* **58** (2008) 75, doi:10.1146/annurev.nucl.58.110707.171200, arXiv:0801.4554.
- [20] J. Ellis et al., "Higgs bosons in a nonminimal supersymmetric model", *Phys. Rev. D* **39** (1989) 844, doi:10.1103/PhysRevD.39.844.
- [21] U. Ellwanger, M. Rausch de Traubenberg, and C. A. Savoy, "Particle spectrum in supersymmetric models with a gauge singlet", *Phys. Lett. B* **315** (1993) 331, doi:10.1016/0370-2693(93)91621-S, arXiv:hep-ph/9307322.
- [22] U. Ellwanger, M. Rausch de Traubenberg, and C. A. Savoy, "Higgs phenomenology of the supersymmetric model with a gauge singlet", *Z. Phys. C* **67** (1995) 665, doi:10.1007/BF01553993, arXiv:hep-ph/9502206.
- [23] B. A. Dobrescu, G. L. Landsberg, and K. T. Matchev, "Higgs boson decays to CP-odd scalars at the Tevatron and beyond", *Phys. Rev. D* **63** (2001) 075003, doi:10.1103/PhysRevD.63.075003, arXiv:hep-ph/0005308.
- [24] D. J. Miller, R. Nevzorov, and P. M. Zerwas, "The Higgs sector of the next-to-minimal supersymmetric standard model", *Nucl. Phys. B* **681** (2004) 3, doi:10.1016/j.nuclphysb.2003.12.021, arXiv:hep-ph/0304049.
- [25] A. Belyaev et al., "LHC discovery potential of the lightest NMSSM Higgs in the $h_1 \rightarrow a_1 a_1 \rightarrow 4\mu$ channel", *Phys. Rev. D* **81** (2010) 075021, doi:10.1103/PhysRevD.81.075021, arXiv:1002.1956.
- [26] R. Dermisek and J. F. Gunion, "New constraints on a light CP-odd Higgs boson and related NMSSM ideal Higgs scenarios", *Phys. Rev. D* **81** (2010) 075003, doi:10.1103/PhysRevD.81.075003, arXiv:1002.1971.
- [27] OPAL Collaboration, "Search for a low mass CP-odd Higgs boson in e^+e^- collisions with the OPAL detector at LEP-2", *Eur. Phys. J. C* **27** (2003) 483, doi:10.1140/epjc/s2003-01139-y, arXiv:hep-ex/0209068.
- [28] ALEPH, DELPHI, L3, OPAL, LEP Working Group for Higgs Boson Searches Collaboration, "Search for neutral MSSM Higgs bosons at LEP", *Eur. Phys. J. C* **47** (2006) 547, doi:10.1140/epjc/s2006-02569-7, arXiv:hep-ex/0602042.
- [29] CLEO Collaboration, "Search for very light CP-odd Higgs boson in radiative decays of $Y(1S)$ ", *Phys. Rev. Lett.* **101** (2008) 151802, doi:10.1103/PhysRevLett.101.151802, arXiv:0807.1427.

- [30] BABAR Collaboration, "Search for dimuon decays of a light scalar boson in radiative transitions $v \rightarrow \gamma a_0$ ", *Phys. Rev. Lett.* **103** (2009) 081803, doi:10.1103/PhysRevLett.103.081803, arXiv:0905.4539.
- [31] D0 Collaboration, "Search for NMSSM Higgs bosons in the $h \rightarrow aa \rightarrow \mu\mu\mu\mu, \mu\mu\tau\tau$ channels using $p\bar{p}$ collisions at $\sqrt{s} = 1.96$ TeV", *Phys. Rev. Lett.* **103** (2009) 061801, doi:10.1103/PhysRevLett.103.061801, arXiv:0905.3381.
- [32] Y. Pakhotin, A. Safonov, and A. Tatarinov, "Search for new light bosons from the Higgs boson decays using multi-muon events at the LHC", *CMS Note* **2011/238** (2011).
- [33] K. Cheung, J. Song, P. Tseng, and Q.-S. Yan, "Production and decays of the light pseudoscalar boson eta at the LHC in the simplest little Higgs model", *Phys. Rev.* **D78** (2008) 055015, doi:10.1103/PhysRevD.78.055015, arXiv:0806.4411.
- [34] N. Arkani-Hamed, D. P. Finkbeiner, T. R. Slatyer, and N. Weiner, "A theory of dark matter", *Phys. Rev. D* **79** (2009) 015014, doi:10.1103/PhysRevD.79.015014, arXiv:0810.0713.
- [35] M. Baumgart et al., "Non-abelian dark sectors and their collider signatures", *JHEP* **04** (2009) 014, doi:10.1088/1126-6708/2009/04/014, arXiv:0901.0283.
- [36] A. Falkowski, J. T. Ruderman, T. Volansky, and J. Zupan, "Hidden Higgs decaying to lepton jets", *JHEP* **05** (2010) 077, doi:10.1007/JHEP05(2010)077, arXiv:1002.2952.
- [37] B. Holdom, "Two U(1)'s and e charge shifts", *Phys. Lett. B* **166** (1986) 196, doi:10.1016/0370-2693(86)91377-8.
- [38] K. R. Dienes, C. F. Kolda, and J. March-Russell, "Kinetic mixing and the supersymmetric gauge hierarchy", *Nucl. Phys. B* **492** (1997) 104, doi:10.1016/S0550-3213(97)00173-9, arXiv:hep-ph/9610479.
- [39] C. Cheung, J. T. Ruderman, L.-T. Wang, and I. Yavin, "Kinetic mixing as the origin of light dark scales", *Phys. Rev. D* **80** (2009) 035008, doi:10.1103/PhysRevD.80.035008, arXiv:0902.3246.
- [40] PAMELA Collaboration, "PAMELA results on the cosmic-ray antiproton flux from 60 MeV to 180 GeV in kinetic energy", *Phys. Rev. Lett.* **105** (2010) 121101, doi:10.1103/PhysRevLett.105.121101, arXiv:1007.0821.
- [41] B. Batell, M. Pospelov, and A. Ritz, "Probing a Secluded U(1) at B-factories", *Phys. Rev. D* **79** (2009) 115008, doi:10.1103/PhysRevD.79.115008, arXiv:0903.0363.
- [42] Particle Data Group Collaboration, "Review of Particle Physics (RPP)", *Phys. Rev. D* **86** (2012) 010001, doi:10.1103/PhysRevD.86.010001.
- [43] V. Ezhela, S. Lugovsky, and O. Zenin, "Hadronic part of the muon g-2 estimated on the sigma**2003(tot)(e+ e- -> hadrons) evaluated data compilation", arXiv:hep-ph/0312114.
- [44] M. Davier, S. Eidelman, A. Hocker, and Z. Zhang, "Confronting spectral functions from e+ e- annihilation and tau decays: Consequences for the muon magnetic moment", *Eur. Phys. J.* **C27** (2003) 497–521, doi:10.1140/epjc/s2003-01136-2, arXiv:hep-ph/0208177.

- [45] D. Curtin et al., "Exotic Decays of the 125 GeV Higgs Boson", arXiv:1312.4992.
- [46] S. Abrahamyan et al., "Search for a new gauge boson in electron-nucleus fixed-target scattering by the apex experiment", *Phys. Rev. Lett.* **107** (Nov, 2011) 191804, doi:10.1103/PhysRevLett.107.191804.
- [47] BaBar Collaboration Collaboration, "Search for a dark photon in e^+e^- collisions at BaBar", *Phys. Rev. Lett.* **113** (Nov, 2014) 201801, doi:10.1103/PhysRevLett.113.201801.
- [48] BaBar Collaboration Collaboration, "Search for Low-Mass Dark-Sector Higgs Bosons", *Phys.Rev.Lett.* **108** (2012) 211801, doi:10.1103/PhysRevLett.108.211801, arXiv:1202.1313.
- [49] G. Agakishiev et al., "Searching a dark photon with hades", *Physics Letters B* **731** (2014), no. 0, 265 – 271, doi:<http://dx.doi.org/10.1016/j.physletb.2014.02.035>.
- [50] Curciarello, Francesca, "Dark forces at kloe/kloe-2", *EPJ Web of Conferences* **72** (2014) 00004, doi:10.1051/epjconf/20147200004.
- [51] KLOE-2 Collaboration Collaboration, "Search for light vector boson production in $e^+e^- \rightarrow \mu^+\mu^-\gamma$ interactions with the KLOE experiment", *Phys.Lett.* **B736** (2014) 459–464, doi:10.1016/j.physletb.2014.08.005, arXiv:1404.7772.
- [52] M. Endo, K. Hamaguchi, and G. Mishima, "Constraints on Hidden Photon Models from Electron g-2 and Hydrogen Spectroscopy", *Phys.Rev.* **D86** (2012) 095029, doi:10.1103/PhysRevD.86.095029, arXiv:1209.2558.
- [53] ATLAS Collaboration Collaboration, "Search for long-lived neutral particles decaying into lepton jets in proton–proton collisions at $\sqrt{s} = 8$ TeV with the ATLAS detector", arXiv:1409.0746.
- [54] CMS Collaboration, "A search for pair production of new light bosons decaying into muons", *Phys. Lett.* **B752** (2016) 146–168, doi:10.1016/j.physletb.2015.10.067, arXiv:1506.00424.
- [55] J. Pivarski, A. Safonov, and A. Tatarinov, "Search for collimated groups of muons", *CMS Note* **2010/462** (2010).
- [56] CMS Collaboration, "Search for light resonances decaying into pairs of muons as a signal of new physics", *JHEP* **07** (2011) 098, doi:10.1007/JHEP07(2011)098, arXiv:1106.2375.
- [57] ATLAS Collaboration, "Search for displaced muonic lepton jets from light Higgs boson decay in proton-proton collisions at $\sqrt{s} = 7$ TeV with the ATLAS detector", arXiv:1210.0435., Submitted to Phys. Lett. B.
- [58] CMS Collaboration, "Search for a non-standard-model Higgs boson decaying to a pair of new light bosons in four-muon final states", arXiv:1210.7619.
- [59] BESIII Collaboration Collaboration, "Search for a light exotic particle in j/ψ radiative decays", *Phys. Rev. D* **85** (May, 2012) 092012, doi:10.1103/PhysRevD.85.092012.
- [60] BESIII Collaboration Collaboration, "Search for a light cp -odd higgs boson in radiative decays of j/ψ ", *Phys. Rev. D* **93** (Mar, 2016) 052005, doi:10.1103/PhysRevD.93.052005.

- [61] CDF Collaboration, "Search for a very light CP-odd Higgs boson in top quark decays from $p\bar{p}$ collisions at 1.96 TeV", *Phys. Rev. Lett.* **107** (2011) 031801, doi:10.1103/PhysRevLett.107.031801, arXiv:1104.5701.
- [62] CMS Collaboration, "Search for a light pseudoscalar Higgs boson in the dimuon decay channel in pp collisions at $\sqrt{s} = 7$ TeV", *Phys. Rev. Lett.* **109** (2012) 121801, doi:10.1103/PhysRevLett.109.121801, arXiv:1206.6326.
- [63] N. Jarosik et al., "Seven-year Wilkinson microwave anisotropy probe (WMAP) observations: sky maps, systematic errors, and basic results", *Astrophys. J. Suppl.* **192** (2011) 14, doi:10.1088/0067-0049/192/2/14, arXiv:1001.4744.
- [64] OPAL Collaboration, "Decay mode independent searches for new scalar bosons with the OPAL detector at LEP", *Eur. Phys. J. C* **27** (2003) 311, doi:10.1140/epjc/s2002-01115-1, arXiv:hep-ex/0206022.
- [65] D0 Collaboration, "Search for dark photons from supersymmetric hidden valleys", *Phys. Rev. Lett.* **103** (2009) 081802, doi:10.1103/PhysRevLett.103.081802, arXiv:0905.1478.
- [66] D0 Collaboration, "Search for events with leptonic jets and missing transverse energy in $p\bar{p}$ collisions at $\sqrt{s} = 1.96$ TeV", *Phys. Rev. Lett.* **105** (2010) 211802, doi:10.1103/PhysRevLett.105.211802, arXiv:1008.3356.
- [67] CDF Collaboration, "Search for anomalous production of multiple leptons in association with W and Z bosons at CDF", *Phys. Rev. D* **85** (2012) 092001, doi:10.1103/PhysRevD.85.092001, arXiv:1202.1260.
- [68] R. D. Ball et al., "Parton distributions with QED corrections", *Nuclear Physics B* **877** (2013), no. 2, 290 – 320, doi:<http://dx.doi.org/10.1016/j.nuclphysb.2013.10.010>.
- [69] P. Skands, S. Carrazza, and J. Rojo, "Tuning pythia 8.1: the monash 2013 tune", *The European Physical Journal C* **74** (2014), no. 8, 1–39, doi:10.1140/epjc/s10052-014-3024-y.
- [70] LHC Higgs Cross Section Working Group Collaboration, "Handbook of LHC Higgs Cross Sections: 4. Deciphering the Nature of the Higgs Sector", doi:10.23731/CYRM-2017-002, arXiv:1610.07922.
- [71] T. Sjöstrand, S. Mrenna, and P. Z. Skands, "PYTHIA 6.4 physics and manual", *JHEP* **05** (2006) 026, doi:10.1088/1126-6708/2006/05/026, arXiv:hep-ph/0603175.
- [72] J. Alwall et al., "MadGraph/MadEvent v4: the new web generation", *JHEP* **09** (2007) 028, doi:10.1088/1126-6708/2007/09/028, arXiv:0706.2334.
- [73] P. Meade and M. Reece, "BRIDGE: Branching ratio inquiry / decay generated events", arXiv:hep-ph/0703031.
- [74] CMS Collaboration, "Measurement of the WZ production cross section in pp collisions at $\sqrt(s) = 13$ TeV", *Phys. Lett.* **B766** (2017) 268–290, doi:10.1016/j.physletb.2017.01.011, arXiv:1607.06943.

- [75] CMS Collaboration, "Particle-flow reconstruction and global event description with the cms detector", *JINST* **12** (2017) P10003, doi:10.1088/1748-0221/12/10/P10003, arXiv:1706.04965.
- [76] A. Belyaev, N. D. Christensen, and A. Pukhov, "CalcHEP 3.4 for collider physics within and beyond the Standard Model", *Comput. Phys. Commun.* **184** (2013) 1729–1769, doi:10.1016/j.cpc.2013.01.014, arXiv:1207.6082.
- [77] C. H. Kom, A. Kulesza, and W. J. Stirling, "Pair production of j/ψ as a probe of double parton scattering at lhcb", *Phys. Rev. Lett.* **107** (Aug, 2011) 082002, doi:10.1103/PhysRevLett.107.082002.
- [78] CMS Collaboration, "CMS Luminosity Measurements for the 2016 Data Taking Period", Technical Report CMS-PAS-LUM-17-001, CERN, Geneva, 2017.
- [79] CMS Collaboration, "Studies of higgs boson production in the four-lepton final state at $\sqrt{s} = 13$ tev", CMS-PAS-HIG-15-004 (Mar, 2016).
- [80] J. Butterworth et al., "Pdf4lhc recommendations for lhc run ii", *Journal of Physics G: Nuclear and Particle Physics* **43** (2016), no. 2, 023001.
- [81] J. M. Campbell and R. Ellis, "Loops and legs in quantum field theory mcfm for the tevatron and the lhc", *Nuclear Physics B - Proceedings Supplements* **205** (2010) 10 – 15, doi:<http://dx.doi.org/10.1016/j.nuclphysbps.2010.08.011>.
- [82] LHC Higgs Cross Section Working Group Collaboration, "Handbook of LHC Higgs Cross Sections: 4. Deciphering the Nature of the Higgs Sector", doi:10.23731/CYRM-2017-002, arXiv:1610.07922.
- [83] CMS Collaboration, "Observation of a new boson with mass near 125 GeV in pp collisions at $\sqrt{s} = 7$ and 8 TeV", *JHEP* **1306** (2013) 081, doi:10.1007/JHEP06(2013)081, arXiv:1303.4571.
- [84] ATLAS and CMS Collaboration, "Procedure for the LHC Higgs boson search combination in summer 2011",.
- [85] CMS Collaboration, "Combined results of searches for the standard model Higgs boson in pp collisions at $\sqrt{s} = 7$ TeV", *Phys.Lett.* **B710** (2012) 26–48, doi:10.1016/j.physletb.2012.02.064, arXiv:1202.1488.

¹⁵⁰⁹ **A List of the Data and MC Signal Samples**

Table 12: Data samples from DoubleMu primary dataset in RECO format used in this analysis. Multi-volume datasets have their volume numbers in brackets.

Dataset name	Run range	No. Events	Integrated Lumi.
/DoubleMuon/Run2016B-07Aug17_ver[1,2]-v1/AOD	272760-275376	86,735,473	5.7
/DoubleMuon/Run2016C-07Aug17-v1/AOD	275656-276283	27,934,629	2.5
/DoubleMuon/Run2016D-07Aug17-v1/AOD	276315-276811	33,861,745	4.2
/DoubleMuon/Run2016E-07Aug17-v1/AOD	276831-277420	28,246,946	4.0
/DoubleMuon/Run2016F-07Aug17-v1/AOD	277932-278808	20,329,921	3.2
/DoubleMuon/Run2016G-07Aug17-v1/AOD	278820-280385	45,235,604	7.5
/DoubleMuon/Run2016H-07Aug17-v1/AOD	281085-284068	49,316,548	8.6

Table 13: The NMSSM MC samples used in the analysis.

$m_{H_{\text{MSSM}}}$, GeV/ c^2	$m_{A_{\text{MSSM}}}$, GeV/ c^2	Number of events
90	0.50	200,000
90	0.75	196,949
90	1.00	194,299
90	2.00	199,598
90	3.00	199,351
90	3.55	199,360
100	0.75	200,000
100	1.00	200,000
100	2.00	200,000
100	3.00	198,826
100	3.55	200,000
110	0.50	199,400
110	0.75	200,000
110	1.00	197,892
110	2.00	200,000
110	3.00	200,000
110	3.55	200,000
125	0.50	192,848
125	0.75	200,000
125	1.00	196,985
125	2.00	190,593
125	3.00	199,015
125	3.55	200,000
150	0.50	200,000
150	0.75	200,000
150	1.00	197,874
150	2.00	195,495
150	3.00	199,004
150	3.55	190,704

Table 14: Names DAS keys for the NMSSM sampleThe NMSSM MC samples used in the analysis.

```
/NMSSMHToAATo4Mu.mH_90_mA_0p25_TuneCUETP8M1_13TeV_pythia8/RunIISummer16DR80Premix-PUMoriond17_80X_mcRun2_asymptotic_201
/NMSSMHToAATo4Mu.mH_90_mA_0p5_TuneCUETP8M1_13TeV_pythia8/RunIISummer16DR80Premix-PUMoriond17_80X_mcRun2_asymptotic_201
/NMSSMHToAATo4Mu.mH_90_mA_0p75_TuneCUETP8M1_13TeV_pythia8/RunIISummer16DR80Premix-PUMoriond17_80X_mcRun2_asymptotic_201
/NMSSMHToAATo4Mu.mH_90_mA_1_TuneCUETP8M1_13TeV_pythia8/RunIISummer16DR80Premix-PUMoriond17_80X_mcRun2_asymptotic_201
/NMSSMHToAATo4Mu.mH_90_mA_2_TuneCUETP8M1_13TeV_pythia8/RunIISummer16DR80Premix-PUMoriond17_80X_mcRun2_asymptotic_201
/NMSSMHToAATo4Mu.mH_90_mA_3_TuneCUETP8M1_13TeV_pythia8/RunIISummer16DR80Premix-PUMoriond17_80X_mcRun2_asymptotic_201
/NMSSMHToAATo4Mu.mH_90_mA_3p55_TuneCUETP8M1_13TeV_pythia8/RunIISummer16DR80Premix-PUMoriond17_80X_mcRun2_asymptotic_201
/NMSSMHToAATo4Mu.mH_100_mA_0p25_TuneCUETP8M1_13TeV_pythia8/RunIISummer16DR80Premix-PUMoriond17_80X_mcRun2_asymptotic_201
/NMSSMHToAATo4Mu.mH_100_mA_0p5_TuneCUETP8M1_13TeV_pythia8/RunIISummer16DR80Premix-PUMoriond17_80X_mcRun2_asymptotic_201
/NMSSMHToAATo4Mu.mH_90_mA_0p55_TuneCUETP8M1_13TeV_pythia8/RunIISummer16DR80Premix-PUMoriond17_80X_mcRun2_asymptotic_201
/NMSSMHToAATo4Mu.mH_100_mA_0p75_TuneCUETP8M1_13TeV_pythia8/RunIISummer16DR80Premix-PUMoriond17_80X_mcRun2_asymptotic_201
/NMSSMHToAATo4Mu.mH_100_mA_1_TuneCUETP8M1_13TeV_pythia8/RunIISummer16DR80Premix-PUMoriond17_80X_mcRun2_asymptotic_201
/NMSSMHToAATo4Mu.mH_100_mA_2_TuneCUETP8M1_13TeV_pythia8/RunIISummer16DR80Premix-PUMoriond17_80X_mcRun2_asymptotic_201
/NMSSMHToAATo4Mu.mH_100_mA_3_TuneCUETP8M1_13TeV_pythia8/RunIISummer16DR80Premix-PUMoriond17_80X_mcRun2_asymptotic_201
/NMSSMHToAATo4Mu.mH_100_mA_3p55_TuneCUETP8M1_13TeV_pythia8/RunIISummer16DR80Premix-PUMoriond17_80X_mcRun2_asymptotic_201
/NMSSMHToAATo4Mu.mH_110_mA_0p25_TuneCUETP8M1_13TeV_pythia8/RunIISummer16DR80Premix-PUMoriond17_80X_mcRun2_asymptotic_201
/NMSSMHToAATo4Mu.mH_110_mA_0p75_TuneCUETP8M1_13TeV_pythia8/RunIISummer16DR80Premix-PUMoriond17_80X_mcRun2_asymptotic_201
/NMSSMHToAATo4Mu.mH_110_mA_1_TuneCUETP8M1_13TeV_pythia8/RunIISummer16DR80Premix-PUMoriond17_80X_mcRun2_asymptotic_201
```

Table 15: Names DAS keys for the NMSSM sampleThe NMSSM MC samples used in the analysis.

/NMSSM_HToAAATo4Mu.mH_110_mA_2_TuneCUETP8M1_13TeV_pythia8/RunIISummer16DR80Premix-PUMoriond17_80X_mcRun2_asymptotic_2016_Tranch
/NMSSM_HToAAATo4Mu.mH_110_mA_3_TuneCUETP8M1_13TeV_pythia8/RunIISummer16DR80Premix-PUMoriond17_80X_mcRun2_asymptotic_2016_Tranch
/NMSSM_HToAAATo4Mu.mH_110_mA_3p55_TuneCUETP8M1_13TeV_pythia8/RunIISummer16DR80Premix-PUMoriond17_80X_mcRun2_asymptotic_2016_Tranch
/NMSSM_HToAAATo4Mu.mH_125_mA_0p25_TuneCUETP8M1_13TeV_pythia8/RunIISummer16DR80Premix-PUMoriond17_80X_mcRun2_asymptotic_2016_Tranch
/NMSSM_HToAAATo4Mu.mH_125_mA_0p5_TuneCUETP8M1_13TeV_pythia8/RunIISummer16DR80Premix-PUMoriond17_80X_mcRun2_asymptotic_2016_Tranch
/NMSSM_HToAAATo4Mu.mH_125_mA_0p75_TuneCUETP8M1_13TeV_pythia8/RunIISummer16DR80Premix-PUMoriond17_80X_mcRun2_asymptotic_2016_Tranch
/NMSSM_HToAAATo4Mu.mH_125_mA_1_TuneCUETP8M1_13TeV_pythia8/RunIISummer16DR80Premix-PUMoriond17_80X_mcRun2_asymptotic_2016_Tranch
/NMSSM_HToAAATo4Mu.mH_125_mA_2_TuneCUETP8M1_13TeV_pythia8/RunIISummer16DR80Premix-PUMoriond17_80X_mcRun2_asymptotic_2016_Tranch
/NMSSM_HToAAATo4Mu.mH_125_mA_3_TuneCUETP8M1_13TeV_pythia8/RunIISummer16DR80Premix-PUMoriond17_80X_mcRun2_asymptotic_2016_Tranch
/NMSSM_HToAAATo4Mu.mH_125_mA_3p55_TuneCUETP8M1_13TeV_pythia8/RunIISummer16DR80Premix-PUMoriond17_80X_mcRun2_asymptotic_2016_Tranch
/NMSSM_HToAAATo4Mu.mH_150_mA_0p25_TuneCUETP8M1_13TeV_pythia8/RunIISummer16DR80Premix-PUMoriond17_80X_mcRun2_asymptotic_2016_Tranch
/NMSSM_HToAAATo4Mu.mH_150_mA_0p5_TuneCUETP8M1_13TeV_pythia8/RunIISummer16DR80Premix-PUMoriond17_80X_mcRun2_asymptotic_2016_Tranch
/NMSSM_HToAAATo4Mu.mH_150_mA_0p75_TuneCUETP8M1_13TeV_pythia8/RunIISummer16DR80Premix-PUMoriond17_80X_mcRun2_asymptotic_2016_Tranch
/NMSSM_HToAAATo4Mu.mH_150_mA_1_TuneCUETP8M1_13TeV_pythia8/RunIISummer16DR80Premix-PUMoriond17_80X_mcRun2_asymptotic_2016_Tranch
/NMSSM_HToAAATo4Mu.mH_150_mA_2_TuneCUETP8M1_13TeV_pythia8/RunIISummer16DR80Premix-PUMoriond17_80X_mcRun2_asymptotic_2016_Tranch
/NMSSM_HToAAATo4Mu.mH_150_mA_3_TuneCUETP8M1_13TeV_pythia8/RunIISummer16DR80Premix-PUMoriond17_80X_mcRun2_asymptotic_2016_Tranch
/NMSSM_HToAAATo4Mu.mH_150_mA_3p55_TuneCUETP8M1_13TeV_pythia8/RunIISummer16DR80Premix-PUMoriond17_80X_mcRun2_asymptotic_2016_Tranch

Table 16: The Dark SUSY MC samples used in the analysis

m_h , GeV/c 2	m_{h_1} , GeV/c 2	m_{n_D} , GeV/c 2	m_{γ_D} , GeV/c 2	$c\tau(\gamma_D)$, mm
125	10	1	0.25	0
125	10	1	0.25	0.05
125	10	1	0.25	0.1
125	10	1	0.25	0.5
125	10	1	0.25	1
125	10	1	0.25	2
125	10	1	0.25	5
125	10	1	0.25	20
125	10	1	0.25	100
125	10	1	0.4	0
125	10	1	0.4	0.5
125	10	1	0.4	1
125	10	1	0.4	2
125	10	1	0.4	5
125	10	1	0.4	20
125	10	1	0.4	100
125	10	1	0.7	0
125	10	1	0.7	0.5
125	10	1	0.7	1
125	10	1	0.7	20
125	10	1	0.7	100
125	10	1	1	0
125	10	1	1	5
125	10	1	1	20
125	10	1	1	100
125	10	1	5	0
125	10	1	5	20
125	10	1	5	100
125	10	1	8.5	0
125	10	1	8.5	2
125	10	1	8.5	20
125	10	1	8.5	100

/DarkSUSY_mH_125_mN1_10_mGammaD_0p25_cT_0.13TeV_20k_MG452_BR224_LHE_pythia8_GEN_SIM_MINIAOD_V2_v1/lpernie-DarkSUSY_mH_125_mN1_10_mGammaD_0p25_cT_0.13TeV_20k_RAW2DIGI_L1Reco_RECO_MINIAOD_V2_v1-2ddd25030f7878ebc0ae5f79cd4b430/USER
/DarkSUSY_mH_125_mN1_10_mGammaD_0p25_cT_0.13TeV_80k_MG452_BR224_LHE_pythia8_GEN_SIM_MINIAOD_V2_v1/lpernie-DarkSUSY_mH_125_mN1_10_mGammaD_0p25_cT_0.13TeV_80k_RAW2DIGI_L1Reco_RECO_MINIAOD_V2_v1-2ddd25030f7878ebc0ae5f79cd4b430/USER
/DarkSUSY_mH_125_mN1_10_mGammaD_0p25_cT_0p05_13TeV_20k_MG452_BR224_LHE_pythia8_GEN_SIM_MINIAOD_V2_v1/lpernie-DarkSUSY_mH_125_mN1_10_mGammaD_0p25_cT_0p05_13TeV_20k_RAW2DIGI_L1Reco_RECO_MINIAOD_V2_v1-2ddd25030f7878ebc0ae5f79cd4b430/USER
/DarkSUSY_mH_125_mN1_10_mGammaD_0p25_cT_0p1_13TeV_20k_MG452_BR224_LHE_pythia8_GEN_SIM_MINIAOD_V2_v1/lpernie-DarkSUSY_mH_125_mN1_10_mGammaD_0p25_cT_0p1_13TeV_20k_RAW2DIGI_L1Reco_RECO_MINIAOD_V2_v1-2ddd25030f7878ebc0ae5f79cd4b430/USER
/DarkSUSY_mH_125_mN1_10_mGammaD_0p25_cT_0p1_13TeV_80k_MG452_BR224_LHE_pythia8_GEN_SIM_MINIAOD_V2_v1/lpernie-DarkSUSY_mH_125_mN1_10_mGammaD_0p25_cT_0p1_13TeV_80k_RAW2DIGI_L1Reco_RECO_MINIAOD_V2_v1-2ddd25030f7878ebc0ae5f79cd4b430/USER
/DarkSUSY_mH_125_mN1_10_mGammaD_0p25_cT_0p5_13TeV_20k_MG452_BR224_LHE_pythia8_GEN_SIM_MINIAOD_V2_v1/lpernie-DarkSUSY_mH_125_mN1_10_mGammaD_0p25_cT_0p5_13TeV_20k_RAW2DIGI_L1Reco_RECO_MINIAOD_V2_v1-2ddd25030f7878ebc0ae5f79cd4b430/USER
/DarkSUSY_mH_125_mN1_10_mGammaD_0p25_cT_0p5_13TeV_80k_MG452_BR224_LHE_pythia8_GEN_SIM_MINIAOD_V2_v1/lpernie-DarkSUSY_mH_125_mN1_10_mGammaD_0p25_cT_0p5_13TeV_80k_RAW2DIGI_L1Reco_RECO_MINIAOD_V2_v1-2ddd25030f7878ebc0ae5f79cd4b430/USER
/DarkSUSY_mH_125_mN1_10_mGammaD_0p25_cT_100_13TeV_60k_MG452_BR224_LHE_pythia8_GEN_SIM_MINIAOD_V2_v1/lpernie-DarkSUSY_mH_125_mN1_10_mGammaD_0p25_cT_100_13TeV_60k_RAW2DIGI_L1Reco_RECO_MINIAOD_V2_v1-2ddd25030f7878ebc0ae5f79cd4b430/USER
/DarkSUSY_mH_125_mN1_10_mGammaD_0p25_cT_100_13TeV_62k_MG452_BR224_LHE_pythia8_GEN_SIM_MINIAOD_V2_v1/lpernie-DarkSUSY_mH_125_mN1_10_mGammaD_0p25_cT_100_13TeV_62k_RAW2DIGI_L1Reco_RECO_MINIAOD_V2_v1-2ddd25030f7878ebc0ae5f79cd4b430/USER
/DarkSUSY_mH_125_mN1_10_mGammaD_0p25_cT_100_13TeV_63k_MG452_BR224_LHE_pythia8_GEN_SIM_MINIAOD_V2_v1/lpernie-DarkSUSY_mH_125_mN1_10_mGammaD_0p25_cT_100_13TeV_63k_RAW2DIGI_L1Reco_RECO_MINIAOD_V2_v1-2ddd25030f7878ebc0ae5f79cd4b430/USER

```

/DarkSUSY_mH_125_mN1_10_mGammaD_0p25_cT_100_13TeV_64k_BR224_LHE_pythia8_GEN_SIM_MINIAOD-
_V2_v1/lpernie-DarkSUSY_mH_125_mN1_10_mGammaD_0p25_cT_100_13TeV_64k_RAW2DIGI_L1Reco_RECOCMINIAOD_V2_v1-
2ddd25030f7878ebc0ae5f7f9cd4b430/USER

/DarkSUSY_mH_125_mN1_10_mGammaD_0p25_cT_100_13TeV_65k_BR224_LHE_pythia8_GEN_SIM_MINIAOD-
_V2_v1/lpernie-DarkSUSY_mH_125_mN1_10_mGammaD_0p25_cT_100_13TeV_65k_RAW2DIGI_L1Reco_RECOCMINIAOD_V2_v1-
2ddd25030f7878ebc0ae5f7f9cd4b430/USER

/DarkSUSY_mH_125_mN1_10_mGammaD_0p25_cT_100_13TeV_66k_BR224_LHE_pythia8_GEN_SIM_MINIAOD-
_V2_v1/lpernie-DarkSUSY_mH_125_mN1_10_mGammaD_0p25_cT_100_13TeV_66k_RAW2DIGI_L1Reco_RECOCMINIAOD_V2_v1-
2ddd25030f7878ebc0ae5f7f9cd4b430/USER

/DarkSUSY_mH_125_mN1_10_mGammaD_0p25_cT_100_13TeV_67k_BR224_LHE_pythia8_GEN_SIM_MINIAOD-
_V2_v1/lpernie-DarkSUSY_mH_125_mN1_10_mGammaD_0p25_cT_100_13TeV_67k_RAW2DIGI_L1Reco_RECOCMINIAOD_V2_v1-
2ddd25030f7878ebc0ae5f7f9cd4b430/USER

/DarkSUSY_mH_125_mN1_10_mGammaD_0p25_cT_100_13TeV_68k_BR224_LHE_pythia8_GEN_SIM_MINIAOD-
_V2_v1/lpernie-DarkSUSY_mH_125_mN1_10_mGammaD_0p25_cT_100_13TeV_68k_RAW2DIGI_L1Reco_RECOCMINIAOD_V2_v1-
2ddd25030f7878ebc0ae5f7f9cd4b430/USER

/DarkSUSY_mH_125_mN1_10_mGammaD_0p25_cT_100_13TeV_69k_BR224_LHE_pythia8_GEN_SIM_MINIAOD-
_V2_v1/lpernie-DarkSUSY_mH_125_mN1_10_mGammaD_0p25_cT_100_13TeV_69k_RAW2DIGI_L1Reco_RECOCMINIAOD_V2_v1-
2ddd25030f7878ebc0ae5f7f9cd4b430/USER

/DarkSUSY_mH_125_mN1_10_mGammaD_0p25_cT_100_13TeV_70k_BR224_LHE_pythia8_GEN_SIM_MINIAOD-
_V2_v1/lpernie-DarkSUSY_mH_125_mN1_10_mGammaD_0p25_cT_100_13TeV_70k_RAW2DIGI_L1Reco_RECOCMINIAOD_V2_v1-
2ddd25030f7878ebc0ae5f7f9cd4b430/USER

/DarkSUSY_mH_125_mN1_10_mGammaD_0p25_cT_100_13TeV_71k_BR224_LHE_pythia8_GEN_SIM_MINIAOD-
_V2_v1/lpernie-DarkSUSY_mH_125_mN1_10_mGammaD_0p25_cT_100_13TeV_71k_RAW2DIGI_L1Reco_RECOCMINIAOD_V2_v1-
2ddd25030f7878ebc0ae5f7f9cd4b430/USER

/DarkSUSY_mH_125_mN1_10_mGammaD_0p25_cT_100_13TeV_72k_BR224_LHE_pythia8_GEN_SIM_MINIAOD-
_V2_v1/lpernie-DarkSUSY_mH_125_mN1_10_mGammaD_0p25_cT_100_13TeV_72k_RAW2DIGI_L1Reco_RECOCMINIAOD_V2_v1-
2ddd25030f7878ebc0ae5f7f9cd4b430/USER

/DarkSUSY_mH_125_mN1_10_mGammaD_0p25_cT_100_13TeV_73k_BR224_LHE_pythia8_GEN_SIM_MINIAOD-
_V2_v1/lpernie-DarkSUSY_mH_125_mN1_10_mGammaD_0p25_cT_100_13TeV_73k_RAW2DIGI_L1Reco_RECOCMINIAOD_V2_v1-
2ddd25030f7878ebc0ae5f7f9cd4b430/USER

```

/DarkSUSY_mH_125_mN1_10_mGammaD_0p25_cT_100_13TeV_74k_BR224_LHE_pythia8_GEN_SIM_MINIAOD-V2_v1/lpernie-DarkSUSY_mH_125_mN1_10_mGammaD_0p25_cT_100_13TeV_74k_RAW2DIGI_L1Reco_REC0_MINIAOD_V2_v1-2ddd25030f7878ebc0ae5f79cd4b430/USER
/DarkSUSY_mH_125_mN1_10_mGammaD_0p25_cT_100_13TeV_75k_BR224_LHE_pythia8_GEN_SIM_MINIAOD-V2_v1/lpernie-DarkSUSY_mH_125_mN1_10_mGammaD_0p25_cT_100_13TeV_75k_RAW2DIGI_L1Reco_REC0_MINIAOD_V2_v1-2ddd25030f7878ebc0ae5f79cd4b430/USER
/DarkSUSY_mH_125_mN1_10_mGammaD_0p25_cT_100_13TeV_76k_BR224_LHE_pythia8_GEN_SIM_MINIAOD-V2_v1/lpernie-DarkSUSY_mH_125_mN1_10_mGammaD_0p25_cT_100_13TeV_76k_RAW2DIGI_L1Reco_REC0_MINIAOD_V2_v1-2ddd25030f7878ebc0ae5f79cd4b430/USER
/DarkSUSY_mH_125_mN1_10_mGammaD_0p25_cT_100_13TeV_77k_BR224_LHE_pythia8_GEN_SIM_MINIAOD-V2_v1/lpernie-DarkSUSY_mH_125_mN1_10_mGammaD_0p25_cT_100_13TeV_77k_RAW2DIGI_L1Reco_REC0_MINIAOD_V2_v1-2ddd25030f7878ebc0ae5f79cd4b430/USER
/DarkSUSY_mH_125_mN1_10_mGammaD_0p25_cT_100_13TeV_78k_BR224_LHE_pythia8_GEN_SIM_MINIAOD-V2_v1/lpernie-DarkSUSY_mH_125_mN1_10_mGammaD_0p25_cT_100_13TeV_78k_RAW2DIGI_L1Reco_REC0_MINIAOD_V2_v1-2ddd25030f7878ebc0ae5f79cd4b430/USER
/DarkSUSY_mH_125_mN1_10_mGammaD_0p25_cT_100_13TeV_79k_BR224_LHE_pythia8_GEN_SIM_MINIAOD-V2_v1/lpernie-DarkSUSY_mH_125_mN1_10_mGammaD_0p25_cT_100_13TeV_79k_RAW2DIGI_L1Reco_REC0_MINIAOD_V2_v1-2ddd25030f7878ebc0ae5f79cd4b430/USER
/DarkSUSY_mH_125_mN1_10_mGammaD_0p25_cT_100_13TeV_80k_BR224_LHE_pythia8_GEN_SIM_MINIAOD-V2_v1/lpernie-DarkSUSY_mH_125_mN1_10_mGammaD_0p25_cT_100_13TeV_80k_RAW2DIGI_L1Reco_REC0_MINIAOD_V2_v1-2ddd25030f7878ebc0ae5f79cd4b430/USER
/DarkSUSY_mH_125_mN1_10_mGammaD_0p25_cT_100_13TeV_47k_BR224_LHE_pythia8_GEN_SIM_MINIAOD-V2_v1/lpernie-DarkSUSY_mH_125_mN1_10_mGammaD_0p25_cT_1_13TeV_47k_RAW2DIGI_L1Reco_REC0_MINIAOD_V2_v1-2ddd25030f7878ebc0ae5f79cd4b430/USER
/DarkSUSY_mH_125_mN1_10_mGammaD_0p25_cT_1_13TeV_48k_BR224_LHE_pythia8_GEN_SIM_MINIAOD-V2_v1/lpernie-DarkSUSY_mH_125_mN1_10_mGammaD_0p25_cT_1_13TeV_48k_RAW2DIGI_L1Reco_REC0_MINIAOD_V2_v1-2ddd25030f7878ebc0ae5f79cd4b430/USER
/DarkSUSY_mH_125_mN1_10_mGammaD_0p25_cT_1_13TeV_51k_BR224_LHE_pythia8_GEN_SIM_MINIAOD-V2_v1/lpernie-DarkSUSY_mH_125_mN1_10_mGammaD_0p25_cT_1_13TeV_51k_RAW2DIGI_L1Reco_REC0_MINIAOD_V2_v1-2ddd25030f7878ebc0ae5f79cd4b430/USER

```

/DarkSUSY_mH_125_mN1_10_mGammaD_0p25_cT_1_13TeV_52k_MG452_BR224_LHE_pythia8_GEN_SIM_MINIAOD-
_V2_v1/lpernie-DarkSUSY_mH_125_mN1_10_mGammaD_0p25_cT_1_13TeV_52k_RAW2DIGI_L1Recو_RECو_MINIAOD_V2_v1-
2ddd25030f7878ebc0ae5f7f9cd4b430/USER

/DarkSUSY_mH_125_mN1_10_mGammaD_0p25_cT_1_13TeV_53k_MG452_BR224_LHE_pythia8_GEN_SIM_MINIAOD-
_V2_v1/lpernie-DarkSUSY_mH_125_mN1_10_mGammaD_0p25_cT_1_13TeV_53k_RAW2DIGI_L1Recو_RECو_MINIAOD_V2_v1-
2ddd25030f7878ebc0ae5f7f9cd4b430/USER

/DarkSUSY_mH_125_mN1_10_mGammaD_0p25_cT_20_13TeV_67k_MG452_BR224_LHE_pythia8_GEN_SIM_MINIAOD-
_V2_v1/lpernie-DarkSUSY_mH_125_mN1_10_mGammaD_0p25_cT_20_13TeV_67k_RAW2DIGI_L1Recو_RECو_MINIAOD_V2_v1-
2ddd25030f7878ebc0ae5f7f9cd4b430/USER

/DarkSUSY_mH_125_mN1_10_mGammaD_0p25_cT_20_13TeV_68k_MG452_BR224_LHE_pythia8_GEN_SIM_MINIAOD-
_V2_v1/lpernie-DarkSUSY_mH_125_mN1_10_mGammaD_0p25_cT_20_13TeV_68k_RAW2DIGI_L1Recو_RECو_MINIAOD_V2_v1-
2ddd25030f7878ebc0ae5f7f9cd4b430/USER

/DarkSUSY_mH_125_mN1_10_mGammaD_0p25_cT_20_13TeV_69k_MG452_BR224_LHE_pythia8_GEN_SIM_MINIAOD-
_V2_v1/lpernie-DarkSUSY_mH_125_mN1_10_mGammaD_0p25_cT_20_13TeV_69k_RAW2DIGI_L1Recو_RECو_MINIAOD_V2_v1-
2ddd25030f7878ebc0ae5f7f9cd4b430/USER

/DarkSUSY_mH_125_mN1_10_mGammaD_0p25_cT_20_13TeV_70k_MG452_BR224_LHE_pythia8_GEN_SIM_MINIAOD-
_V2_v1/lpernie-DarkSUSY_mH_125_mN1_10_mGammaD_0p25_cT_20_13TeV_70k_RAW2DIGI_L1Recو_RECو_MINIAOD_V2_v1-
2ddd25030f7878ebc0ae5f7f9cd4b430/USER

/DarkSUSY_mH_125_mN1_10_mGammaD_0p25_cT_20_13TeV_71k_MG452_BR224_LHE_pythia8_GEN_SIM_MINIAOD-
_V2_v1/lpernie-DarkSUSY_mH_125_mN1_10_mGammaD_0p25_cT_20_13TeV_71k_RAW2DIGI_L1Recو_RECو_MINIAOD_V2_v1-
2ddd25030f7878ebc0ae5f7f9cd4b430/USER

/DarkSUSY_mH_125_mN1_10_mGammaD_0p25_cT_20_13TeV_72k_MG452_BR224_LHE_pythia8_GEN_SIM_MINIAOD-
_V2_v1/lpernie-DarkSUSY_mH_125_mN1_10_mGammaD_0p25_cT_20_13TeV_72k_RAW2DIGI_L1Recو_RECو_MINIAOD_V2_v1-
2ddd25030f7878ebc0ae5f7f9cd4b430/USER

/DarkSUSY_mH_125_mN1_10_mGammaD_0p25_cT_20_13TeV_73k_MG452_BR224_LHE_pythia8_GEN_SIM_MINIAOD-
_V2_v1/lpernie-DarkSUSY_mH_125_mN1_10_mGammaD_0p25_cT_20_13TeV_73k_RAW2DIGI_L1Recو_RECو_MINIAOD_V2_v1-
2ddd25030f7878ebc0ae5f7f9cd4b430/USER

/DarkSUSY_mH_125_mN1_10_mGammaD_0p25_cT_20_13TeV_74k_MG452_BR224_LHE_pythia8_GEN_SIM_MINIAOD-
_V2_v1/lpernie-DarkSUSY_mH_125_mN1_10_mGammaD_0p25_cT_20_13TeV_74k_RAW2DIGI_L1Recو_RECو_MINIAOD_V2_v1-
2ddd25030f7878ebc0ae5f7f9cd4b430/USER

```

/DarkSUSY_mH_125_mN1_10_mGammaD_0p25_cT_20_13TeV_75k_BR224_LHE_pythia8_GEN_SIM_MINIAOD_V2_v1/lpernie-DarkSUSY_mH_125_mN1_10_mGammaD_0p25_cT_20_13TeV_75k_RAW2DIGI_L1Reco_RECO_MINIAOD_V2_v1-2ddd25030f7878ebc0ae5f79cd4b430/USER
/DarkSUSY_mH_125_mN1_10_mGammaD_0p25_cT_20_13TeV_76k_BR224_LHE_pythia8_GEN_SIM_MINIAOD_V2_v1/lpernie-DarkSUSY_mH_125_mN1_10_mGammaD_0p25_cT_20_13TeV_76k_RAW2DIGI_L1Reco_RECO_MINIAOD_V2_v1-2ddd25030f7878ebc0ae5f79cd4b430/USER
/DarkSUSY_mH_125_mN1_10_mGammaD_0p25_cT_20_13TeV_77k_BR224_LHE_pythia8_GEN_SIM_MINIAOD_V2_v1/lpernie-DarkSUSY_mH_125_mN1_10_mGammaD_0p25_cT_20_13TeV_77k_RAW2DIGI_L1Reco_RECO_MINIAOD_V2_v1-2ddd25030f7878ebc0ae5f79cd4b430/USER
/DarkSUSY_mH_125_mN1_10_mGammaD_0p25_cT_20_13TeV_78k_BR224_LHE_pythia8_GEN_SIM_MINIAOD_V2_v1/lpernie-DarkSUSY_mH_125_mN1_10_mGammaD_0p25_cT_20_13TeV_78k_RAW2DIGI_L1Reco_RECO_MINIAOD_V2_v1-2ddd25030f7878ebc0ae5f79cd4b430/USER
/DarkSUSY_mH_125_mN1_10_mGammaD_0p25_cT_20_13TeV_79k_BR224_LHE_pythia8_GEN_SIM_MINIAOD_V2_v1/lpernie-DarkSUSY_mH_125_mN1_10_mGammaD_0p25_cT_20_13TeV_79k_RAW2DIGI_L1Reco_RECO_MINIAOD_V2_v1-2ddd25030f7878ebc0ae5f79cd4b430/USER
/DarkSUSY_mH_125_mN1_10_mGammaD_0p25_cT_20_13TeV_80k_BR224_LHE_pythia8_GEN_SIM_MINIAOD_V2_v1/lpernie-DarkSUSY_mH_125_mN1_10_mGammaD_0p25_cT_20_13TeV_80k_RAW2DIGI_L1Reco_RECO_MINIAOD_V2_v1-2ddd25030f7878ebc0ae5f79cd4b430/USER
/DarkSUSY_mH_125_mN1_10_mGammaD_0p25_cT_20_13TeV_847k_BR224_LHE_pythia8_GEN_SIM_MINIAOD_V2_v1/lpernie-DarkSUSY_mH_125_mN1_10_mGammaD_0p25_cT_2_13TeV_47k_RAW2DIGI_L1Reco_RECO_MINIAOD_V2_v1-2ddd25030f7878ebc0ae5f79cd4b430/USER
/DarkSUSY_mH_125_mN1_10_mGammaD_0p25_cT_2_13TeV_48k_BR224_LHE_pythia8_GEN_SIM_MINIAOD_V2_v1/lpernie-DarkSUSY_mH_125_mN1_10_mGammaD_0p25_cT_2_13TeV_48k_RAW2DIGI_L1Reco_RECO_MINIAOD_V2_v1-2ddd25030f7878ebc0ae5f79cd4b430/USER
/DarkSUSY_mH_125_mN1_10_mGammaD_0p25_cT_2_13TeV_49k_BR224_LHE_pythia8_GEN_SIM_MINIAOD_V2_v1/lpernie-DarkSUSY_mH_125_mN1_10_mGammaD_0p25_cT_2_13TeV_49k_RAW2DIGI_L1Reco_RECO_MINIAOD_V2_v1-2ddd25030f7878ebc0ae5f79cd4b430/USER
/DarkSUSY_mH_125_mN1_10_mGammaD_0p25_cT_2_13TeV_51k_BR224_LHE_pythia8_GEN_SIM_MINIAOD_V2_v1/lpernie-DarkSUSY_mH_125_mN1_10_mGammaD_0p25_cT_2_13TeV_51k_RAW2DIGI_L1Reco_RECO_MINIAOD_V2_v1-2ddd25030f7878ebc0ae5f79cd4b430/USER

```

/DarkSUSY_mH_125_mN1_10_mGammaD_0p25_cT_2_13TeV_52k_BR224_LHE_pythia8_GEN_SIM_MINIAOD-
_V2_v1/lpernie-DarkSUSY_mH_125_mN1_10_mGammaD_0p25_cT_2_13TeV_52k_RAW2DIGI_L1Reco_RECO_MINIAOD_V2_v1-
2ddd25030f7878ebc0ae5f7f9cd4b430/USER

/DarkSUSY_mH_125_mN1_10_mGammaD_0p25_cT_2_13TeV_53k_BR224_LHE_pythia8_GEN_SIM_MINIAOD-
_V2_v1/lpernie-DarkSUSY_mH_125_mN1_10_mGammaD_0p25_cT_2_13TeV_53k_RAW2DIGI_L1Reco_RECO_MINIAOD_V2_v1-
2ddd25030f7878ebc0ae5f7f9cd4b430/USER

/DarkSUSY_mH_125_mN1_10_mGammaD_0p25_cT_5_13TeV_47k_BR224_LHE_pythia8_GEN_SIM_MINIAOD-
_V2_v1/lpernie-DarkSUSY_mH_125_mN1_10_mGammaD_0p25_cT_5_13TeV_47k_RAW2DIGI_L1Reco_RECO_MINIAOD_V2_v1-
2ddd25030f7878ebc0ae5f7f9cd4b430/USER

/DarkSUSY_mH_125_mN1_10_mGammaD_0p25_cT_5_13TeV_48k_BR224_LHE_pythia8_GEN_SIM_MINIAOD-
_V2_v1/lpernie-DarkSUSY_mH_125_mN1_10_mGammaD_0p25_cT_5_13TeV_48k_RAW2DIGI_L1Reco_RECO_MINIAOD_V2_v1-
2ddd25030f7878ebc0ae5f7f9cd4b430/USER

/DarkSUSY_mH_125_mN1_10_mGammaD_0p25_cT_5_13TeV_49k_BR224_LHE_pythia8_GEN_SIM_MINIAOD-
_V2_v1/lpernie-DarkSUSY_mH_125_mN1_10_mGammaD_0p25_cT_5_13TeV_49k_RAW2DIGI_L1Reco_RECO_MINIAOD_V2_v1-
2ddd25030f7878ebc0ae5f7f9cd4b430/USER

/DarkSUSY_mH_125_mN1_10_mGammaD_0p25_cT_5_13TeV_51k_BR224_LHE_pythia8_GEN_SIM_MINIAOD-
_V2_v1/lpernie-DarkSUSY_mH_125_mN1_10_mGammaD_0p25_cT_5_13TeV_51k_RAW2DIGI_L1Reco_RECO_MINIAOD_V2_v1-
2ddd25030f7878ebc0ae5f7f9cd4b430/USER

/DarkSUSY_mH_125_mN1_10_mGammaD_0p25_cT_5_13TeV_52k_BR224_LHE_pythia8_GEN_SIM_MINIAOD-
_V2_v1/lpernie-DarkSUSY_mH_125_mN1_10_mGammaD_0p25_cT_5_13TeV_52k_RAW2DIGI_L1Reco_RECO_MINIAOD_V2_v1-
2ddd25030f7878ebc0ae5f7f9cd4b430/USER

/DarkSUSY_mH_125_mN1_10_mGammaD_0p25_cT_5_13TeV_53k_BR224_LHE_pythia8_GEN_SIM_MINIAOD-
_V2_v1/lpernie-DarkSUSY_mH_125_mN1_10_mGammaD_0p25_cT_5_13TeV_53k_RAW2DIGI_L1Reco_RECO_MINIAOD_V2_v1-
2ddd25030f7878ebc0ae5f7f9cd4b430/USER

/DarkSUSY_mH_125_mN1_10_mGammaD_0p25_cT_0_13TeV_20k_BR224_LHE_pythia8_GEN_SIM_MINIAOD-
_V2_v1/wshi-DarkSUSY_mH_125_mN1_10_mGammaD_0p25_cT_0_13TeV_20k_RAW2DIGI_L1Reco_RECO_MINIAOD_V2_v1-
2ddd25030f7878ebc0ae5f7f9cd4b430/USER

/DarkSUSY_mH_125_mN1_10_mGammaD_0p4_cT_0_13TeV_80k_BR224_LHE_pythia8_GEN_SIM_MINIAOD-
_V2_v1/wshi-DarkSUSY_mH_125_mN1_10_mGammaD_0p4_cT_0_13TeV_80k_RAW2DIGI_L1Reco_RECO_MINIAOD_V2_v1-
2ddd25030f7878ebc0ae5f7f9cd4b430/USER

```

/DarkSUSY_mH_125_mN1_10_mGammaD_0p4_cT_0p5_13TeV_20k_BR224_LHE_pythia8_GEN_SIM_MINIAOD_V2_v1/wshi-DarkSUSY_mH_125_mN1_10_mGammaD_0p4_cT_0p5_13TeV_20k_RAW2DIGI_L1Reco_RECO_MINIAOD_V2_v1-2ddd25030f7878ebc0ae5f79cd4b430/USER
/DarkSUSY_mH_125_mN1_10_mGammaD_0p4_cT_0p5_13TeV_80k_BR224_LHE_pythia8_GEN_SIM_MINIAOD_V2_v1/wshi-DarkSUSY_mH_125_mN1_10_mGammaD_0p4_cT_0p5_13TeV_80k_RAW2DIGI_L1Reco_RECO_MINIAOD_V2_v1-2ddd25030f7878ebc0ae5f79cd4b430/USER
/DarkSUSY_mH_125_mN1_10_mGammaD_0p4_cT_100_13TeV_59k_BR224_LHE_pythia8_GEN_SIM_MINIAOD_V2_v1/wshi-DarkSUSY_mH_125_mN1_10_mGammaD_0p4_cT_100_13TeV_59k_RAW2DIGI_L1Reco_RECO_MINIAOD_V2_v1-2ddd25030f7878ebc0ae5f79cd4b430/USER
/DarkSUSY_mH_125_mN1_10_mGammaD_0p4_cT_100_13TeV_60k_BR224_LHE_pythia8_GEN_SIM_MINIAOD_V2_v1/wshi-DarkSUSY_mH_125_mN1_10_mGammaD_0p4_cT_100_13TeV_60k_RAW2DIGI_L1Reco_RECO_MINIAOD_V2_v1-2ddd25030f7878ebc0ae5f79cd4b430/USER
/DarkSUSY_mH_125_mN1_10_mGammaD_0p4_cT_100_13TeV_61k_BR224_LHE_pythia8_GEN_SIM_MINIAOD_V2_v1/wshi-DarkSUSY_mH_125_mN1_10_mGammaD_0p4_cT_100_13TeV_61k_RAW2DIGI_L1Reco_RECO_MINIAOD_V2_v1-2ddd25030f7878ebc0ae5f79cd4b430/USER
/DarkSUSY_mH_125_mN1_10_mGammaD_0p4_cT_100_13TeV_62k_BR224_LHE_pythia8_GEN_SIM_MINIAOD_V2_v1/wshi-DarkSUSY_mH_125_mN1_10_mGammaD_0p4_cT_100_13TeV_62k_RAW2DIGI_L1Reco_RECO_MINIAOD_V2_v1-2ddd25030f7878ebc0ae5f79cd4b430/USER
/DarkSUSY_mH_125_mN1_10_mGammaD_0p4_cT_100_13TeV_63k_BR224_LHE_pythia8_GEN_SIM_MINIAOD_V2_v1/wshi-DarkSUSY_mH_125_mN1_10_mGammaD_0p4_cT_100_13TeV_63k_RAW2DIGI_L1Reco_RECO_MINIAOD_V2_v1-2ddd25030f7878ebc0ae5f79cd4b430/USER
/DarkSUSY_mH_125_mN1_10_mGammaD_0p4_cT_100_13TeV_65k_BR224_LHE_pythia8_GEN_SIM_MINIAOD_V2_v1/wshi-DarkSUSY_mH_125_mN1_10_mGammaD_0p4_cT_100_13TeV_65k_RAW2DIGI_L1Reco_RECO_MINIAOD_V2_v1-2ddd25030f7878ebc0ae5f79cd4b430/USER
/DarkSUSY_mH_125_mN1_10_mGammaD_0p4_cT_100_13TeV_66k_BR224_LHE_pythia8_GEN_SIM_MINIAOD_V2_v1/wshi-DarkSUSY_mH_125_mN1_10_mGammaD_0p4_cT_100_13TeV_66k_RAW2DIGI_L1Reco_RECO_MINIAOD_V2_v1-2ddd25030f7878ebc0ae5f79cd4b430/USER
/DarkSUSY_mH_125_mN1_10_mGammaD_0p4_cT_100_13TeV_67k_BR224_LHE_pythia8_GEN_SIM_MINIAOD_V2_v1/wshi-DarkSUSY_mH_125_mN1_10_mGammaD_0p4_cT_100_13TeV_67k_RAW2DIGI_L1Reco_RECO_MINIAOD_V2_v1-2ddd25030f7878ebc0ae5f79cd4b430/USER

```

/DarkSUSY_mH_125_mN1_10_mGammaD_0p4_cT_100_13TeV_69k_MG452_BR224_LHE_pythia8_GEN_SIM_MINIAOD-
_V2_v1/wshi-DarkSUSY_mH_125_mN1_10_mGammaD_0p4_cT_100_13TeV_69k_RAW2DIGI_L1Reco_RECOPROJECTOR_MINIAOD_V2_v1-
2ddd25030f7878ebc0ae5f7f9cd4b430/USER

/DarkSUSY_mH_125_mN1_10_mGammaD_0p4_cT_100_13TeV_70k_MG452_BR224_LHE_pythia8_GEN_SIM_MINIAOD-
_V2_v1/wshi-DarkSUSY_mH_125_mN1_10_mGammaD_0p4_cT_100_13TeV_70k_RAW2DIGI_L1Reco_RECOPROJECTOR_MINIAOD_V2_v1-
2ddd25030f7878ebc0ae5f7f9cd4b430/USER

/DarkSUSY_mH_125_mN1_10_mGammaD_0p4_cT_100_13TeV_72k_MG452_BR224_LHE_pythia8_GEN_SIM_MINIAOD-
_V2_v1/wshi-DarkSUSY_mH_125_mN1_10_mGammaD_0p4_cT_100_13TeV_72k_RAW2DIGI_L1Reco_RECOPROJECTOR_MINIAOD_V2_v1-
2ddd25030f7878ebc0ae5f7f9cd4b430/USER

/DarkSUSY_mH_125_mN1_10_mGammaD_0p4_cT_100_13TeV_73k_MG452_BR224_LHE_pythia8_GEN_SIM_MINIAOD-
_V2_v1/wshi-DarkSUSY_mH_125_mN1_10_mGammaD_0p4_cT_100_13TeV_73k_RAW2DIGI_L1Reco_RECOPROJECTOR_MINIAOD_V2_v1-
2ddd25030f7878ebc0ae5f7f9cd4b430/USER

/DarkSUSY_mH_125_mN1_10_mGammaD_0p4_cT_100_13TeV_76k_MG452_BR224_LHE_pythia8_GEN_SIM_MINIAOD-
_V2_v1/wshi-DarkSUSY_mH_125_mN1_10_mGammaD_0p4_cT_100_13TeV_76k_RAW2DIGI_L1Reco_RECOPROJECTOR_MINIAOD_V2_v1-
2ddd25030f7878ebc0ae5f7f9cd4b430/USER

/DarkSUSY_mH_125_mN1_10_mGammaD_0p4_cT_100_13TeV_79k_MG452_BR224_LHE_pythia8_GEN_SIM_MINIAOD-
_V2_v1/wshi-DarkSUSY_mH_125_mN1_10_mGammaD_0p4_cT_100_13TeV_79k_RAW2DIGI_L1Reco_RECOPROJECTOR_MINIAOD_V2_v1-
2ddd25030f7878ebc0ae5f7f9cd4b430/USER

/DarkSUSY_mH_125_mN1_10_mGammaD_0p4_cT_100_13TeV_80k_MG452_BR224_LHE_pythia8_GEN_SIM_MINIAOD-
_V2_v1/wshi-DarkSUSY_mH_125_mN1_10_mGammaD_0p4_cT_100_13TeV_80k_RAW2DIGI_L1Reco_RECOPROJECTOR_MINIAOD_V2_v1-
2ddd25030f7878ebc0ae5f7f9cd4b430/USER

/DarkSUSY_mH_125_mN1_10_mGammaD_0p4_cT_100_13TeV_80k_MG452_BR224_LHE_pythia8_GEN_SIM_MINIAOD-
_V2_v1/wshi-DarkSUSY_mH_125_mN1_10_mGammaD_0p4_cT_100_13TeV_80k_RAW2DIGI_L1Reco_RECOPROJECTOR_MINIAOD_V2_v1-
2ddd25030f7878ebc0ae5f7f9cd4b430/USER

/DarkSUSY_mH_125_mN1_10_mGammaD_0p4_cT_11_13TeV_47k_MG452_BR224_LHE_pythia8_GEN_SIM_MINIAOD-
_V2_v1/wshi-DarkSUSY_mH_125_mN1_10_mGammaD_0p4_cT_11_13TeV_47k_RAW2DIGI_L1Reco_RECOPROJECTOR_MINIAOD_V2_v1-
2ddd25030f7878ebc0ae5f7f9cd4b430/USER

/DarkSUSY_mH_125_mN1_10_mGammaD_0p4_cT_11_13TeV_48k_MG452_BR224_LHE_pythia8_GEN_SIM_MINIAOD-
_V2_v1/wshi-DarkSUSY_mH_125_mN1_10_mGammaD_0p4_cT_11_13TeV_48k_RAW2DIGI_L1Reco_RECOPROJECTOR_MINIAOD_V2_v1-
2ddd25030f7878ebc0ae5f7f9cd4b430/USER

/DarkSUSY_mH_125_mN1_10_mGammaD_0p4_cT_1_13TeV_49k_MG452_BR224_LHE_pythia8_GEN_SIM_MINIAOD-
_V2_v1/wshi-DarkSUSY_mH_125_mN1_10_mGammaD_0p4_cT_1_13TeV_49k_RAW2DIGI_L1Reco_RECOPROJECTOR_MINIAOD_V2_v1-
2ddd25030f7878ebc0ae5f7f9cd4b430/USER

```

/DarkSUSY_mH_125_mN1_10_mGammaD_0p4_cT_1_13TeV_51k_BR224_LHE_pythia8_GEN_SIM_MINIAOD-V2_v1/wshi-DarkSUSY_mH_125_mN1_10_mGammaD_0p4_cT_1_13TeV_51k_RAW2DIGI_L1Reco_RECO_MINIAOD_V2_v1-2ddd25030f7878ebc0ae5f79cd4b430/USER
/DarkSUSY_mH_125_mN1_10_mGammaD_0p4_cT_1_13TeV_52k_BR452_BR224_LHE_pythia8_GEN_SIM_MINIAOD-V2_v1/wshi-DarkSUSY_mH_125_mN1_10_mGammaD_0p4_cT_1_13TeV_52k_RAW2DIGI_L1Reco_RECO_MINIAOD_V2_v1-2ddd25030f7878ebc0ae5f79cd4b430/USER
/DarkSUSY_mH_125_mN1_10_mGammaD_0p4_cT_1_13TeV_53k_BR452_BR224_LHE_pythia8_GEN_SIM_MINIAOD-V2_v1/wshi-DarkSUSY_mH_125_mN1_10_mGammaD_0p4_cT_1_13TeV_53k_RAW2DIGI_L1Reco_RECO_MINIAOD_V2_v1-2ddd25030f7878ebc0ae5f79cd4b430/USER
/DarkSUSY_mH_125_mN1_10_mGammaD_0p4_cT_20_13TeV_67k_BR452_BR224_LHE_pythia8_GEN_SIM_MINIAOD-V2_v1/wshi-DarkSUSY_mH_125_mN1_10_mGammaD_0p4_cT_20_13TeV_67k_RAW2DIGI_L1Reco_RECO_MINIAOD_V2_v1-2ddd25030f7878ebc0ae5f79cd4b430/USER
/DarkSUSY_mH_125_mN1_10_mGammaD_0p4_cT_20_13TeV_69k_BR452_BR224_LHE_pythia8_GEN_SIM_MINIAOD-V2_v1/wshi-DarkSUSY_mH_125_mN1_10_mGammaD_0p4_cT_20_13TeV_69k_RAW2DIGI_L1Reco_RECO_MINIAOD_V2_v1-2ddd25030f7878ebc0ae5f79cd4b430/USER
/DarkSUSY_mH_125_mN1_10_mGammaD_0p4_cT_20_13TeV_70k_BR452_BR224_LHE_pythia8_GEN_SIM_MINIAOD-V2_v1/wshi-DarkSUSY_mH_125_mN1_10_mGammaD_0p4_cT_20_13TeV_70k_RAW2DIGI_L1Reco_RECO_MINIAOD_V2_v1-2ddd25030f7878ebc0ae5f79cd4b430/USER
/DarkSUSY_mH_125_mN1_10_mGammaD_0p4_cT_20_13TeV_71k_BR452_BR224_LHE_pythia8_GEN_SIM_MINIAOD-V2_v1/wshi-DarkSUSY_mH_125_mN1_10_mGammaD_0p4_cT_20_13TeV_71k_RAW2DIGI_L1Reco_RECO_MINIAOD_V2_v1-2ddd25030f7878ebc0ae5f79cd4b430/USER
/DarkSUSY_mH_125_mN1_10_mGammaD_0p4_cT_20_13TeV_72k_BR452_BR224_LHE_pythia8_GEN_SIM_MINIAOD-V2_v1/wshi-DarkSUSY_mH_125_mN1_10_mGammaD_0p4_cT_20_13TeV_72k_RAW2DIGI_L1Reco_RECO_MINIAOD_V2_v1-2ddd25030f7878ebc0ae5f79cd4b430/USER
/DarkSUSY_mH_125_mN1_10_mGammaD_0p4_cT_20_13TeV_73k_BR452_BR224_LHE_pythia8_GEN_SIM_MINIAOD-V2_v1/wshi-DarkSUSY_mH_125_mN1_10_mGammaD_0p4_cT_20_13TeV_73k_RAW2DIGI_L1Reco_RECO_MINIAOD_V2_v1-2ddd25030f7878ebc0ae5f79cd4b430/USER
/DarkSUSY_mH_125_mN1_10_mGammaD_0p4_cT_20_13TeV_74k_BR452_BR224_LHE_pythia8_GEN_SIM_MINIAOD-V2_v1/wshi-DarkSUSY_mH_125_mN1_10_mGammaD_0p4_cT_20_13TeV_74k_RAW2DIGI_L1Reco_RECO_MINIAOD_V2_v1-2ddd25030f7878ebc0ae5f79cd4b430/USER

```
/DarkSUSY_mH_125_mN1_10_mGammaD_0p4_cT_20_13TeV_75k_MG452_BR224_LHE_pythia8_GEN_SIM_MINIAOD-
_V2_v1/wshi-DarkSUSY_mH_125_mN1_10_mGammaD_0p4_cT_20_13TeV_75k_RAW2DIGI_L1Reco_REC0_MINIAOD_V2_v1-
2dd25030F7878ebc0ae5f7f9cd4b430/USER
/DarkSUSY_mH_125_mN1_10_mGammaD_0p4_cT_20_13TeV_76k_MG452_BR224_LHE_pythia8_GEN_SIM_MINIAOD-
_V2_v1/wshi-DarkSUSY_mH_125_mN1_10_mGammaD_0p4_cT_20_13TeV_76k_RAW2DIGI_L1Reco_REC0_MINIAOD_V2_v1-
2dd25030F7878ebc0ae5f7f9cd4b430/USER
/DarkSUSY_mH_125_mN1_10_mGammaD_0p4_cT_20_13TeV_78k_MG452_BR224_LHE_pythia8_GEN_SIM_MINIAOD-
_V2_v1/wshi-DarkSUSY_mH_125_mN1_10_mGammaD_0p4_cT_20_13TeV_78k_RAW2DIGI_L1Reco_REC0_MINIAOD_V2_v1-
2dd25030F7878ebc0ae5f7f9cd4b430/USER
/DarkSUSY_mH_125_mN1_10_mGammaD_0p4_cT_20_13TeV_79k_MG452_BR224_LHE_pythia8_GEN_SIM_MINIAOD-
_V2_v1/wshi-DarkSUSY_mH_125_mN1_10_mGammaD_0p4_cT_20_13TeV_79k_RAW2DIGI_L1Reco_REC0_MINIAOD_V2_v1-
2dd25030F7878ebc0ae5f7f9cd4b430/USER
/DarkSUSY_mH_125_mN1_10_mGammaD_0p4_cT_2_13TeV_47k_MG452_BR224_LHE_pythia8_GEN_SIM_MINIAOD-
_V2_v1/wshi-DarkSUSY_mH_125_mN1_10_mGammaD_0p4_cT_2_13TeV_47k_RAW2DIGI_L1Reco_REC0_MINIAOD_V2_v1-
2dd25030F7878ebc0ae5f7f9cd4b430/USER
/V2_v1/wshi-DarkSUSY_mH_125_mN1_10_mGammaD_0p4_cT_2_13TeV_48k_MG452_BR224_LHE_pythia8_GEN_SIM_MINIAOD-
2dd25030F7878ebc0ae5f7f9cd4b430/USER
/DarkSUSY_mH_125_mN1_10_mGammaD_0p4_cT_2_13TeV_48k_MG452_BR224_LHE_pythia8_GEN_SIM_MINIAOD-
_V2_v1/wshi-DarkSUSY_mH_125_mN1_10_mGammaD_0p4_cT_2_13TeV_48k_RAW2DIGI_L1Reco_REC0_MINIAOD_V2_v1-
2dd25030F7878ebc0ae5f7f9cd4b430/USER
/V2_v1/wshi-DarkSUSY_mH_125_mN1_10_mGammaD_0p4_cT_2_13TeV_48k_MG452_BR224_LHE_pythia8_GEN_SIM_MINIAOD-
2dd25030F7878ebc0ae5f7f9cd4b430/USER
/V2_v1/wshi-DarkSUSY_mH_125_mN1_10_mGammaD_0p4_cT_2_13TeV_49k_MG452_BR224_LHE_pythia8_GEN_SIM_MINIAOD-
2dd25030F7878ebc0ae5f7f9cd4b430/USER
/V2_v1/wshi-DarkSUSY_mH_125_mN1_10_mGammaD_0p4_cT_2_13TeV_51k_MG452_BR224_LHE_pythia8_GEN_SIM_MINIAOD-
2dd25030F7878ebc0ae5f7f9cd4b430/USER
/V2_v1/wshi-DarkSUSY_mH_125_mN1_10_mGammaD_0p4_cT_2_13TeV_51k_RAW2DIGI_L1Reco_REC0_MINIAOD_V2_v1-
2dd25030F7878ebc0ae5f7f9cd4b430/USER
/DarkSUSY_mH_125_mN1_10_mGammaD_0p4_cT_2_13TeV_52k_MG452_BR224_LHE_pythia8_GEN_SIM_MINIAOD-
_V2_v1/wshi-DarkSUSY_mH_125_mN1_10_mGammaD_0p4_cT_2_13TeV_52k_RAW2DIGI_L1Reco_REC0_MINIAOD_V2_v1-
2dd25030F7878ebc0ae5f7f9cd4b430/USER
/DarkSUSY_mH_125_mN1_10_mGammaD_0p4_cT_2_13TeV_53k_RAW2DIGI_L1Reco_REC0_MINIAOD_V2_v1-
2dd25030F7878ebc0ae5f7f9cd4b430/USER
```

/DarkSUSY_mH_125_mN1_10_mGammaD_0p4_cT_5_13TeV_47k_MG452_BR224_LHE_pythia8_GEN_SIM_MINIAOD-V2_v1/wshi-DarkSUSY_mH_125_mN1_10_mGammaD_0p4_cT_5_13TeV_47k_RAW2DIGI_L1Reco_RECO_MINIAOD_V2_v1-2ddd25030f7878ebc0ae5f79cd4b430/USER
/DarkSUSY_mH_125_mN1_10_mGammaD_0p4_cT_5_13TeV_48k_MG452_BR224_LHE_pythia8_GEN_SIM_MINIAOD-V2_v1/wshi-DarkSUSY_mH_125_mN1_10_mGammaD_0p4_cT_5_13TeV_48k_RAW2DIGI_L1Reco_RECO_MINIAOD_V2_v1-2ddd25030f7878ebc0ae5f79cd4b430/USER
/DarkSUSY_mH_125_mN1_10_mGammaD_0p4_cT_5_13TeV_49k_MG452_BR224_LHE_pythia8_GEN_SIM_MINIAOD-V2_v1/wshi-DarkSUSY_mH_125_mN1_10_mGammaD_0p4_cT_5_13TeV_49k_RAW2DIGI_L1Reco_RECO_MINIAOD_V2_v1-2ddd25030f7878ebc0ae5f79cd4b430/USER
/DarkSUSY_mH_125_mN1_10_mGammaD_0p4_cT_5_13TeV_51k_MG452_BR224_LHE_pythia8_GEN_SIM_MINIAOD-V2_v1/wshi-DarkSUSY_mH_125_mN1_10_mGammaD_0p4_cT_5_13TeV_51k_RAW2DIGI_L1Reco_RECO_MINIAOD_V2_v1-2ddd25030f7878ebc0ae5f79cd4b430/USER
/DarkSUSY_mH_125_mN1_10_mGammaD_0p4_cT_5_13TeV_52k_MG452_BR224_LHE_pythia8_GEN_SIM_MINIAOD-V2_v1/wshi-DarkSUSY_mH_125_mN1_10_mGammaD_0p4_cT_5_13TeV_52k_RAW2DIGI_L1Reco_RECO_MINIAOD_V2_v1-2ddd25030f7878ebc0ae5f79cd4b430/USER
/DarkSUSY_mH_125_mN1_10_mGammaD_0p4_cT_5_13TeV_53k_MG452_BR224_LHE_pythia8_GEN_SIM_MINIAOD-V2_v1/wshi-DarkSUSY_mH_125_mN1_10_mGammaD_0p4_cT_5_13TeV_53k_RAW2DIGI_L1Reco_RECO_MINIAOD_V2_v1-2ddd25030f7878ebc0ae5f79cd4b430/USER
/DarkSUSY_mH_125_mN1_10_mGammaD_0p4_cT_5_13TeV_80k_MG452_BR224_LHE_pythia8_GEN_SIM_MINIAOD-V2_v1/wshi-DarkSUSY_mH_125_mN1_10_mGammaD_0p7_cT_0_13TeV_80k_RAW2DIGI_L1Reco_RECO_MINIAOD_V2_v1-2ddd25030f7878ebc0ae5f79cd4b430/USER
/DarkSUSY_mH_125_mN1_10_mGammaD_0p7_cT_0_13TeV_13TeV_20k_MG452_BR224_LHE_pythia8_GEN_SIM_MINIAOD-V2_v1/wshi-DarkSUSY_mH_125_mN1_10_mGammaD_0p7_cT_0_13TeV_20k_RAW2DIGI_L1Reco_RECO_MINIAOD_V2_v1-2ddd25030f7878ebc0ae5f79cd4b430/USER
/DarkSUSY_mH_125_mN1_10_mGammaD_0p7_cT_0_13TeV_13TeV_20k_MG452_BR224_LHE_pythia8_GEN_SIM_MINIAOD-V2_v1/wshi-DarkSUSY_mH_125_mN1_10_mGammaD_0p7_cT_0_13TeV_20k_RAW2DIGI_L1Reco_RECO_MINIAOD_V2_v1-2ddd25030f7878ebc0ae5f79cd4b430/USER
/DarkSUSY_mH_125_mN1_10_mGammaD_0p7_cT_100_13TeV_59k_MG452_BR224_LHE_pythia8_GEN_SIM_MINIAOD-V2_v1/wshi-DarkSUSY_mH_125_mN1_10_mGammaD_0p7_cT_100_13TeV_59k_RAW2DIGI_L1Reco_RECO_MINIAOD_V2_v1-2ddd25030f7878ebc0ae5f79cd4b430/USER
/DarkSUSY_mH_125_mN1_10_mGammaD_0p7_cT_100_13TeV_64k_MG452_BR224_LHE_pythia8_GEN_SIM_MINIAOD-V2_v1/wshi-DarkSUSY_mH_125_mN1_10_mGammaD_0p7_cT_100_13TeV_64k_RAW2DIGI_L1Reco_RECO_MINIAOD_V2_v1-2ddd25030f7878ebc0ae5f79cd4b430/USER

```

/DarkSUSY_mH_125_mN1_10_mGammaD_0p7_cT_100_13TeV_65k_MG452_BR224_LHE_pythia8_GEN_SIM_MINIAOD-
_V2_v1/wshi-DarkSUSY_mH_125_mN1_10_mGammaD_0p7_cT_100_13TeV_65k_RAW2DIGI_L1Reco_RECOPROJECTOR_MINIAOD_V2_v1-
2ddd25030f7878ebc0ae5f7f9cd4b430/USER

/DarkSUSY_mH_125_mN1_10_mGammaD_0p7_cT_100_13TeV_67k_MG452_BR224_LHE_pythia8_GEN_SIM_MINIAOD-
_V2_v1/wshi-DarkSUSY_mH_125_mN1_10_mGammaD_0p7_cT_100_13TeV_67k_RAW2DIGI_L1Reco_RECOPROJECTOR_MINIAOD_V2_v1-
2ddd25030f7878ebc0ae5f7f9cd4b430/USER

/DarkSUSY_mH_125_mN1_10_mGammaD_0p7_cT_100_13TeV_68k_MG452_BR224_LHE_pythia8_GEN_SIM_MINIAOD-
_V2_v1/wshi-DarkSUSY_mH_125_mN1_10_mGammaD_0p7_cT_100_13TeV_68k_RAW2DIGI_L1Reco_RECOPROJECTOR_MINIAOD_V2_v1-
2ddd25030f7878ebc0ae5f7f9cd4b430/USER

/DarkSUSY_mH_125_mN1_10_mGammaD_0p7_cT_100_13TeV_70k_MG452_BR224_LHE_pythia8_GEN_SIM_MINIAOD-
_V2_v1/wshi-DarkSUSY_mH_125_mN1_10_mGammaD_0p7_cT_100_13TeV_70k_MG452_BR224_LHE_pythia8_GEN_SIM_MINIAOD-
_V2_v1/wshi-DarkSUSY_mH_125_mN1_10_mGammaD_0p7_cT_100_13TeV_70k_RAW2DIGI_L1Reco_RECOPROJECTOR_MINIAOD_V2_v1-
2ddd25030f7878ebc0ae5f7f9cd4b430/USER

/DarkSUSY_mH_125_mN1_10_mGammaD_0p7_cT_100_13TeV_74k_MG452_BR224_LHE_pythia8_GEN_SIM_MINIAOD-
_V2_v1/wshi-DarkSUSY_mH_125_mN1_10_mGammaD_0p7_cT_100_13TeV_74k_RAW2DIGI_L1Reco_RECOPROJECTOR_MINIAOD_V2_v1-
2ddd25030f7878ebc0ae5f7f9cd4b430/USER

/DarkSUSY_mH_125_mN1_10_mGammaD_0p7_cT_100_13TeV_75k_MG452_BR224_LHE_pythia8_GEN_SIM_MINIAOD-
_V2_v1/wshi-DarkSUSY_mH_125_mN1_10_mGammaD_0p7_cT_100_13TeV_75k_RAW2DIGI_L1Reco_RECOPROJECTOR_MINIAOD_V2_v1-
2ddd25030f7878ebc0ae5f7f9cd4b430/USER

/DarkSUSY_mH_125_mN1_10_mGammaD_0p7_cT_100_13TeV_76k_MG452_BR224_LHE_pythia8_GEN_SIM_MINIAOD-
_V2_v1/wshi-DarkSUSY_mH_125_mN1_10_mGammaD_0p7_cT_100_13TeV_76k_RAW2DIGI_L1Reco_RECOPROJECTOR_MINIAOD_V2_v1-
2ddd25030f7878ebc0ae5f7f9cd4b430/USER

/DarkSUSY_mH_125_mN1_10_mGammaD_0p7_cT_100_13TeV_77k_MG452_BR224_LHE_pythia8_GEN_SIM_MINIAOD-
_V2_v1/wshi-DarkSUSY_mH_125_mN1_10_mGammaD_0p7_cT_100_13TeV_77k_RAW2DIGI_L1Reco_RECOPROJECTOR_MINIAOD_V2_v1-
2ddd25030f7878ebc0ae5f7f9cd4b430/USER

/DarkSUSY_mH_125_mN1_10_mGammaD_0p7_cT_100_13TeV_80k_MG452_BR224_LHE_pythia8_GEN_SIM_MINIAOD-
_V2_v1/wshi-DarkSUSY_mH_125_mN1_10_mGammaD_0p7_cT_100_13TeV_80k_RAW2DIGI_L1Reco_RECOPROJECTOR_MINIAOD_V2_v1-
2ddd25030f7878ebc0ae5f7f9cd4b430/USER

/DarkSUSY_mH_125_mN1_10_mGammaD_0p7_cT_100_13TeV_47k_MG452_BR224_LHE_pythia8_GEN_SIM_MINIAOD-
_V2_v1/wshi-DarkSUSY_mH_125_mN1_10_mGammaD_0p7_cT_100_13TeV_47k_RAW2DIGI_L1Reco_RECOPROJECTOR_MINIAOD_V2_v1-
2ddd25030f7878ebc0ae5f7f9cd4b430/USER

```

/DarkSUSY_mH_125_mN1_10_mGammaD_0p7_cT_1_13TeV_48k_MG452_BR224_LHE_pythia8_GEN_SIM_MINIAOD_V2_v1/wshi-DarkSUSY_mH_125_mN1_10_mGammaD_0p7_cT_1_13TeV_48k_RAW2DIGI_L1Reco_RECO_MINIAOD_V2_v1-2ddd25030f7878ebc0ae5f79cd4b430/USER
/DarkSUSY_mH_125_mN1_10_mGammaD_0p7_cT_1_13TeV_51k_MG452_BR224_LHE_pythia8_GEN_SIM_MINIAOD_V2_v1/wshi-DarkSUSY_mH_125_mN1_10_mGammaD_0p7_cT_1_13TeV_51k_RAW2DIGI_L1Reco_RECO_MINIAOD_V2_v1-2ddd25030f7878ebc0ae5f79cd4b430/USER
/DarkSUSY_mH_125_mN1_10_mGammaD_0p7_cT_1_13TeV_52k_MG452_BR224_LHE_pythia8_GEN_SIM_MINIAOD_V2_v1/wshi-DarkSUSY_mH_125_mN1_10_mGammaD_0p7_cT_1_13TeV_52k_RAW2DIGI_L1Reco_RECO_MINIAOD_V2_v1-2ddd25030f7878ebc0ae5f79cd4b430/USER
/DarkSUSY_mH_125_mN1_10_mGammaD_0p7_cT_1_13TeV_53k_MG452_BR224_LHE_pythia8_GEN_SIM_MINIAOD_V2_v1/wshi-DarkSUSY_mH_125_mN1_10_mGammaD_0p7_cT_1_13TeV_53k_RAW2DIGI_L1Reco_RECO_MINIAOD_V2_v1-2ddd25030f7878ebc0ae5f79cd4b430/USER
/DarkSUSY_mH_125_mN1_10_mGammaD_0p7_cT_1_13TeV_68k_MG452_BR224_LHE_pythia8_GEN_SIM_MINIAOD_V2_v1/wshi-DarkSUSY_mH_125_mN1_10_mGammaD_0p7_cT_1_13TeV_68k_RAW2DIGI_L1Reco_RECO_MINIAOD_V2_v1-2ddd25030f7878ebc0ae5f79cd4b430/USER
/DarkSUSY_mH_125_mN1_10_mGammaD_0p7_cT_20_13TeV_70k_MG452_BR224_LHE_pythia8_GEN_SIM_MINIAOD_V2_v1/wshi-DarkSUSY_mH_125_mN1_10_mGammaD_0p7_cT_20_13TeV_70k_RAW2DIGI_L1Reco_RECO_MINIAOD_V2_v1-2ddd25030f7878ebc0ae5f79cd4b430/USER
/DarkSUSY_mH_125_mN1_10_mGammaD_0p7_cT_20_13TeV_71k_MG452_BR224_LHE_pythia8_GEN_SIM_MINIAOD_V2_v1/wshi-DarkSUSY_mH_125_mN1_10_mGammaD_0p7_cT_20_13TeV_71k_RAW2DIGI_L1Reco_RECO_MINIAOD_V2_v1-2ddd25030f7878ebc0ae5f79cd4b430/USER
/DarkSUSY_mH_125_mN1_10_mGammaD_0p7_cT_20_13TeV_72k_MG452_BR224_LHE_pythia8_GEN_SIM_MINIAOD_V2_v1/wshi-DarkSUSY_mH_125_mN1_10_mGammaD_0p7_cT_20_13TeV_72k_RAW2DIGI_L1Reco_RECO_MINIAOD_V2_v1-2ddd25030f7878ebc0ae5f79cd4b430/USER
/DarkSUSY_mH_125_mN1_10_mGammaD_0p7_cT_20_13TeV_73k_MG452_BR224_LHE_pythia8_GEN_SIM_MINIAOD_V2_v1/wshi-DarkSUSY_mH_125_mN1_10_mGammaD_0p7_cT_20_13TeV_73k_RAW2DIGI_L1Reco_RECO_MINIAOD_V2_v1-2ddd25030f7878ebc0ae5f79cd4b430/USER
/DarkSUSY_mH_125_mN1_10_mGammaD_0p7_cT_20_13TeV_75k_MG452_BR224_LHE_pythia8_GEN_SIM_MINIAOD_V2_v1/wshi-DarkSUSY_mH_125_mN1_10_mGammaD_0p7_cT_20_13TeV_75k_RAW2DIGI_L1Reco_RECO_MINIAOD_V2_v1-2ddd25030f7878ebc0ae5f79cd4b430/USER

```

/DarkSUSY_mH_125_mN1_10_mGammaD_0p7_cT_20_13TeV_76k_BR224_LHE_pythia8_GEN_SIM_MINIAOD-
_V2_v1/wshi-DarkSUSY_mH_125_mN1_10_mGammaD_0p7_cT_20_13TeV_76k_RAW2DIGI_L1Reco_RECO_MINIAOD_V2_v1-
2ddd25030f7878ebc0ae5f7f9cd4b430/USER

/DarkSUSY_mH_125_mN1_10_mGammaD_0p7_cT_20_13TeV_77k_BR224_LHE_pythia8_GEN_SIM_MINIAOD-
_V2_v1/wshi-DarkSUSY_mH_125_mN1_10_mGammaD_0p7_cT_20_13TeV_77k_RAW2DIGI_L1Reco_RECO_MINIAOD_V2_v1-
2ddd25030f7878ebc0ae5f7f9cd4b430/USER

/DarkSUSY_mH_125_mN1_10_mGammaD_0p7_cT_20_13TeV_78k_BR224_LHE_pythia8_GEN_SIM_MINIAOD-
_V2_v1/wshi-DarkSUSY_mH_125_mN1_10_mGammaD_0p7_cT_20_13TeV_78k_RAW2DIGI_L1Reco_RECO_MINIAOD_V2_v1-
2ddd25030f7878ebc0ae5f7f9cd4b430/USER

/DarkSUSY_mH_125_mN1_10_mGammaD_0p7_cT_20_13TeV_79k_BR224_LHE_pythia8_GEN_SIM_MINIAOD-
_V2_v1/wshi-DarkSUSY_mH_125_mN1_10_mGammaD_0p7_cT_20_13TeV_79k_RAW2DIGI_L1Reco_RECO_MINIAOD_V2_v1-
2ddd25030f7878ebc0ae5f7f9cd4b430/USER

/DarkSUSY_mH_125_mN1_10_mGammaD_0p7_cT_20_13TeV_80k_BR224_LHE_pythia8_GEN_SIM_MINIAOD-
_V2_v1/wshi-DarkSUSY_mH_125_mN1_10_mGammaD_0p7_cT_20_13TeV_80k_RAW2DIGI_L1Reco_RECO_MINIAOD_V2_v1-
2ddd25030f7878ebc0ae5f7f9cd4b430/USER

/DarkSUSY_mH_125_mN1_10_mGammaD_0p7_cT_5_13TeV_47k_BR224_LHE_pythia8_GEN_SIM_MINIAOD-
_V2_v1/wshi-DarkSUSY_mH_125_mN1_10_mGammaD_0p7_cT_5_13TeV_47k_RAW2DIGI_L1Reco_RECO_MINIAOD_V2_v1-
2ddd25030f7878ebc0ae5f7f9cd4b430/USER

/DarkSUSY_mH_125_mN1_10_mGammaD_0p7_cT_5_13TeV_48k_BR224_LHE_pythia8_GEN_SIM_MINIAOD-
_V2_v1/wshi-DarkSUSY_mH_125_mN1_10_mGammaD_0p7_cT_5_13TeV_48k_RAW2DIGI_L1Reco_RECO_MINIAOD_V2_v1-
2ddd25030f7878ebc0ae5f7f9cd4b430/USER

/DarkSUSY_mH_125_mN1_10_mGammaD_0p7_cT_5_13TeV_49k_BR224_LHE_pythia8_GEN_SIM_MINIAOD-
_V2_v1/wshi-DarkSUSY_mH_125_mN1_10_mGammaD_0p7_cT_5_13TeV_49k_RAW2DIGI_L1Reco_RECO_MINIAOD_V2_v1-
2ddd25030f7878ebc0ae5f7f9cd4b430/USER

/DarkSUSY_mH_125_mN1_10_mGammaD_0p7_cT_5_13TeV_52k_BR224_LHE_pythia8_GEN_SIM_MINIAOD-
_V2_v1/wshi-DarkSUSY_mH_125_mN1_10_mGammaD_0p7_cT_5_13TeV_52k_RAW2DIGI_L1Reco_RECO_MINIAOD_V2_v1-
2ddd25030f7878ebc0ae5f7f9cd4b430/USER

/DarkSUSY_mH_125_mN1_10_mGammaD_0p7_cT_5_13TeV_53k_BR224_LHE_pythia8_GEN_SIM_MINIAOD-
_V2_v1/wshi-DarkSUSY_mH_125_mN1_10_mGammaD_0p7_cT_5_13TeV_53k_RAW2DIGI_L1Reco_RECO_MINIAOD_V2_v1-
2ddd25030f7878ebc0ae5f7f9cd4b430/USER

```

/DarkSUSY_mH_125_mN1_10_mGammaD_1_cT_100_13TeV_65k_BR224_LHE_pythia8_GEN_SIM_MINIAOD-V2_v1/wshi-DarkSUSY_mH_125_mN1_10_mGammaD_1_cT_100_13TeV_65k_RAW2DIGI_L1Reco_RECO_MINIAOD_V2_v1-2ddd25030f7878ebc0ae5f79cd4b430/USER
/DarkSUSY_mH_125_mN1_10_mGammaD_1_cT_100_13TeV_70k_BR224_LHE_pythia8_GEN_SIM_MINIAOD-V2_v1/wshi-DarkSUSY_mH_125_mN1_10_mGammaD_1_cT_100_13TeV_70k_RAW2DIGI_L1Reco_RECO_MINIAOD_V2_v1-2ddd25030f7878ebc0ae5f79cd4b430/USER
/DarkSUSY_mH_125_mN1_10_mGammaD_1_cT_100_13TeV_73k_BR224_LHE_pythia8_GEN_SIM_MINIAOD-V2_v1/wshi-DarkSUSY_mH_125_mN1_10_mGammaD_1_cT_100_13TeV_73k_RAW2DIGI_L1Reco_RECO_MINIAOD_V2_v1-2ddd25030f7878ebc0ae5f79cd4b430/USER
/DarkSUSY_mH_125_mN1_10_mGammaD_1_cT_100_13TeV_75k_BR224_LHE_pythia8_GEN_SIM_MINIAOD-V2_v1/wshi-DarkSUSY_mH_125_mN1_10_mGammaD_1_cT_100_13TeV_75k_RAW2DIGI_L1Reco_RECO_MINIAOD_V2_v1-2ddd25030f7878ebc0ae5f79cd4b430/USER
/DarkSUSY_mH_125_mN1_10_mGammaD_1_cT_100_13TeV_76k_BR224_LHE_pythia8_GEN_SIM_MINIAOD-V2_v1/wshi-DarkSUSY_mH_125_mN1_10_mGammaD_1_cT_100_13TeV_76k_RAW2DIGI_L1Reco_RECO_MINIAOD_V2_v1-2ddd25030f7878ebc0ae5f79cd4b430/USER
/DarkSUSY_mH_125_mN1_10_mGammaD_1_cT_100_13TeV_78k_BR224_LHE_pythia8_GEN_SIM_MINIAOD-V2_v1/wshi-DarkSUSY_mH_125_mN1_10_mGammaD_1_cT_100_13TeV_78k_RAW2DIGI_L1Reco_RECO_MINIAOD_V2_v1-2ddd25030f7878ebc0ae5f79cd4b430/USER
/DarkSUSY_mH_125_mN1_10_mGammaD_1_cT_100_13TeV_48k_BR224_LHE_pythia8_GEN_SIM_MINIAOD-V2_v1/wshi-DarkSUSY_mH_125_mN1_10_mGammaD_1_cT_100_13TeV_48k_RAW2DIGI_L1Reco_RECO_MINIAOD_V2_v1-2ddd25030f7878ebc0ae5f79cd4b430/USER
/DarkSUSY_mH_125_mN1_10_mGammaD_1_cT_1_13TeV_49k_BR224_LHE_pythia8_GEN_SIM_MINIAOD-V2_v1/wshi-DarkSUSY_mH_125_mN1_10_mGammaD_1_cT_1_13TeV_49k_RAW2DIGI_L1Reco_RECO_MINIAOD_V2_v1-2ddd25030f7878ebc0ae5f79cd4b430/USER
/DarkSUSY_mH_125_mN1_10_mGammaD_1_cT_20_13TeV_67k_BR224_LHE_pythia8_GEN_SIM_MINIAOD-V2_v1/wshi-DarkSUSY_mH_125_mN1_10_mGammaD_1_cT_20_13TeV_67k_RAW2DIGI_L1Reco_RECO_MINIAOD_V2_v1-2ddd25030f7878ebc0ae5f79cd4b430/USER
/DarkSUSY_mH_125_mN1_10_mGammaD_1_cT_20_13TeV_70k_BR224_LHE_pythia8_GEN_SIM_MINIAOD-V2_v1/wshi-DarkSUSY_mH_125_mN1_10_mGammaD_1_cT_20_13TeV_70k_RAW2DIGI_L1Reco_RECO_MINIAOD_V2_v1-2ddd25030f7878ebc0ae5f79cd4b430/USER

```

/DarkSUSY_mH_125_mN1_10_mGammaD_1_cT_20_13TeV_71k_MG452_BR224_LHE_pythia8_GEN_SIM_MINIAOD-
_V2_v1/wshi-DarkSUSY_mH_125_mN1_10_mGammaD_1_cT_20_13TeV_71k_RAW2DIGI_L1Reco_REC0_MINIAOD_V2_v1-
2ddd25030f7878ebc0ae5f7f9cd4b430/USER

/DarkSUSY_mH_125_mN1_10_mGammaD_1_cT_20_13TeV_72k_MG452_BR224_LHE_pythia8_GEN_SIM_MINIAOD-
_V2_v1/wshi-DarkSUSY_mH_125_mN1_10_mGammaD_1_cT_20_13TeV_72k_RAW2DIGI_L1Reco_REC0_MINIAOD_V2_v1-
2ddd25030f7878ebc0ae5f7f9cd4b430/USER

/DarkSUSY_mH_125_mN1_10_mGammaD_1_cT_20_13TeV_74k_MG452_BR224_LHE_pythia8_GEN_SIM_MINIAOD-
_V2_v1/wshi-DarkSUSY_mH_125_mN1_10_mGammaD_1_cT_20_13TeV_74k_RAW2DIGI_L1Reco_REC0_MINIAOD_V2_v1-
2ddd25030f7878ebc0ae5f7f9cd4b430/USER

/DarkSUSY_mH_125_mN1_10_mGammaD_1_cT_20_13TeV_77k_MG452_BR224_LHE_pythia8_GEN_SIM_MINIAOD-
_V2_v1/wshi-DarkSUSY_mH_125_mN1_10_mGammaD_1_cT_20_13TeV_77k_RAW2DIGI_L1Reco_REC0_MINIAOD_V2_v1-
2ddd25030f7878ebc0ae5f7f9cd4b430/USER

/DarkSUSY_mH_125_mN1_10_mGammaD_1_cT_20_13TeV_78k_MG452_BR224_LHE_pythia8_GEN_SIM_MINIAOD-
_V2_v1/wshi-DarkSUSY_mH_125_mN1_10_mGammaD_1_cT_20_13TeV_78k_RAW2DIGI_L1Reco_REC0_MINIAOD_V2_v1-
2ddd25030f7878ebc0ae5f7f9cd4b430/USER

/DarkSUSY_mH_125_mN1_10_mGammaD_5_cT_0_13TeV_80k_MG452_BR224_LHE_pythia8_GEN_SIM_MINIAOD-
_V2_v1/wshi-DarkSUSY_mH_125_mN1_10_mGammaD_5_cT_0_13TeV_80k_RAW2DIGI_L1Reco_REC0_MINIAOD_V2_v1-
2ddd25030f7878ebc0ae5f7f9cd4b430/USER

/DarkSUSY_mH_125_mN1_10_mGammaD_5_cT_100_13TeV_64k_MG452_BR224_LHE_pythia8_GEN_SIM_MINIAOD-
_V2_v1/wshi-DarkSUSY_mH_125_mN1_10_mGammaD_5_cT_100_13TeV_64k_RAW2DIGI_L1Reco_REC0_MINIAOD_V2_v1-
2ddd25030f7878ebc0ae5f7f9cd4b430/USER

/DarkSUSY_mH_125_mN1_10_mGammaD_5_cT_100_13TeV_68k_MG452_BR224_LHE_pythia8_GEN_SIM_MINIAOD-
_V2_v1/wshi-DarkSUSY_mH_125_mN1_10_mGammaD_5_cT_100_13TeV_68k_RAW2DIGI_L1Reco_REC0_MINIAOD_V2_v1-
2ddd25030f7878ebc0ae5f7f9cd4b430/USER

/DarkSUSY_mH_125_mN1_10_mGammaD_5_cT_100_13TeV_72k_MG452_BR224_LHE_pythia8_GEN_SIM_MINIAOD-
_V2_v1/wshi-DarkSUSY_mH_125_mN1_10_mGammaD_5_cT_100_13TeV_72k_RAW2DIGI_L1Reco_REC0_MINIAOD_V2_v1-
2ddd25030f7878ebc0ae5f7f9cd4b430/USER

/DarkSUSY_mH_125_mN1_10_mGammaD_5_cT_100_13TeV_75k_MG452_BR224_LHE_pythia8_GEN_SIM_MINIAOD-
_V2_v1/wshi-DarkSUSY_mH_125_mN1_10_mGammaD_5_cT_100_13TeV_75k_RAW2DIGI_L1Reco_REC0_MINIAOD_V2_v1-
2ddd25030f7878ebc0ae5f7f9cd4b430/USER

```

/DarkSUSY_mH_125_mN1_10_mGammaD_5_cT_100_13TeV_77k_MG452_BR224_LHE_pythia8_GEN_SIM_MINIAOD-V2_v1/wshi-DarkSUSY_mH_125_mN1_10_mGammaD_5_cT_100_13TeV_77k_RAW2DIGI_L1Reco_RECO_MINIAOD_V2_v1-2ddd25030ff78ebc0ae5f79cd4b430/USER
/DarkSUSY_mH_125_mN1_10_mGammaD_5_cT_20_13TeV_79k_MG452_BR224_LHE_pythia8_GEN_SIM_MINIAOD-V2_v1-2ddd25030ff78ebc0ae5f79cd4b430/USER
/DarkSUSY_mH_125_mN1_10_mGammaD_8p5_cT_0_13TeV_100k_MG452_BR224_LHE_pythia8_GEN_SIM_Private/wshi-DarkSUSY_mH_125_mN1_10_mGammaD_8p5_cT_0_13TeV_100k_RAW_RECO_Private-3bed5cc6739ae96e62f5788adf997763/USER
/DarkSUSY_mH_125_mN1_10_mGammaD_8p5_cT_100_13TeV_59k_MG452_BR224_LHE_pythia8_GEN_SIM_Private/wshi-DarkSUSY_mH_125_mN1_10_mGammaD_8p5_cT_100_13TeV_59k_RAW_RECO_Private-3bed5cc6739ae96e62f5788adf997763/USER
/DarkSUSY_mH_125_mN1_10_mGammaD_8p5_cT_100_13TeV_60k_MG452_BR224_LHE_pythia8_GEN_SIM_Private/wshi-DarkSUSY_mH_125_mN1_10_mGammaD_8p5_cT_100_13TeV_60k_RAW_RECO_Private-3bed5cc6739ae96e62f5788adf997763/USER
/DarkSUSY_mH_125_mN1_10_mGammaD_8p5_cT_100_13TeV_62k_MG452_BR224_LHE_pythia8_GEN_SIM_Private/wshi-DarkSUSY_mH_125_mN1_10_mGammaD_8p5_cT_100_13TeV_62k_RAW_RECO_Private-3bed5cc6739ae96e62f5788adf997763/USER
/DarkSUSY_mH_125_mN1_10_mGammaD_8p5_cT_100_13TeV_63k_MG452_BR224_LHE_pythia8_GEN_SIM_Private/wshi-DarkSUSY_mH_125_mN1_10_mGammaD_8p5_cT_100_13TeV_63k_RAW_RECO_Private-3bed5cc6739ae96e62f5788adf997763/USER
/DarkSUSY_mH_125_mN1_10_mGammaD_8p5_cT_100_13TeV_70k_MG452_BR224_LHE_pythia8_GEN_SIM_Private/wshi-DarkSUSY_mH_125_mN1_10_mGammaD_8p5_cT_100_13TeV_70k_RAW_RECO_Private-3bed5cc6739ae96e62f5788adf997763/USER
/DarkSUSY_mH_125_mN1_10_mGammaD_8p5_cT_100_13TeV_71k_MG452_BR224_LHE_pythia8_GEN_SIM_Private/wshi-DarkSUSY_mH_125_mN1_10_mGammaD_8p5_cT_100_13TeV_71k_RAW_RECO_Private-3bed5cc6739ae96e62f5788adf997763/USER
/DarkSUSY_mH_125_mN1_10_mGammaD_8p5_cT_100_13TeV_72k_MG452_BR224_LHE_pythia8_GEN_SIM_Private/wshi-DarkSUSY_mH_125_mN1_10_mGammaD_8p5_cT_100_13TeV_72k_RAW_RECO_Private-3bed5cc6739ae96e62f5788adf997763/USER

```

/DarkSUSY_mH_125_mN1_10_mGammaD_8p5_cT_100_13TeV_73k_RAW_LHE_pythia8_GEN_SIM_Private/wshi-
DarkSUSY_mH_125_mN1_10_mGammaD_8p5_cT_100_13TeV_73k_RAW_RECOPrivate-3bed5cc6739ae96e62f5788adf997763/USER
/DarkSUSY_mH_125_mN1_10_mGammaD_8p5_cT_100_13TeV_74k_MG452_BR224_LHE_pythia8_GEN_SIM_Private/wshi-
DarkSUSY_mH_125_mN1_10_mGammaD_8p5_cT_100_13TeV_74k_RAW_RECOPrivate-3bed5cc6739ae96e62f5788adf997763/USER
/DarkSUSY_mH_125_mN1_10_mGammaD_8p5_cT_100_13TeV_75k_MG452_BR224_LHE_pythia8_GEN_SIM_Private/wshi-
DarkSUSY_mH_125_mN1_10_mGammaD_8p5_cT_100_13TeV_75k_RAW_RECOPrivate-3bed5cc6739ae96e62f5788adf997763/USER
/DarkSUSY_mH_125_mN1_10_mGammaD_8p5_cT_100_13TeV_76k_MG452_BR224_LHE_pythia8_GEN_SIM_Private/wshi-
DarkSUSY_mH_125_mN1_10_mGammaD_8p5_cT_100_13TeV_76k_RAW_RECOPrivate-3bed5cc6739ae96e62f5788adf997763/USER
/DarkSUSY_mH_125_mN1_10_mGammaD_8p5_cT_100_13TeV_77k_MG452_BR224_LHE_pythia8_GEN_SIM_Private/wshi-
DarkSUSY_mH_125_mN1_10_mGammaD_8p5_cT_100_13TeV_77k_RAW_RECOPrivate-3bed5cc6739ae96e62f5788adf997763/USER
/DarkSUSY_mH_125_mN1_10_mGammaD_8p5_cT_100_13TeV_78k_MG452_BR224_LHE_pythia8_GEN_SIM_Private/wshi-
DarkSUSY_mH_125_mN1_10_mGammaD_8p5_cT_100_13TeV_78k_RAW_RECOPrivate-3bed5cc6739ae96e62f5788adf997763/USER
/DarkSUSY_mH_125_mN1_10_mGammaD_8p5_cT_100_13TeV_79k_MG452_BR224_LHE_pythia8_GEN_SIM_Private/wshi-
DarkSUSY_mH_125_mN1_10_mGammaD_8p5_cT_100_13TeV_79k_RAW_RECOPrivate-3bed5cc6739ae96e62f5788adf997763/USER
/DarkSUSY_mH_125_mN1_10_mGammaD_8p5_cT_100_13TeV_80k_MG452_BR224_LHE_pythia8_GEN_SIM_Private/wshi-
DarkSUSY_mH_125_mN1_10_mGammaD_8p5_cT_100_13TeV_80k_RAW_RECOPrivate-3bed5cc6739ae96e62f5788adf997763/USER
/DarkSUSY_mH_125_mN1_10_mGammaD_8p5_cT_20_13TeV_69k_MG452_BR224_LHE_pythia8_GEN_SIM_Private/wshi-
DarkSUSY_mH_125_mN1_10_mGammaD_8p5_cT_20_13TeV_69k_RAW_RECOPrivate-3bed5cc6739ae96e62f5788adf997763/USER
/DarkSUSY_mH_125_mN1_10_mGammaD_8p5_cT_20_13TeV_70k_MG452_BR224_LHE_pythia8_GEN_SIM_Private/wshi-
DarkSUSY_mH_125_mN1_10_mGammaD_8p5_cT_20_13TeV_70k_RAW_RECOPrivate-3bed5cc6739ae96e62f5788adf997763/USER

```

```

/DarkSUSY_mH_125_mN1_10_mGammaD_8p5_ct_20_13TeV_71k_MG452_BR224_LHE_pythia8_GEN_SIM_Private/wshi-
DarkSUSY_mH_125_mN1_10_mGammaD_8p5_ct_20_13TeV_71k_RAW_RECO_Private-3bed5cc6739ae96e62f5788adf997763/USER
/DarkSUSY_mH_125_mN1_10_mGammaD_8p5_ct_20_13TeV_72k_MG452_BR224_LHE_pythia8_GEN_SIM_Private/wshi-
DarkSUSY_mH_125_mN1_10_mGammaD_8p5_ct_20_13TeV_72k_RAW_RECO_Private-3bed5cc6739ae96e62f5788adf997763/USER
/DarkSUSY_mH_125_mN1_10_mGammaD_8p5_ct_20_13TeV_74k_MG452_BR224_LHE_pythia8_GEN_SIM_Private/wshi-
DarkSUSY_mH_125_mN1_10_mGammaD_8p5_ct_20_13TeV_74k_RAW_RECO_Private-3bed5cc6739ae96e62f5788adf997763/USER
/DarkSUSY_mH_125_mN1_10_mGammaD_8p5_ct_20_13TeV_75k_MG452_BR224_LHE_pythia8_GEN_SIM_Private/wshi-
DarkSUSY_mH_125_mN1_10_mGammaD_8p5_ct_20_13TeV_75k_RAW_RECO_Private-3bed5cc6739ae96e62f5788adf997763/USER
/DarkSUSY_mH_125_mN1_10_mGammaD_8p5_ct_20_13TeV_76k_MG452_BR224_LHE_pythia8_GEN_SIM_Private/wshi-
DarkSUSY_mH_125_mN1_10_mGammaD_8p5_ct_20_13TeV_76k_RAW_RECO_Private-3bed5cc6739ae96e62f5788adf997763/USER
/DarkSUSY_mH_125_mN1_10_mGammaD_8p5_ct_20_13TeV_77k_MG452_BR224_LHE_pythia8_GEN_SIM_Private/wshi-
DarkSUSY_mH_125_mN1_10_mGammaD_8p5_ct_20_13TeV_77k_RAW_RECO_Private-3bed5cc6739ae96e62f5788adf997763/USER
/DarkSUSY_mH_125_mN1_10_mGammaD_8p5_ct_20_13TeV_78k_MG452_BR224_LHE_pythia8_GEN_SIM_Private/wshi-
DarkSUSY_mH_125_mN1_10_mGammaD_8p5_ct_20_13TeV_78k_RAW_RECO_Private-3bed5cc6739ae96e62f5788adf997763/USER
/DarkSUSY_mH_125_mN1_10_mGammaD_8p5_ct_20_13TeV_79k_MG452_BR224_LHE_pythia8_GEN_SIM_Private/wshi-
DarkSUSY_mH_125_mN1_10_mGammaD_8p5_ct_20_13TeV_79k_RAW_RECO_Private-3bed5cc6739ae96e62f5788adf997763/USER
/DarkSUSY_mH_125_mN1_10_mGammaD_8p5_ct_20_13TeV_80k_MG452_BR224_LHE_pythia8_GEN_SIM_Private/wshi-
DarkSUSY_mH_125_mN1_10_mGammaD_8p5_ct_20_13TeV_80k_RAW_RECO_Private-3bed5cc6739ae96e62f5788adf997763/USER
/DarkSUSY_mH_125_mN1_10_mGammaD_8p5_ct_2_13TeV_47k_MG452_BR224_LHE_pythia8_GEN_SIM_Private/wshi-
DarkSUSY_mH_125_mN1_10_mGammaD_8p5_ct_2_13TeV_47k_RAW_RECO_Private-3bed5cc6739ae96e62f5788adf997763/USER

```

```
/DarkSUSY_mH_125_mN1_10_mGammaD_8p5_cT_2.13TeV_48k_MG452_BR224_LHE_pythia8_GEN_SIM_Private/wshi-
DarkSUSY_mH_125_mN1_10_mGammaD_8p5_cT_2.13TeV_48k_RAW_RECOPrivate-3bed5cc6739ae96e62f5788adf997763/USER
/DarkSUSY_mH_125_mN1_10_mGammaD_8p5_cT_2.13TeV_49k_MG452_BR224_LHE_pythia8_GEN_SIM_Private/wshi-
DarkSUSY_mH_125_mN1_10_mGammaD_8p5_cT_2.13TeV_49k_RAW_RECOPrivate-3bed5cc6739ae96e62f5788adf997763/USER
/DarkSUSY_mH_125_mN1_10_mGammaD_8p5_cT_2.13TeV_51k_MG452_BR224_LHE_pythia8_GEN_SIM_Private/wshi-
DarkSUSY_mH_125_mN1_10_mGammaD_8p5_cT_2.13TeV_51k_RAW_RECOPrivate-3bed5cc6739ae96e62f5788adf997763/USER
/DarkSUSY_mH_125_mN1_10_mGammaD_8p5_cT_2.13TeV_52k_MG452_BR224_LHE_pythia8_GEN_SIM_Private/wshi-
DarkSUSY_mH_125_mN1_10_mGammaD_8p5_cT_2.13TeV_52k_RAW_RECOPrivate-3bed5cc6739ae96e62f5788adf997763/USER
/DarkSUSY_mH_125_mN1_10_mGammaD_8p5_cT_2.13TeV_53k_MG452_BR224_LHE_pythia8_GEN_SIM_Private/wshi-
DarkSUSY_mH_125_mN1_10_mGammaD_8p5_cT_2.13TeV_53k_RAW_RECOPrivate-3bed5cc6739ae96e62f5788adf997763/USER
```

1510 **B Efficiencies of the Event Selection Requirements for Bench-**
1511 **mark MC Samples**

DRAFT

Sample	$m_H = 90 \text{ GeV}, m_A = 0.25 \text{ GeV}$			$m_H = 90 \text{ GeV}, m_A = 0.5 \text{ GeV}$		
Selection	Events	Tot. Eff. [%]	Rel. Eff. [%]	Events	Tot. Eff. [%]	Rel. Eff. [%]
All events	200001	1.000 ± 0.000	1.000 ± 0.000	200001	1.000 ± 0.000	1.000 ± 0.000
Basic GEN level selections						
$p_{T_1} > 17 \text{ GeV}, \eta < 0.9$	87490	0.437 ± 0.001	0.437 ± 0.001	92109	0.461 ± 0.001	0.461 ± 0.001
$p_{T_2} > 8 \text{ GeV}, \eta < 2.4$	86689	0.433 ± 0.001	0.991 ± 0.000	87924	0.440 ± 0.001	0.955 ± 0.001
$p_{T_3} > 8 \text{ GeV}, \eta < 2.4$	79856	0.399 ± 0.001	0.921 ± 0.001	73519	0.368 ± 0.001	0.836 ± 0.001
$p_{T_4} > 8 \text{ GeV}, \eta < 2.4$	69837	0.349 ± 0.001	0.875 ± 0.001	33836	0.169 ± 0.001	0.460 ± 0.002
$L_{xy} < 9.8 \text{ cm and } L_z < 46.5 \text{ cm}$	69837	0.349 ± 0.001	1.000 ± 0.000	33836	0.169 ± 0.001	1.000 ± 0.000
Basic RECO level selections						
$p_{T_1} > 17 \text{ GeV}, \eta < 0.9$	86974	0.435 ± 0.001	0.435 ± 0.001	91840	0.459 ± 0.001	0.459 ± 0.001
$p_{T_2} > 8 \text{ GeV}, \eta < 2.4$	85786	0.429 ± 0.001	0.986 ± 0.000	87499	0.437 ± 0.001	0.953 ± 0.001
$p_{T_3} > 8 \text{ GeV}, \eta < 2.4$	78141	0.391 ± 0.001	0.911 ± 0.001	72090	0.360 ± 0.001	0.824 ± 0.001
$p_{T_4} > 8 \text{ GeV}, \eta < 2.4$	61778	0.309 ± 0.001	0.791 ± 0.001	32447	0.162 ± 0.001	0.450 ± 0.002
Extra RECO level selections						
Good primary vertex	61778	0.309 ± 0.001	1.000 ± 0.000	32447	0.162 ± 0.001	1.000 ± 0.000
Two muon-jets	59757	0.299 ± 0.001	0.967 ± 0.001	28129	0.141 ± 0.001	0.867 ± 0.002
Two dimuons	59727	0.299 ± 0.001	0.999 ± 0.000	28118	0.141 ± 0.001	1.000 ± 0.000
Pixel hit requirement	59263	0.296 ± 0.001	0.992 ± 0.000	28089	0.140 ± 0.001	0.999 ± 0.000
$ z_{\mu\mu_1} - z_{\mu\mu_2} < 0.1 \text{ cm}$	59043	0.295 ± 0.001	0.996 ± 0.000	28013	0.140 ± 0.001	0.997 ± 0.000
$m_{\mu\mu_1} \approx m_{\mu\mu_2}$	58837	0.294 ± 0.001	0.997 ± 0.000	27906	0.140 ± 0.001	0.996 ± 0.000
Dimuon isolation < 2 GeV	47599	0.238 ± 0.001	0.809 ± 0.002	22460	0.112 ± 0.001	0.805 ± 0.002
Trigger	45205	0.226 ± 0.001	0.950 ± 0.001	21784	0.109 ± 0.001	0.970 ± 0.001
α_{GEN}						
ϵ_{SIM}						
$\epsilon_{\text{SIM}} / \alpha_{\text{GEN}}$						
		0.647 ± 0.002				0.644 ± 0.003

Sample	$m_H = 90 \text{ GeV}, m_A = 0.75 \text{ GeV}$			$m_H = 90 \text{ GeV}, m_A = 1 \text{ GeV}$		
Selection	Events	Tot. Eff. [%]	Rel. Eff. [%]	Events	Tot. Eff. [%]	Rel. Eff. [%]
All events	200001	1.000 ± 0.000	1.000 ± 0.000	200000	1.000 ± 0.000	1.000 ± 0.000
Basic GEN level selections						
$p_{T_1} > 17 \text{ GeV}, \eta < 0.9$	92437	0.462 ± 0.001	0.462 ± 0.001	92521	0.463 ± 0.001	0.463 ± 0.001
$p_{T_2} > 8 \text{ GeV}, \eta < 2.4$	87923	0.440 ± 0.001	0.951 ± 0.001	87868	0.439 ± 0.001	0.950 ± 0.001
$p_{T_3} > 8 \text{ GeV}, \eta < 2.4$	71588	0.358 ± 0.001	0.814 ± 0.001	70651	0.353 ± 0.001	0.804 ± 0.001
$p_{T_4} > 8 \text{ GeV}, \eta < 2.4$	30322	0.152 ± 0.001	0.424 ± 0.002	28962	0.145 ± 0.001	0.410 ± 0.002
$L_{xy} < 9.8 \text{ cm and } L_z < 46.5 \text{ cm}$	30322	0.152 ± 0.001	1.000 ± 0.000	28962	0.145 ± 0.001	1.000 ± 0.000
Basic RECO level selections						
$p_{T_1} > 17 \text{ GeV}, \eta < 0.9$	92182	0.461 ± 0.001	0.461 ± 0.001	92216	0.461 ± 0.001	0.461 ± 0.001
$p_{T_2} > 8 \text{ GeV}, \eta < 2.4$	87524	0.438 ± 0.001	0.949 ± 0.001	87390	0.437 ± 0.001	0.948 ± 0.001
$p_{T_3} > 8 \text{ GeV}, \eta < 2.4$	70182	0.351 ± 0.001	0.802 ± 0.001	69363	0.347 ± 0.001	0.794 ± 0.001
$p_{T_4} > 8 \text{ GeV}, \eta < 2.4$	29167	0.146 ± 0.001	0.416 ± 0.002	27824	0.139 ± 0.001	0.401 ± 0.002
Extra RECO level selections						
Good primary vertex	29167	0.146 ± 0.001	1.000 ± 0.000	27824	0.139 ± 0.001	1.000 ± 0.000
Two muon-jets	25108	0.126 ± 0.001	0.861 ± 0.002	23927	0.120 ± 0.001	0.860 ± 0.002
Two dimuons	25093	0.125 ± 0.001	0.999 ± 0.000	23910	0.120 ± 0.001	0.999 ± 0.000
Pixel hit requirement	25083	0.125 ± 0.001	1.000 ± 0.000	23907	0.120 ± 0.001	1.000 ± 0.000
$ z_{\mu\mu_1} - z_{\mu\mu_2} < 0.1 \text{ cm}$	25041	0.125 ± 0.001	0.998 ± 0.000	23881	0.119 ± 0.001	0.999 ± 0.000
$m_{\mu\mu_1} \approx m_{\mu\mu_2}$	24824	0.124 ± 0.001	0.991 ± 0.001	23578	0.118 ± 0.001	0.987 ± 0.001
Dimuon isolation < 2 GeV	20078	0.100 ± 0.001	0.809 ± 0.002	19039	0.095 ± 0.001	0.807 ± 0.003
Trigger	19492	0.097 ± 0.001	0.971 ± 0.001	18527	0.093 ± 0.001	0.973 ± 0.001
α_{GEN}						
ϵ_{SIM}						
$\epsilon_{\text{SIM}}/\alpha_{\text{GEN}}$						
		0.643 ± 0.003				
						0.640 ± 0.003

Sample	$m_H = 90 \text{ GeV}, m_A = 2 \text{ GeV}$			$m_H = 90 \text{ GeV}, m_A = 3 \text{ GeV}$		
Selection	Events	Tot. Eff. [%]	Rel. Eff. [%]	Events	Tot. Eff. [%]	Rel. Eff. [%]
All events	200000	1.000 ± 0.000	1.000 ± 0.000	199308	1.000 ± 0.000	1.000 ± 0.000
Basic GEN level selections						
$p_{T_1} > 17 \text{ GeV}, \eta < 0.9$	93027	0.465 ± 0.001	0.465 ± 0.001	92655	0.465 ± 0.001	0.465 ± 0.001
$p_{T_2} > 8 \text{ GeV}, \eta < 2.4$	88299	0.441 ± 0.001	0.949 ± 0.001	87862	0.441 ± 0.001	0.948 ± 0.001
$p_{T_3} > 8 \text{ GeV}, \eta < 2.4$	70051	0.350 ± 0.001	0.793 ± 0.001	69577	0.349 ± 0.001	0.792 ± 0.001
$p_{T_4} > 8 \text{ GeV}, \eta < 2.4$	27857	0.139 ± 0.001	0.398 ± 0.002	27625	0.139 ± 0.001	0.397 ± 0.002
$L_{xy} < 9.8 \text{ cm and } L_z < 46.5 \text{ cm}$	27857	0.139 ± 0.001	1.000 ± 0.000	27625	0.139 ± 0.001	1.000 ± 0.000
Basic RECO level selections						
$p_{T_1} > 17 \text{ GeV}, \eta < 0.9$	92768	0.464 ± 0.001	0.464 ± 0.001	92390	0.464 ± 0.001	0.464 ± 0.001
$p_{T_2} > 8 \text{ GeV}, \eta < 2.4$	87878	0.439 ± 0.001	0.947 ± 0.001	87470	0.439 ± 0.001	0.947 ± 0.001
$p_{T_3} > 8 \text{ GeV}, \eta < 2.4$	68906	0.345 ± 0.001	0.784 ± 0.001	68417	0.343 ± 0.001	0.782 ± 0.001
$p_{T_4} > 8 \text{ GeV}, \eta < 2.4$	27111	0.136 ± 0.001	0.393 ± 0.002	26943	0.135 ± 0.001	0.394 ± 0.002
Extra RECO level selections						
Good primary vertex	27111	0.136 ± 0.001	1.000 ± 0.000	26943	0.135 ± 0.001	1.000 ± 0.000
Two muon-jets	23247	0.116 ± 0.001	0.857 ± 0.002	23237	0.117 ± 0.001	0.862 ± 0.002
Two dimuons	23229	0.116 ± 0.001	0.999 ± 0.000	23216	0.116 ± 0.001	0.999 ± 0.000
Pixel hit requirement	23225	0.116 ± 0.001	1.000 ± 0.000	23211	0.116 ± 0.001	1.000 ± 0.000
$ z_{\mu\mu_1} - z_{\mu\mu_2} < 0.1 \text{ cm}$	23206	0.116 ± 0.001	0.999 ± 0.000	23194	0.116 ± 0.001	0.999 ± 0.000
$m_{\mu\mu_1} \approx m_{\mu\mu_2}$	22586	0.113 ± 0.001	0.973 ± 0.001	22279	0.112 ± 0.001	0.961 ± 0.001
Dimuon isolation < 2 GeV	18216	0.091 ± 0.001	0.807 ± 0.003	17913	0.090 ± 0.001	0.804 ± 0.003
Trigger	1796	0.088 ± 0.001	0.971 ± 0.001	17383	0.087 ± 0.001	0.970 ± 0.001
α_{GEN}			0.139 ± 0.001			0.139 ± 0.001
ϵ_{SIM}			0.088 ± 0.001			0.087 ± 0.001
$\epsilon_{\text{SIM}} / \alpha_{\text{GEN}}$			0.635 ± 0.003			0.629 ± 0.003

Sample	$m_H = 100 \text{ GeV}, m_A = 0.25 \text{ GeV}$			$m_H = 100 \text{ GeV}, m_A = 0.5 \text{ GeV}$		
Selection	Events	Tot. Eff. [%]	Rel. Eff. [%]	Events	Tot. Eff. [%]	Rel. Eff. [%]
All events	199065	1.000 ± 0.000	1.000 ± 0.000	199215	1.000 ± 0.000	1.000 ± 0.000
Basic GEN level selections						
$p_{T_1} > 17 \text{ GeV}, \eta < 0.9$	93494	0.470 ± 0.001	0.470 ± 0.001	96955	0.487 ± 0.001	0.487 ± 0.001
$p_{T_2} > 8 \text{ GeV}, \eta < 2.4$	92701	0.466 ± 0.001	0.992 ± 0.000	92545	0.465 ± 0.001	0.955 ± 0.001
$p_{T_3} > 8 \text{ GeV}, \eta < 2.4$	85163	0.428 ± 0.001	0.919 ± 0.001	79529	0.399 ± 0.001	0.859 ± 0.001
$p_{T_4} > 8 \text{ GeV}, \eta < 2.4$	77741	0.391 ± 0.001	0.913 ± 0.001	40784	0.205 ± 0.001	0.513 ± 0.002
$L_{xy} < 9.8 \text{ cm and } L_z < 46.5 \text{ cm}$	77741	0.391 ± 0.001	1.000 ± 0.000	40784	0.205 ± 0.001	1.000 ± 0.000
Basic RECO level selections						
$p_{T_1} > 17 \text{ GeV}, \eta < 0.9$	93066	0.468 ± 0.001	0.468 ± 0.001	96691	0.485 ± 0.001	0.485 ± 0.001
$p_{T_2} > 8 \text{ GeV}, \eta < 2.4$	91827	0.461 ± 0.001	0.987 ± 0.000	92097	0.462 ± 0.001	0.952 ± 0.001
$p_{T_3} > 8 \text{ GeV}, \eta < 2.4$	83562	0.420 ± 0.001	0.910 ± 0.001	78119	0.392 ± 0.001	0.848 ± 0.001
$p_{T_4} > 8 \text{ GeV}, \eta < 2.4$	68361	0.343 ± 0.001	0.818 ± 0.001	38892	0.195 ± 0.001	0.498 ± 0.002
Extra RECO level selections						
Good primary vertex	68361	0.343 ± 0.001	1.000 ± 0.000	38892	0.195 ± 0.001	1.000 ± 0.000
Two muon-jets	66229	0.333 ± 0.001	0.969 ± 0.001	33823	0.170 ± 0.001	0.870 ± 0.002
Two dimuons	66194	0.333 ± 0.001	0.999 ± 0.000	33808	0.170 ± 0.001	1.000 ± 0.000
Pixel hit requirement	65576	0.329 ± 0.001	0.991 ± 0.000	33769	0.170 ± 0.001	0.999 ± 0.000
$ z_{\mu\mu_1} - z_{\mu\mu_2} < 0.1 \text{ cm}$	65325	0.328 ± 0.001	0.996 ± 0.000	33661	0.169 ± 0.001	0.997 ± 0.000
$m_{\mu\mu_1} \approx m_{\mu\mu_2}$	65047	0.327 ± 0.001	0.996 ± 0.000	33488	0.168 ± 0.001	0.995 ± 0.000
Dimuon isolation < 2 GeV	52164	0.262 ± 0.001	0.802 ± 0.002	27152	0.136 ± 0.001	0.811 ± 0.002
Trigger	49547	0.249 ± 0.001	0.950 ± 0.001	26356	0.132 ± 0.001	0.971 ± 0.001
α_{GEN}						
ϵ_{SIM}						
$\epsilon_{\text{SIM}}/\alpha_{\text{GEN}}$				0.637 ± 0.002	0.205 ± 0.001	0.132 ± 0.001
						0.646 ± 0.002

Sample	$m_H = 100 \text{ GeV}, m_A = 0.75 \text{ GeV}$			$m_H = 100 \text{ GeV}, m_A = 1 \text{ GeV}$		
Selection	Events	Tot. Eff. [%]	Rel. Eff. [%]	Events	Tot. Eff. [%]	Rel. Eff. [%]
All events	200000	1.000 ± 0.000	1.000 ± 0.000	198250	1.000 ± 0.000	1.000 ± 0.000
Basic GEN level selections						
$p_{T_1} > 17 \text{ GeV}, \eta < 0.9$	98057	0.490 ± 0.001	0.490 ± 0.001	97141	0.490 ± 0.001	0.490 ± 0.001
$p_{T_2} > 8 \text{ GeV}, \eta < 2.4$	93159	0.466 ± 0.001	0.950 ± 0.001	92106	0.465 ± 0.001	0.948 ± 0.001
$p_{T_3} > 8 \text{ GeV}, \eta < 2.4$	77827	0.389 ± 0.001	0.835 ± 0.001	76235	0.385 ± 0.001	0.828 ± 0.001
$p_{T_4} > 8 \text{ GeV}, \eta < 2.4$	36480	0.182 ± 0.001	0.469 ± 0.002	34629	0.175 ± 0.001	0.454 ± 0.002
$L_{xy} < 9.8 \text{ cm and } L_z < 46.5 \text{ cm}$	36480	0.182 ± 0.001	1.000 ± 0.000	34629	0.175 ± 0.001	1.000 ± 0.000
Basic RECO level selections						
$p_{T_1} > 17 \text{ GeV}, \eta < 0.9$	97781	0.489 ± 0.001	0.489 ± 0.001	96951	0.489 ± 0.001	0.489 ± 0.001
$p_{T_2} > 8 \text{ GeV}, \eta < 2.4$	92716	0.464 ± 0.001	0.948 ± 0.001	91766	0.463 ± 0.001	0.947 ± 0.001
$p_{T_3} > 8 \text{ GeV}, \eta < 2.4$	76430	0.382 ± 0.001	0.824 ± 0.001	74906	0.378 ± 0.001	0.816 ± 0.001
$p_{T_4} > 8 \text{ GeV}, \eta < 2.4$	35049	0.175 ± 0.001	0.459 ± 0.002	33304	0.168 ± 0.001	0.445 ± 0.002
Extra RECO level selections						
Good primary vertex	35049	0.175 ± 0.001	1.000 ± 0.000	33304	0.168 ± 0.001	1.000 ± 0.000
Two muon-jets	30200	0.151 ± 0.001	0.862 ± 0.002	28657	0.145 ± 0.001	0.860 ± 0.002
Two dimuons	30191	0.151 ± 0.001	1.000 ± 0.000	28647	0.144 ± 0.001	1.000 ± 0.000
Pixel hit requirement	30181	0.151 ± 0.001	1.000 ± 0.000	28643	0.144 ± 0.001	1.000 ± 0.000
$ z_{\mu\mu_1} - z_{\mu\mu_2} < 0.1 \text{ cm}$	30113	0.151 ± 0.001	0.998 ± 0.000	28612	0.144 ± 0.001	0.999 ± 0.000
$m_{\mu\mu_1} \approx m_{\mu\mu_2}$	29848	0.149 ± 0.001	0.991 ± 0.001	28231	0.142 ± 0.001	0.987 ± 0.001
Dimuon isolation < 2 GeV	23950	0.120 ± 0.001	0.802 ± 0.002	22636	0.114 ± 0.001	0.802 ± 0.002
Trigger	23225	0.116 ± 0.001	0.970 ± 0.001	21973	0.111 ± 0.001	0.971 ± 0.001
α_{GEN}						
ϵ_{SIM}						
$\epsilon_{\text{SIM}} / \alpha_{\text{GEN}}$				0.637 ± 0.003		0.635 ± 0.003

Sample	$m_H = 100 \text{ GeV}, m_A = 2 \text{ GeV}$				$m_H = 100 \text{ GeV}, m_A = 3 \text{ GeV}$			
	Events	Tot. Eff. [%]	Rel. Eff. [%]	Events	Tot. Eff. [%]	Rel. Eff. [%]	Events	Tot. Eff. [%]
All events	200000	1.000 ± 0.000	1.000 ± 0.000	198865	1.000 ± 0.000	1.000 ± 0.000	98026	0.493 ± 0.001
Basic GEN level selections							93107	0.468 ± 0.001
$p_{T_1} > 17 \text{ GeV}, \eta < 0.9$	98468	0.492 ± 0.001	0.492 ± 0.001	76550	0.383 ± 0.001	0.819 ± 0.001	76071	0.383 ± 0.001
$p_{T_2} > 8 \text{ GeV}, \eta < 2.4$	93521	0.468 ± 0.001	0.950 ± 0.001	33727	0.169 ± 0.001	0.441 ± 0.002	33470	0.168 ± 0.001
$p_{T_3} > 8 \text{ GeV}, \eta < 2.4$	76550	0.383 ± 0.001	0.819 ± 0.001	33727	0.169 ± 0.001	1.000 ± 0.000	33470	0.168 ± 0.001
$p_{T_4} > 8 \text{ GeV}, \eta < 2.4$	33727	0.169 ± 0.001	0.441 ± 0.002				97765	0.492 ± 0.001
$L_{xy} < 9.8 \text{ cm and } L_z < 46.5 \text{ cm}$	33727	0.169 ± 0.001	1.000 ± 0.000				92709	0.466 ± 0.001
Basic RECO level selections							74943	0.377 ± 0.001
$p_{T_1} > 17 \text{ GeV}, \eta < 0.9$	98201	0.491 ± 0.001	0.491 ± 0.001	75257	0.376 ± 0.001	0.808 ± 0.001	32520	0.164 ± 0.001
$p_{T_2} > 8 \text{ GeV}, \eta < 2.4$	93113	0.466 ± 0.001	0.948 ± 0.001	32710	0.164 ± 0.001	0.435 ± 0.002		
$p_{T_3} > 8 \text{ GeV}, \eta < 2.4$	75257	0.376 ± 0.001	0.808 ± 0.001				97765	0.492 ± 0.001
$p_{T_4} > 8 \text{ GeV}, \eta < 2.4$	32710	0.164 ± 0.001	0.435 ± 0.002				92709	0.466 ± 0.001
Extra RECO level selections							74943	0.377 ± 0.001
Good primary vertex	32710	0.164 ± 0.001	1.000 ± 0.000				32520	0.164 ± 0.001
Two muon-jets	28191	0.141 ± 0.001	0.862 ± 0.002				27960	0.141 ± 0.001
Two dimuons	28174	0.141 ± 0.001	0.999 ± 0.000				27942	0.141 ± 0.001
Pixel hit requirement	28168	0.141 ± 0.001	1.000 ± 0.000				27940	0.140 ± 0.001
$ z_{\mu\mu_1} - z_{\mu\mu_2} < 0.1 \text{ cm}$	28143	0.141 ± 0.001	0.999 ± 0.000				27920	0.140 ± 0.001
$m_{\mu\mu_1} \approx m_{\mu\mu_2}$	27367	0.137 ± 0.001	0.972 ± 0.001				26893	0.135 ± 0.001
Dimuon isolation < 2 GeV	21920	0.110 ± 0.001	0.801 ± 0.002				21527	0.108 ± 0.001
Trigger	21291	0.106 ± 0.001	0.971 ± 0.001				20937	0.105 ± 0.001
α_{GEN}								0.973 ± 0.001
ϵ_{SIM}								0.168 ± 0.001
$\epsilon_{\text{SIM}} / \alpha_{\text{GEN}}$								0.105 ± 0.001
								0.626 ± 0.003

Sample	$m_H = 110 \text{ GeV}, m_A = 0.25 \text{ GeV}$		
Selection	Events	Tot. Eff. [%]	Rel. Eff. [%]
All events	200000	1.000 ± 0.000	1.000 ± 0.000
Basic GEN level selections			
$p_{T_1} > 17 \text{ GeV}, \eta < 0.9$	98832	0.494 ± 0.001	0.494 ± 0.001
$p_{T_2} > 8 \text{ GeV}, \eta < 2.4$	98032	0.490 ± 0.001	0.992 ± 0.000
$p_{T_3} > 8 \text{ GeV}, \eta < 2.4$	89512	0.448 ± 0.001	0.913 ± 0.001
$p_{T_4} > 8 \text{ GeV}, \eta < 2.4$	83808	0.419 ± 0.001	0.936 ± 0.001
$L_{xy} < 9.8 \text{ cm and } L_z < 46.5 \text{ cm}$	83808	0.419 ± 0.001	1.000 ± 0.000
Basic RECO level selections			
$p_{T_1} > 17 \text{ GeV}, \eta < 0.9$	98336	0.492 ± 0.001	0.492 ± 0.001
$p_{T_2} > 8 \text{ GeV}, \eta < 2.4$	97103	0.486 ± 0.001	0.987 ± 0.000
$p_{T_3} > 8 \text{ GeV}, \eta < 2.4$	87848	0.439 ± 0.001	0.905 ± 0.001
$p_{T_4} > 8 \text{ GeV}, \eta < 2.4$	73146	0.366 ± 0.001	0.833 ± 0.001
Extra RECO level selections			
Good primary vertex	73146	0.366 ± 0.001	1.000 ± 0.000
Two muon-jets	71000	0.355 ± 0.001	0.971 ± 0.001
Two dimuons	70957	0.355 ± 0.001	0.999 ± 0.000
Pixel hit requirement	70292	0.351 ± 0.001	0.991 ± 0.000
$ z_{\mu\mu_1} - z_{\mu\mu_2} < 0.1 \text{ cm}$	69991	0.350 ± 0.001	0.996 ± 0.000
$m_{\mu\mu_1} \approx m_{\mu\mu_2}$	69671	0.348 ± 0.001	0.995 ± 0.000
Dimuon isolation < 2 GeV	56141	0.281 ± 0.001	0.806 ± 0.001
Trigger	53158	0.266 ± 0.001	0.947 ± 0.001
α_{GEN}			0.419 ± 0.001
ϵ_{SIM}			0.266 ± 0.001
$\epsilon_{\text{SIM}} / \alpha_{\text{GEN}}$			0.634 ± 0.002

Sample	$m_H = 110 \text{ GeV}, m_A = 0.75 \text{ GeV}$			$m_H = 110 \text{ GeV}, m_A = 1 \text{ GeV}$		
Selection	Events	Tot. Eff. [%]	Rel. Eff. [%]	Events	Tot. Eff. [%]	Rel. Eff. [%]
All events	199065	1.000 ± 0.000	1.000 ± 0.000	197097	1.000 ± 0.000	1.000 ± 0.000
Basic GEN level selections						
$p_{T_1} > 17 \text{ GeV}, \eta < 0.9$	101665	0.511 ± 0.001	0.511 ± 0.001	101218	0.514 ± 0.001	0.514 ± 0.001
$p_{T_2} > 8 \text{ GeV}, \eta < 2.4$	96713	0.486 ± 0.001	0.951 ± 0.001	96012	0.487 ± 0.001	0.949 ± 0.001
$p_{T_3} > 8 \text{ GeV}, \eta < 2.4$	82352	0.414 ± 0.001	0.852 ± 0.001	81050	0.411 ± 0.001	0.844 ± 0.001
$p_{T_4} > 8 \text{ GeV}, \eta < 2.4$	41515	0.209 ± 0.001	0.504 ± 0.002	39722	0.202 ± 0.001	0.490 ± 0.002
$L_{xy} < 9.8 \text{ cm and } L_z < 46.5 \text{ cm}$	41515	0.209 ± 0.001	1.000 ± 0.000	39722	0.202 ± 0.001	1.000 ± 0.000
Basic RECO level selections						
$p_{T_1} > 17 \text{ GeV}, \eta < 0.9$	101405	0.509 ± 0.001	0.509 ± 0.001	100938	0.512 ± 0.001	0.512 ± 0.001
$p_{T_2} > 8 \text{ GeV}, \eta < 2.4$	96297	0.484 ± 0.001	0.950 ± 0.001	95560	0.485 ± 0.001	0.947 ± 0.001
$p_{T_3} > 8 \text{ GeV}, \eta < 2.4$	80897	0.406 ± 0.001	0.840 ± 0.001	79632	0.404 ± 0.001	0.833 ± 0.001
$p_{T_4} > 8 \text{ GeV}, \eta < 2.4$	39643	0.199 ± 0.001	0.490 ± 0.002	37985	0.193 ± 0.001	0.477 ± 0.002
Extra RECO level selections						
Good primary vertex	39643	0.199 ± 0.001	1.000 ± 0.000	37985	0.193 ± 0.001	1.000 ± 0.000
Two muon-jets	34205	0.172 ± 0.001	0.863 ± 0.002	32709	0.166 ± 0.001	0.861 ± 0.002
Two dimuons	34191	0.172 ± 0.001	1.000 ± 0.000	32687	0.166 ± 0.001	0.999 ± 0.000
Pixel hit requirement	34170	0.172 ± 0.001	0.999 ± 0.000	32676	0.166 ± 0.001	1.000 ± 0.000
$ z_{\mu\mu_1} - z_{\mu\mu_2} < 0.1 \text{ cm}$	34091	0.171 ± 0.001	0.998 ± 0.000	32632	0.166 ± 0.001	0.999 ± 0.000
$m_{\mu\mu_1} \approx m_{\mu\mu_2}$	33767	0.170 ± 0.001	0.990 ± 0.001	32139	0.163 ± 0.001	0.985 ± 0.001
Dimuon isolation < 2 GeV	27010	0.136 ± 0.001	0.800 ± 0.002	25798	0.131 ± 0.001	0.803 ± 0.002
Trigger	26260	0.132 ± 0.001	0.972 ± 0.001	25069	0.127 ± 0.001	0.972 ± 0.001
α_{GEN}						
ϵ_{SIM}						
$\epsilon_{\text{SIM}}/\alpha_{\text{GEN}}$						
		0.633 ± 0.002				0.631 ± 0.002

Sample	$m_H = 110 \text{ GeV}, m_A = 2 \text{ GeV}$			$m_H = 110 \text{ GeV}, m_A = 3 \text{ GeV}$		
Selection	Events	Tot. Eff. [%]	Rel. Eff. [%]	Events	Tot. Eff. [%]	Rel. Eff. [%]
All events	198634	1.000 ± 0.000	1.000 ± 0.000	200000	1.000 ± 0.000	1.000 ± 0.000
Basic GEN level selections						
$p_{T_1} > 17 \text{ GeV}, \eta < 0.9$	101807	0.513 ± 0.001	0.513 ± 0.001	102786	0.514 ± 0.001	0.514 ± 0.001
$p_{T_2} > 8 \text{ GeV}, \eta < 2.4$	96587	0.486 ± 0.001	0.949 ± 0.001	97581	0.488 ± 0.001	0.949 ± 0.001
$p_{T_3} > 8 \text{ GeV}, \eta < 2.4$	80783	0.407 ± 0.001	0.836 ± 0.001	81648	0.408 ± 0.001	0.837 ± 0.001
$p_{T_4} > 8 \text{ GeV}, \eta < 2.4$	38572	0.194 ± 0.001	0.477 ± 0.002	38481	0.192 ± 0.001	0.471 ± 0.002
$L_{xy} < 9.8 \text{ cm and } L_z < 46.5 \text{ cm}$	38572	0.194 ± 0.001	1.000 ± 0.000	38481	0.192 ± 0.001	1.000 ± 0.000
Basic RECO level selections						
$p_{T_1} > 17 \text{ GeV}, \eta < 0.9$	101557	0.511 ± 0.001	0.511 ± 0.001	102477	0.512 ± 0.001	0.512 ± 0.001
$p_{T_2} > 8 \text{ GeV}, \eta < 2.4$	96213	0.484 ± 0.001	0.947 ± 0.001	97156	0.486 ± 0.001	0.948 ± 0.001
$p_{T_3} > 8 \text{ GeV}, \eta < 2.4$	79487	0.400 ± 0.001	0.826 ± 0.001	80327	0.402 ± 0.001	0.827 ± 0.001
$p_{T_4} > 8 \text{ GeV}, \eta < 2.4$	37196	0.187 ± 0.001	0.468 ± 0.002	37248	0.186 ± 0.001	0.464 ± 0.002
Extra RECO level selections						
Good primary vertex	37196	0.187 ± 0.001	1.000 ± 0.000	37248	0.186 ± 0.001	1.000 ± 0.000
Two muon-jets	32095	0.162 ± 0.001	0.863 ± 0.002	32105	0.161 ± 0.001	0.862 ± 0.002
Two dimuons	32066	0.161 ± 0.001	0.999 ± 0.000	32069	0.160 ± 0.001	0.999 ± 0.000
Pixel hit requirement	32060	0.161 ± 0.001	1.000 ± 0.000	32066	0.160 ± 0.001	1.000 ± 0.000
$ z_{\mu\mu_1} - z_{\mu\mu_2} < 0.1 \text{ cm}$	32031	0.161 ± 0.001	0.999 ± 0.000	32043	0.160 ± 0.001	0.999 ± 0.000
$m_{\mu\mu_1} \approx m_{\mu\mu_2}$	31092	0.157 ± 0.001	0.971 ± 0.001	30776	0.154 ± 0.001	0.960 ± 0.001
Dimuon isolation < 2 GeV	24887	0.125 ± 0.001	0.800 ± 0.002	24666	0.123 ± 0.001	0.801 ± 0.002
Trigger	24140	0.122 ± 0.001	0.970 ± 0.001	23930	0.120 ± 0.001	0.970 ± 0.001
α_{GEN}		0.194 ± 0.001		0.192 ± 0.001		0.192 ± 0.001
ϵ_{SIM}		0.122 ± 0.001		0.120 ± 0.001		0.120 ± 0.001
$\epsilon_{\text{SIM}}/\alpha_{\text{GEN}}$		0.626 ± 0.002		0.622 ± 0.002		0.622 ± 0.002

Sample	$m_H = 125 \text{ GeV}, m_A = 0.25 \text{ GeV}$			$m_H = 125 \text{ GeV}, m_A = 0.5 \text{ GeV}$		
Selection	Events	Tot. Eff. [%]	Rel. Eff. [%]	Events	Tot. Eff. [%]	Rel. Eff. [%]
All events	200000	1.000 ± 0.000	1.000 ± 0.000	200000	1.000 ± 0.000	1.000 ± 0.000
Basic GEN level selections						
$p_{T_1} > 17 \text{ GeV}, \eta < 0.9$	105303	0.527 ± 0.001	0.527 ± 0.001	107340	0.537 ± 0.001	0.537 ± 0.001
$p_{T_2} > 8 \text{ GeV}, \eta < 2.4$	104555	0.523 ± 0.001	0.993 ± 0.000	102519	0.513 ± 0.001	0.955 ± 0.001
$p_{T_3} > 8 \text{ GeV}, \eta < 2.4$	94856	0.474 ± 0.001	0.907 ± 0.001	90431	0.452 ± 0.001	0.882 ± 0.001
$p_{T_4} > 8 \text{ GeV}, \eta < 2.4$	90982	0.455 ± 0.001	0.959 ± 0.001	54814	0.274 ± 0.001	0.606 ± 0.002
$L_{xy} < 9.8 \text{ cm and } L_z < 46.5 \text{ cm}$	90982	0.455 ± 0.001	1.000 ± 0.000	54814	0.274 ± 0.001	1.000 ± 0.000
Basic RECO level selections						
$p_{T_1} > 17 \text{ GeV}, \eta < 0.9$	104904	0.525 ± 0.001	0.525 ± 0.001	107052	0.535 ± 0.001	0.535 ± 0.001
$p_{T_2} > 8 \text{ GeV}, \eta < 2.4$	103689	0.518 ± 0.001	0.988 ± 0.000	102092	0.510 ± 0.001	0.954 ± 0.001
$p_{T_3} > 8 \text{ GeV}, \eta < 2.4$	93191	0.466 ± 0.001	0.899 ± 0.001	88835	0.444 ± 0.001	0.870 ± 0.001
$p_{T_4} > 8 \text{ GeV}, \eta < 2.4$	78216	0.391 ± 0.001	0.839 ± 0.001	51624	0.258 ± 0.001	0.581 ± 0.002
Extra RECO level selections						
Good primary vertex	78216	0.391 ± 0.001	1.000 ± 0.000	51624	0.258 ± 0.001	1.000 ± 0.000
Two muon-jets	75871	0.379 ± 0.001	0.970 ± 0.001	44884	0.224 ± 0.001	0.869 ± 0.001
Two dimuons	75818	0.379 ± 0.001	0.999 ± 0.000	44864	0.224 ± 0.001	1.000 ± 0.000
Pixel hit requirement	74936	0.375 ± 0.001	0.988 ± 0.000	44816	0.224 ± 0.001	0.999 ± 0.000
$ z_{\mu\mu_1} - z_{\mu\mu_2} < 0.1 \text{ cm}$	74543	0.373 ± 0.001	0.995 ± 0.000	44655	0.223 ± 0.001	0.996 ± 0.000
$m_{\mu\mu_1} \approx m_{\mu\mu_2}$	74091	0.370 ± 0.001	0.994 ± 0.000	44390	0.222 ± 0.001	0.994 ± 0.000
Dimuon isolation < 2 GeV	59350	0.297 ± 0.001	0.801 ± 0.001	35381	0.177 ± 0.001	0.797 ± 0.002
Trigger	56039	0.280 ± 0.001	0.944 ± 0.001	34288	0.171 ± 0.001	0.969 ± 0.001
α_{GEN}						
ϵ_{SIM}						
$\epsilon_{\text{SIM}} / \alpha_{\text{GEN}}$				0.616 ± 0.002		0.626 ± 0.002

Sample	$m_H = 125 \text{ GeV}, m_A = 0.75 \text{ GeV}$			$m_H = 125 \text{ GeV}, m_A = 1 \text{ GeV}$		
Selection	Events	Tot. Eff. [%]	Rel. Eff. [%]	Events	Tot. Eff. [%]	Rel. Eff. [%]
All events	195695	1.000 ± 0.000	1.000 ± 0.000	198388	1.000 ± 0.000	1.000 ± 0.000
Basic GEN level selections						
$p_{T_1} > 17 \text{ GeV}, \eta < 0.9$	105445	0.539 ± 0.001	0.539 ± 0.001	106979	0.539 ± 0.001	0.539 ± 0.001
$p_{T_2} > 8 \text{ GeV}, \eta < 2.4$	100131	0.512 ± 0.001	0.950 ± 0.001	101631	0.512 ± 0.001	0.950 ± 0.001
$p_{T_3} > 8 \text{ GeV}, \eta < 2.4$	86611	0.443 ± 0.001	0.865 ± 0.001	87296	0.440 ± 0.001	0.859 ± 0.001
$p_{T_4} > 8 \text{ GeV}, \eta < 2.4$	48016	0.245 ± 0.001	0.554 ± 0.002	46795	0.236 ± 0.001	0.536 ± 0.002
$L_{xy} < 9.8 \text{ cm and } L_z < 46.5 \text{ cm}$	48016	0.245 ± 0.001	1.000 ± 0.000	46795	0.236 ± 0.001	1.000 ± 0.000
Basic RECO level selections						
$p_{T_1} > 17 \text{ GeV}, \eta < 0.9$	105208	0.538 ± 0.001	0.538 ± 0.001	106698	0.538 ± 0.001	0.538 ± 0.001
$p_{T_2} > 8 \text{ GeV}, \eta < 2.4$	99760	0.510 ± 0.001	0.948 ± 0.001	101186	0.510 ± 0.001	0.948 ± 0.001
$p_{T_3} > 8 \text{ GeV}, \eta < 2.4$	85187	0.435 ± 0.001	0.854 ± 0.001	85688	0.432 ± 0.001	0.847 ± 0.001
$p_{T_4} > 8 \text{ GeV}, \eta < 2.4$	45651	0.233 ± 0.001	0.536 ± 0.002	44534	0.224 ± 0.001	0.520 ± 0.002
Extra RECO level selections						
Good primary vertex	45651	0.233 ± 0.001	1.000 ± 0.000	44534	0.224 ± 0.001	1.000 ± 0.000
Two muon-jets	39376	0.201 ± 0.001	0.863 ± 0.002	38357	0.193 ± 0.001	0.861 ± 0.002
Two dimuons	39351	0.201 ± 0.001	0.999 ± 0.000	38325	0.193 ± 0.001	0.999 ± 0.000
Pixel hit requirement	39324	0.201 ± 0.001	0.999 ± 0.000	38302	0.193 ± 0.001	0.999 ± 0.000
$ z_{\mu\mu_1} - z_{\mu\mu_2} < 0.1 \text{ cm}$	39223	0.200 ± 0.001	0.997 ± 0.000	38243	0.193 ± 0.001	0.998 ± 0.000
$m_{\mu\mu_1} \approx m_{\mu\mu_2}$	38805	0.198 ± 0.001	0.989 ± 0.001	37656	0.190 ± 0.001	0.985 ± 0.001
Dimuon isolation < 2 GeV	30972	0.158 ± 0.001	0.798 ± 0.002	29965	0.151 ± 0.001	0.796 ± 0.002
Trigger	30120	0.154 ± 0.001	0.972 ± 0.001	29122	0.147 ± 0.001	0.972 ± 0.001
α_{GEN}			0.245 ± 0.001			0.236 ± 0.001
ϵ_{SIM}			0.154 ± 0.001			0.147 ± 0.001
$\epsilon_{\text{SIM}}/\alpha_{\text{GEN}}$			0.627 ± 0.002			0.622 ± 0.002

Sample	$m_H = 125 \text{ GeV}, m_A = 2 \text{ GeV}$			$m_H = 125 \text{ GeV}, m_A = 3 \text{ GeV}$		
Selection	Events	Tot. Eff. [%]	Rel. Eff. [%]	Events	Tot. Eff. [%]	Rel. Eff. [%]
All events	200000	1.000 ± 0.000	1.000 ± 0.000	200001	1.000 ± 0.000	1.000 ± 0.000
Basic GEN level selections						
$p_{T_1} > 17 \text{ GeV}, \eta < 0.9$	108063	0.540 ± 0.001	0.540 ± 0.001	108342	0.542 ± 0.001	0.542 ± 0.001
$p_{T_2} > 8 \text{ GeV}, \eta < 2.4$	102538	0.513 ± 0.001	0.949 ± 0.001	102787	0.514 ± 0.001	0.949 ± 0.001
$p_{T_3} > 8 \text{ GeV}, \eta < 2.4$	87363	0.437 ± 0.001	0.852 ± 0.001	87284	0.436 ± 0.001	0.849 ± 0.001
$p_{T_4} > 8 \text{ GeV}, \eta < 2.4$	45674	0.228 ± 0.001	0.523 ± 0.002	44992	0.225 ± 0.001	0.515 ± 0.002
$L_{xy} < 9.8 \text{ cm and } L_z < 46.5 \text{ cm}$	45674	0.228 ± 0.001	1.000 ± 0.000	44992	0.225 ± 0.001	1.000 ± 0.000
Basic RECO level selections						
$p_{T_1} > 17 \text{ GeV}, \eta < 0.9$	107840	0.539 ± 0.001	0.539 ± 0.001	108099	0.540 ± 0.001	0.540 ± 0.001
$p_{T_2} > 8 \text{ GeV}, \eta < 2.4$	102164	0.511 ± 0.001	0.947 ± 0.001	102407	0.512 ± 0.001	0.947 ± 0.001
$p_{T_3} > 8 \text{ GeV}, \eta < 2.4$	86066	0.430 ± 0.001	0.842 ± 0.001	86041	0.430 ± 0.001	0.840 ± 0.001
$p_{T_4} > 8 \text{ GeV}, \eta < 2.4$	43862	0.219 ± 0.001	0.510 ± 0.002	43357	0.217 ± 0.001	0.504 ± 0.002
Extra RECO level selections						
Good primary vertex	43862	0.219 ± 0.001	1.000 ± 0.000	43357	0.217 ± 0.001	1.000 ± 0.000
Two muon-jets	37645	0.188 ± 0.001	0.858 ± 0.002	37227	0.186 ± 0.001	0.859 ± 0.002
Two dimuons	37616	0.188 ± 0.001	0.999 ± 0.000	37183	0.186 ± 0.001	0.999 ± 0.000
Pixel hit requirement	37610	0.188 ± 0.001	1.000 ± 0.000	37175	0.186 ± 0.001	1.000 ± 0.000
$ z_{\mu\mu_1} - z_{\mu\mu_2} < 0.1 \text{ cm}$	37572	0.188 ± 0.001	0.999 ± 0.000	37147	0.186 ± 0.001	0.999 ± 0.000
$m_{\mu\mu_1} \approx m_{\mu\mu_2}$	36441	0.182 ± 0.001	0.970 ± 0.001	35656	0.178 ± 0.001	0.960 ± 0.001
Dimuon isolation < 2 GeV	29065	0.145 ± 0.001	0.798 ± 0.002	28342	0.142 ± 0.001	0.795 ± 0.002
Trigger	28251	0.141 ± 0.001	0.972 ± 0.001	27522	0.138 ± 0.001	0.971 ± 0.001
α_{GEN}						
ϵ_{SIM}						
$\epsilon_{\text{SIM}} / \alpha_{\text{GEN}}$						
		0.619 ± 0.002				
		0.141 ± 0.001				
		0.228 ± 0.001				
		0.138 ± 0.001				
		0.612 ± 0.002				

Sample	$m_H = 150 \text{ GeV}, m_A = 0.25 \text{ GeV}$			$m_H = 150 \text{ GeV}, m_A = 0.5 \text{ GeV}$		
Selection	Events	Tot. Eff. [%]	Rel. Eff. [%]	Events	Tot. Eff. [%]	Rel. Eff. [%]
All events	200001	1.000 ± 0.000	1.000 ± 0.002	200001	1.000 ± 0.000	1.000 ± 0.000
Basic GEN level selections						
$p_{T_1} > 17 \text{ GeV}, \eta < 0.9$	112770	0.564 ± 0.001	0.564 ± 0.001	114310	0.572 ± 0.001	0.572 ± 0.001
$p_{T_2} > 8 \text{ GeV}, \eta < 2.4$	112162	0.561 ± 0.001	0.995 ± 0.000	109658	0.548 ± 0.001	0.959 ± 0.001
$p_{T_3} > 8 \text{ GeV}, \eta < 2.4$	100458	0.502 ± 0.001	0.896 ± 0.001	97405	0.487 ± 0.001	0.888 ± 0.001
$p_{T_4} > 8 \text{ GeV}, \eta < 2.4$	98493	0.492 ± 0.001	0.980 ± 0.000	66806	0.334 ± 0.001	0.686 ± 0.001
$L_{xy} < 9.8 \text{ cm and } L_z < 46.5 \text{ cm}$	98493	0.492 ± 0.001	1.000 ± 0.000	66806	0.334 ± 0.001	1.000 ± 0.000
Basic RECO level selections						
$p_{T_1} > 17 \text{ GeV}, \eta < 0.9$	112426	0.562 ± 0.001	0.562 ± 0.002	114047	0.570 ± 0.001	0.570 ± 0.001
$p_{T_2} > 8 \text{ GeV}, \eta < 2.4$	111197	0.556 ± 0.001	0.989 ± 0.000	109195	0.546 ± 0.001	0.957 ± 0.001
$p_{T_3} > 8 \text{ GeV}, \eta < 2.4$	98738	0.494 ± 0.001	0.888 ± 0.001	95735	0.479 ± 0.001	0.877 ± 0.001
$p_{T_4} > 8 \text{ GeV}, \eta < 2.4$	82647	0.413 ± 0.001	0.837 ± 0.001	62361	0.312 ± 0.001	0.651 ± 0.002
Extra RECO level selections						
Good primary vertex	82647	0.413 ± 0.001	1.000 ± 0.000	62361	0.312 ± 0.001	1.000 ± 0.000
Two muon-jets	80120	0.401 ± 0.001	0.969 ± 0.001	54550	0.273 ± 0.001	0.875 ± 0.001
Two dimuons	80078	0.400 ± 0.001	0.999 ± 0.000	54525	0.273 ± 0.001	1.000 ± 0.000
Pixel hit requirement	78913	0.395 ± 0.001	0.985 ± 0.000	54436	0.272 ± 0.001	0.998 ± 0.000
$ z_{\mu\mu_1} - z_{\mu\mu_2} < 0.1 \text{ cm}$	78433	0.392 ± 0.001	0.994 ± 0.000	54139	0.271 ± 0.001	0.995 ± 0.000
$m_{\mu\mu_1} \approx m_{\mu\mu_2}$	77707	0.389 ± 0.001	0.991 ± 0.000	53793	0.269 ± 0.001	0.994 ± 0.000
Dimuon isolation < 2 GeV	61880	0.309 ± 0.001	0.796 ± 0.001	42491	0.212 ± 0.001	0.790 ± 0.002
Trigger	58218	0.291 ± 0.001	0.941 ± 0.001	41216	0.206 ± 0.001	0.970 ± 0.001
α_{GEN}						
ϵ_{SIM}						
$\epsilon_{\text{SIM}}/\alpha_{\text{GEN}}$						
		0.591 ± 0.002				0.617 ± 0.002

Sample	$m_H = 150 \text{ GeV}, m_A = 0.75 \text{ GeV}$			$m_H = 150 \text{ GeV}, m_A = 1 \text{ GeV}$		
Selection	Events	Tot. Eff. [%]	Rel. Eff. [%]	Events	Tot. Eff. [%]	Rel. Eff. [%]
All events	200001	1.000 ± 0.000	1.000 ± 0.622	200001	1.000 ± 0.000	1.000 ± 0.000
Basic GEN level selections						
$p_{T_1} > 17 \text{ GeV}, \eta < 0.9$	114774	0.574 ± 0.001	0.574 ± 0.001	114733	0.574 ± 0.001	0.574 ± 0.001
$p_{T_2} > 8 \text{ GeV}, \eta < 2.4$	109455	0.547 ± 0.001	0.954 ± 0.001	109226	0.546 ± 0.001	0.952 ± 0.001
$p_{T_3} > 8 \text{ GeV}, \eta < 2.4$	96123	0.481 ± 0.001	0.878 ± 0.001	95293	0.476 ± 0.001	0.872 ± 0.001
$p_{T_4} > 8 \text{ GeV}, \eta < 2.4$	59862	0.299 ± 0.001	0.623 ± 0.002	57543	0.288 ± 0.001	0.604 ± 0.002
$L_{xy} < 9.8 \text{ cm and } L_z < 46.5 \text{ cm}$	59862	0.299 ± 0.001	1.000 ± 0.000	57543	0.288 ± 0.001	1.000 ± 0.000
Basic RECO level selections						
$p_{T_1} > 17 \text{ GeV}, \eta < 0.9$	114545	0.573 ± 0.001	0.573 ± 0.001	114428	0.572 ± 0.001	0.572 ± 0.001
$p_{T_2} > 8 \text{ GeV}, \eta < 2.4$	109069	0.545 ± 0.001	0.952 ± 0.001	108774	0.544 ± 0.001	0.951 ± 0.001
$p_{T_3} > 8 \text{ GeV}, \eta < 2.4$	94524	0.473 ± 0.001	0.867 ± 0.001	93710	0.469 ± 0.001	0.862 ± 0.001
$p_{T_4} > 8 \text{ GeV}, \eta < 2.4$	56445	0.282 ± 0.001	0.597 ± 0.002	54166	0.271 ± 0.001	0.578 ± 0.002
Extra RECO level selections						
Good primary vertex	56445	0.282 ± 0.001	1.000 ± 0.000	54166	0.271 ± 0.001	1.000 ± 0.000
Two muon-jets	48808	0.244 ± 0.001	0.865 ± 0.001	46636	0.233 ± 0.001	0.861 ± 0.001
Two dimuons	48775	0.244 ± 0.001	0.999 ± 0.617	46609	0.233 ± 0.001	0.999 ± 0.000
Pixel hit requirement	48739	0.244 ± 0.001	0.999 ± 0.000	46588	0.233 ± 0.001	1.000 ± 0.000
$ z_{\mu\mu_1} - z_{\mu\mu_2} < 0.1 \text{ cm}$	48576	0.243 ± 0.001	0.997 ± 0.000	46481	0.232 ± 0.001	0.998 ± 0.000
$m_{\mu\mu_1} \approx m_{\mu\mu_2}$	48001	0.240 ± 0.001	0.988 ± 0.000	45682	0.228 ± 0.001	0.983 ± 0.001
Dimuon isolation < 2 GeV	38048	0.190 ± 0.001	0.793 ± 0.002	36214	0.181 ± 0.001	0.793 ± 0.002
Trigger	36951	0.185 ± 0.001	0.971 ± 0.001	35147	0.176 ± 0.001	0.971 ± 0.001
α_{GEN}						
ϵ_{SIM}						
$\epsilon_{\text{SIM}} / \alpha_{\text{GEN}}$						
		0.617 ± 0.002				
			0.299 ± 0.001			0.288 ± 0.001
			0.185 ± 0.001			0.176 ± 0.001
						0.611 ± 0.002

Sample	$m_H = 150 \text{ GeV}, m_A = 2 \text{ GeV}$			$m_H = 150 \text{ GeV}, m_A = 3 \text{ GeV}$		
Selection	Events	Tot. Eff. [%]	Rel. Eff. [%]	Events	Tot. Eff. [%]	Rel. Eff. [%]
All events	200001	1.000 ± 0.000	1.000 ± 0.000	199066	1.000 ± 0.000	1.000 ± 0.000
Basic GEN level selections						
$p_{T_1} > 17 \text{ GeV}, \eta < 0.9$	115039	0.575 ± 0.001	0.575 ± 0.001	114421	0.575 ± 0.001	0.575 ± 0.001
$p_{T_2} > 8 \text{ GeV}, \eta < 2.4$	109461	0.547 ± 0.001	0.952 ± 0.001	108903	0.547 ± 0.001	0.952 ± 0.001
$p_{T_3} > 8 \text{ GeV}, \eta < 2.4$	94815	0.474 ± 0.001	0.866 ± 0.001	94412	0.474 ± 0.001	0.867 ± 0.001
$p_{T_4} > 8 \text{ GeV}, \eta < 2.4$	55447	0.277 ± 0.001	0.585 ± 0.002	54660	0.275 ± 0.001	0.579 ± 0.002
$L_{xy} < 9.8 \text{ cm and } L_z < 46.5 \text{ cm}$	55447	0.277 ± 0.001	1.000 ± 0.000	54660	0.275 ± 0.001	1.000 ± 0.000
Basic RECO level selections						
$p_{T_1} > 17 \text{ GeV}, \eta < 0.9$	114803	0.574 ± 0.001	0.574 ± 0.001	114132	0.573 ± 0.001	0.573 ± 0.001
$p_{T_2} > 8 \text{ GeV}, \eta < 2.4$	109048	0.545 ± 0.001	0.950 ± 0.001	108457	0.545 ± 0.001	0.950 ± 0.001
$p_{T_3} > 8 \text{ GeV}, \eta < 2.4$	93405	0.467 ± 0.001	0.857 ± 0.001	93149	0.468 ± 0.001	0.859 ± 0.001
$p_{T_4} > 8 \text{ GeV}, \eta < 2.4$	52881	0.264 ± 0.001	0.566 ± 0.002	52408	0.263 ± 0.001	0.563 ± 0.002
Extra RECO level selections						
Good primary vertex	52881	0.264 ± 0.001	1.000 ± 0.000	52408	0.263 ± 0.001	1.000 ± 0.000
Two muon-jets	45437	0.227 ± 0.001	0.859 ± 0.002	45045	0.226 ± 0.001	0.860 ± 0.002
Two dimuons	45393	0.227 ± 0.001	0.999 ± 0.000	44994	0.226 ± 0.001	0.999 ± 0.000
Pixel hit requirement	45379	0.227 ± 0.001	1.000 ± 0.000	44987	0.226 ± 0.001	1.000 ± 0.000
$ z_{\mu\mu_1} - z_{\mu\mu_2} < 0.1 \text{ cm}$	45332	0.227 ± 0.001	0.999 ± 0.000	44932	0.226 ± 0.001	0.999 ± 0.000
$m_{\mu\mu_1} \approx m_{\mu\mu_2}$	43865	0.219 ± 0.001	0.968 ± 0.001	43040	0.216 ± 0.001	0.958 ± 0.001
Dimuon isolation < 2 GeV	34691	0.173 ± 0.001	0.791 ± 0.002	33937	0.170 ± 0.001	0.788 ± 0.002
Trigger	33696	0.168 ± 0.001	0.971 ± 0.001	32919	0.165 ± 0.001	0.970 ± 0.001
α_{GEN}			0.277 ± 0.001		0.275 ± 0.001	
ϵ_{SIM}			0.168 ± 0.001		0.165 ± 0.001	
$\epsilon_{\text{SIM}} / \alpha_{\text{GEN}}$			0.608 ± 0.002		0.602 ± 0.002	

Table 17: Acceptances and efficiencies of the event selection requirements for several representative dark SUSY benchmark models in MC simulation.

Sample	$m_{\gamma_D} = 0.25 \text{ GeV}, c\tau_{\gamma_D} = 0 \text{ mm}$			$m_{\gamma_D} = 0.25 \text{ GeV}, c\tau_{\gamma_D} = 0.05 \text{ mm}$		
Selection	Events	Tot. Eff. [%]	Rel. Eff. [%]	Events	Tot. Eff. [%]	Rel. Eff. [%]
All events	19400	1.000 ± 0.000	1.000 ± 0.000	19200	1.000 ± 0.000	1.000 ± 0.000
Basic GEN level selections						
$p_{T_1} > 17 \text{ GeV}, \eta < 0.9$	6160	0.318 ± 0.003	0.318 ± 0.003	6092	0.317 ± 0.003	0.317 ± 0.003
$p_{T_2} > 8 \text{ GeV}, \eta < 2.4$	6041	0.311 ± 0.003	0.981 ± 0.002	5951	0.310 ± 0.003	0.977 ± 0.002
$p_{T_3} > 8 \text{ GeV}, \eta < 2.4$	4024	0.207 ± 0.003	0.666 ± 0.006	3995	0.208 ± 0.003	0.671 ± 0.006
$p_{T_4} > 8 \text{ GeV}, \eta < 2.4$	2622	0.135 ± 0.002	0.652 ± 0.008	2666	0.139 ± 0.002	0.667 ± 0.007
$L_{xy} < 9.8 \text{ cm and } L_z < 46.5 \text{ cm}$	2622	0.135 ± 0.002	1.000 ± 0.000	2654	0.138 ± 0.002	0.995 ± 0.001
Basic RECO level selections						
$p_{T_1} > 17 \text{ GeV}, \eta < 0.9$	6129	0.316 ± 0.003	0.316 ± 0.003	6057	0.315 ± 0.003	0.315 ± 0.003
$p_{T_2} > 8 \text{ GeV}, \eta < 2.4$	5952	0.307 ± 0.003	0.971 ± 0.002	5830	0.304 ± 0.003	0.963 ± 0.002
$p_{T_3} > 8 \text{ GeV}, \eta < 2.4$	3945	0.203 ± 0.003	0.663 ± 0.006	3904	0.203 ± 0.003	0.670 ± 0.006
$p_{T_4} > 8 \text{ GeV}, \eta < 2.4$	2440	0.126 ± 0.002	0.619 ± 0.008	2442	0.127 ± 0.002	0.626 ± 0.008
Extra RECO level selections						
Good primary vertex	2440	0.126 ± 0.002	1.000 ± 0.000	2442	0.127 ± 0.002	1.000 ± 0.000
Two muon-jets	2349	0.121 ± 0.002	0.963 ± 0.004	2332	0.121 ± 0.002	0.955 ± 0.004
Two dimuons	2349	0.121 ± 0.002	1.000 ± 0.000	2330	0.121 ± 0.002	0.999 ± 0.001
Pixel hit requirement	2334	0.120 ± 0.002	0.994 ± 0.002	2301	0.120 ± 0.002	0.988 ± 0.002
$ z_{\mu\mu_1} - z_{\mu\mu_2} < 0.1 \text{ cm}$	2324	0.120 ± 0.002	0.996 ± 0.001	2288	0.119 ± 0.002	0.994 ± 0.002
$m_{\mu\mu_1} \approx m_{\mu\mu_2}$	2319	0.120 ± 0.002	0.998 ± 0.001	2283	0.119 ± 0.002	0.998 ± 0.001
Dimuon isolation < 2 GeV	1870	0.096 ± 0.002	0.806 ± 0.008	1854	0.097 ± 0.002	0.812 ± 0.008
Trigger	1769	0.091 ± 0.002	0.946 ± 0.005	1748	0.091 ± 0.002	0.943 ± 0.005
α_{GEN}			0.135 ± 0.002			0.138 ± 0.002
ϵ_{SIM}			0.091 ± 0.002			0.091 ± 0.002
$\epsilon_{\text{SIM}}/\alpha_{\text{GEN}}$			0.675 ± 0.009			0.659 ± 0.009

Table 18: Acceptances and efficiencies of the event selection requirements for several representative dark SUSY benchmark models in MC simulation.

Sample	$m_{\tau_D} = 0.25 \text{ GeV}, c\tau_{\tau_D} = 0.1 \text{ mm}$			$m_{\tau_D} = 0.25 \text{ GeV}, c\tau_{\tau_D} = 0.5 \text{ mm}$		
Selection	Events	Tot. Eff. [%]	Rel. Eff. [%]	Events	Tot. Eff. [%]	Rel. Eff. [%]
All events	97900	1.000 ± 0.000	1.000 ± 0.000	98100	1.000 ± 0.000	1.000 ± 0.000
Basic GEN level selections						
$p_{T_1} > 17 \text{ GeV}, \eta < 0.9$	31178	0.318 ± 0.001	0.318 ± 0.001	31515	0.321 ± 0.001	0.321 ± 0.001
$p_{T_2} > 8 \text{ GeV}, \eta < 2.4$	30501	0.312 ± 0.001	0.978 ± 0.001	30851	0.314 ± 0.001	0.979 ± 0.001
$p_{T_3} > 8 \text{ GeV}, \eta < 2.4$	20407	0.208 ± 0.001	0.669 ± 0.003	20480	0.209 ± 0.001	0.664 ± 0.003
$p_{T_4} > 8 \text{ GeV}, \eta < 2.4$	13707	0.140 ± 0.001	0.672 ± 0.003	13706	0.140 ± 0.001	0.669 ± 0.003
$L_{xy} < 9.8 \text{ cm and } L_z < 46.5 \text{ cm}$	13318	0.136 ± 0.001	0.972 ± 0.001	6337	0.065 ± 0.001	0.462 ± 0.004
Basic RECO level selections						
$p_{T_1} > 17 \text{ GeV}, \eta < 0.9$	30993	0.317 ± 0.001	0.317 ± 0.001	30704	0.313 ± 0.001	0.313 ± 0.001
$p_{T_2} > 8 \text{ GeV}, \eta < 2.4$	29823	0.305 ± 0.001	0.962 ± 0.001	28903	0.295 ± 0.001	0.941 ± 0.001
$p_{T_3} > 8 \text{ GeV}, \eta < 2.4$	19896	0.203 ± 0.001	0.667 ± 0.003	18812	0.192 ± 0.001	0.651 ± 0.003
$p_{T_4} > 8 \text{ GeV}, \eta < 2.4$	12242	0.125 ± 0.001	0.615 ± 0.003	10391	0.106 ± 0.001	0.552 ± 0.004
Extra RECO level selections						
Good primary vertex	12242	0.125 ± 0.001	1.000 ± 0.000	10391	0.106 ± 0.001	1.000 ± 0.000
Two muon-jets	11597	0.118 ± 0.001	0.947 ± 0.002	8634	0.088 ± 0.001	0.831 ± 0.004
Two dimuons	11592	0.118 ± 0.001	1.000 ± 0.000	8632	0.088 ± 0.001	1.000 ± 0.000
Pixel hit requirement	11310	0.116 ± 0.001	0.976 ± 0.001	5446	0.056 ± 0.001	0.631 ± 0.005
$ z_{\mu\mu_1} - z_{\mu\mu_2} < 0.1 \text{ cm}$	11269	0.115 ± 0.001	0.996 ± 0.001	5315	0.054 ± 0.001	0.976 ± 0.002
$m_{\mu\mu_1} \approx m_{\mu\mu_2}$	11252	0.115 ± 0.001	0.998 ± 0.000	5306	0.054 ± 0.001	0.998 ± 0.001
Dimuon isolation < 2 GeV	8919	0.091 ± 0.001	0.793 ± 0.004	4216	0.043 ± 0.001	0.795 ± 0.006
Trigger	8357	0.085 ± 0.001	0.937 ± 0.003	3901	0.040 ± 0.001	0.925 ± 0.004
α_{GEN}						
ϵ_{SM}						
$\epsilon_{\text{SM}} / \alpha_{\text{GEN}}$						
		0.627 ± 0.004				0.616 ± 0.006

Table 19: Acceptances and efficiencies of the event selection requirements for several representative dark SUSY benchmark models in MC simulation.

Sample	$m_{\gamma_D} = 0.25 \text{ GeV}, c\tau_{\gamma_D} = 1 \text{ mm}$			$m_{\gamma_D} = 0.25 \text{ GeV}, c\tau_{\gamma_D} = 2 \text{ mm}$		
Selection	Events	Tot. Eff. [%]	Rel. Eff. [%]	Events	Tot. Eff. [%]	Rel. Eff. [%]
All events	52100	1.000 ± 0.000	1.000 ± 0.000	294400	1.000 ± 0.000	1.000 ± 0.000
Basic GEN level selections						
$p_{T_1} > 17 \text{ GeV}, \eta < 0.9$	16812	0.323 ± 0.002	0.323 ± 0.002	94481	0.321 ± 0.001	0.321 ± 0.001
$p_{T_2} > 8 \text{ GeV}, \eta < 2.4$	16475	0.316 ± 0.002	0.980 ± 0.001	92452	0.314 ± 0.001	0.979 ± 0.000
$p_{T_3} > 8 \text{ GeV}, \eta < 2.4$	11017	0.211 ± 0.002	0.669 ± 0.004	61569	0.209 ± 0.001	0.666 ± 0.002
$p_{T_4} > 8 \text{ GeV}, \eta < 2.4$	7368	0.141 ± 0.002	0.669 ± 0.004	41465	0.141 ± 0.001	0.673 ± 0.002
$L_{xy} < 9.8 \text{ cm and } L_z < 46.5 \text{ cm}$	1484	0.028 ± 0.001	0.201 ± 0.005	2836	0.010 ± 0.000	0.068 ± 0.001
Basic RECO level selections						
$p_{T_1} > 17 \text{ GeV}, \eta < 0.9$	15509	0.298 ± 0.002	0.298 ± 0.002	73712	0.250 ± 0.001	0.250 ± 0.001
$p_{T_2} > 8 \text{ GeV}, \eta < 2.4$	14177	0.272 ± 0.002	0.914 ± 0.002	64032	0.218 ± 0.001	0.869 ± 0.001
$p_{T_3} > 8 \text{ GeV}, \eta < 2.4$	8875	0.170 ± 0.002	0.626 ± 0.004	35234	0.120 ± 0.001	0.550 ± 0.002
$p_{T_4} > 8 \text{ GeV}, \eta < 2.4$	4315	0.083 ± 0.001	0.486 ± 0.005	14786	0.050 ± 0.000	0.420 ± 0.003
Extra RECO level selections						
Good primary vertex	4315	0.083 ± 0.001	1.000 ± 0.000	14786	0.050 ± 0.000	1.000 ± 0.000
Two muon-jets	3216	0.062 ± 0.001	0.745 ± 0.007	9838	0.033 ± 0.000	0.665 ± 0.004
Two dimuons	3214	0.062 ± 0.001	0.999 ± 0.000	9834	0.033 ± 0.000	1.000 ± 0.000
Pixel hit requirement	1315	0.025 ± 0.001	0.409 ± 0.009	2771	0.009 ± 0.000	0.282 ± 0.005
$ z_{\mu\mu_1} - z_{\mu\mu_2} < 0.1 \text{ cm}$	1236	0.024 ± 0.001	0.940 ± 0.007	2540	0.009 ± 0.000	0.917 ± 0.005
$m_{\mu\mu_1} \approx m_{\mu\mu_2}$	1233	0.024 ± 0.001	0.998 ± 0.001	2537	0.009 ± 0.000	0.999 ± 0.001
Dimuon isolation < 2 GeV	992	0.019 ± 0.001	0.805 ± 0.011	2058	0.007 ± 0.000	0.811 ± 0.008
Trigger	894	0.017 ± 0.001	0.901 ± 0.009	1862	0.006 ± 0.000	0.905 ± 0.006
α_{GEN}			0.028 ± 0.001			0.010 ± 0.000
ϵ_{SIM}			0.017 ± 0.001			0.006 ± 0.000
$\epsilon_{\text{SIM}}/\alpha_{\text{GEN}}$			0.602 ± 0.013			0.657 ± 0.009

Table 20: Acceptances and efficiencies of the event selection requirements for several representative dark SUSY benchmark models in MC simulation.

Sample	$m_{\gamma_D} = 0.25 \text{ GeV}, c\tau_{\gamma_D} = 5 \text{ mm}$			$m_{\gamma_D} = 0.25 \text{ GeV}, c\tau_{\gamma_D} = 20 \text{ mm}$		
Selection	Events	Tot. Eff. [%]	Rel. Eff. [%]	Events	Tot. Eff. [%]	Rel. Eff. [%]
All events	295800	1.000 ± 0.000	1.000 ± 0.000	1155200	1.000 ± 0.000	1.000 ± 0.000
Basic GEN level selections						
$p_{T_1} > 17 \text{ GeV}, \eta < 0.9$	94753	0.320 ± 0.001	0.320 ± 0.001	370951	0.321 ± 0.000	0.321 ± 0.000
$p_{T_2} > 8 \text{ GeV}, \eta < 2.4$	92786	0.314 ± 0.001	0.979 ± 0.000	362825	0.314 ± 0.000	0.978 ± 0.000
$p_{T_3} > 8 \text{ GeV}, \eta < 2.4$	61945	0.209 ± 0.001	0.668 ± 0.002	242335	0.210 ± 0.000	0.668 ± 0.001
$p_{T_4} > 8 \text{ GeV}, \eta < 2.4$	41630	0.141 ± 0.001	0.672 ± 0.002	162845	0.141 ± 0.000	0.672 ± 0.001
$L_{xy} < 9.8 \text{ cm and } L_z < 46.5 \text{ cm}$	584	0.002 ± 0.000	0.014 ± 0.001	154	0.000 ± 0.000	0.001 ± 0.000
Basic RECO level selections						
$p_{T_1} > 17 \text{ GeV}, \eta < 0.9$	48479	0.164 ± 0.001	0.164 ± 0.001	74241	0.064 ± 0.000	0.064 ± 0.000
$p_{T_2} > 8 \text{ GeV}, \eta < 2.4$	37872	0.128 ± 0.001	0.781 ± 0.002	45285	0.039 ± 0.000	0.610 ± 0.002
$p_{T_3} > 8 \text{ GeV}, \eta < 2.4$	14991	0.051 ± 0.000	0.396 ± 0.003	8491	0.007 ± 0.000	0.188 ± 0.002
$p_{T_4} > 8 \text{ GeV}, \eta < 2.4$	4947	0.017 ± 0.000	0.330 ± 0.004	2008	0.002 ± 0.000	0.236 ± 0.005
Extra RECO level selections						
Good primary vertex	4947	0.017 ± 0.000	1.000 ± 0.000	2008	0.002 ± 0.000	1.000 ± 0.000
Two muon-jets	2928	0.010 ± 0.000	0.592 ± 0.007	1077	0.001 ± 0.000	0.536 ± 0.011
Two dimuons	2925	0.010 ± 0.000	0.999 ± 0.001	1077	0.001 ± 0.000	1.000 ± 0.000
Pixel hit requirement	553	0.002 ± 0.000	0.189 ± 0.007	163	0.000 ± 0.000	0.151 ± 0.011
$ z_{\mu\mu_1} - z_{\mu\mu_2} < 0.1 \text{ cm}$	496	0.002 ± 0.000	0.897 ± 0.013	136	0.000 ± 0.000	0.834 ± 0.029
$m_{\mu\mu_1} \approx m_{\mu\mu_2}$	495	0.002 ± 0.000	0.998 ± 0.002	136	0.000 ± 0.000	1.000 ± 0.000
Dimuon isolation < 2 GeV	380	0.001 ± 0.000	0.768 ± 0.019	100	0.000 ± 0.000	0.735 ± 0.038
Trigger	341	0.001 ± 0.000	0.897 ± 0.016	90	0.000 ± 0.000	0.900 ± 0.030
α_{GEN}			0.002 ± 0.000			0.000 ± 0.000
ϵ_{SM}			0.001 ± 0.000			0.000 ± 0.000
$\epsilon_{\text{SM}} / \alpha_{\text{GEN}}$			0.584 ± 0.020			0.584 ± 0.040

Table 21: Acceptances and efficiencies of the event selection requirements for several representative dark SUSY benchmark models in MC simulation.

Sample	$m_{\gamma_D} = 0.25 \text{ GeV}, c\tau_{\gamma_D} = 100 \text{ mm}$			$m_{\gamma_D} = 0.4 \text{ GeV}, c\tau_{\gamma_D} = 0 \text{ mm}$		
Selection	Events	Tot. Eff. [%]	Rel. Eff. [%]	Events	Tot. Eff. [%]	Rel. Eff. [%]
All events	1048700	1.000 ± 0.000	1.000 ± 0.000	97900	1.000 ± 0.000	1.000 ± 0.000
Basic GEN level selections						
$p_{T_1} > 17 \text{ GeV}, \eta < 0.9$	336474	0.321 ± 0.000	0.321 ± 0.000	32982	0.337 ± 0.002	0.337 ± 0.002
$p_{T_2} > 8 \text{ GeV}, \eta < 2.4$	329123	0.314 ± 0.000	0.978 ± 0.000	30417	0.311 ± 0.001	0.922 ± 0.001
$p_{T_3} > 8 \text{ GeV}, \eta < 2.4$	219579	0.209 ± 0.000	0.667 ± 0.001	20088	0.205 ± 0.001	0.660 ± 0.003
$p_{T_4} > 8 \text{ GeV}, \eta < 2.4$	147387	0.141 ± 0.000	0.671 ± 0.001	9614	0.098 ± 0.001	0.479 ± 0.004
$L_{xy} < 9.8 \text{ cm and } L_z < 46.5 \text{ cm}$	4	0.000 ± 0.000	0.000 ± 0.000	9614	0.098 ± 0.001	1.000 ± 0.000
Basic RECO level selections						
$p_{T_1} > 17 \text{ GeV}, \eta < 0.9$	19227	0.018 ± 0.000	0.018 ± 0.000	32917	0.336 ± 0.002	0.336 ± 0.002
$p_{T_2} > 8 \text{ GeV}, \eta < 2.4$	8435	0.008 ± 0.000	0.439 ± 0.004	30181	0.308 ± 0.001	0.917 ± 0.002
$p_{T_3} > 8 \text{ GeV}, \eta < 2.4$	581	0.001 ± 0.000	0.069 ± 0.003	19875	0.203 ± 0.001	0.659 ± 0.003
$p_{T_4} > 8 \text{ GeV}, \eta < 2.4$	100	0.000 ± 0.000	0.172 ± 0.016	9340	0.095 ± 0.001	0.470 ± 0.004
Extra RECO level selections						
Good primary vertex	100	0.000 ± 0.000	1.000 ± 0.000	9340	0.095 ± 0.001	1.000 ± 0.000
Two muon-jets	44	0.000 ± 0.000	0.440 ± 0.050	8357	0.085 ± 0.001	0.895 ± 0.003
Two dimuons	44	0.000 ± 0.000	1.000 ± 0.000	8353	0.085 ± 0.001	1.000 ± 0.000
Pixel hit requirement	6	0.000 ± 0.000	0.136 ± 0.052	8345	0.085 ± 0.001	0.999 ± 0.000
$ z_{\mu\mu_1} - z_{\mu\mu_2} < 0.1 \text{ cm}$	4	0.000 ± 0.000	0.667 ± 0.192	8324	0.085 ± 0.001	0.997 ± 0.001
$m_{\mu\mu_1} \approx m_{\mu\mu_2}$	3	0.000 ± 0.000	0.750 ± 0.217	8304	0.085 ± 0.001	0.998 ± 0.001
Dimuon isolation < 2 GeV	2	0.000 ± 0.000	0.667 ± 0.272	6562	0.067 ± 0.001	0.790 ± 0.004
Trigger	1	0.000 ± 0.000	0.500 ± 0.354	6320	0.065 ± 0.001	0.963 ± 0.002
α_{GEN}			0.000 ± 0.000			0.098 ± 0.001
ϵ_{SIM}			0.000 ± 0.000			0.065 ± 0.001
$\epsilon_{\text{SIM}}/\alpha_{\text{GEN}}$			0.250 ± 0.217			0.657 ± 0.005

Table 22: Acceptances and efficiencies of the event selection requirements for several representative dark SUSY benchmark models in MC simulation.

Sample	$m_{\tau_D} = 0.4 \text{ GeV}, c\tau_{\tau_D} = 0.5 \text{ mm}$			$m_{\tau_D} = 0.4 \text{ GeV}, c\tau_{\tau_D} = 1 \text{ mm}$		
Selection	Events	Tot. Eff. [%]	Rel. Eff. [%]	Events	Tot. Eff. [%]	Rel. Eff. [%]
All events	98800	1.000 ± 0.000	1.000 ± 0.000	281600	1.000 ± 0.000	1.000 ± 0.000
Basic GEN level selections						
$p_{T_1} > 17 \text{ GeV}, \eta < 0.9$	33187	0.336 ± 0.002	0.336 ± 0.002	95487	0.339 ± 0.001	0.339 ± 0.001
$p_{T_2} > 8 \text{ GeV}, \eta < 2.4$	30495	0.309 ± 0.001	0.919 ± 0.001	87803	0.312 ± 0.001	0.920 ± 0.001
$p_{T_3} > 8 \text{ GeV}, \eta < 2.4$	20221	0.205 ± 0.001	0.663 ± 0.003	58189	0.207 ± 0.001	0.663 ± 0.002
$p_{T_4} > 8 \text{ GeV}, \eta < 2.4$	9572	0.097 ± 0.001	0.473 ± 0.004	27587	0.098 ± 0.001	0.474 ± 0.002
$L_{xy} < 9.8 \text{ cm and } L_z < 46.5 \text{ cm}$	6381	0.065 ± 0.001	0.667 ± 0.005	9740	0.035 ± 0.000	0.353 ± 0.003
Basic RECO level selections						
$p_{T_1} > 17 \text{ GeV}, \eta < 0.9$	32774	0.332 ± 0.001	0.332 ± 0.001	91886	0.326 ± 0.001	0.326 ± 0.001
$p_{T_2} > 8 \text{ GeV}, \eta < 2.4$	29357	0.297 ± 0.001	0.896 ± 0.002	80530	0.286 ± 0.001	0.876 ± 0.001
$p_{T_3} > 8 \text{ GeV}, \eta < 2.4$	18903	0.191 ± 0.001	0.644 ± 0.003	49793	0.177 ± 0.001	0.618 ± 0.002
$p_{T_4} > 8 \text{ GeV}, \eta < 2.4$	7916	0.080 ± 0.001	0.419 ± 0.004	18975	0.067 ± 0.000	0.381 ± 0.002
Extra RECO level selections						
Good primary vertex	7916	0.080 ± 0.001	1.000 ± 0.000	18975	0.067 ± 0.000	1.000 ± 0.000
Two muon-jets	6667	0.067 ± 0.001	0.842 ± 0.004	15162	0.054 ± 0.000	0.799 ± 0.003
Two dimuons	6663	0.067 ± 0.001	0.999 ± 0.000	15155	0.054 ± 0.000	1.000 ± 0.000
Pixel hit requirement	5186	0.052 ± 0.001	0.778 ± 0.005	7990	0.028 ± 0.000	0.527 ± 0.004
$ z_{\mu\mu_1} - z_{\mu\mu_2} < 0.1 \text{ cm}$	5119	0.052 ± 0.001	0.987 ± 0.002	7707	0.027 ± 0.000	0.965 ± 0.002
$m_{\mu\mu_1} \approx m_{\mu\mu_2}$	5110	0.052 ± 0.001	0.998 ± 0.001	7692	0.027 ± 0.000	0.998 ± 0.001
Dimuon isolation < 2 GeV	4038	0.041 ± 0.001	0.790 ± 0.006	6122	0.022 ± 0.000	0.796 ± 0.005
Trigger	3813	0.039 ± 0.001	0.944 ± 0.004	5718	0.020 ± 0.000	0.934 ± 0.003
α_{GEN}						
ϵ_{SM}						
$\epsilon_{\text{SM}} / \alpha_{\text{GEN}}$						
		0.598 ± 0.006				0.587 ± 0.005

Table 23: Acceptances and efficiencies of the event selection requirements for several representative dark SUSY benchmark models in MC simulation.

Sample	$m_{\gamma_D} = 0.4 \text{ GeV}, c\tau_{\gamma_D} = 2 \text{ mm}$			$m_{\gamma_D} = 0.4 \text{ GeV}, c\tau_{\gamma_D} = 5 \text{ mm}$		
Selection	Events	Tot. Eff. [%]	Rel. Eff. [%]	Events	Tot. Eff. [%]	Rel. Eff. [%]
All events	296400	1.000 ± 0.000	1.000 ± 0.000	146200	1.000 ± 0.000	1.000 ± 0.000
Basic GEN level selections						
$p_{T_1} > 17 \text{ GeV}, \eta < 0.9$	100134	0.338 ± 0.001	0.338 ± 0.001	49255	0.337 ± 0.001	0.337 ± 0.001
$p_{T_2} > 8 \text{ GeV}, \eta < 2.4$	92034	0.311 ± 0.001	0.919 ± 0.001	45395	0.310 ± 0.001	0.922 ± 0.001
$p_{T_3} > 8 \text{ GeV}, \eta < 2.4$	60730	0.205 ± 0.001	0.660 ± 0.002	30007	0.205 ± 0.001	0.661 ± 0.002
$p_{T_4} > 8 \text{ GeV}, \eta < 2.4$	28891	0.097 ± 0.001	0.476 ± 0.002	14310	0.098 ± 0.001	0.477 ± 0.003
$L_{xy} < 9.8 \text{ cm and } L_z < 46.5 \text{ cm}$	3802	0.013 ± 0.000	0.132 ± 0.002	457	0.003 ± 0.000	0.032 ± 0.001
Basic RECO level selections						
$p_{T_1} > 17 \text{ GeV}, \eta < 0.9$	88761	0.299 ± 0.001	0.299 ± 0.001	32936	0.225 ± 0.001	0.225 ± 0.001
$p_{T_2} > 8 \text{ GeV}, \eta < 2.4$	74427	0.251 ± 0.001	0.839 ± 0.001	24595	0.168 ± 0.001	0.747 ± 0.002
$p_{T_3} > 8 \text{ GeV}, \eta < 2.4$	42098	0.142 ± 0.001	0.566 ± 0.002	11071	0.076 ± 0.001	0.450 ± 0.003
$p_{T_4} > 8 \text{ GeV}, \eta < 2.4$	13968	0.047 ± 0.000	0.332 ± 0.002	2902	0.020 ± 0.000	0.262 ± 0.004
Extra RECO level selections						
Good primary vertex	13968	0.047 ± 0.000	1.000 ± 0.000	2902	0.020 ± 0.000	1.000 ± 0.000
Two muon-jets	10240	0.035 ± 0.000	0.733 ± 0.004	1948	0.013 ± 0.000	0.671 ± 0.009
Two dimuons	10237	0.035 ± 0.000	1.000 ± 0.000	1947	0.013 ± 0.000	0.999 ± 0.001
Pixel hit requirement	3294	0.011 ± 0.000	0.322 ± 0.005	433	0.003 ± 0.000	0.222 ± 0.009
$ z_{\mu\mu_1} - z_{\mu\mu_2} < 0.1 \text{ cm}$	3083	0.010 ± 0.000	0.936 ± 0.004	390	0.003 ± 0.000	0.901 ± 0.014
$m_{\mu\mu_1} \approx m_{\mu\mu_2}$	3075	0.010 ± 0.000	0.997 ± 0.001	386	0.003 ± 0.000	0.990 ± 0.005
Dimuon isolation < 2 GeV	2421	0.008 ± 0.000	0.787 ± 0.007	300	0.002 ± 0.000	0.777 ± 0.021
Trigger	2245	0.008 ± 0.000	0.927 ± 0.005	285	0.002 ± 0.000	0.950 ± 0.013
α_{GEN}			0.013 ± 0.000		0.003 ± 0.000	
ϵ_{SIM}			0.008 ± 0.000		0.002 ± 0.000	
$\epsilon_{\text{SIM}}/\alpha_{\text{GEN}}$			0.590 ± 0.008		0.624 ± 0.023	

Table 24: Acceptances and efficiencies of the event selection requirements for several representative dark SUSY benchmark models in MC simulation.

Sample	$m_{\gamma_D} = 0.4 \text{ GeV}, c\tau_{\gamma_D} = 20 \text{ mm}$			$m_{\gamma_D} = 0.4 \text{ GeV}, c\tau_{\gamma_D} = 100 \text{ mm}$		
Selection	Events	Tot. Eff. [%]	Rel. Eff. [%]	Events	Tot. Eff. [%]	Rel. Eff. [%]
All events	581200	1.000 ± 0.000	1.000 ± 0.000	623400	1.000 ± 0.000	1.000 ± 0.000
Basic GEN level selections						
$p_{T_1} > 17 \text{ GeV}, \eta < 0.9$	196990	0.339 ± 0.001	0.339 ± 0.001	210808	0.338 ± 0.001	0.338 ± 0.001
$p_{T_2} > 8 \text{ GeV}, \eta < 2.4$	181018	0.311 ± 0.001	0.919 ± 0.001	193725	0.311 ± 0.001	0.919 ± 0.001
$p_{T_3} > 8 \text{ GeV}, \eta < 2.4$	119508	0.206 ± 0.001	0.660 ± 0.001	127543	0.205 ± 0.001	0.658 ± 0.001
$p_{T_4} > 8 \text{ GeV}, \eta < 2.4$	57076	0.098 ± 0.000	0.478 ± 0.001	60868	0.098 ± 0.000	0.477 ± 0.001
$L_{xy} < 9.8 \text{ cm and } L_z < 46.5 \text{ cm}$	133	0.000 ± 0.000	0.002 ± 0.000	4	0.000 ± 0.000	0.000 ± 0.000
Basic RECO level selections						
$p_{T_1} > 17 \text{ GeV}, \eta < 0.9$	56741	0.098 ± 0.000	0.098 ± 0.000	17655	0.028 ± 0.000	0.028 ± 0.000
$p_{T_2} > 8 \text{ GeV}, \eta < 2.4$	31552	0.054 ± 0.000	0.556 ± 0.002	6751	0.011 ± 0.000	0.382 ± 0.004
$p_{T_3} > 8 \text{ GeV}, \eta < 2.4$	7563	0.013 ± 0.000	0.240 ± 0.002	629	0.001 ± 0.000	0.093 ± 0.004
$p_{T_4} > 8 \text{ GeV}, \eta < 2.4$	1539	0.003 ± 0.000	0.203 ± 0.005	78	0.000 ± 0.000	0.124 ± 0.013
Extra RECO level selections						
Good primary vertex	1539	0.003 ± 0.000	1.000 ± 0.000	78	0.000 ± 0.000	1.000 ± 0.000
Two muon-jets	886	0.002 ± 0.000	0.576 ± 0.013	34	0.000 ± 0.000	0.436 ± 0.056
Two dimuons	886	0.002 ± 0.000	1.000 ± 0.000	34	0.000 ± 0.000	1.000 ± 0.000
Pixel hit requirement	123	0.000 ± 0.000	0.139 ± 0.012	1	0.000 ± 0.000	0.029 ± 0.029
$ z_{\mu\mu_1} - z_{\mu\mu_2} < 0.1 \text{ cm}$	104	0.000 ± 0.000	0.846 ± 0.033	1	0.000 ± 0.000	1.000 ± 0.000
$m_{\mu\mu_1} \approx m_{\mu\mu_2}$	103	0.000 ± 0.000	0.990 ± 0.010	1	0.000 ± 0.000	1.000 ± 0.000
Dimuon isolation < 2 GeV	83	0.000 ± 0.000	0.806 ± 0.039	1	0.000 ± 0.000	1.000 ± 0.000
Trigger	78	0.000 ± 0.000	0.940 ± 0.026	1	0.000 ± 0.000	1.000 ± 0.000
α_{GEN}			0.000 ± 0.000			0.000 ± 0.000
ϵ_{SIM}			0.000 ± 0.000			0.000 ± 0.000
$\epsilon_{\text{SIM}}/\alpha_{\text{GEN}}$			0.586 ± 0.043			0.250 ± 0.217

Table 25: Acceptances and efficiencies of the event selection requirements for several representative dark SUSY benchmark models in MC simulation.

Sample	$m_{\gamma_D} = 0.7 \text{ GeV}, c\tau_{\gamma_D} = 0 \text{ mm}$			$m_{\gamma_D} = 0.7 \text{ GeV}, c\tau_{\gamma_D} = 0.5 \text{ mm}$		
Selection	Events	Tot. Eff. [%]	Rel. Eff. [%]	Events	Tot. Eff. [%]	Rel. Eff. [%]
All events	76800	1.000 ± 0.000	1.000 ± 0.000	19400	1.000 ± 0.000	1.000 ± 0.000
Basic GEN level selections						
$p_{T_1} > 17 \text{ GeV}, \eta < 0.9$	26147	0.340 ± 0.002	0.340 ± 0.002	6648	0.343 ± 0.003	0.343 ± 0.003
$p_{T_2} > 8 \text{ GeV}, \eta < 2.4$	23820	0.310 ± 0.002	0.911 ± 0.002	6064	0.313 ± 0.003	0.912 ± 0.003
$p_{T_3} > 8 \text{ GeV}, \eta < 2.4$	15760	0.205 ± 0.001	0.662 ± 0.003	4009	0.207 ± 0.003	0.661 ± 0.006
$p_{T_4} > 8 \text{ GeV}, \eta < 2.4$	7131	0.093 ± 0.001	0.452 ± 0.004	1804	0.093 ± 0.002	0.450 ± 0.008
$L_{xy} < 9.8 \text{ cm and } L_z < 46.5 \text{ cm}$	7131	0.093 ± 0.001	1.000 ± 0.000	1582	0.082 ± 0.002	0.877 ± 0.008
Basic RECO level selections						
$p_{T_1} > 17 \text{ GeV}, \eta < 0.9$	26118	0.340 ± 0.002	0.340 ± 0.002	6610	0.341 ± 0.003	0.341 ± 0.003
$p_{T_2} > 8 \text{ GeV}, \eta < 2.4$	23703	0.309 ± 0.002	0.908 ± 0.002	5943	0.306 ± 0.003	0.899 ± 0.004
$p_{T_3} > 8 \text{ GeV}, \eta < 2.4$	15610	0.203 ± 0.001	0.659 ± 0.003	3866	0.199 ± 0.003	0.651 ± 0.006
$p_{T_4} > 8 \text{ GeV}, \eta < 2.4$	6926	0.090 ± 0.001	0.444 ± 0.004	1639	0.084 ± 0.002	0.424 ± 0.008
Extra RECO level selections						
Good primary vertex	6926	0.090 ± 0.001	1.000 ± 0.000	1639	0.084 ± 0.002	1.000 ± 0.000
Two muon-jets	6096	0.079 ± 0.001	0.880 ± 0.004	1439	0.074 ± 0.002	0.878 ± 0.008
Two dimuons	6094	0.079 ± 0.001	1.000 ± 0.000	1437	0.074 ± 0.002	0.999 ± 0.001
Pixel hit requirement	6090	0.079 ± 0.001	0.999 ± 0.000	1313	0.068 ± 0.002	0.914 ± 0.007
$ z_{\mu\mu_1} - z_{\mu\mu_2} < 0.1 \text{ cm}$	6079	0.079 ± 0.001	0.998 ± 0.001	1306	0.067 ± 0.002	0.995 ± 0.002
$m_{\mu\mu_1} \approx m_{\mu\mu_2}$	6044	0.079 ± 0.001	0.994 ± 0.001	1288	0.066 ± 0.002	0.986 ± 0.003
Dimuon isolation < 2 GeV	4822	0.063 ± 0.001	0.798 ± 0.005	1006	0.052 ± 0.002	0.781 ± 0.012
Trigger	4643	0.060 ± 0.001	0.963 ± 0.003	959	0.049 ± 0.002	0.953 ± 0.007
α_{GEN}			0.093 ± 0.001			0.082 ± 0.002
ϵ_{SIM}			0.060 ± 0.001			0.049 ± 0.002
$\epsilon_{\text{SIM}}/\alpha_{\text{GEN}}$			0.651 ± 0.006			0.606 ± 0.012

Table 26: Acceptances and efficiencies of the event selection requirements for several representative dark SUSY benchmark models in MC simulation.

Sample	$m_{\tau_D} = 0.7 \text{ GeV}, c\tau_{\tau_D} = 1 \text{ mm}$			$m_{\tau_D} = 0.7 \text{ GeV}, c\tau_{\tau_D} = 20 \text{ mm}$		
	Events	Tot. Eff. [%]	Rel. Eff. [%]	Events	Tot. Eff. [%]	Rel. Eff. [%]
Selection	144000	1.000 ± 0.000	1.000 ± 0.000	677400	1.000 ± 0.000	1.000 ± 0.000
All events						
Basic GEN level selections						
$p_{T_1} > 17 \text{ GeV}, \eta < 0.9$	48722	0.338 ± 0.001	0.338 ± 0.001	231533	0.342 ± 0.001	0.342 ± 0.001
$p_{T_2} > 8 \text{ GeV}, \eta < 2.4$	44342	0.308 ± 0.001	0.910 ± 0.001	210649	0.311 ± 0.001	0.910 ± 0.001
$p_{T_3} > 8 \text{ GeV}, \eta < 2.4$	29159	0.202 ± 0.001	0.658 ± 0.002	138098	0.204 ± 0.000	0.656 ± 0.001
$p_{T_4} > 8 \text{ GeV}, \eta < 2.4$	13175	0.091 ± 0.001	0.452 ± 0.003	62408	0.092 ± 0.000	0.452 ± 0.001
$L_{xy} < 9.8 \text{ cm and } L_z < 46.5 \text{ cm}$	7989	0.055 ± 0.001	0.606 ± 0.004	370	0.001 ± 0.000	0.006 ± 0.000
Basic RECO level selections						
$p_{T_1} > 17 \text{ GeV}, \eta < 0.9$	48011	0.333 ± 0.001	0.333 ± 0.001	99462	0.147 ± 0.000	0.147 ± 0.000
$p_{T_2} > 8 \text{ GeV}, \eta < 2.4$	42470	0.295 ± 0.001	0.885 ± 0.001	62735	0.093 ± 0.000	0.631 ± 0.002
$p_{T_3} > 8 \text{ GeV}, \eta < 2.4$	26876	0.187 ± 0.001	0.633 ± 0.002	20080	0.030 ± 0.000	0.320 ± 0.002
$p_{T_4} > 8 \text{ GeV}, \eta < 2.4$	10632	0.074 ± 0.001	0.396 ± 0.003	4350	0.006 ± 0.000	0.217 ± 0.003
Extra RECO level selections						
Good primary vertex	10632	0.074 ± 0.001	1.000 ± 0.000	4350	0.006 ± 0.000	1.000 ± 0.000
Two muon-jets	8913	0.062 ± 0.001	0.838 ± 0.004	2759	0.004 ± 0.000	0.634 ± 0.007
Two dimuons	8906	0.062 ± 0.001	0.999 ± 0.000	2757	0.004 ± 0.000	0.999 ± 0.001
Pixel hit requirement	6485	0.045 ± 0.001	0.728 ± 0.005	387	0.001 ± 0.000	0.140 ± 0.007
$ z_{\mu\mu_1} - z_{\mu\mu_2} < 0.1 \text{ cm}$	6411	0.045 ± 0.001	0.989 ± 0.001	319	0.000 ± 0.000	0.824 ± 0.019
$m_{\mu\mu_1} \approx m_{\mu\mu_2}$	6367	0.044 ± 0.001	0.993 ± 0.001	317	0.000 ± 0.000	0.994 ± 0.004
Dimuon isolation < 2 GeV	5037	0.035 ± 0.000	0.791 ± 0.005	253	0.000 ± 0.000	0.798 ± 0.023
Trigger	4729	0.033 ± 0.000	0.939 ± 0.003	234	0.000 ± 0.000	0.925 ± 0.017
α_{GEN}						0.001 ± 0.000
ϵ_{SM}						0.000 ± 0.000
$\epsilon_{\text{SM}} / \alpha_{\text{GEN}}$						0.592 ± 0.005
						0.632 ± 0.025

Table 27: Acceptances and efficiencies of the event selection requirements for several representative dark SUSY benchmark models in MC simulation.

Sample	$m_{\gamma_D} = 0.7 \text{ GeV}, c\tau_{\gamma_D} = 100 \text{ mm}$			$m_{\gamma_D} = 1 \text{ GeV}, c\tau_{\gamma_D} = 0 \text{ mm}$		
Selection	Events	Tot. Eff. [%]	Rel. Eff. [%]	Events	Tot. Eff. [%]	Rel. Eff. [%]
All events	231100	1.000 ± 0.000	1.000 ± 0.000	77999	1.000 ± 0.000	1.000 ± 0.000
Basic GEN level selections						
$p_{T_1} > 17 \text{ GeV}, \eta < 0.9$	78603	0.340 ± 0.001	0.340 ± 0.001	26774	0.343 ± 0.002	0.343 ± 0.002
$p_{T_2} > 8 \text{ GeV}, \eta < 2.4$	71546	0.310 ± 0.001	0.910 ± 0.001	24398	0.313 ± 0.002	0.911 ± 0.002
$p_{T_3} > 8 \text{ GeV}, \eta < 2.4$	46981	0.203 ± 0.001	0.657 ± 0.002	16187	0.208 ± 0.001	0.663 ± 0.003
$p_{T_4} > 8 \text{ GeV}, \eta < 2.4$	21031	0.091 ± 0.001	0.448 ± 0.002	7110	0.091 ± 0.001	0.439 ± 0.004
$L_{xy} < 9.8 \text{ cm and } L_z < 46.5 \text{ cm}$	12	0.000 ± 0.000	0.001 ± 0.000	7110	0.091 ± 0.001	1.000 ± 0.000
Basic RECO level selections						
$p_{T_1} > 17 \text{ GeV}, \eta < 0.9$	10472	0.045 ± 0.000	0.045 ± 0.000	26716	0.343 ± 0.002	0.343 ± 0.002
$p_{T_2} > 8 \text{ GeV}, \eta < 2.4$	46116	0.020 ± 0.000	0.441 ± 0.005	24241	0.311 ± 0.002	0.907 ± 0.002
$p_{T_3} > 8 \text{ GeV}, \eta < 2.4$	593	0.003 ± 0.000	0.128 ± 0.005	15990	0.205 ± 0.001	0.660 ± 0.003
$p_{T_4} > 8 \text{ GeV}, \eta < 2.4$	96	0.000 ± 0.000	0.162 ± 0.015	6920	0.089 ± 0.001	0.433 ± 0.004
Extra RECO level selections						
Good primary vertex	96	0.000 ± 0.000	1.000 ± 0.000	6920	0.089 ± 0.001	1.000 ± 0.000
Two muon-jets	58	0.000 ± 0.000	0.604 ± 0.050	6076	0.078 ± 0.001	0.878 ± 0.004
Two dimuons	58	0.000 ± 0.000	1.000 ± 0.000	6071	0.078 ± 0.001	0.999 ± 0.000
Pixel hit requirement	6	0.000 ± 0.000	0.103 ± 0.040	6069	0.078 ± 0.001	1.000 ± 0.000
$ z_{\mu\mu_1} - z_{\mu\mu_2} < 0.1 \text{ cm}$	6	0.000 ± 0.000	1.000 ± 0.000	6062	0.078 ± 0.001	0.999 ± 0.000
$m_{\mu\mu_1} \approx m_{\mu\mu_2}$	6	0.000 ± 0.000	1.000 ± 0.000	5993	0.077 ± 0.001	0.989 ± 0.001
Dimuon isolation < 2 GeV	6	0.000 ± 0.000	1.000 ± 0.000	4726	0.061 ± 0.001	0.789 ± 0.005
Trigger	6	0.000 ± 0.000	1.000 ± 0.000	4582	0.059 ± 0.001	0.970 ± 0.003
α_{GEN}			0.000 ± 0.000			0.091 ± 0.001
ϵ_{SIM}			0.000 ± 0.000			0.059 ± 0.001
$\epsilon_{\text{SIM}}/\alpha_{\text{GEN}}$			0.500 ± 0.144			0.644 ± 0.006

Table 28: Acceptances and efficiencies of the event selection requirements for several representative dark SUSY benchmark models in MC simulation.

Sample	$m_{\tilde{\tau}_D} = 1 \text{ GeV}, c\tau_{\tilde{\tau}_D} = 5 \text{ mm}$			$m_{\tilde{\tau}_D} = 1 \text{ GeV}, c\tau_{\tilde{\tau}_D} = 20 \text{ mm}$		
	Events	Tot. Eff. [%]	Rel. Eff. [%]	Events	Tot. Eff. [%]	Rel. Eff. [%]
Selection	170200	1.000 ± 0.000	1.000 ± 0.000	303300	1.000 ± 0.000	1.000 ± 0.000
All events						
Basic GEN level selections						
$p_{T_1} > 17 \text{ GeV}, \eta < 0.9$	58196	0.342 ± 0.001	0.342 ± 0.001	104206	0.344 ± 0.001	0.344 ± 0.001
$p_{T_2} > 8 \text{ GeV}, \eta < 2.4$	52792	0.310 ± 0.001	0.907 ± 0.001	94863	0.313 ± 0.001	0.910 ± 0.001
$p_{T_3} > 8 \text{ GeV}, \eta < 2.4$	34733	0.204 ± 0.001	0.658 ± 0.002	62487	0.206 ± 0.001	0.659 ± 0.002
$p_{T_4} > 8 \text{ GeV}, \eta < 2.4$	15199	0.089 ± 0.001	0.438 ± 0.003	27422	0.090 ± 0.001	0.439 ± 0.002
$L_{xy} < 9.8 \text{ cm and } L_z < 46.5 \text{ cm}$	2125	0.012 ± 0.000	0.140 ± 0.003	360	0.001 ± 0.000	0.013 ± 0.001
Basic RECO level selections						
$p_{T_1} > 17 \text{ GeV}, \eta < 0.9$	52369	0.308 ± 0.001	0.308 ± 0.001	56101	0.185 ± 0.001	0.185 ± 0.001
$p_{T_2} > 8 \text{ GeV}, \eta < 2.4$	44019	0.259 ± 0.001	0.841 ± 0.002	39006	0.129 ± 0.001	0.695 ± 0.002
$p_{T_3} > 8 \text{ GeV}, \eta < 2.4$	25170	0.148 ± 0.001	0.572 ± 0.002	14941	0.049 ± 0.000	0.383 ± 0.002
$p_{T_4} > 8 \text{ GeV}, \eta < 2.4$	8306	0.049 ± 0.001	0.330 ± 0.003	3698	0.012 ± 0.000	0.248 ± 0.004
Extra RECO level selections						
Good primary vertex	8305	0.049 ± 0.001	1.000 ± 0.000	3698	0.012 ± 0.000	1.000 ± 0.000
Two muon-jets	6366	0.037 ± 0.000	0.767 ± 0.005	2485	0.008 ± 0.000	0.672 ± 0.008
Two dimuons	6359	0.037 ± 0.000	0.999 ± 0.000	2485	0.008 ± 0.000	1.000 ± 0.000
Pixel hit requirement	1962	0.012 ± 0.000	0.309 ± 0.006	385	0.001 ± 0.000	0.155 ± 0.007
$ z_{\mu\mu_1} - z_{\mu\mu_2} < 0.1 \text{ cm}$	1834	0.011 ± 0.000	0.935 ± 0.006	325	0.001 ± 0.000	0.844 ± 0.018
$m_{\mu\mu_1} \approx m_{\mu\mu_2}$	1814	0.011 ± 0.000	0.989 ± 0.002	321	0.001 ± 0.000	0.988 ± 0.006
Dimuon isolation $< 2 \text{ GeV}$	1445	0.008 ± 0.000	0.797 ± 0.009	252	0.001 ± 0.000	0.785 ± 0.023
Trigger	1333	0.008 ± 0.000	0.922 ± 0.007	237	0.001 ± 0.000	0.940 ± 0.015
α_{GEN}			0.012 ± 0.000			0.001 ± 0.000
ϵ_{SM}			0.008 ± 0.000			0.001 ± 0.000
$\epsilon_{\text{SM}} / \alpha_{\text{GEN}}$			0.627 ± 0.010			0.658 ± 0.025

Table 29: Acceptances and efficiencies of the event selection requirements for several representative dark SUSY benchmark models in MC simulation.

Sample	$m_{\gamma_D} = 1 \text{ GeV}, c\tau_{\gamma_D} = 100 \text{ mm}$			$m_{\gamma_D} = 5 \text{ GeV}, c\tau_{\gamma_D} = 0 \text{ mm}$		
Selection	Events	Tot. Eff. [%]	Rel. Eff. [%]	Events	Tot. Eff. [%]	Rel. Eff. [%]
All events	115400	1.000 ± 0.000	1.000 ± 0.000	79400	1.000 ± 0.000	1.000 ± 0.000
Basic GEN level selections						
$p_{T_1} > 17 \text{ GeV}, \eta < 0.9$	39995	0.347 ± 0.001	0.347 ± 0.001	35254	0.444 ± 0.002	0.444 ± 0.002
$p_{T_2} > 8 \text{ GeV}, \eta < 2.4$	36407	0.315 ± 0.001	0.910 ± 0.001	33472	0.422 ± 0.002	0.949 ± 0.001
$p_{T_3} > 8 \text{ GeV}, \eta < 2.4$	23838	0.207 ± 0.001	0.655 ± 0.002	24446	0.308 ± 0.002	0.730 ± 0.002
$p_{T_4} > 8 \text{ GeV}, \eta < 2.4$	10489	0.091 ± 0.001	0.440 ± 0.003	8302	0.105 ± 0.001	0.340 ± 0.003
$L_{xy} < 9.8 \text{ cm and } L_z < 46.5 \text{ cm}$	5	0.000 ± 0.000	0.000 ± 0.000	8302	0.105 ± 0.001	1.000 ± 0.000
Basic RECO level selections						
$p_{T_1} > 17 \text{ GeV}, \eta < 0.9$	7098	0.062 ± 0.001	0.062 ± 0.001	35188	0.443 ± 0.002	0.443 ± 0.002
$p_{T_2} > 8 \text{ GeV}, \eta < 2.4$	3515	0.030 ± 0.001	0.495 ± 0.006	33356	0.420 ± 0.002	0.948 ± 0.001
$p_{T_3} > 8 \text{ GeV}, \eta < 2.4$	584	0.005 ± 0.000	0.166 ± 0.006	24167	0.304 ± 0.002	0.725 ± 0.002
$p_{T_4} > 8 \text{ GeV}, \eta < 2.4$	82	0.001 ± 0.000	0.140 ± 0.014	8277	0.104 ± 0.001	0.342 ± 0.003
Extra RECO level selections						
Good primary vertex	82	0.001 ± 0.000	1.000 ± 0.000	8277	0.104 ± 0.001	1.000 ± 0.000
Two muon-jets	44	0.000 ± 0.000	0.537 ± 0.055	7238	0.091 ± 0.001	0.874 ± 0.004
Two dimuons	44	0.000 ± 0.000	1.000 ± 0.000	7232	0.091 ± 0.001	0.999 ± 0.000
Pixel hit requirement	4	0.000 ± 0.000	0.091 ± 0.043	7231	0.091 ± 0.001	1.000 ± 0.000
$ z_{\mu\mu_1} - z_{\mu\mu_2} < 0.1 \text{ cm}$	4	0.000 ± 0.000	1.000 ± 0.000	7228	0.091 ± 0.001	1.000 ± 0.000
$m_{\mu\mu_1} \approx m_{\mu\mu_2}$	4	0.000 ± 0.000	1.000 ± 0.000	6869	0.087 ± 0.001	0.950 ± 0.003
Dimuon isolation < 2 GeV	1	0.000 ± 0.000	0.250 ± 0.217	5466	0.069 ± 0.001	0.796 ± 0.005
Trigger	1	0.000 ± 0.000	1.000 ± 0.000	5220	0.066 ± 0.001	0.955 ± 0.003
α_{GEN}			0.000 ± 0.000			0.105 ± 0.001
ϵ_{SIM}			0.000 ± 0.000			0.066 ± 0.001
$\epsilon_{\text{SIM}}/\alpha_{\text{GEN}}$			0.200 ± 0.179			0.629 ± 0.005

Table 30: Acceptances and efficiencies of the event selection requirements for several representative dark SUSY benchmark models in MC simulation.

Sample	$m_{\tau_D} = 5 \text{ GeV}, c\tau_{\tau_D} = 20 \text{ mm}$			$m_{\tau_D} = 5 \text{ GeV}, c\tau_{\tau_D} = 100 \text{ mm}$		
	Events	Tot. Eff. [%]	Rel. Eff. [%]	Events	Tot. Eff. [%]	Rel. Eff. [%]
Selection	78300	1.000 ± 0.000	1.000 ± 0.000	227600	1.000 ± 0.000	1.000 ± 0.000
All events						
Basic GEN level selections						
$p_{T_1} > 17 \text{ GeV}, \eta < 0.9$	34982	0.447 ± 0.002	0.447 ± 0.002	101990	0.448 ± 0.001	0.448 ± 0.001
$p_{T_2} > 8 \text{ GeV}, \eta < 2.4$	33192	0.424 ± 0.002	0.949 ± 0.001	96799	0.425 ± 0.001	0.949 ± 0.001
$p_{T_3} > 8 \text{ GeV}, \eta < 2.4$	23953	0.306 ± 0.002	0.722 ± 0.002	70180	0.308 ± 0.001	0.725 ± 0.001
$p_{T_4} > 8 \text{ GeV}, \eta < 2.4$	7946	0.101 ± 0.001	0.332 ± 0.003	23802	0.105 ± 0.001	0.339 ± 0.002
$L_{xy} < 9.8 \text{ cm and } L_z < 46.5 \text{ cm}$	1456	0.019 ± 0.000	0.183 ± 0.004	256	0.001 ± 0.000	0.011 ± 0.001
Basic RECO level selections						
$p_{T_1} > 17 \text{ GeV}, \eta < 0.9$	32695	0.418 ± 0.002	0.418 ± 0.002	56073	0.246 ± 0.001	0.246 ± 0.001
$p_{T_2} > 8 \text{ GeV}, \eta < 2.4$	29501	0.377 ± 0.002	0.902 ± 0.002	36936	0.162 ± 0.001	0.659 ± 0.002
$p_{T_3} > 8 \text{ GeV}, \eta < 2.4$	18111	0.231 ± 0.002	0.614 ± 0.003	14410	0.063 ± 0.001	0.390 ± 0.003
$p_{T_4} > 8 \text{ GeV}, \eta < 2.4$	4850	0.062 ± 0.001	0.268 ± 0.003	2811	0.012 ± 0.000	0.195 ± 0.003
Extra RECO level selections						
Good primary vertex	4850	0.062 ± 0.001	1.000 ± 0.000	2811	0.012 ± 0.000	1.000 ± 0.000
Two muon-jets	3686	0.047 ± 0.001	0.760 ± 0.006	1882	0.008 ± 0.000	0.670 ± 0.009
Two dimuons	3682	0.047 ± 0.001	0.999 ± 0.001	1882	0.008 ± 0.000	1.000 ± 0.000
Pixel hit requirement	1335	0.017 ± 0.000	0.363 ± 0.008	289	0.001 ± 0.000	0.154 ± 0.008
$ z_{\mu\mu_1} - z_{\mu\mu_2} < 0.1 \text{ cm}$	1253	0.016 ± 0.000	0.939 ± 0.007	243	0.001 ± 0.000	0.841 ± 0.022
$m_{\mu\mu_1} \approx m_{\mu\mu_2}$	1208	0.015 ± 0.000	0.964 ± 0.005	235	0.001 ± 0.000	0.967 ± 0.011
Dimuon isolation < 2 GeV	945	0.012 ± 0.000	0.782 ± 0.012	186	0.001 ± 0.000	0.791 ± 0.027
Trigger	843	0.011 ± 0.000	0.892 ± 0.010	172	0.001 ± 0.000	0.925 ± 0.019
α_{GEN}						0.001 ± 0.000
ϵ_{SM}						0.001 ± 0.000
$\epsilon_{\text{SM}} / \alpha_{\text{GEN}}$						0.579 ± 0.013
						0.672 ± 0.029

Table 31: Acceptances and efficiencies of the event selection requirements for several representative dark SUSY benchmark models in MC simulation.

Sample	$m_{\gamma_D} = 8.5 \text{ GeV}, c\tau_{\gamma_D} = 0 \text{ mm}$			$m_{\gamma_D} = 8.5 \text{ GeV}, c\tau_{\gamma_D} = 2 \text{ mm}$		
Selection	Events	Tot. Eff. [%]	Rel. Eff. [%]	Events	Tot. Eff. [%]	Rel. Eff. [%]
All events	79099	1.000 ± 0.000	1.000 ± 0.000	276700	1.000 ± 0.000	1.000 ± 0.000
Basic GEN level selections						
$p_{T_1} > 17 \text{ GeV}, \eta < 0.9$	44037	0.557 ± 0.002	0.557 ± 0.002	153847	0.556 ± 0.001	0.556 ± 0.001
$p_{T_2} > 8 \text{ GeV}, \eta < 2.4$	42211	0.534 ± 0.002	0.959 ± 0.001	147153	0.532 ± 0.001	0.956 ± 0.001
$p_{T_3} > 8 \text{ GeV}, \eta < 2.4$	35071	0.443 ± 0.002	0.831 ± 0.002	122355	0.442 ± 0.001	0.831 ± 0.001
$p_{T_4} > 8 \text{ GeV}, \eta < 2.4$	16205	0.205 ± 0.001	0.462 ± 0.003	56138	0.203 ± 0.001	0.459 ± 0.001
$L_{xy} < 9.8 \text{ cm and } L_z < 46.5 \text{ cm}$	16205	0.205 ± 0.001	1.000 ± 0.000	55479	0.201 ± 0.001	0.988 ± 0.000
Basic RECO level selections						
$p_{T_1} > 17 \text{ GeV}, \eta < 0.9$	44017	0.556 ± 0.002	0.556 ± 0.002	153526	0.555 ± 0.001	0.555 ± 0.001
$p_{T_2} > 8 \text{ GeV}, \eta < 2.4$	42165	0.533 ± 0.002	0.958 ± 0.001	146660	0.530 ± 0.001	0.955 ± 0.001
$p_{T_3} > 8 \text{ GeV}, \eta < 2.4$	34945	0.442 ± 0.002	0.829 ± 0.002	120802	0.437 ± 0.001	0.824 ± 0.001
$p_{T_4} > 8 \text{ GeV}, \eta < 2.4$	16161	0.204 ± 0.001	0.462 ± 0.003	54939	0.199 ± 0.001	0.455 ± 0.001
Extra RECO level selections						
Good primary vertex	16161	0.204 ± 0.001	1.000 ± 0.000	54939	0.199 ± 0.001	1.000 ± 0.000
Two muon-jets	14115	0.178 ± 0.001	0.873 ± 0.003	47869	0.173 ± 0.001	0.871 ± 0.001
Two dimuons	14098	0.178 ± 0.001	0.999 ± 0.000	47831	0.173 ± 0.001	0.999 ± 0.000
Pixel hit requirement	14098	0.178 ± 0.001	1.000 ± 0.000	47461	0.172 ± 0.001	0.992 ± 0.000
$ z_{\mu\mu_1} - z_{\mu\mu_2} < 0.1 \text{ cm}$	14092	0.178 ± 0.001	1.000 ± 0.000	47127	0.170 ± 0.001	0.993 ± 0.000
$m_{\mu\mu_1} \approx m_{\mu\mu_2}$	13165	0.166 ± 0.001	0.934 ± 0.002	44240	0.160 ± 0.001	0.939 ± 0.001
Dimuon isolation < 2 GeV	10392	0.131 ± 0.001	0.789 ± 0.004	35048	0.127 ± 0.001	0.792 ± 0.002
Trigger	10105	0.128 ± 0.001	0.972 ± 0.002	33898	0.123 ± 0.001	0.967 ± 0.001
α_{GEN}			0.205 ± 0.001			0.201 ± 0.001
ϵ_{SIM}			0.128 ± 0.001			0.123 ± 0.001
$\epsilon_{\text{SIM}}/\alpha_{\text{GEN}}$			0.624 ± 0.004			0.611 ± 0.002

Table 32: Acceptances and efficiencies of the event selection requirements for several representative dark SUSY benchmark models in MC simulation.

Sample	$m_{\gamma_D} = 8.5 \text{ GeV}, c\tau_{\gamma_D} = 20 \text{ mm}$			$m_{\gamma_D} = 8.5 \text{ GeV}, c\tau_{\gamma_D} = 100 \text{ mm}$		
Selection	Events	Tot. Eff. [%]	Rel. Eff. [%]	Events	Tot. Eff. [%]	Rel. Eff. [%]
All events	708100	1.000 ± 0.000	1.000 ± 0.000	918100	1.000 ± 0.000	1.000 ± 0.000
Basic GEN level selections						
$p_{T_1} > 17 \text{ GeV}, \eta < 0.9$	394162	0.557 ± 0.001	0.557 ± 0.001	510675	0.556 ± 0.001	0.556 ± 0.001
$p_{T_2} > 8 \text{ GeV}, \eta < 2.4$	377302	0.533 ± 0.001	0.957 ± 0.000	488761	0.532 ± 0.001	0.957 ± 0.000
$p_{T_3} > 8 \text{ GeV}, \eta < 2.4$	313365	0.443 ± 0.001	0.831 ± 0.001	406687	0.443 ± 0.001	0.832 ± 0.001
$p_{T_4} > 8 \text{ GeV}, \eta < 2.4$	144443	0.204 ± 0.000	0.461 ± 0.001	187200	0.204 ± 0.000	0.460 ± 0.001
$L_{xy} < 9.8 \text{ cm and } L_z < 46.5 \text{ cm}$	43590	0.062 ± 0.000	0.302 ± 0.001	4346	0.005 ± 0.000	0.023 ± 0.000
Basic RECO level selections						
$p_{T_1} > 17 \text{ GeV}, \eta < 0.9$	381349	0.539 ± 0.001	0.539 ± 0.001	343484	0.374 ± 0.001	0.374 ± 0.001
$p_{T_2} > 8 \text{ GeV}, \eta < 2.4$	354475	0.501 ± 0.001	0.930 ± 0.000	248625	0.271 ± 0.000	0.724 ± 0.001
$p_{T_3} > 8 \text{ GeV}, \eta < 2.4$	263409	0.372 ± 0.001	0.743 ± 0.001	118293	0.129 ± 0.000	0.476 ± 0.001
$p_{T_4} > 8 \text{ GeV}, \eta < 2.4$	100626	0.142 ± 0.000	0.382 ± 0.001	33378	0.036 ± 0.000	0.282 ± 0.001
Extra RECO level selections						
Good primary vertex	100626	0.142 ± 0.000	1.000 ± 0.000	33378	0.036 ± 0.000	1.000 ± 0.000
Two muon-jets	76753	0.108 ± 0.000	0.763 ± 0.001	19496	0.021 ± 0.000	0.584 ± 0.003
Two dimuons	76700	0.108 ± 0.000	0.999 ± 0.000	19484	0.021 ± 0.000	0.999 ± 0.000
Pixel hit requirement	38488	0.054 ± 0.000	0.502 ± 0.002	4164	0.005 ± 0.000	0.214 ± 0.003
$ z_{\mu\mu_1} - z_{\mu\mu_2} < 0.1 \text{ cm}$	35925	0.051 ± 0.000	0.933 ± 0.001	3623	0.004 ± 0.000	0.870 ± 0.005
$m_{\mu\mu_1} \approx m_{\mu\mu_2}$	34384	0.049 ± 0.000	0.957 ± 0.001	3494	0.004 ± 0.000	0.964 ± 0.003
Dimuon isolation < 2 GeV	27526	0.039 ± 0.000	0.801 ± 0.002	2808	0.003 ± 0.000	0.804 ± 0.007
Trigger	25586	0.036 ± 0.000	0.930 ± 0.002	2575	0.003 ± 0.000	0.917 ± 0.005
α_{GEN}						
ϵ_{SM}						
$\epsilon_{\text{SM}} / \alpha_{\text{GEN}}$						
		0.062 ± 0.000	0.036 ± 0.000		0.005 ± 0.000	0.003 ± 0.000
		0.587 ± 0.002			0.592 ± 0.007	

1527 **C BB Background Fit Results**

DRAFT

Table 33: S17 fit parameters

Parameter	Fit Value	Fit Error
p_η	2.77e+01	3.26e+01
p_ω	1.01e+02	3.25e+01
p_ϕ	9.47e+01	2.67e+01
$p_{J/\psi}$	5.85e+03	8.54e+02
p_ψ	9.47e+01	2.67e+01
$\alpha_{J/\psi}$	1.70e+00	5.50e-02
$\sigma_{J/\psi}$	2.76e-02	4.37e-04
$m_{J/\psi}$	3.09e+00	4.37e-04
p_B	1.29e+04	3.01e+03
p_{06}	1.29e+01	5.94e+00
p_{16}	7.78e-07	5.32e-01
p_{26}	1.60e-05	4.37e-01
p_{36}	9.81e-01	6.67e-01
p_{46}	1.40e+00	4.73e-01
p_{56}	2.64e-01	2.24e-01
p_{66}	7.01e-01	3.67e-01
p_{AH}	6.92e+02	7.31e+01
$m_{0,AH}$	3.09e-01	1.66e-03
σ_{AH}	6.82e-02	8.01e-03
p_{E0}	1.83e-02	1.79e-04
p_{E1}	1.18e-00	1.99e-02
p_{E2}	9.92e+03	1.75ee+02

Table 34: Smix fit parameters

Parameter	Fit Value	Fit Error
p_η	7.45e-13	5.57e-01
p_ω	1.87e+01	1.55e+01
p_ϕ	4.13e+01	1.65e+01
$p_{J/\psi}$	2.17e+03	5.90e+01
p_ψ	4.13e+01	1.65e+01
$\alpha_{J/\psi}$	1.62e+00	1.02e-01
$\sigma_{J/\psi}$	3.92e-02	1.07e-03
$m_{J/\psi}$	3.09e+00	1.11e-03
p_B	3.87e+03	2.78e+02
p_{06}	1.29e+01	8.68e+00
p_{16}	1.45e-04	7.44e-01
p_{26}	1.49e-13	4.54e-01
p_{36}	7.70e-13	2.65e+00
p_{46}	1.40e+00	8.96e-01
p_{56}	4.49e-01	2.22e-01
p_{66}	9.10e-01	6.74e-01
p_{AH}	1.43e+02	5.83e+01
$m_{0,AH}$	3.3745e-01	1.92e-02
σ_{AH}	7.32e-02	1.88ee-02
p_{E0}	2.03e-02	1.21e-03
p_{E1}	1.09e-02	1.21e-03
p_{E2}	5.71e+03	2.39e+02

1528 D Separation of prompt and non-prompt J/Psi using the lifetime method 1529

1530 An alternative method to separate the prompt and non-prompt double J/ψ 's relies on the
1531 dimuon lifetime. We assume that promptly produced double J/ψ typically have a smaller
1532 lifetime than those from b decay. In that case, the "corrected L_{xy} " variable can discriminate
1533 between the prompt and non-prompt contributions.

1534 Region A has both prompt ($f_{A,\text{prompt}}$) and non-prompt ($f_{A,\text{non-prompt}}$) double J/ψ events. The
1535 L_{xy} is denoted as $L_{xy,\text{Data } A}$. The prompt template, $L_{xy,\text{MC}}$, was obtained from a double J/ψ
1536 MC sample. Here, either SPS or DPS can be used since they have similar lifetimes (see Fig. 37).
1537 Events in the non-isolated sideband region C determine the non-prompt L_{xy} template, $L_{xy,\text{Data } C}$.
1538 These L_{xy} are shown in Fig. 47 (top left). The fit of the combined template $f_{A,\text{prompt}}L_{xy,\text{MC}} +$
1539 $f_{A,\text{non-prompt}}L_{xy,\text{Data } C}$ to $L_{xy,\text{Data } A}$ yields the fraction of each contribution. The fit is shown
1540 top right and has a goodness of $\chi^2/\text{ndf} = 1.39$. Figure 47 (bottom left) is the same fit, but
1541 shown with logarithmic scale on the y -axis. The contributions were $f_{A,\text{prompt}} = 27 \pm 2\%$ and
1542 $f_{A,\text{non-prompt}} = 73\% \pm 3$. These results are consistent with those obtained using the ABCD
1543 method, i.e. $f_{A,\text{prompt}}^{ABCD} = (33.6 \pm 6)\%$ and $f_{A,\text{non-prompt}}^{ABCD} = (66.4 \pm 6)\%$. The ratio of fit over data
1544 is shown bottom right.

DRAFT

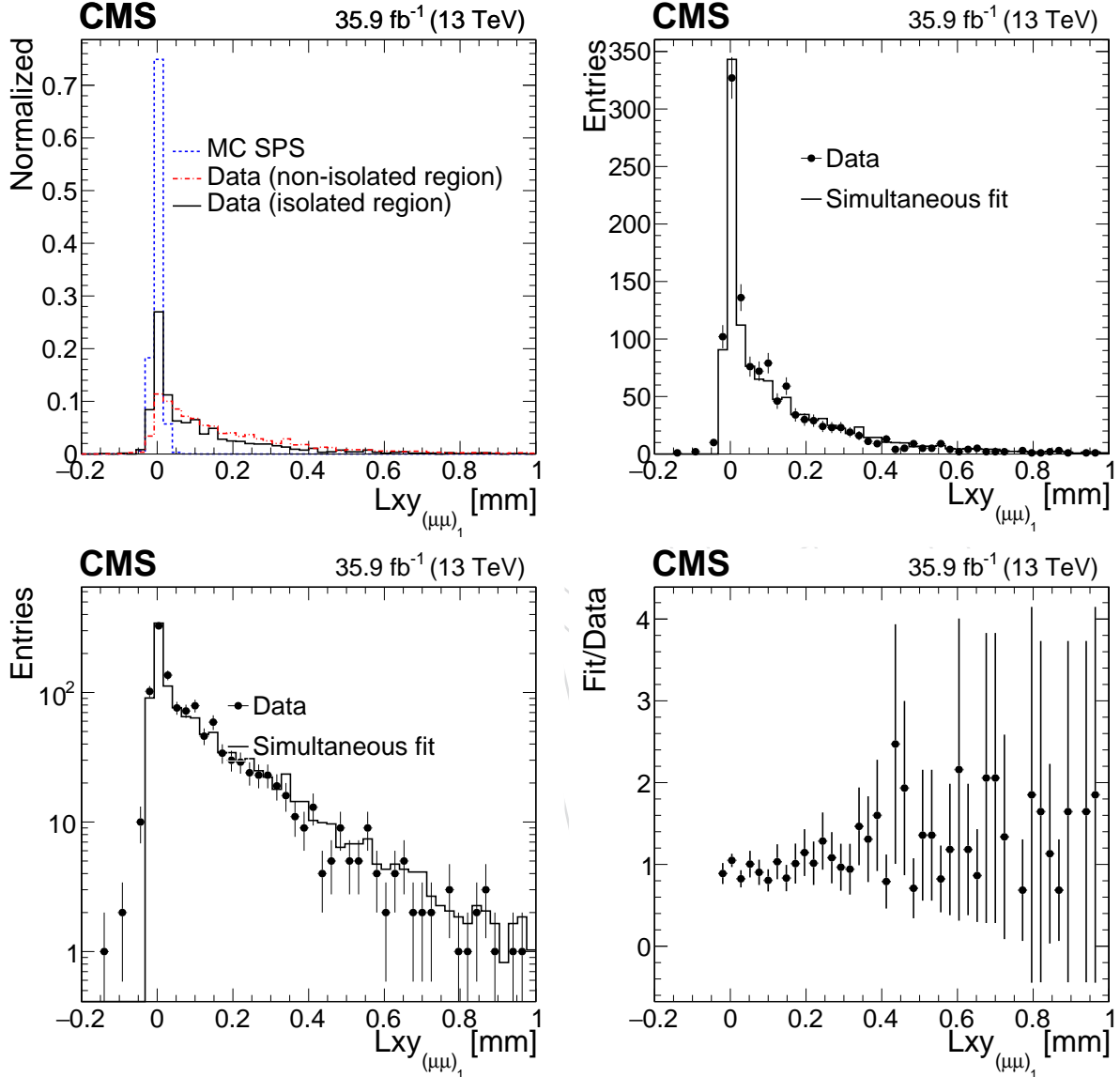


Figure 47: Top left: L_{xy} distributions for SPS MC simulation, non-prompt double J/ψ events from a non-isolated distribution in data and prompt double J/ψ events in data. Top right: fit of the combined L_{xy} template, from MC simulation and the non-prompt using a non-isolated distribution in data, to the L_{xy} distribution for double J/ψ events in data. Bottom left: same as top right, but with logarithmic scale on the y -axis. Bottom right: distribution of the ratio between fit and data.

1545 E Vertex Recovery for Parallel Muon Pairs

1546 As described in Section 4.3, for models with small values of $m(\gamma_D)$ the muons from the γ_D
 1547 decay are often both highly parallel and spatially close to one another. In some events with this
 1548 topology the Kalman filter is unable to select a satisfactory dimuon vertex due to the parallel
 1549 nature of the tracks. For events in which this is the case the point of closest approach between
 1550 the two muon tracks is used as the vertex, and the dimuon kinematics are recalculated to take
 1551 this into account. Fig. 48 shows the value of $\epsilon_{full}/\alpha_{gen}$ as a function of $c\tau$ for several different
 1552 values of $m(\gamma_D)$, where ϵ_{full} is the full analysis acceptance at RECO level, and α_{gen} is the basic
 1553 analysis acceptance at GEN level. Both of these quantities, ϵ_{full} and α_{gen} , are described in detail
 1554 in Section 4.4. There is a clear improvement in the case of the low mass sample once this vertex
 1555 recovery approach is included. Signal samples with larger values of $m(\gamma_D)$ are not affected as
 1556 the opening angle between the muons larger.

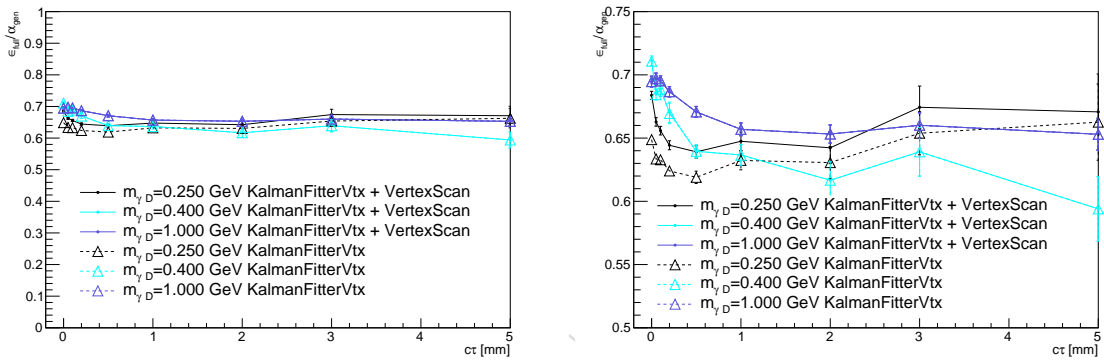


Figure 48: $\epsilon_{full}/\alpha_{gen}$ as a function of $c\tau$ for several different values of $m(\gamma_D)$ for the case where only the Kalman filter is used to select dimuon vertices, and also when the vertex scan extension is used. Left shows the complete $\epsilon_{full}/\alpha_{gen}$ range. Right shows the region of interest in closer detail.

F Dimuon Tracker Isolation

Figures 49, 50, 51, 52, 53, 54, 55, 56, and 57, show the dimuon tracker isolation distributions for dark SUSY MC samples and background-enriched parts of the data. All dark photon mass samples are presented, and for each mass the full dimuon isolation distribution is shown (left) and a close-up log-scaled plot (right) is shown in the region near the 2.0 GeV cut.

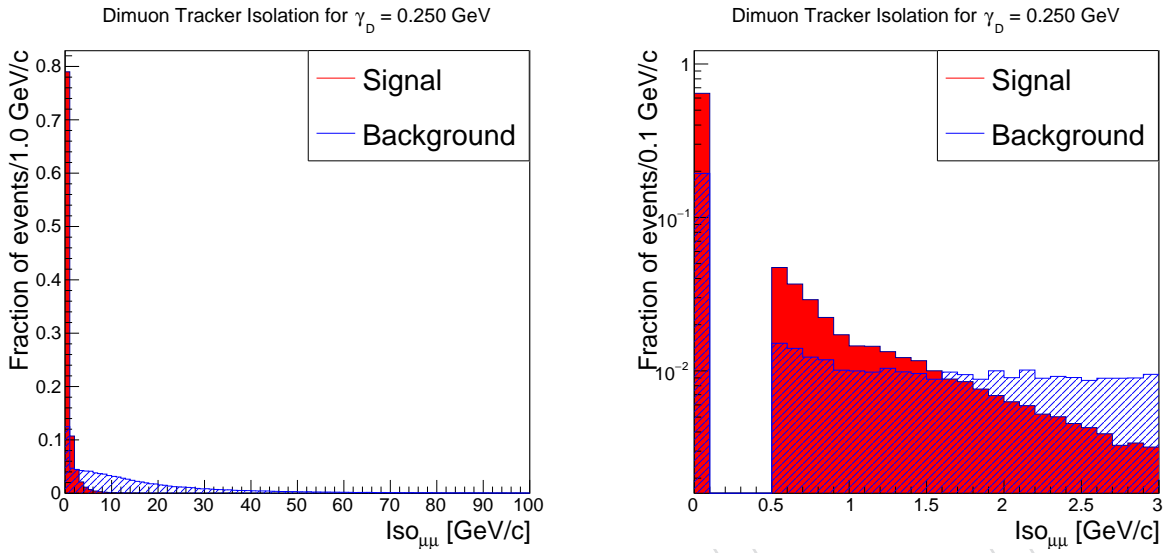


Figure 49: Isolation of the dimuons in events from the dark SUSY MC sample with a dark photon mass of 0.25 GeV and in events from the background-enriched part of data. The full normalized distribution (left) and a log-scale close-up near the 2.0 GeV isolation cut (right) are shown.

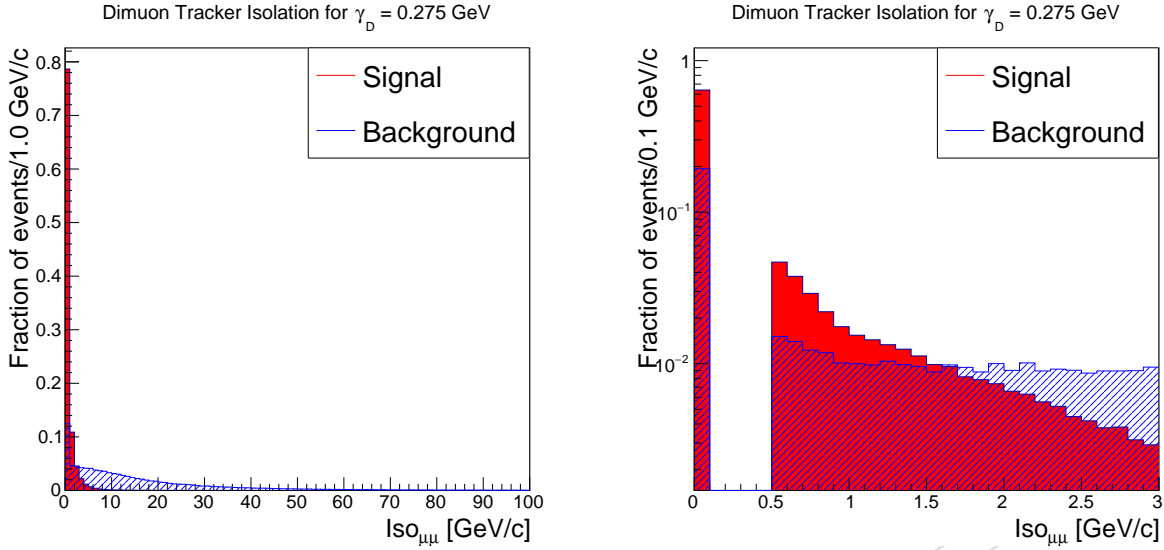


Figure 50: Isolation of the dimuons in events from the dark SUSY MC sample with a dark photon mass of 0.275 GeV and in events from the background-enriched part of data. The full normalized distribution (left) and a log-scale close-up near the 2.0 GeV isolation cut (right) are shown.

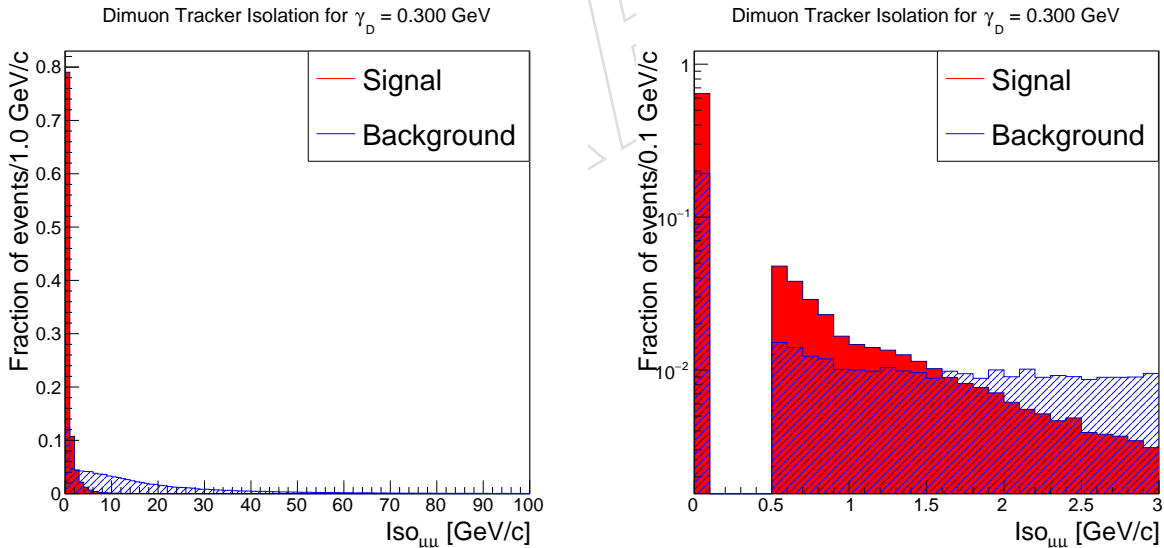


Figure 51: Isolation of the dimuons in events from the dark SUSY MC sample with a dark photon mass of 0.3 GeV and in events from the background-enriched part of data. The full normalized distribution (left) and a log-scale close-up near the 2.0 GeV isolation cut (right) are shown.

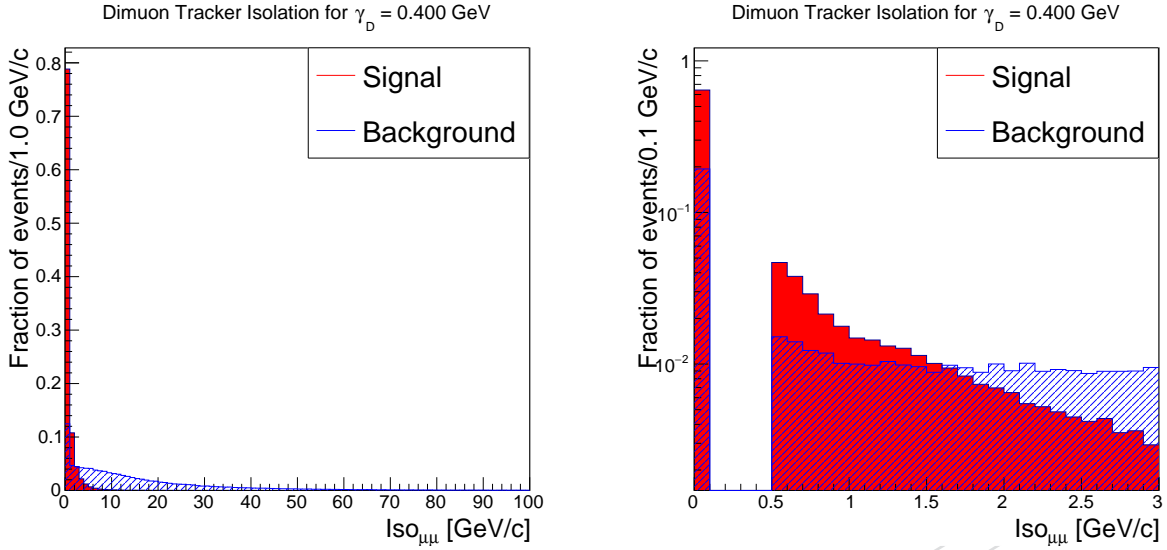


Figure 52: Isolation of the dimuons in events from the dark SUSY MC sample with a dark photon mass of 0.4 GeV and in events from the background-enriched part of data. The full normalized distribution (left) and a log-scale close-up near the 2.0 GeV isolation cut (right) are shown.

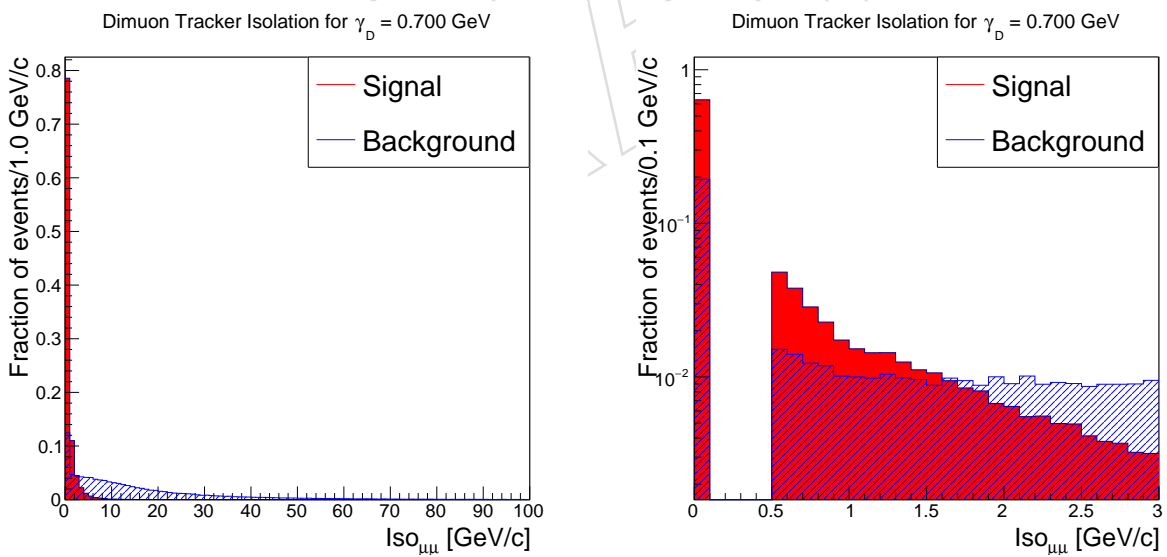


Figure 53: Isolation of the dimuons in events from the dark SUSY MC sample with a dark photon mass of 0.7 GeV and in events from the background-enriched part of data. The full normalized distribution (left) and a log-scale close-up near the 2.0 GeV isolation cut (right) are shown.

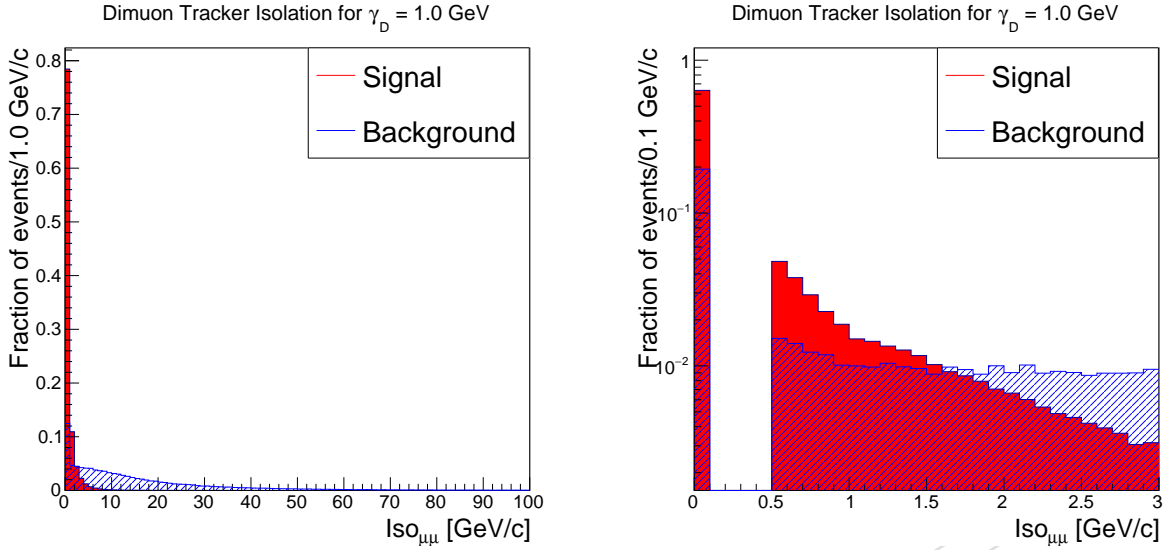


Figure 54: Isolation of the dimuons in events from the dark SUSY MC sample with a dark photon mass of 1.0 GeV and in events from the background-enriched part of data. The full normalized distribution (left) and a log-scale close-up near the 2.0 GeV isolation cut (right) are shown.

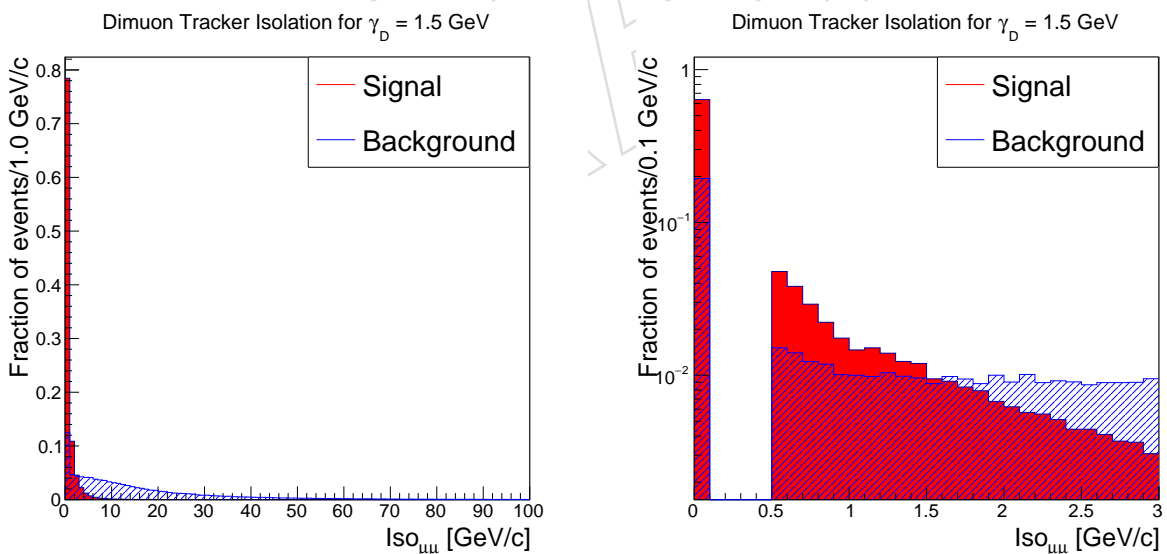


Figure 55: Isolation of the dimuons in events from the dark SUSY MC sample with a dark photon mass of 1.5 GeV and in events from the background-enriched part of data. The full normalized distribution (left) and a log-scale close-up near the 2.0 GeV isolation cut (right) are shown.

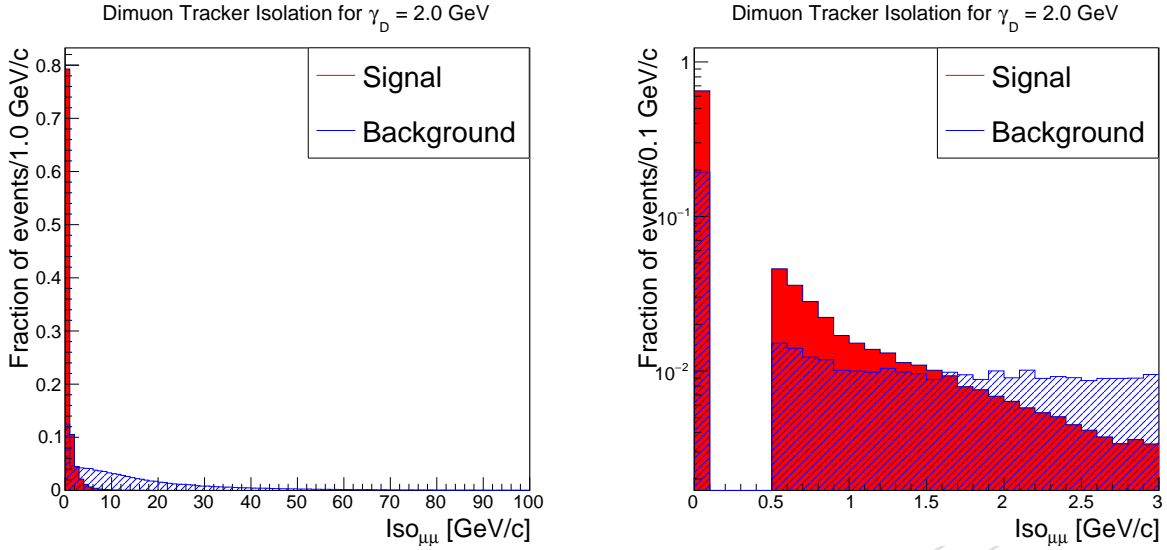


Figure 56: Isolation of the dimuons in events from the dark SUSY MC sample with a dark photon mass of 2.0 GeV and in events from the background-enriched part of data. The full normalized distribution (left) and a log-scale close-up near the 2.0 GeV isolation cut (right) are shown.

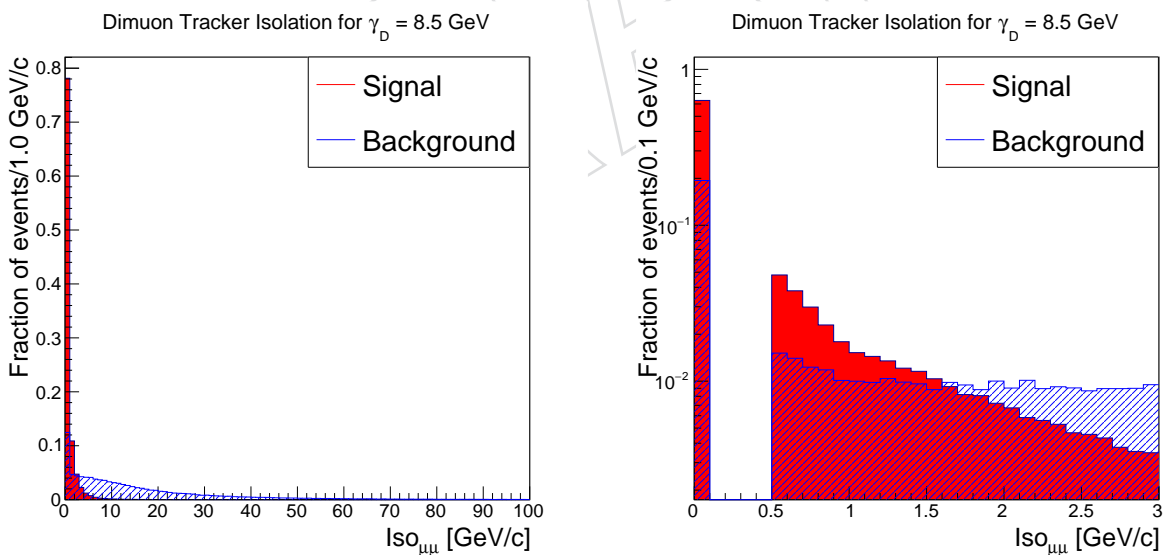


Figure 57: Isolation of the dimuons in events from the dark SUSY MC sample with a dark photon mass of 8.5 GeV and in events from the background-enriched part of data. The full normalized distribution (left) and a log-scale close-up near the 2.0 GeV isolation cut (right) are shown.

1562 G Extraction SF for muon ID and Isolation

1563 The corrections DATA to MC for muon ID and isolation are extracted with the official muonPG
 1564 T&P tool as a function of pT and η as shown in Figures 58, 59, 60. Our selection uses a loose
 1565 muon ID and track isolation, our SFs are extracted using the DY samples and the low p_T part is
 1566 validated using the J/ψ resonance.

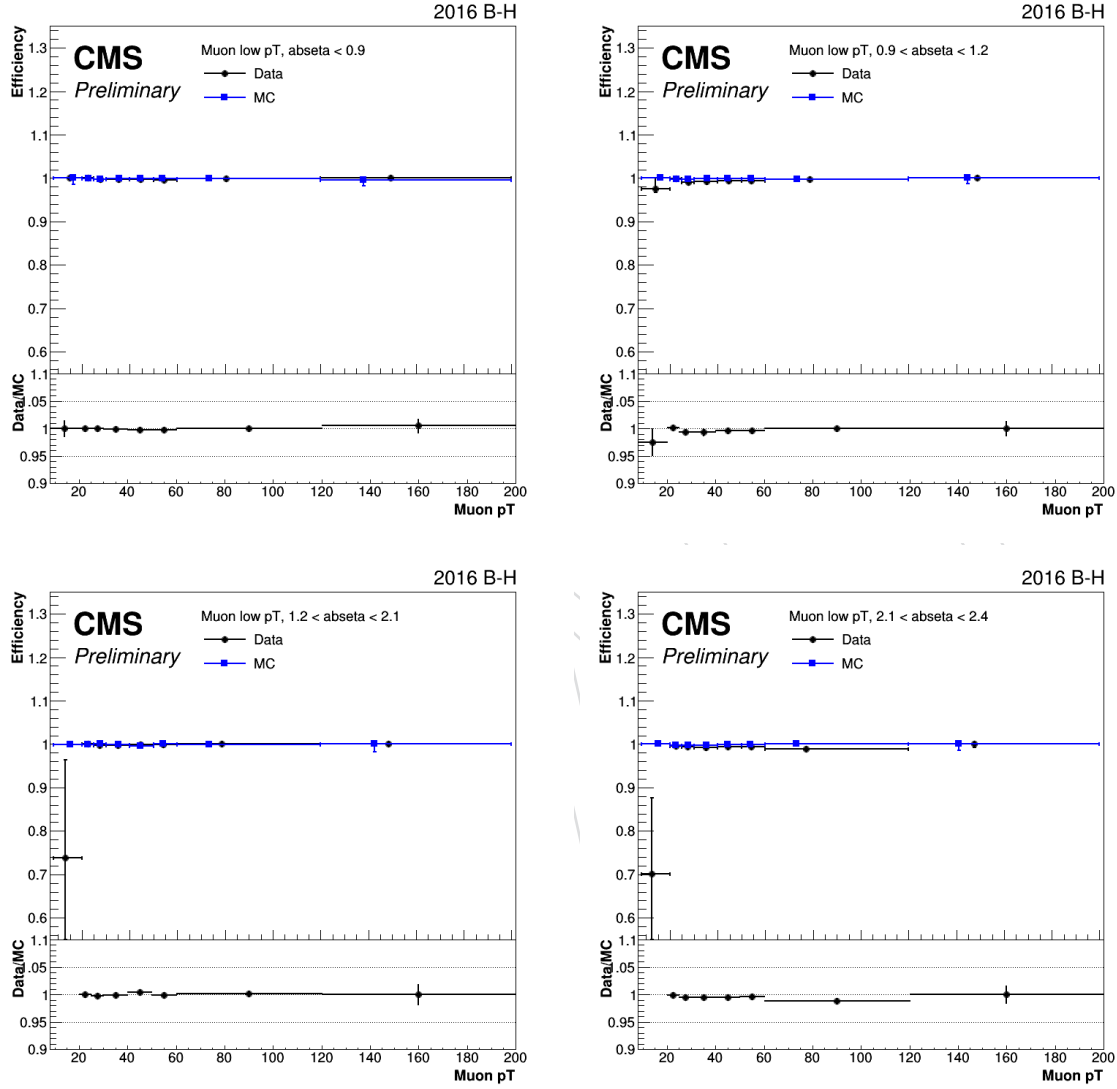


Figure 58: SF for muon ID extracted with T&P method using the DY samples with a muon p_T threshold of 8 GeV

1567 G.1 Cross-check of the low-pT contribution with J/ψ

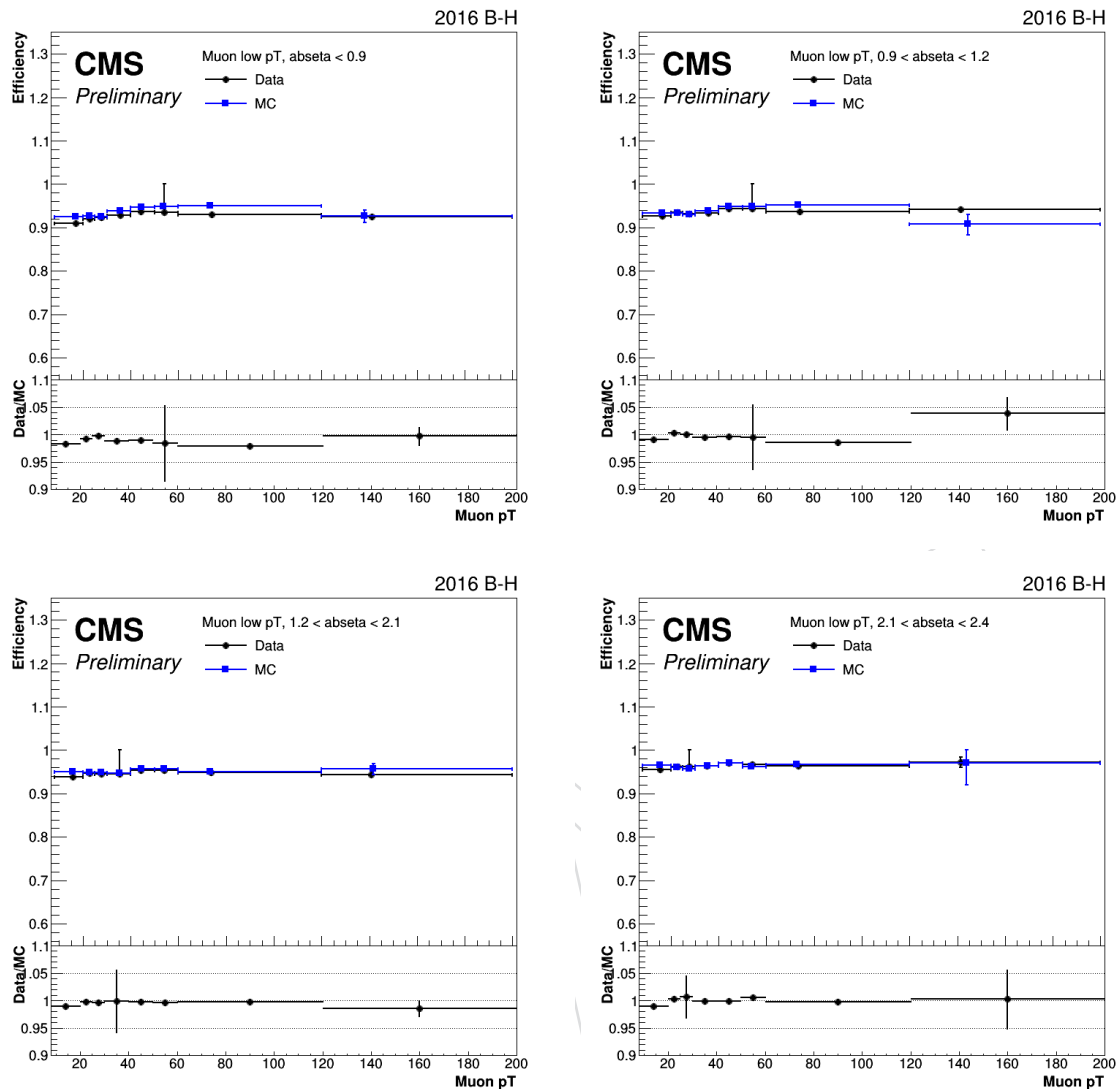


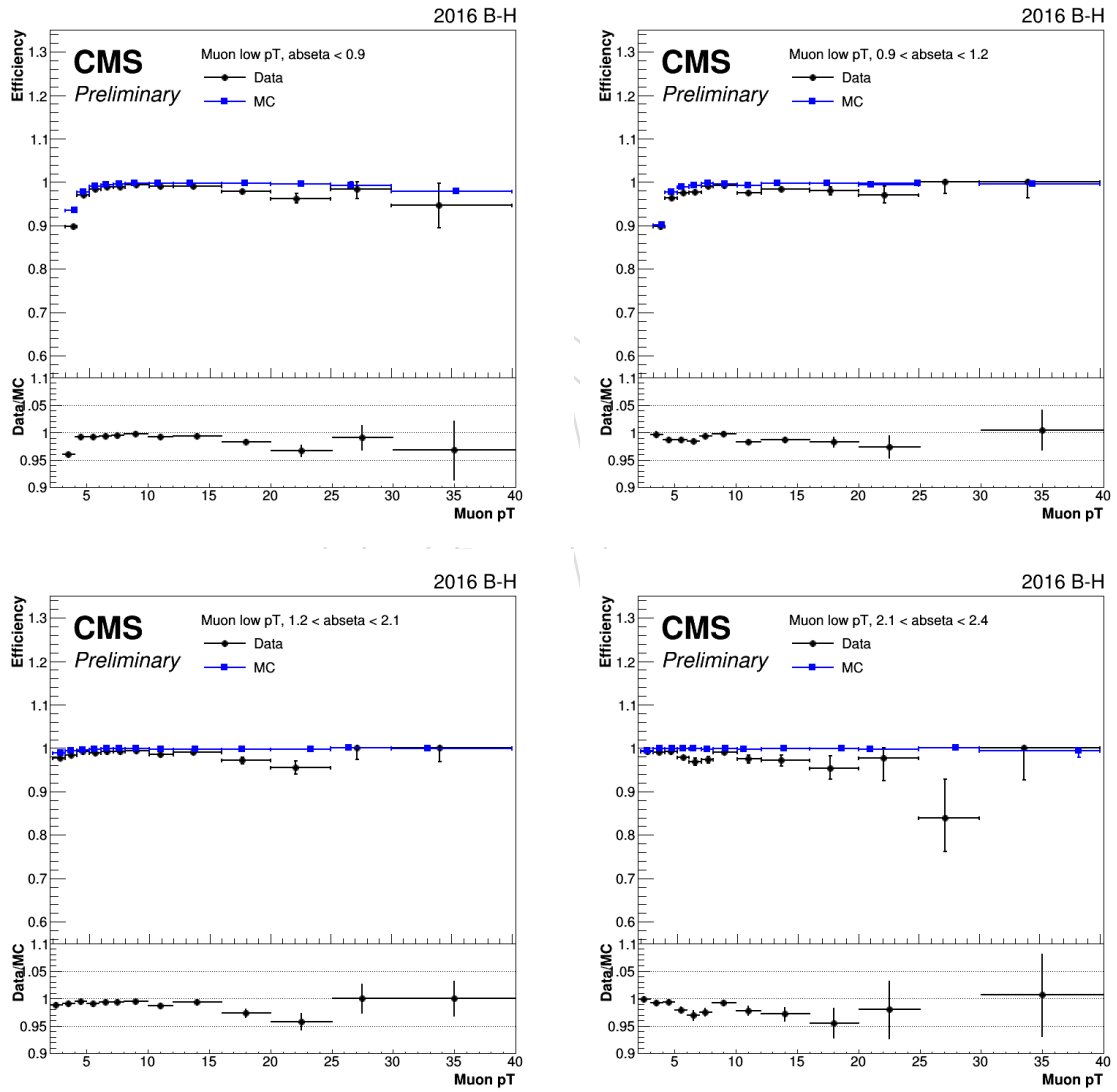
Figure 59: SF for muon isolation extracted with T&P method using the DY samples with a muon pT threshold of 8 GeV

Table 35: Summary of SF for muon ID

η Region	SF (weighted avg)	Uncertainty %
0-0.9	0.99842	0.6
0.9-1.2	0.995928	0.3
1.2-2.1	1.001099	0.4
2.1-2.4	0.995141	0.2
Total	0.997647	0.6

Table 36: Summary of SF for muonIso

η Region	SF (weighted avg)	Uncertainty %
0-0.9	0.989105	0.02
0.9-1.2	0.9957	0.1
1.2-2.1	0.996674	0.1
2.1-2.4	0.998705	0.1
Total	0.995046	0.1

Figure 60: SF for muon ID extracted with T&P method using the J/ψ resonance with a muon pT threshold of 2 GeV

1568 H Model of the Event Acceptance as a Function of m_{γ_D} and $c\tau_{\gamma_D}$

1569 In order to construct smooth Dark SUSY efficiency curves to input to the limit machinery we
 1570 needed to construct an analytic expression that describes this how the efficiency behaves as a
 1571 function of m_{γ_D} and $c\tau$.

1572 Gamma factor as a function of the m_{γ_D} for a given energy:

$$\gamma(m_{\gamma_D}, E_{\gamma_D}) = \frac{E_{\gamma_D}}{m_{\gamma_D}} \quad (27)$$

1573 The acceptance measured with the $c\tau = 0$ mm MC samples is used as a normalization.

1574 We can construct a function for $\frac{dN}{dz} dR$, corresponding to the number of γ_D which decay within
 1575 a cone that points to a “belt” on a cylinder with radius R , at z , where the γ_D originates from the
 1576 center of the coordinate frame at $R = z = 0$.

$$f_1(m_{\gamma_D}, E_{\gamma_D}, c\tau, R) = \frac{1}{2} \cdot \frac{1}{\gamma(m_{\gamma_D}, E_{\gamma_D}) \cdot c\tau} \cdot \frac{R}{R^2 + z^2} \cdot e^{-\frac{\sqrt{R^2 + z^2}}{\gamma(m_{\gamma_D}, E_{\gamma_D}) \cdot c\tau}} \quad (28)$$

$$z_{\max}(m_{\gamma_D}, E_{\gamma_D}, c\tau, R) = \begin{cases} 10.0 \cdot \frac{E_{\gamma_D}}{m_{\gamma_D}}, & \text{if } 10.0 \cdot \frac{E_{\gamma_D}}{m_{\gamma_D}} < 10.0 \cdot R \\ 10.0 \cdot R, & \text{otherwise} \end{cases} \quad (29)$$

1577 We then integrate over z from $-5R$ to $+5R$. Ideally we should integrate from $\pm\infty$ but numerical
 1578 convergence is achieved in the range $\pm 5R$.

$$f_2(m_{\gamma_D}, E_{\gamma_D}, c\tau, R) = 2 \left(\int_0^{z_{\max}} f_1(m_{\gamma_D}, E_{\gamma_D}, c\tau, R) dz \right) \quad (30)$$

1579 For this analysis the efficiency as a function of R is a constant up to $R = 9.8$ cm, the radius of
 1580 the third layer in the pixel detector, and beyond this the efficiency is set to 0 (this is consistent
 1581 with the effective fiducial cut described in Sec. 4.3). Prior to including the effective fiducial
 1582 requirement the efficiency as a function of R was still a constant in the region $R < 9.8$ cm, but
 1583 beyond this it decreased as $\sim \frac{1}{R}$, until 600 cm, at which point it was set to 0:

$$\epsilon_R(R_0, R) = \begin{cases} \text{if } R < R_0 \\ \begin{cases} 1.0, & \text{if } R > 0.0 \\ 0.0, & \text{otherwise} \end{cases} \\ \text{otherwise:} \\ \begin{cases} \frac{R_0}{R}, & \text{if } R < 600.0 \\ 0.0, & \text{otherwise} \end{cases} \end{cases} \quad (31)$$

1584 where R_0 is set to the radius of the third layer in the pixel detector.

¹⁵⁸⁵ **I Example of an Candidate Signal Event**

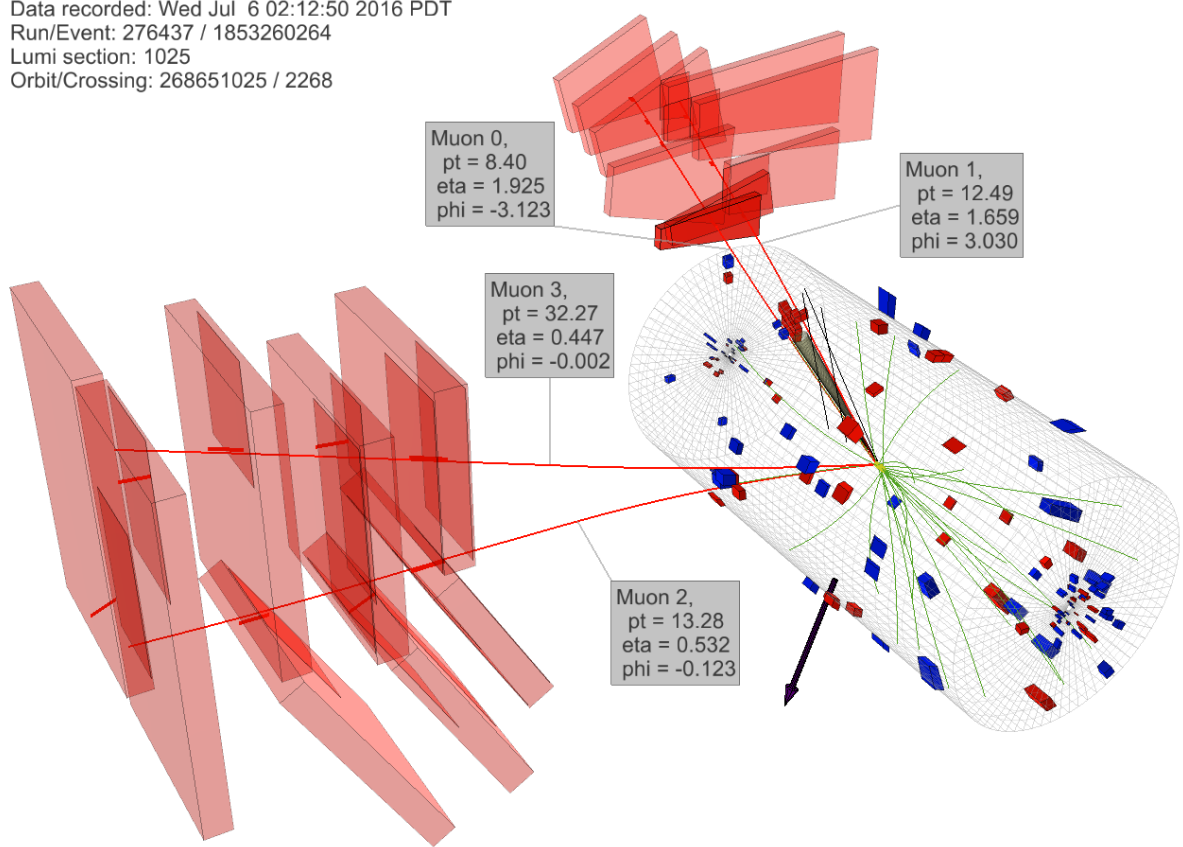
¹⁵⁸⁶ Table 37 shows some of the main parameters of the 13 data events passing the event selection.
¹⁵⁸⁷ The first event in the table is displayed in Fig. 61. The two isolated dimuons are clearly shown.

Table 37: Parameters of the 13 events in data that pass all selection criteria. Note: LS stands for “luminosity section”

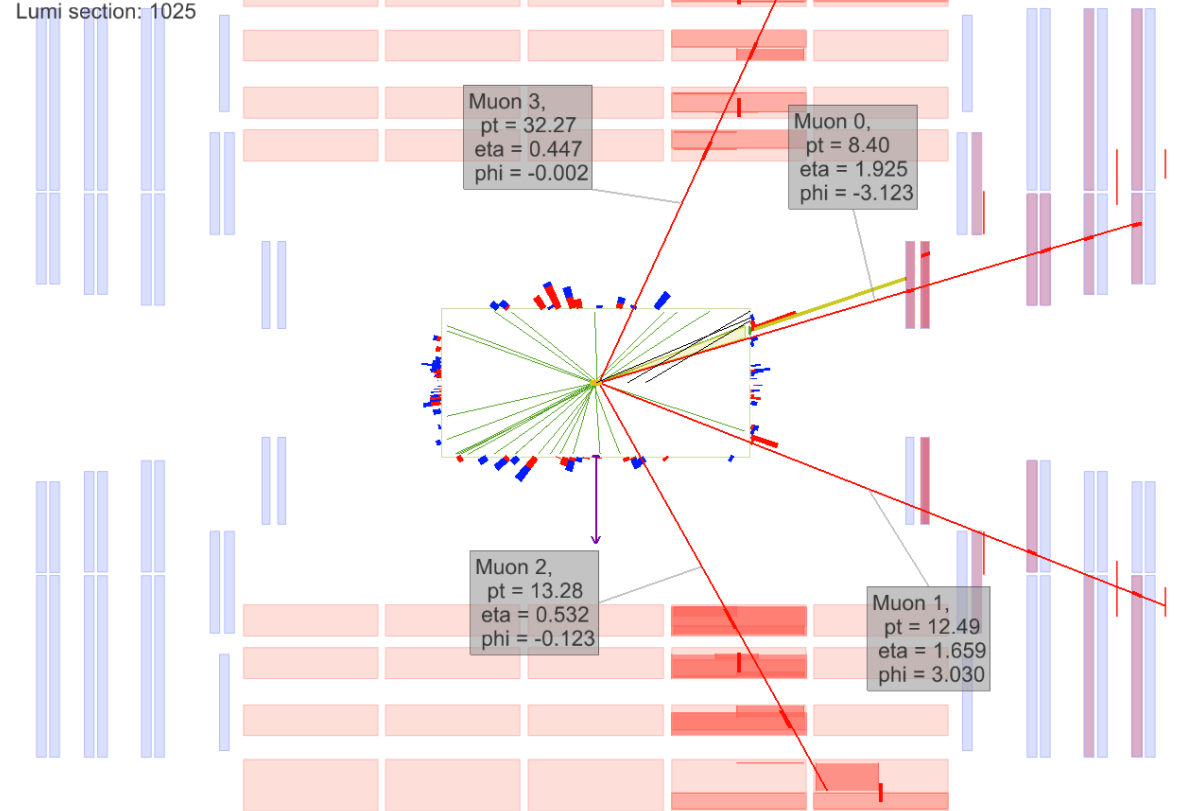
Row	Run	LS	Event	$m_{\mu\mu_1}$ [GeV]	$m_{\mu\mu_1}$ [GeV]	$\text{Iso}_{\mu\mu_1}$ [GeV]	$\text{Iso}_{\mu\mu_2}$ [GeV]
1	275847	1705	2106699737	2.860	3.002	0	0.530
2	275913	32	66565962	0.808	0.727	1.784	1.856
3	276437	1025	1853260264	3.073	3.054	1.745	0.564
4	276458	316	401282019	0.426	0.585	0	0
5	276582	844	1519428017	3.072	3.266	0	0
6	276950	1504	1571001039	3.095	3.362	0	0
7	278273	83	40062290	2.825	2.650	0.838	0
8	278769	83	26539721	3.152	2.855	1.238	0.944
9	279760	154	174402676	1.254	1.152	0	1.084
10	281707	695	1065646434	1.354	1.483	1.451	1.055
11	282814	1028	1890506418	2.386	2.358	0.657	1.966
12	283306	151	277427894	3.064	3.097	1.708	0
13	283453	122	100162832	1.940	1.820	0	0

DRAFT

CMS Experiment at LHC, CERN
 Data recorded: Wed Jul 6 02:12:50 2016 PDT
 Run/Event: 276437 / 1853260264
 Lumi section: 1025
 Orbit/Crossing: 268651025 / 2268



CMS Experiment at LHC, CERN
 Data recorded: Wed Jul 6 02:12:50 2016 PDT
 Run/Event: 276437 / 1853260264
 Lumi section: 1025



1588 J Comparison 8 vs 13 TeV

1589 This search constrains a large area of the parameter space. The previous published result
 1590 excluded the dark SUSY model with kinematic mixing ϵ between 5×10^{-6} at 0.25 GeV and
 1591 6×10^{-7} at 2 GeV [54]. The current limits improve to 2×10^{-6} at 0.25 GeV and 5×10^{-8} at
 1592 8.5 GeV.

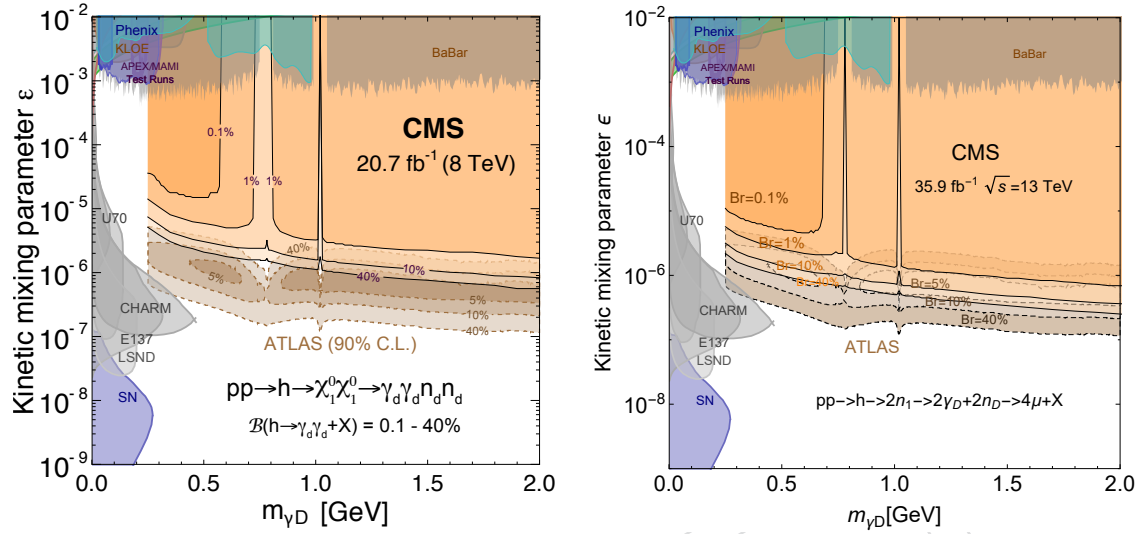


Figure 62: Comparison of the limit obtained in the ϵ vs $m_{\gamma D}$ plane for the Run-1 search (8 TeV) and the expected Run-2 with data collected during 2016 at 13 TeV